



NTNU – Trondheim
Norwegian University of
Science and Technology

Investigation of Hydrodynamic Performance of a Twin-Screw Trawler Using CFD

Nikolas Øksdal Svoren

Marine Technology

Submission date: June 2015

Supervisor: Sverre Steen, IMT

Norwegian University of Science and Technology
Department of Marine Technology

Scope of work



NTNU Trondheim

Norwegian University of Science and Technology

Department of Marine Technology

MASTER THESIS IN MARINE TECHNOLOGY

SPRING 2015

FOR

Nikolas Øksdal Svoren

Investigation of Hydrodynamic Performance of a Twin-Screw Trawler Using CFD

The ship design consultants Seacon have designed a twin-screw trawler, with large ducted propellers and steerable ducts. Before the final model tests are performed, there is a need for verifying and possibly optimizing the hull shape of the ship. Therefore, the objective of the combined project and master thesis is to verify the hydrodynamic performance and propose improvements to the design. It is acknowledged that it might not be possible to assess all aspects of the hydrodynamic performance in detail. Therefore, the priority is to be put on calm water performance in transit and trawling, in straight ahead and in a turn.

For the master thesis, the following issues and activities shall be covered:

- Give an introduction to the proposed trawler design, and how it stands out from the previous design and typical trawler designs, with focus on hydrodynamic aspects.
- Discuss potential hydrodynamics-related problems of the current design, and what can be done to address these problems.
- Perform a resistance and flow prediction of the current design in straight-ahead cruising condition. Do basic validation and convergence study.
- Special emphasis shall be put on the inflow conditions for the propeller. Derive the nominal wake in straight-ahead at different speeds. Consider the effect of the suction of the propeller (effective wake). Consider the effect of a turn on the inflow to the propeller
- Give recommendations for improvements of the hull design.

In the thesis the candidate shall present his personal contribution to the resolution of problem within the scope of the thesis work.



NTNU Trondheim

Norwegian University of Science and Technology

Department of Marine Technology

Theories and conclusions shall be based on mathematical derivations and/or logic reasoning identifying the various steps in the deduction.

The thesis work shall be based on the current state of knowledge in the field of study. The current state of knowledge shall be established through a thorough literature study, the results of this study shall be written into the thesis. The candidate should utilize the existing possibilities for obtaining relevant literature.

The thesis should be organized in a rational manner to give a clear exposition of results, assessments, and conclusions. The text should be brief and to the point, with a clear language. Telegraphic language should be avoided.

The thesis shall contain the following elements: A text defining the scope, preface, list of contents, summary, main body of thesis, conclusions with recommendations for further work, list of symbols and acronyms, reference and (optional) appendices. All figures, tables and equations shall be numerated.

The supervisor may require that the candidate, in an early stage of the work, present a written plan for the completion of the work. The plan should include a budget for the use of computer and laboratory resources that will be charged to the department. Overruns shall be reported to the supervisor.

The original contribution of the candidate and material taken from other sources shall be clearly defined. Work from other sources shall be properly referenced using an acknowledged referencing system.

The thesis shall be submitted electronically (pdf) in DAIM:

- Signed by the candidate
- The text defining the scope (signed by the supervisor) included
- Computer code, input files, videos and other electronic appendages can be uploaded in a zip-file in DAIM. Any electronic appendages shall be listed in the main thesis.

The candidate will receive a printed copy of the thesis.

Supervisor : Professor Sverre Steen

Start : 15.01.2015

Deadline : 09.06.2015

Trondheim, 15.01.2015

Sverre Steen
Supervisor

Preface

This master's thesis work has been carried out at the department of Marine Technology at the Norwegian University of Science and Technology, NTNU, during the spring of 2015. This is the final work towards my M.Sc. degree, where I specialize within hydrodynamics.

Before starting this work I had no previous experience working with CFD, only some knowledge on theory applied. I have had a steep learning curve, and it has been an interesting adventure familiarizing with the software. During this work I have been greatly dependent of the computational resources provided by the HPC group at NTNU. Without the access to Vilje this work would not have been possible to carry out. A grand total of 5200 licencing hours have been used when performing simulations for this thesis.

I would like to express my deepest gratitude to my supervisor Professor Sverre Steen at NTNU for his valuable help and guidance throughout this semester. Also I would like to thank the contributing companies for letting me take a part of this interesting innovation project. My appreciation goes to the ship-owner *Roaldnes AS* for letting me take a part in the design process of their ship, and *Seacon as* for providing me with necessary data and models. I would especially like to thank Vegard Larsen at *Stadt Towing Tank* for providing support beyond expectations, and for the creation of the 3D model referred to as Hull 2 in this thesis. My appreciation also goes to the engineering team at CD-adapco for support, and for letting me use their software for free.

Lastly I would like to thank my fellow students at *Champagnesvingen* for valuable discussions during the work of this Master's thesis, and all the good moments over the last 5 years.

Trondheim, 10th June 2015



Nikolas Øksdal Svoren.

Abstract

Previously experimental methods or empirical knowledge laid the foundation for ship design. Performing a model test in a towing tank is time consuming and expensive. In addition to this, studying detailed effects in a laboratory proves to be difficult.

The exponential growth in computer power allows engineers to use computers and software to solve Navier-Stokes equations using *computational fluid dynamics* (CFD). This method allows the engineers to test different models, in a time and cost-efficient manner.

In this master thesis, a study of CFD codes to perform a resistance prediction on two different hull design for the trawler, Roaldnes, have been made. The first design being the current design from Seacon, Hull 1, the second being a design based on findings from project report (Svoren, 2014), Hull 2. The difference between these hulls can be found at the aft shoulder where Season's hull is designed with chines while the second design is without. Special emphasis was made on the inflow conditions for the propeller. This was done in order to compare and observe the effect of the changes made to the hull. STAR CCM+ from CD-adapco was chosen as CFD software, due to its user-friendly interface and powerful built in post processing tools.

A detailed and thorough convergence study was performed to find the optimal simulation setup. This study resulted in a mesh with approx. 2 mill cells, time step of 0.01s, and a domain which stretched 4 lwl aft and forth, 5 lwl to the side, 1.7 lwl up, and 3.5 lwl down. Due to symmetry, half of the model is simulated.

A total of eight simulations on both hulls, at trawl and transit speed, and with and without nozzle and virtual disk, were performed. Hull 1 displayed a low-pressure ridge over the sharp edge created by the chines. This lead to increased vorticities in this area compared to Hull 2. These vorticities propagated onto the propeller plane, where Hull 2 showed a slightly better wake field at trawl speed, and similar wake field at transit speed. A plot of the streamlines showed a low-velocity swirl of water on the inside of each skeg at both velocities. These were however almost gone when introducing suction from the virtual disk simulating the propeller.

Calculation of thrust reduction on Hull 2 showed an improvement of 3.75% compared to Hull 1. Full-scale calculations showed an improvement in total hull resistance of 6.7% at 4 knots, and 2.2% at 10 knots in favor of Hull 2.

Validation of results were made to known experimental data for a similar vessel, R/V Gunnerus. This investigation showed that the results obtained in this report was within an acceptable range from the reference vessel.

As CDF is a numerical tool to replicate reality, error sources, and uncertainty will always be of presence. Nevertheless, it can be used to show trends. Results obtained in this report suggests that Hull 2 might produce a more uniform inflow, and a better wake field for the propellers, than what can be seen from Hull 1. It also indicates that Hull 2 might produce lower thrust reduction, as well as an overall lower hull resistance at both trawling and transit.

Sammendrag

Tidligere la eksperimentelle metoder eller empirisk kunnskap grunnlaget for skipsdesign. Å utføre modelltester i slepetank er tidkrevende og kostbart. I tillegg til dette er det utfordrende å studere detaljerte effekter ved propellområdet i et laboratorium.

Den voldsomme veksten i datakraft gjør det mulig å bruke datamaskiner og programvare til å løse Navier-Stokes ligninger ved hjelp av *Computational Fluid Dynamics* (CFD). Denne metoden gjør det mulig for ingeniører å teste forskjellige modeller på en effektiv og økonomisk besparende måte.

Denne masteroppgaven omhandler bruk av CFD-koder til å utføre en motstandsberegning samt studere innstrømningsfeltet til propellene. Dette gjøres på to forskjellige skrog design for tråleren Roaldnes. Det første skroget, Skrog 1, er designet av konsulentselskapet Seacon as, og er tegnet med knekkspant i akterskipet, med håp om å redusere rull bevegelsen. Skrog 2 er designet basert på foreslåtte endringer fra prosjektoppgaven tilhørende denne masteroppgaven (Svoren, 2014). Dette skroget har rundet spant i akterskipet, i håp om å redusere skrogmotstand og forbedre innstrømningen til propellene. Programvaren, STAR CCM+, fra CD-adapco ble valgt som CFD programvare på grunn av sitt brukervennlige grensesnitt og kraftige innebyggede post-prosesseringsverktøy.

En grundig og detaljert konvergens analyse ble gjennomført for å finne et optimalt oppsett for denne simuleringen. Denne studien resulterte i et oppsett med rundt 2 millioner celler, et tids steg på 0.01s og et domene som strekker seg 4 lwl forover og akterover, 5 lwl til siden, 1.7 lwl oppover og 3.5 lwl nedover. Grunnet symmetri simuleres kun halve modellen.

Totalt ble åtte simuleringer kjørt, bestående av begge skrog, både ved transitt og trålhastighet. Skrog 1 viste et lavt dynamisk trykk over knekken som fremkommer av knekkspantene. Dette ledet til økt virvelavløsning i dette området, sammenlignet med Skrog 2. Denne virvelavløsningen forplantet seg

bak i innstrømmingen til propellen, hvor Skrog 2 viste et noe bedre medstrøms felt ved trålhastighet sammenlignet med Skrog 1, og tilsynelatende likt medstrøms felt vel transitt. Et plot av strømningslinjene langs skroget viser virveldannelse på innsiden av skeggene med lav vannhastighet. Denne forsvinner nesten helt når sug fra propell blir introdusert i simuleringen.

Beregning av thrustreduksjon på Skrog 2 viser en forbedring på 3,75% i forhold til Skrog 1. Kalkulering av skalert motstand, for Skrog 2, viste en forbedring av total skrogmotstand på 6,7% ved trål hastighet, og 2,2% ved transitt sammenlignet med Skrog 1.

Validering av resultatene ble gjort ved å sammenligne beregnede verdier med resultat fra slepeforsøk på et tilsvarende fartøy, R/V Gunnerus. Denne undersøkelsen viste at de oppnådde resultater i denne rapport var innenfor akseptable verdier sammenlignet med referansefartøyet.

Siden CFD er et numeriskverktøy som brukes for å replisere virkeligheten vil det alltid inneholde usikkerheter og unøyaktigheter, men kan likevel brukes til å studere trender. Resultater fra denne masteroppgaven viser at Skrog 2 kan se ut til å produsere et bedre innstrømningsfelt til propellene, samt et bedre medstrømsfelt i propell planet, sammenlignet med Skrog 1. Resultatene indikerer også at Skrog 2 vil kunne produsere en lavere thrustreduksjon enn Skrog 1. Skrog 2 ser også ut til å produsere mindre skrog motstand i fullskala, både ved tråling og transitt.

Table of Contents

SCOPE OF WORK.....	III
PREFACE	V
ABSTRACT	VII
SAMMENDRAG	IX
TABLE OF CONTENTS.....	XI
LIST OF FIGURES.....	XV
LIST OF TABLES	XIX
LIST OF ABBREVIATIONS	XXI
NOMENCLATURE	XXIII
1 INTRODUCTION	1
1.1 BACKGROUND	1
1.2 OBJECTIVES.....	1
1.3 STRUCTURE OF REPORT	1
2 DESIGN OF A TRAWLER.....	3
2.1 DEFINITION OF A TRAWLER.....	3
2.2 TYPICAL TRAWLER	4
2.2.1 <i>Design</i>	4
2.2.2 <i>Hydrodynamics</i>	5
2.3 CURRENT DESIGN	6
3 HYDRODYNAMICS.....	9
3.1 HYDRODYNAMIC CHALLENGES.....	9
3.1.1 <i>Bulbous bow</i>	9
3.1.2 <i>Stern design</i>	10
3.1.3 <i>Twin skeg and wake field</i>	13
4 THEORETICAL FOUNDATION	15
4.1 CFD BACKGROUND	15
4.2 GOVERNING EQUATIONS.....	16
4.3 TURBULENCE MODELLING	16

4.4	COURANT NUMBER.....	18
4.5	LAW OF THE WALL, Y+ VALUE.....	19
4.6	STAR CCM+	20
4.7	3D MODELLING	21
4.8	COMPUTATIONAL DOMAIN.....	22
4.9	MESHING	22
4.9.1	<i>Surface remesher</i>	23
4.9.2	<i>Volume mesher</i>	23
4.10	PHYSICAL MODELS	23
4.10.1	<i>K-epsilon turbulence and realizable K-epsilon two-layer</i>	24
4.10.2	<i>Eulerian multiphase</i>	24
4.10.3	<i>Volume of fluid (VOF)</i>	24
4.10.4	<i>VOF Waves</i>	25
4.10.5	<i>Virtual Disk</i>	25
4.11	INITIAL CONDITIONS	27
4.11.1	<i>Segregated Flow</i>	27
4.12	BOUNDARY CONDITIONS	27
4.12.1	<i>Wall</i>	27
4.12.2	<i>Symmetry plane</i>	27
4.12.3	<i>Velocity inlet</i>	28
4.12.4	<i>Pressure outlet</i>	28
4.13	RIGID BODY MOTIONS	28
4.14	SOLVERS AND STOPPING CRITERIA	28
4.15	SCALING OF RESISTANCE	29
4.16	THRUST REDUCTION	30
4.17	WAKE FIELD	30
5	METHOD OF ANALYSIS FOR ROALDNES	31
5.1	3D MODELLING	31
5.2	DOMAIN.....	36
5.3	MESHING	37
5.3.1	<i>Reference values</i>	37
5.3.2	<i>Volumetric control</i>	37
5.4	REGIONS	43
5.5	RESULTING MESH	43
5.6	PHYSICAL MODELS.....	48

5.6.1	<i>Virtual disk</i>	49
5.7	INITIAL CONDITIONS.....	50
5.8	BOUNDARY CONDITIONS.....	50
5.9	RIGID BODY MOTIONS.....	51
5.10	SOLVERS AND STOPPING CRITERIA.....	53
5.11	SETUP OF 4 KNOT SIMULATIONS.....	54
6	RESULTS AND DISCUSSION	55
6.1	CONVERGENCES STUDY.....	55
6.1.1	<i>Mesh</i>	55
6.1.2	<i>Time step</i>	60
6.1.3	<i>Domain</i>	66
6.1.4	<i>Summary of Convergence Study</i>	70
6.2	RESULTS WITH OPTIMAL SIMULATIONS SETUP.....	73
6.2.1	<i>Comparison of Dynamic Pressure</i>	73
6.2.2	<i>Comparison of Vorticity</i>	74
6.2.1	<i>Axial Velocity</i>	78
6.2.2	<i>Wake field</i>	83
6.2.3	<i>Tangential Velocity</i>	86
6.2.4	<i>Dynamic Pressure</i>	86
6.2.5	<i>Streamlines</i>	88
6.2.1	<i>Wave pattern Hull 1</i>	95
6.2.1	<i>Wave Pattern Hull 2</i>	96
6.2.2	<i>Hull Forces at 4 Knots</i>	97
6.2.3	<i>Hull Forces at 10 Knots</i>	99
6.2.1	<i>Thrust Reduction</i>	101
6.2.2	<i>Form Factor</i>	101
6.2.3	<i>Full-Scale Hull Resistance</i>	102
6.3	COMPARISON WITH R/V GUNNERUS.....	103
6.4	UNCERTAINTIES OF RESULTS.....	105
7	CONCLUSION	107
8	FURTHER WORK	111
9	REFERENCE	113
10	APPENDIX	I

List of Figures

FIGURE 2-1 - BOTTOM TRAWLING	3
FIGURE 2-2 - TORBAS. REAR/MID MOUNTED SUPERSTRUCTURE	4
FIGURE 2-3 - GADUS NEPTUN. FRONT MOUNTED SUPERSTRUCTURE	5
FIGURE 2-4 - ILLUSTRATION OF STEERABLE NOZZLE SYSTEM	7
FIGURE 2-5 - STERN SHOWING TWIN SKEG	7
FIGURE 2-6 - CURRENT DESIGN OF TRAWLER ROALDNES	8
FIGURE 3-1 - BULBOUS BOW	9
FIGURE 3-2 - ROALDNES HULL DISPLAYING CHINE FRAMES AND SHARP AFT EDGES, HULL 1	10
FIGURE 3-3 - CHINE ANGLE	10
FIGURE 3-4 - HULL DESIGN WITH ROUNDED AFT SIDES, HULL 2	11
FIGURE 3-5 - RESISTANCE CURVE OF A SHIP WITH AND WITHOUT CHINE	12
FIGURE 3-6 - PERCENTAGE DIFFERENCE IN TOTAL SHIP RESISTANCE BETWEEN A SHIP WITH AND WITHOUT CHINE.....	12
FIGURE 3-7 - DISTRIBUTION OF COMPUTATIONAL VELOCITY COMPONENTS	13
FIGURE 4-1 – DIRECT NUMERICAL SIMULATION, DNS	17
FIGURE 4-2 - LARGE EDDY SIMULATION, LES	17
FIGURE 4-3 - REYNOLDS-AVERAGED NAVIER-STOKES	18
FIGURE 4-4 - Y+ VALUE REGIONS.	20
FIGURE 4-5 - EXAMPLE OF 2D AND 3D DOMAIN	22
FIGURE 4-6 - EXAMPLE OF BEFORE AND AFTER REMESHING	23
FIGURE 5-1 - EXTRA REFINEMENT LAYER BETWEEN TWO VOLUMETRIC CONTROLS.....	31
FIGURE 5-2 - IMPORTED 3D MODEL, HULL 1	33
FIGURE 5-3 - SURFACE ERRORS, HULL 2	33
FIGURE 5-4 REMESHED 3D MODEL, HULL 1	34
FIGURE 5-5 - REMESHED 3D MODEL, HULL 2	34
FIGURE 5-6 - BEFORE AND AFTER REPAIRING DENT IN SKEG, HULL 1	35
FIGURE 5-7 - SURFACE DISTORTION IN KEEL, HULL 1	35
FIGURE 5-8 - START DOMAIN FOR SIMULATIONS.....	36
FIGURE 5-9 - RESULTING MESH, HULL 1 AND HULL 2	44
FIGURE 5-10 - TRANSITION FROM PRISM LAYER TO CORE MESH.....	44
FIGURE 5-11 - TOP VIEW OF MESH	45
FIGURE 5-12 - MESH REFINEMENT ON FREE SURFACE.....	46
FIGURE 5-13 - FRONT VIEW OF MESH.....	46
FIGURE 5-14 - SIDE VIEW OF MESH.....	47
FIGURE 5-15 - MESH OF NOZZLE.....	47

FIGURE 5-16 - SINKAGE AND TRIM FROM 10-KNOT SIMULATION WITH HEAVE AND PITCH ALLOWED	51
FIGURE 5-17 - LAST 35% PERCENTILE OF SIMULATION WITH HEAVE	52
FIGURE 6-1 - TOTAL FORCE, FULL RUNTIME – MESH	56
FIGURE 6-2 - PRESSURE AND SHEAR FORCE, FULL RUNTIME - MESH.....	57
FIGURE 6-3 - LAST 20% PERCENTILE OF RUNTIME - MESH.....	58
FIGURE 6-4 - LAST 20% OF RUNTIME SHEAR AND PRESSURE - MESH	58
FIGURE 6-5 - MEAN FORCE VS NUMBER OF CELLS – MESH	59
FIGURE 6-6 - TOTAL FORCE, FULL RUNTIME - TIME STEP.....	60
FIGURE 6-7 - PRESSURE AND SHEAR FORCE, FULL RUNTIME - TIME STEP	61
FIGURE 6-8 - LAST 20% PERCENTILE OF RUNTIME – TIME STEP	62
FIGURE 6-9 - LAST 20% OF RUNTIME SHEAR AND PRESSURE – TIME STEP	63
FIGURE 6-10 - MEAN FORCE VS LOGARITHMIC TIME STEP.....	64
FIGURE 6-11 - WAVE PATTERN WITH TIME STEP OF 0.01s	65
FIGURE 6-12 - WAVE PATTERN WITH TIME STEP OF 0.8s	65
FIGURE 6-13 – DIFFERENT DOMAIN SIZE.	66
FIGURE 6-14 - TOTAL FORCE, FULL RUNTIME – DOMAIN.....	67
FIGURE 6-15 - PRESSURE AND SHEAR FORCE, FULL RUNTIME – DOMAIN	67
FIGURE 6-16 - LAST 20% PERCENTILE OF RUNTIME - DOMAIN	68
FIGURE 6-17 - LAST 20% OF RUNTIME SHEAR AND PRESSURE - DOMAIN.....	68
FIGURE 6-18 - MEAN FORCE VS DOMAIN SIZE	69
FIGURE 6-19 - CHOSEN DOMAIN.....	70
FIGURE 6-20 - SIMULATION HIERARCHY.....	70
FIGURE 6-21 - WALL Y+ VALUE 10-KNOT MESH SETUP FROM CONVERGENCE STUDY	71
FIGURE 6-22 - WALL Y+ VALUE 10-KNOT NEW MESH SETUP.....	71
FIGURE 6-23 - WALL Y+ VALUE 4 KNOTS WITH MESH SETUP FROM CONVERGENCE STUDY.....	72
FIGURE 6-24 - WALL Y+ VALUE 4 KNOTS WITH FINAL MESH SETUP	72
FIGURE 6-25 – PRESSURE [PA], HULL 1 AT 10 KNOTS WITHOUT NOZZLE AND DISK	73
FIGURE 6-26 – PRESSURE [PA], HULL 2 AT 10 KNOTS WITHOUT NOZZLE AND DISK	73
FIGURE 6-27 - VORTICITY HULL 1 AND 2 AT 10 KNOTS WITH NOZZLE AND DISK, -0.2M.....	74
FIGURE 6-28 - VORTICITY HULL 1 AND 2 AT 10 KNOTS WITH NOZZLE AND DISK, -0.3M.....	75
FIGURE 6-29 - VORTICITY HULL 1 AND 2 AT 10 KNOTS WITH NOZZLE AND DISK, -0.2M.....	75
FIGURE 6-30 - VORTICITY HULL 1 AND 2 AT 10 KNOTS WITH NOZZLE AND DISK, -0.3M.....	76
FIGURE 6-31 - VORTICITY PROPELLER PLANE HULL 1 AT 10 KNOTS WITH NOZZLE AND DISK	77
FIGURE 6-32 - VORTICITY PROPELLER PLANE HULL 2 AT 10 KNOTS WITH NOZZLE AND DISK	77
FIGURE 6-33 - AXIAL VELOCITY HULL 1 AT 4 KNOTS WITHOUT NOZZLE AND DISK.....	79
FIGURE 6-34 - AXIAL VELOCITY HULL 2 AT 4 KNOTS WITHOUT NOZZLE AND DISK.....	79

FIGURE 6-35 - AXIAL VELOCITY HULL 1 AT 4 KNOTS WITH NOZZLE AND DISK	80
FIGURE 6-36 - AXIAL VELOCITY HULL 2 AT 4 KNOTS WITH NOZZLE AND DISK	80
FIGURE 6-37 - AXIAL VELOCITY HULL 1 AT 10 KNOTS WITHOUT NOZZLE AND DISK	81
FIGURE 6-38 - AXIAL VELOCITY HULL 2 AT 10 KNOTS WITHOUT NOZZLE AND DISK	81
FIGURE 6-39 - AXIAL VELOCITY HULL 1 AT 10 KNOTS WITH NOZZLE AND DISK	82
FIGURE 6-40 - AXIAL VELOCITY HULL 2 AT 10 KNOTS WITH NOZZLE AND DISK	82
FIGURE 6-41 - NOMINAL WAKE FIELD HULL 1 AT 4 KNOTS	84
FIGURE 6-42 - NOMINAL WAKE FIELD HULL 2 AT 4 KNOTS	84
FIGURE 6-43 - NOMINAL WAKE FIELD HULL 1 AT 10-KNOTS	85
FIGURE 6-44 - NOMINAL WAKE FIELD HULL 2 AT 10-KNOTS	85
FIGURE 6-45 - TANGENTIAL VELOCITY HULL 2 AT 10 KNOTS	86
FIGURE 6-46 - DYNAMIC PRESSURE [PA] HULL 2 WITHOUT NOZZLE AND DISK AT 10 KNOTS	87
FIGURE 6-47 - DYNAMIC PRESSURE [PA] HULL 2 WITH NOZZLE AND DISK AT 10 KNOTS	87
FIGURE 6-48 - STREAMLINES HULL 1, AT 4 KNOTS WITHOUT AND WITH PROPELLER AND NOZZLE	89
FIGURE 6-49 - STREAMLINES HULL 1, AT 4 KNOTS WITH PROPELLER AND NOZZLE, TOP OF NOZZLE	90
FIGURE 6-50 - STREAMLINES HULL 2, AT 4 KNOTS WITH PROPELLER AND NOZZLE, TOP OF NOZZLE	90
FIGURE 6-51 - STREAMLINES SHOWING PARTICLE PATH ON TOP OF NOZZLE, HULL 1 AT 4 KNOTS	91
FIGURE 6-52 - STREAMLINES SHOWING PARTICLE PATH ON TOP OF NOZZLE, HULL 2 AT 4 KNOTS	91
FIGURE 6-53 - STREAMLINES HULL 1, AT 10 KNOTS WITHOUT AND WITH PROPELLER AND NOZZLE	93
FIGURE 6-54 - STREAMLINES HULL 1 AT HULL SURFACE WITHOUT PROPELLER AND NOZZLE, 10 KNOTS	94
FIGURE 6-55 - STREAMLINES HULL 1 AT HULL SURFACE WITH PROPELLER AND NOZZLE, 10 KNOTS	94
FIGURE 6-56 - WAVE ELEVATION AND PATTERN, HULL 1 AT 10 KNOTS	95
FIGURE 6-57 - WAVE ELEVATION AND PATTERN, HULL 2 AT 10 KNOTS	96
FIGURE 6-58 - TOTAL RUNTIME AT 4 KNOTS	97
FIGURE 6-59 - TOTAL RUNTIME AT 4 KNOTS, DECOMPOSED TO SHEAR AND PRESSURE FORCES	97
FIGURE 6-60 - CONVERGED FORCES AT 4 KNOTS	98
FIGURE 6-61 - CONVERGED SHEAR AND PRESSURE FORCES AT 4 KNOTS	98
FIGURE 6-62 - TOTAL RUNTIME AT 10 KNOTS	99
FIGURE 6-63 - TOTAL RUNTIME AT 10 KNOTS, DECOMPOSED TO SHEAR AND PRESSURE FORCES	99
FIGURE 6-64 - CONVERGED FORCES AT 10 KNOTS	100
FIGURE 6-65 - CONVERGED SHEAR AND PRESSURE FORCES AT 4 KNOTS	100
FIGURE 6-66 - HULL RESISTANCE WITH VIRTUAL DISK AND WITHOUT NOZZLE	101
FIGURE 6-67 - COMPARISON CFM AT $F_n = .02776$	103
FIGURE 6-68 - COMPARISON CTM AT $F_n = .02776$	104
FIGURE 6-69 - COMPARISON OF CR AT $F_n = .02776$	104
FIGURE 6-70 - COMPARISON OF CTS AT $F_n = .02776$	104

List of Tables

TABLE 1 - TABLE OF DIMENSIONS ROALDNES.....	32
TABLE 2 - ERRORS IN THE 3D MODEL, HULL 1.....	32
TABLE 3 - ERRORS IN THE 3D MODEL, HULL 2.....	33
TABLE 4 - OPEN WATER DATA FOR PROPELLER	49
TABLE 5 - VOF DAMPING BOUNDARIES, ROALDNES	50
TABLE 6 - BASE VALUE AND NUMBER OF CELLS	55
TABLE 7 - DIFFERENCE BETWEEN MESH SIMULATIONS.....	59
TABLE 8 - DIFFERENCE BETWEEN TIME STEPS.....	64
TABLE 9 - NUMBER OF CELLS IN EACH DOMAIN SIZE.....	66
TABLE 10 - DIFFERENCE BETWEEN DOMAIN SIZES.....	69
TABLE 11 – THRUST DEDUCTION FACTOR.....	101
TABLE 12 - FORM FACTORS	101
TABLE 13 - SCALED RESULTS	102

List of Abbreviations

CFD	Computational Fluid Dynamics
Loa	Length Over All
Lwl	Length in Water Line
RSW	Refrigerated Sea Water
RPM	Revolutions Per Minute
LNG	Liquid Natural Gas
CAD	Computer-Aided Design
RANS	Reynolds-Averaged Navier-Stokes
VOF	Volume Of Fluid
DOF	Degrees Of Freedom
DFBI	Dynamic Fluid Body Interaction
CFL	Courant-Friedrichs-Lewy number/ Courant number
HRIC	High-Resolution Interface Capturing

Nomenclature

F_n	Froude Number
ρ	Density of fluid
ν	Kinematic viscosity of fluid
V	Velocity
y^+	Dimensionless distance from the wall
τ_ω	Wall shear stress
u_τ	Friction velocity
f_{bx}	Rotationally averaged volume force
$f_{b\theta}$	Radially component of volume force
T	Thrust
Q	Torque
K_T	Thrust coefficient
K_Q	Moment coefficient
J	Advanced ration number
n	Propeller revolution
D	Propeller diameter
R_{TM}	Model scale hull resistance
C_{TM}	Model scale total resistance coefficient

C_{RM}	Residual resistance coefficient
k	Form factor
C_{FM}	Friction resistance coefficient
C_R	Residual resistance coefficient
C_{TS}	Full scale total resistance coefficient
ΔC_F	Roughness coefficient
R_{TS}	Full scale hull resistance
S	Wetted surface
R	Reynolds number
t	Thrust deduction factor
F_S	External tow force
T_M	Model propeller thrust
$R_{W,prop}$	Model resistance with acting propeller
R_0	Model resistance without acting propeller
V_A	Velocity seen by the propeller
V_S	Ship velocity
w	Wake fraction
λ	Scaling factor
Base	Reference value for all mesh controls

M

Mass

I

Moment of inertia

1 Introduction

1.1 Background

The ship-owner Roaldnes AS has through The Research Council of Norway's MAROFF-program received a grant to develop a new type of trawler that will ensure sustainable development of the future fishing vessel. This innovation project intends to investigate the possibility of reducing emissions of trawlers. One important way of achieving this goal is to increase the efficiency during trawling. The ship design company Seacon as was chosen to develop the hull for this ship, and has designed a preliminary hull. To validate the performance of this hull, a model test is planned to be performed at Stadt Towing Tank.

1.2 Objectives

This combined Master's and project thesis will verify the hydrodynamic performance on the preliminary design and propose improvements on it. An alternative hull design will be presented based upon findings from project thesis (Svoren, 2014), and compared to the initial design by use of CFD. An introduction to the current design, and how it stands out from typical trawler, with focus on hydrodynamic aspects will be covered. Potential hydrodynamic-related challenges along with suggested solutions will be discussed. Priority in this report is however to be put on calm water performance in transit and trawling, with special emphasis on inflow conditions for the propellers. A convergence study and basic validation of results will also be covered. This Master's thesis aims to lay the foundation for the creation of model to be tested in the towing tank. The main goal is to check whether the proposed hull design is an improvement compared to the current design, and quantify the difference in full scale hull resistance.

1.3 Structure of Report

This thesis work is divided into four different parts; background information and challenges, theoretical foundation, method, and results and discussion. Chapter 2 and 3 gives an overview over typical trawler designs, and how this design stands out. Chapter 4 describes the theory behind CFD and scaling of resistance. Chapter 5 explains the method of simulations and describes the setup used in this thesis. Chapter 6 covers results on both convergence study and final simulations, as well as discussion of results. Finally, conclusions of results and recommendations is covered in Chapter 7.

2 Design of a Trawler

2.1 Definition of a trawler

A trawler is a fishing vessel designed to tow a mesh bag, called trawl, behind itself to catch fish. These ships range in size depending on the area of operation, and size of trawl used. They can vary from small 5meter open boats, powered by outboard engines, up to a 150-meter large freezer and factory trawlers used on the open seas. The equipment and construction of trawlers strongly depend on the fishing method, and the species of fish aimed at. The two most important types of trawlers are derrick-cutter and stern trawler (Dokkum, 2007). The size and design of the trawl are governed by the species to be caught, and can vary in size from 200m² opening up to over 20.000m² (R. Haugen, personal communication, October 10, 2014). In earlier years, ideas about the behavior of the trawls in action were only hypothetical. In the past decades, direct and indirect observations have made it possible to understand the action and behavior of the net in relation to the vessel. As a result of this, different designs have evolved to reduce drag, improve water filtration, and reduce swirls in front of the net that would otherwise repel the entering fish (Traung, 1960).

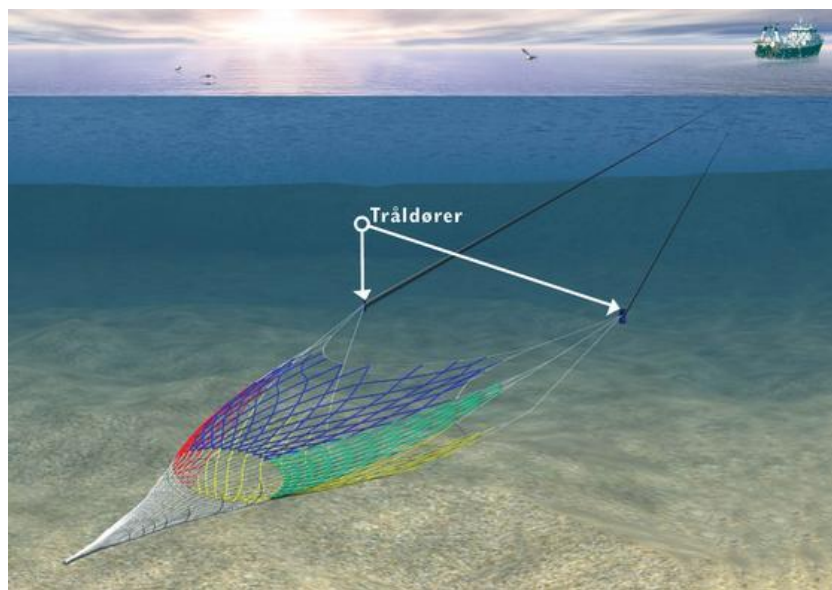


Figure 2-1 - Bottom trawling, (Havforskningsinstituttet, 2011)

There are two main types of stern trawlers; bottom trawls and pelagic/mid-water trawls. The trawler discussed in this report is a relatively small trawler with 35m Loa, designed to trawl at shallow waters on the coast outside of Ålesund. It is a stern trawler, intended to tow the trawl at a speed of 4 knots. Its primary purpose is bottom trawling, which increases the needed thrust, due to increased drag forces towards the seabed.

Trawlers can be compared to a tugboat, as it pulls the trawl at low speed with enormous power demands, especially at the end of a pull when the net is full. For this reason, the propellers are fitted with kort-nozzle to increase the propeller performance by up to 20%, and the bollard pull accordingly (Steen, 2007). These ships had diesel engines similar in power to tugboats, but designed with a longer lwl as they need space for cargo (Dokkum, 2007). The fish may either be stored in frozen blocks of 25kg each, or in refrigerated sea water tanks (RSW tank).

According to Statistics Norway, a total of 74 trawlers with a combined gross tonnage of 77590 m³ was registered in NOR(Norsk ordinært skipsregister) in 2013, making it an important part of Norwegian fishing industry (SSB, 2015).

“Trawling is the most important and one of the most efficient fishing methods used today.”(Ellingsen & Endal, 2007)

2.2 Typical trawler

2.2.1 Design

There are three main types of trawlers when it comes to deck arrangement; side trawler, stern trawler, and outrigger trawler. The design will vary from one ship to another, but the main equipment they all share is a trawl winch for handling and storage of the trawl, gilson winches, net drums, and other auxiliary equipment to handle gear and catch. Placement of the superstructure can also vary for mid/rear mounted, to front mounted superstructure, as seen in Figure 2-2 and Figure 2-3. These are two new trawlers from 2013/2014, both approx. 70m long designed respectively by Seacon and Vard.



Figure 2-2 - Torbas. Rear/mid mounted superstructure (Seacon, 2014)



Figure 2-3 - Gadus Neptun. Front mounted superstructure (Havfisk, 2014)

2.2.2 Hydrodynamics

Desired hydro dynamical properties on a trawler are different than for other fishing vessels. Purse seine and longline ships often need to move quickly from one region to another, or even from the North Sea to the Antarctic Sea. This requires high speed and low operating cost at that speed. Trawlers, on the other hand, have different requirements. They operate at low speeds with high bollard pull (towing power) majority of the operational time. For this reason, trawlers can be compared to tugboat more than other fishing vessels.

Trawlers have low requirements regarding maximum speed, however since they operate at “high power - low speed” majority of the time, there is a large profit in increasing efficiency. To overcome this challenge, trawlers often install large ducted propellers. Having a nozzle surrounding the propeller may increase efficiency on ships with a plump stern by up to 30- 40% (Steen, 2007). Another challenge when designing these ships is to get enough water onto the propeller, and with as much of a uniform flow field as possible. This is where stern design, and design of the skeg, plays a significant role. Results regarding flow field in the propeller plane on this ship will be discussed later on in this report.

Stability is also of concern on trawlers and other fishing vessels. They are equipped with heavy cranes rising high above the deck, and the trawl itself is attached to the trawl winch, which is above center of gravity. Stability is however not to be covered in this project, but an important point to mention.

2.3 Current design

The trawler in this report stands out in several ways. The ship owner Roaldnes is ambitious, and hopes to help evolve the design of the future fishing fleet. Some of the biggest differences between this vessel and other conventional trawlers, are the machinery, its fuel system, and the propulsion system. The machinery is planned to consist of a direct mechanical drive - dual fuel system, running on LNG as main fuel with a 10% diesel injection to control the RPM and ensure for an easier start up. The LNG tank is planned as a DNVGL type C tank and will be fitted beneath the accommodation area, which is in compliance with the new class rule published by DNVGL (2014).

There are several reasons why Roaldnes decided on this dual-fuel LNG system. NHO, "Næringslivets Hovedorganisasjon" gathered in 2008 15 commercial organisations and created an NOx fund (NHO, 2008). Organizations producing NOx pays a fee to this fund, depending on the amount of NOx emissions. LNG is a fuel low on NOx emission compared to marine diesel oil. Not only will Roaldnes help save the environment by using LNG as fuel, they will also save money due to building costs of an LNG system qualifies for subsidies from the NOx fund. Running on LNG also has its limitations when it comes to bunkering, due to the preliminary low availability in ports. This ship will primarily operate on the coast of Ålesund, bunkering and amount of fuel needed will therefore not be an issue.

A second fuel system is also of interest. This consists of a diesel engine system with a battery package to cover peak energy demands during trawl operation.

The propulsion system on this ship will be composed of two mechanical direct drive propellers, with a steerable nozzle system (mounted propellers with steerable nozzles, Figure 2-4). Finnøy Gear and Propeller AS has been chosen to design the propeller nozzle system. The size of propellers are set to a diameter of 3.8m. This ship will trawl for about 75% of its operational time, as mentioned above it is therefore important to have great towing power/high thrust. Two sets of propellers with nozzles, along with big propeller diameter, will aid to fulfill this need. This ship will trawl in shallow waters with the presence of subsea mountains where strong manoeuvrability is required. To further improve the maneuvering of the nozzle system, mounted rudders may be fitted at the aft of the nozzles.

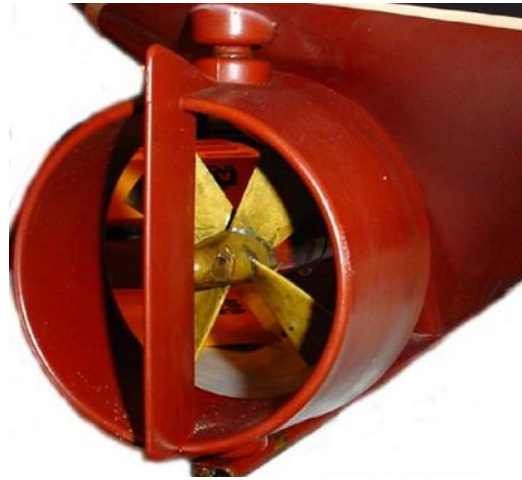


Figure 2-4 - Illustration of steerable nozzle system (Maritime, 2008)

This trawler will also be designed with twin skegs as seen in Figure 2-5, which is unusual for ship of this size. This will be discussed and explained further in section 3.1.3.

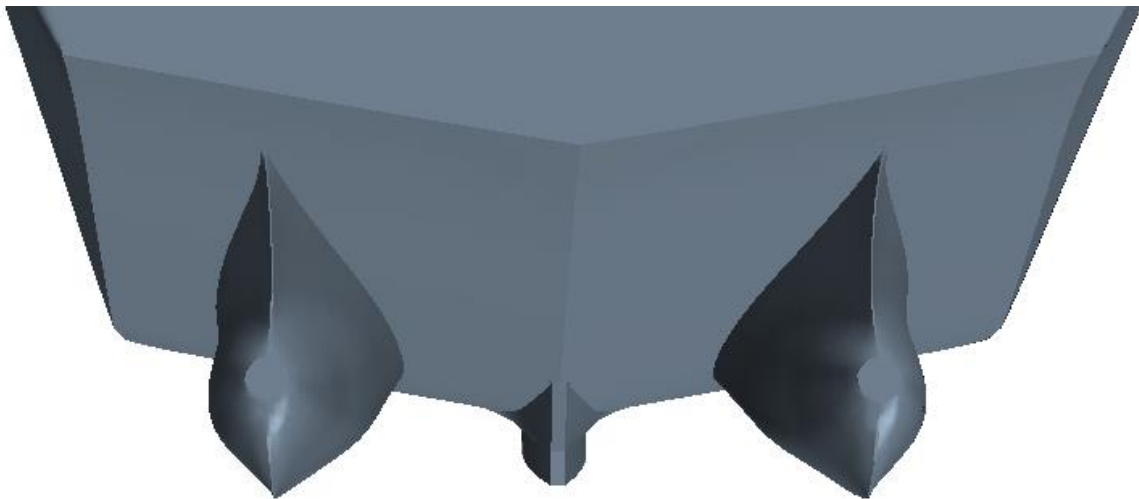


Figure 2-5 - Stern showing twin skeg

The superstructure of this ship is front mounted. Ship-motions are smallest at flotation center of the ship which makes for a better work environment mid ship.

Figure 2-6 presents the current design of Roaldnes.

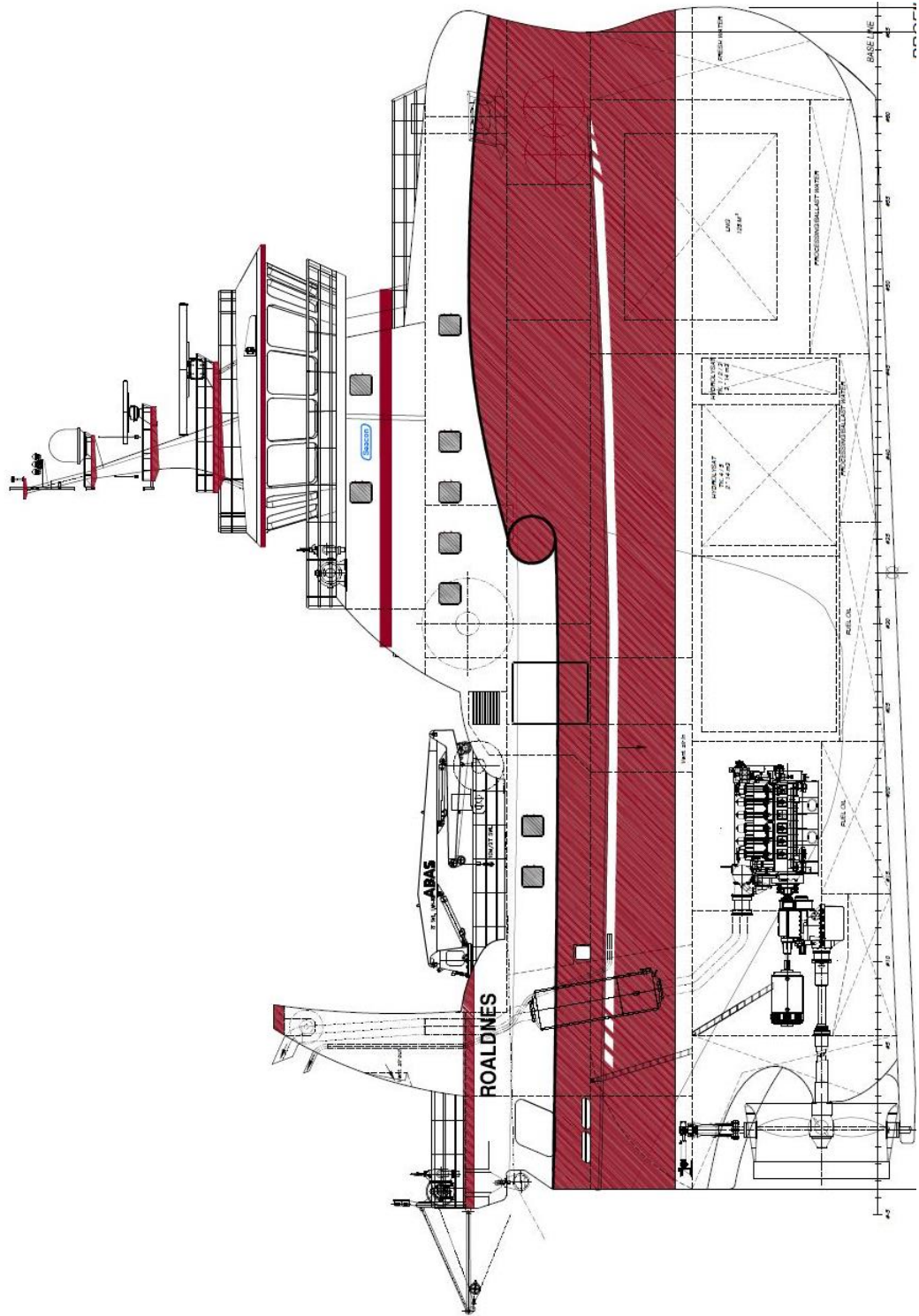


Figure 2-6 - Current design of trawler *Roaldnes* (Retrieved from *Seacon as*)

3 Hydrodynamics

3.1 Hydrodynamic challenges

There are several interesting hydrodynamic challenges regarding this design. The main focus areas are the design of the bow and stern of the ship. This will be covered in this section.

3.1.1 Bulbous bow

The first thing to point out is the bow design. This ship will operate at a trawling speed of 4 knots about 75% of its operational time, the rest steaming back and forth and between different sites. The classic antiphase bulbous bow works best at a design speed, when the bulb creates waves with destructive frequency to the ships shoulder waves. At low speeds, little or no waves are created, and the ship is left only with prolonged waterline length and increased wetted surface, and therefore left only with increased drag. When designing the bow for a trawler like this, compromises are inevitable. This ship is of short length, and have a large displacement compared to its size. To keep the displacement, while maintaining good speed, volume is “taken” from the ship’s shoulder and moved forward into the bulb. This might increase drag at lower speeds, but makes for a slimmer shoulder, which may lead to lower wave resistance at high speeds. This bulb adds to the waterline length, which is beneficial at higher speeds, and is also narrow to give a smaller entrance angle, seen in Figure 3-1. It also increases the waterline length, and therefore slightly increases the longitudinal stability of the ship.

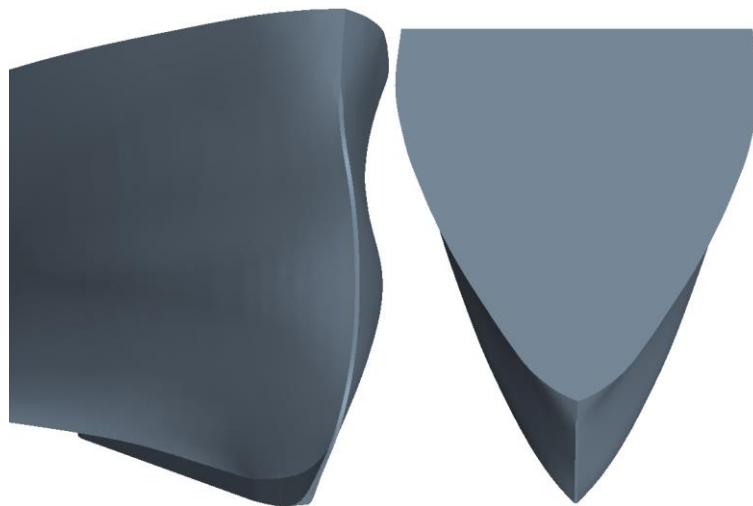


Figure 3-1 - Bulbous bow

3.1.2 Stern design

This ship is going to be fitted with two 3.8m diameter propellers, which is relatively large in comparison to the ship size. This increases the risk of sucking air into the nozzle at heavy roll motions, thus reducing trust. For this reason, anti-roll measures should be looked at.

One solution to reduce roll is designing the stern side with chines (as seen in Figure 3-2) and/or bilge keel.

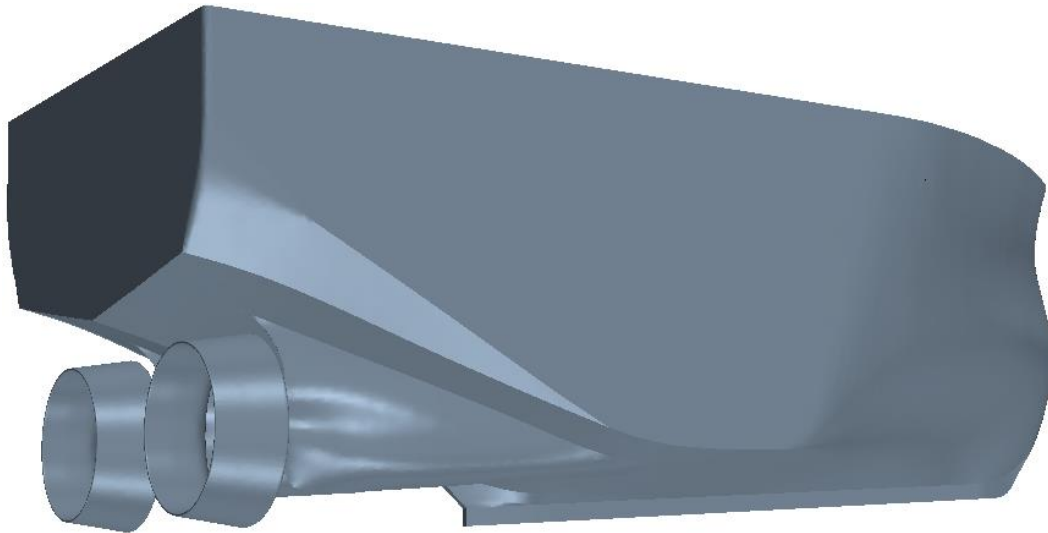


Figure 3-2 - Roaldnes hull displaying chine frames and sharp aft edges, hull 1

The principle behind these anti-roll measurements is to create vortex sheddings in roll. This will consume kinetic energy and, therefore, reduce roll motion. However, the drawback of these solutions are the possibility of increased resistance in straight-ahead cruising. This is a consequence of increased drag and vortex sheddings. Numerical or experimental data is needed to conclude.

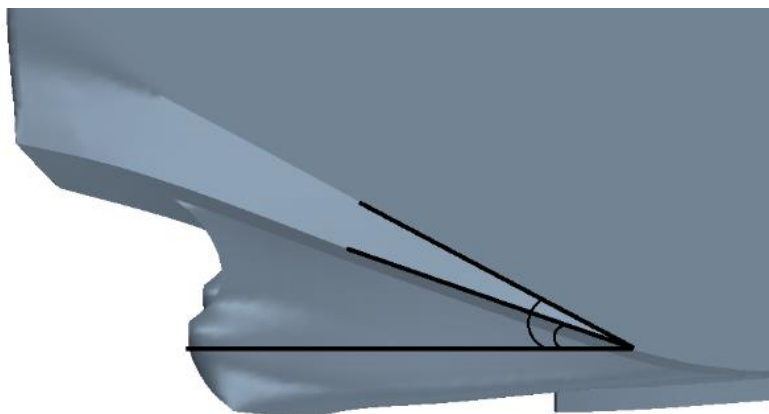


Figure 3-3 - Chine angle

Seacon does not normally use bilge keels in their designs. R. S. Nybakk (personal communication, October 10, 2014) states that fishing vessels operate in many different loading conditions and trim, which makes it near impossible to design a bilge keel optimal enough for all these conditions. This model, however, is considered designed with chines. This creates two sharp edges that leads from the stern all the way mid-ship. These sharp edges as seen in Figure 3-3, have a quite steep angle of up to approx. 30° . Marintek use a “rule of thumb” with a maximum angle of 19° on their design, as well as for their guidance (E. Jullumstrø, personal communication, November 14 2014). This may have an impact on the wake field into the propeller. Results from project thesis (Svoren (2014)) indicates that designing this sharp edge at the stern may cause low pressure and separation at propeller area, and may have little effect in roll. For this reason, a second model was designed with rounded aft sides (Figure 3-4). These models will from now on be referred to as Hull 1 and Hull 2.

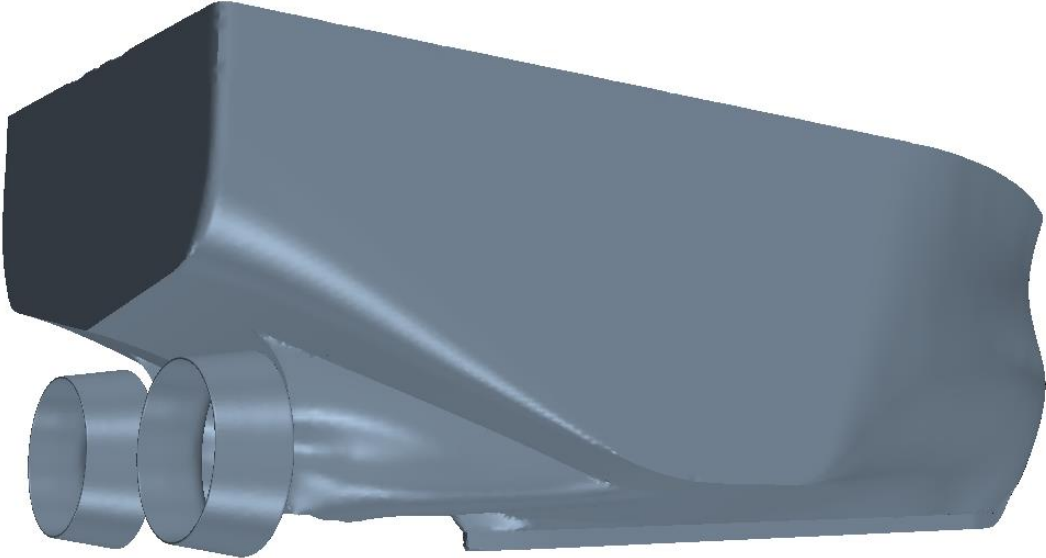


Figure 3-4 - Hull design with rounded aft sides, Hull 2

Figure 3-5 and Figure 3-6 are gathered from a towing test performed by Marintek in 1988 (Marintek, 1988). It displays the full-scale results of a 27meter long fishing vessel, tested on one model with chine at 13° angle, and one without chine. The model had a scale factor of $\lambda = 10.68$.

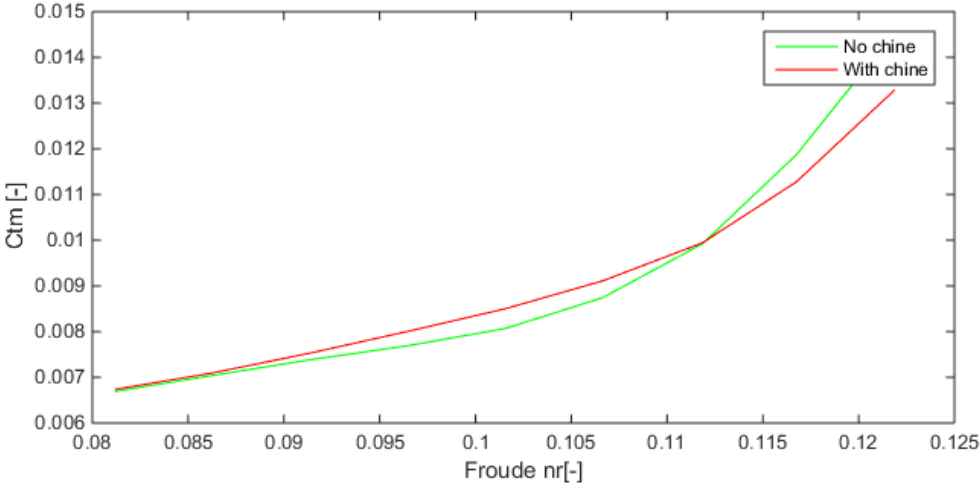


Figure 3-5 - Resistance curve of a ship with and without chine

As seen in Figure 3-5, the model with chines has a greater resistance than the model without chines have at lower Fn. Figure 3-6 shows the percentage difference between the two models. Rounded stern seems to be the solution, with lowest resistance up until about $Fn = 0.11$. Why the model with chines has a lower resistance at high speeds is hard to say, and has not been concluded by Marintek (E. Jullumstrø, personal communication, November 14 2014). This experiment shows that chines increases the total resistance coefficient by up to 5% in straightforward cruising, and should therefore be investigated on the current ship model.

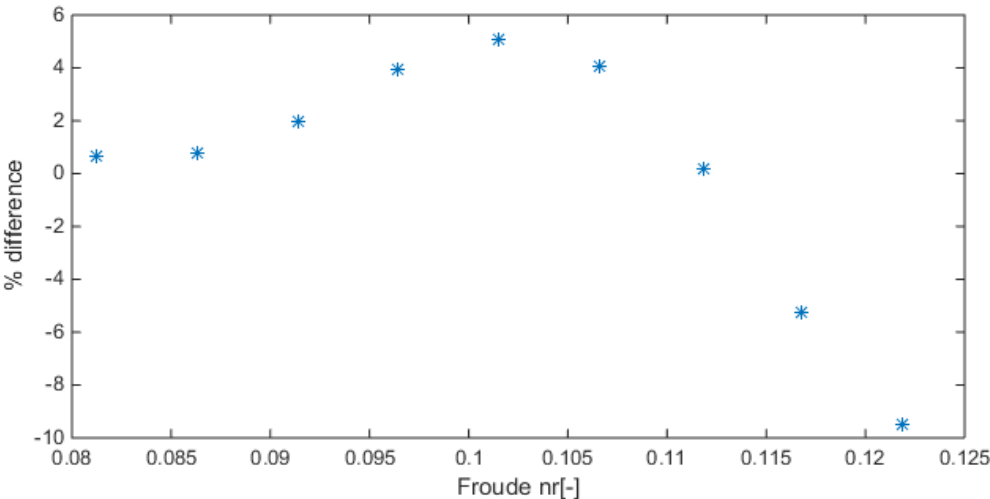


Figure 3-6 - Percentage difference in total ship resistance between a ship with and without chine.

3.1.3 Twin skeg and wake field

This ship is designed with twin-skeg that leads to a more complicated design. Some of the important hydrodynamic points in need to investigate here are the high axial velocities in the skeg tunnel, the flow lines along the skeg, and the balance between inner and outer flow intensity. Park and Chun (2009) performed a CFD analysis on a twin-skeg ship. The main focus was to alter the distance between skegs, skeg angle, and skeg shape to observe the effect on the total resistance. The article shows a 0.5% improvement in effective horsepower between the optimized hull and the mother hull from the skeg shape alone. The wake in the propeller plane was also more evenly distributed. As seen in Figure 3-7, a higher axial flow distribution, in addition to a more evenly velocity distribution in the top part of the propeller plane, is achieved. Furthermore, the wake fraction was reduced by 6%, but the thrust deduction fraction reduced by 17.4%, which indicates that the modified hull was effective in self-propulsion. As a result of this, the advance ratio of the propeller increased, and a total of 2% increase in quasi-propulsive efficiency was achieved. This led to a total of 2.5% increase in efficiency, and 0.15 knots was gained on the optimized hull compared to the mother hull (Park & Chun, 2009). Adding uncertainties on top of this, 2.5% may not be that big of a difference, but nevertheless it is a difference.

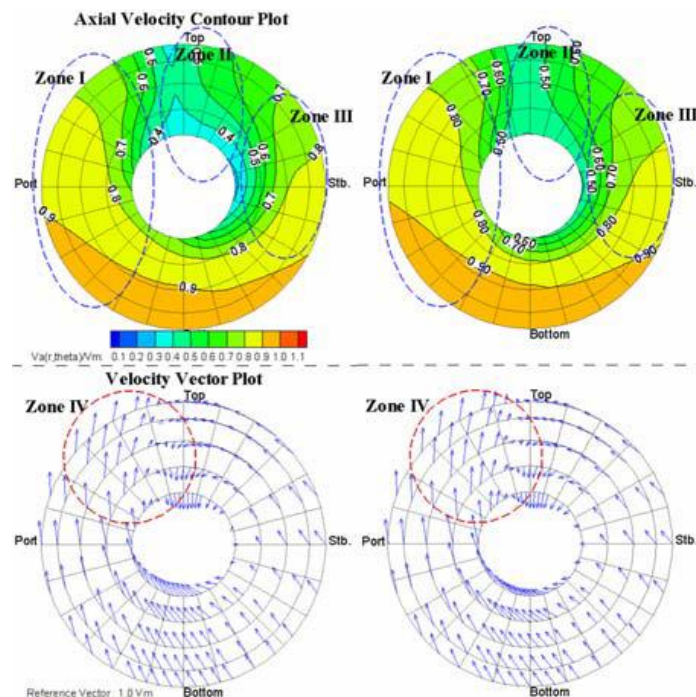


Figure 3-7 - Distribution of computational velocity components in the propeller plane (left mother ship, right optimized ship) (Park & Chun, 2009)

The velocity and pressure field at the stern and propeller area depends on the inlet of water flow. As mentioned, skeg design plays a part in the flow field. By adding a skeg, one may increase the risk of added resistance in favor of obtaining a higher pressure field at the top of the propeller plane, thus reducing the risk of cavitation (R. S. Nybakk, personal communication, October 10, 2014). This is highly important on trawlers under operation, since high trust is crucial during trawling.

4 Theoretical Foundation

4.1 CFD Background

Computational Fluid Dynamics, or CFD, is the science of using mathematics and computer power to solve Navier-Stokes equations to simulate and describe fluid behavior and fluid flow. This method was introduced in the 80's as a powerful engineering and design tool, adopted early by the automotive and aerospace industry. The introduction of CFD in the design of conventional merchant vessels has been disappointingly slow. This part of the naval industry relied in a long history of evolutionary design developed over centuries, during which scientific methods were not available. Younger industries such as the aviation industry had no historical data to rely on, and were therefore forced to adapt to new technological approaches (Dejhalla & Prpi, 2006). The availability of robust commercial CFD software and high-speed computing has led to an increased usage of CFD in several industries, as well as the marine sector.

CFD is applied in marine industry to assess problems related to hydrodynamics. The main concerns here are to compute the global pressure and fluid velocity components in a three-dimensional space surrounding the structure of interest. From this, it is possible to calculate forces acting on the structure. For ship resistance, the forces are divided into shear forces (viscous forces) along the hull, and pressure forces (mostly separation, vortices and boundary layer effects) induced by the presence of a hull. The CFD codes used today are commonly written to solve general cases of compressible, viscous, turbulent flows with heat transfer. These can be used in marine hydrodynamical problems as long as the correct choices are made regarding the equations of state, fluid properties, and boundary equations. What differentiates marine CFD from the other industries, is the presence of a free surface between two different fluids, which represents a considerable challenge (Dejhalla & Prpi, 2006). It is therefore crucial for the marine engineer to understand the physics of the problem, the limitation of the equations used, and how to incorporate this to obtain the most accurate result. In marine hydrodynamics, CFD is used to examine flows that are steady or unsteady, incompressible, laminar or turbulent, and with or without free surface.

For ship design, unless a new design is close to an experimental series or a known ship, towing tests are still used. Use of CFD allows the designer to analyse several different designs in an early stage, and preselect the best design to be tested experimentally, which may help save time and money.

4.2 Governing equations

Computational Fluid Dynamics is based on three governing equations; Continuity equation, Navier-Stokes equation, and Energy equation. The continuity equation (4-1) is a mass conservation equation, while equation 4-2 is a transportation equation that represents transport of linear momentum throughout the domain (Cengel & Cimbala, 2010).

$$\vec{\nabla} \cdot \vec{V} = \frac{\partial u}{\partial x} + \frac{\partial v}{\partial y} + \frac{\partial w}{\partial z} = 0 \quad 4-1$$

$$(\vec{\nabla} \cdot \vec{\nabla})\vec{V} = -\frac{1}{\rho}\vec{\nabla}P' + \nu\vec{\nabla} \quad 4-2$$

ρ is the density of the fluid, ν is the kinematic viscosity and P' is the modified pressure. The energy conservation equation for an isotropic fluid flow is shown by (Fitzpatrick (2014)) to take the following general form:

$$\frac{D\varepsilon}{Dt} = -\frac{p}{\rho}\nabla \cdot \mathbf{v} + \frac{x}{\rho} + \frac{\nabla(\kappa\nabla T)}{\rho} \quad 4-3$$

According to equation 4-3; for a co-moving fluid element, the internal energy per unit mass evolves in time. This is a consequence of work done on the element by pressure, as its volume changes, viscous heat generation due to shear forces, as well as heat conduction. However, for a turbulent simulation with fine enough grids to resolve the three-dimensional turbulent eddies, a CFD solution can approach the exact solution without energy conservation equation (Cengel & Cimbala, 2010). This solution method is however usually not possible for practical engineering, due to computer limitations. Turbulent models are therefore implemented to generate additional transport equations that model the enhanced mixing and diffusion of turbulence. These are then solved together with equations for mass and momentum (4-1 and 4-2).

4.3 Turbulence modelling

CFD simulations of turbulent flow are more difficult than those of laminar flow. The reason for this, is that the finer features of the turbulent flow field are always unsteady, and three-dimensional random, swirling vertical structures called turbulent eddies arise in the turbulent flow shown in Figure 4-1. Some CFD codes use a technique called

Direct Numerical Simulation (DNS), where an attempt to resolve the unsteady motion of these eddies are made. DNS calculations get harder as Reynolds number increases. These calculations demand extreme fine grids, large computers, and an enormous amount of CPU time. DNS is therefore not feasible for high Reynolds number.



Figure 4-1 – Direct Numerical Simulation, DNS (Cengel & Cimbala, 2010)

Next step down is a method called Large Eddy Simulation (LES). In this method, large unsteady features of the turbulent eddies are resolved while the smaller eddies are modeled (Figure 4-2). Due to this, LES requires significantly less CPU time than DNS. Despite this, the computer requirements for this method are still formidable using today’s technology.

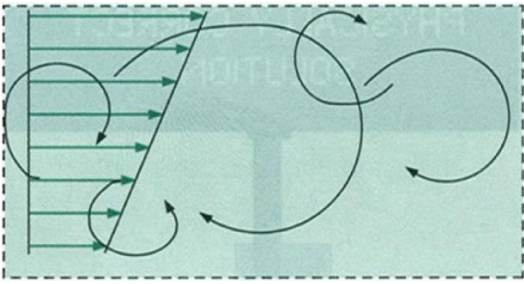


Figure 4-2 - Large Eddy Simulation, LES (Cengel & Cimbala, 2010)

The next step down is the model used in this project called Reynolds-averaged Navier-Stokes (RANS). This technique models all the unsteady turbulent eddies with a turbulence model. No attempt is made to resolve even the largest eddies. Mathematical models are instead used to take into account the mixing and diffusion caused by turbulent eddies. Only the Reynolds-averaged flow properties are calculated, as seen in Figure 4-3.

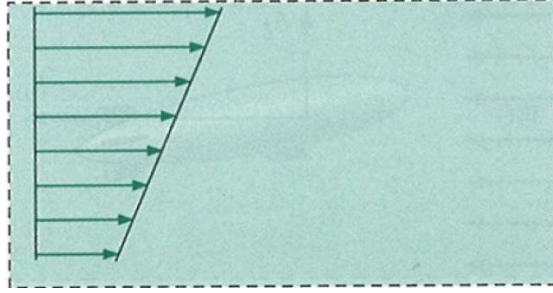


Figure 4-3 - Reynolds-averaged Navier-Stokes, RANS (Cengel & Cimbala, 2010)

The steady Navier-Stokes equation (4-2), is replaced by the RANS equation (4-4).

$$(\vec{V} \cdot \vec{\nabla})\vec{V} = -\frac{1}{\rho}\vec{\nabla}P' + \nu\nabla^2\vec{V} + \vec{\nabla} \cdot (\tau_{ij,turbulent}) \quad 4-4$$

Compared to equation 4-2, there is an additional term on right-hand side of equation 4-4 that accounts for the turbulent fluctuations. This term is known as the Reynold stress tensor, which has the following definition:

$$\tau_{ij} = -\rho\overline{v'v'} = -\rho \begin{bmatrix} \overline{u'u'} & \overline{u'v'} & \overline{u'w'} \\ \overline{u'v'} & \overline{v'v'} & \overline{u'w'} \\ \overline{u'w'} & \overline{u'w'} & \overline{w'w'} \end{bmatrix} \quad 4-5$$

The bar indicates the time average of the product of two fluctuating velocity components. Further information on this can be found in Cengel and Cimbala (2010).

4.4 Courant number

The courant number is a key dimensionless number used in CFD. It is the ratio of the time step Δt to the characteristic convection time, $u/\Delta x$ which is the time required for a particle to be convected a distance Δx (Ferzinger & Peric, 2002).

$$C = \frac{u\Delta t}{\Delta x} \quad 4-6$$

4.5 Law of the wall, y^+ value

The law of the wall explains that the average velocity of a turbulent flow at some point is proportional to the logarithm of the distance from that point to the wall. The y^+ value is the distance from the wall, which is made dimensionless due to friction velocity u_τ , and kinematic viscosity ν . The friction velocity/shear velocity is defined by wall shear stress τ_ω , and the fluid density ρ .

$$y^+ = \frac{y u_\tau}{\nu} \quad 4-7$$

$$u_\tau = \sqrt{\frac{\tau_\omega}{\rho}} \quad 4-8$$

It is important to have control over the y^+ value when setting up the simulation. Depending on which wall treatment is used, one should set up the simulation accordingly. STAR CC+ offers three different wall treatment models.

Low y^+ Wall Treatment is consistent with low Reynolds number simulations. Use of this model assumes that the viscous sublayer is fully resolved, and STAR CCM+ is therefore solving the boundary layer (eq.4-9), which means no wall laws are needed. For this model, one should try to keep y^+ values in between 1 to 5.

The High y^+ Wall Treatment is a wall function approach, which uses equilibrium turbulent boundary layer theory (eq.4-10) to derive wall shear stress τ_ω , turbulent production, and turbulent dissipation. For this model it is desired to have y^+ values over 30, which is within the logarithmic region of the boundary layer. Some surface cells may fall beneath 30, especially near and around stagnation and separation points. Nevertheless this is acceptable.

$$u^+ = y^+ \quad 4-9$$

$$u^+ = \frac{1}{k(\text{von Karman's const.} (\approx 0.41))} \ln(y^+) + B(\text{const.} \approx 5.1) \quad 4-10$$

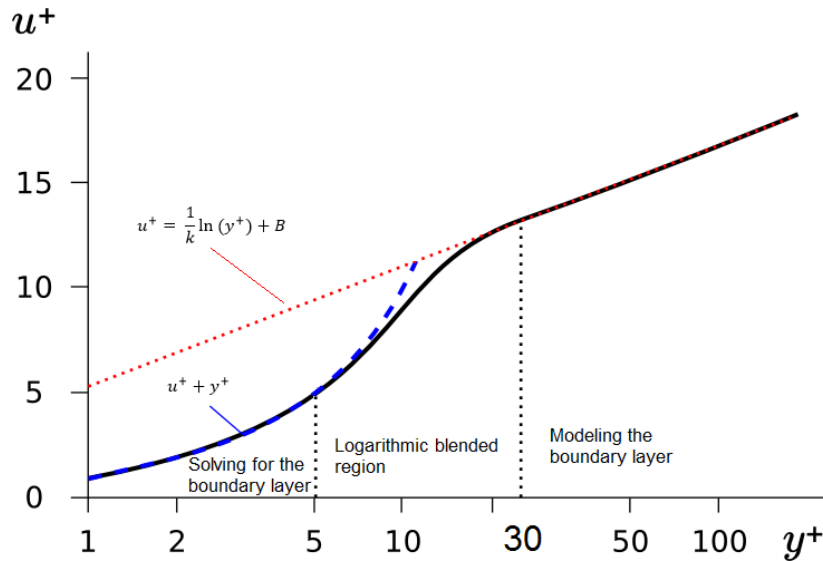


Figure 4-4 - y^+ value regions. Edited from CFD-online (2015) and CD-Adapco (2014)

The last model is a hybrid approach, All y^+ Wall Treatment. This model seeks to behave like the two previous wall treatments both at fine and coarse mesh. Its goal is to give results similar to the low y^+ wall treatment as y^+ approaches 0, and the high y^+ wall treatment as y^+ exceeds 30. It will also give reasonable results at values in between 5 and 30 as well, in case some cells fall in this region.

4.6 STAR CCM+

STAR CCM+ is a CFD-software developed by CD-adapco, designed to handle large models quickly and efficiently. The developers have used object-oriented programming in order to make it easy to use, both for experienced users, as well as for newcomers to CFD (CD-Adapco, 2014). It is also a versatile program capable of handling almost all modeling needs, such as:

- 3D CAD modeler
- CAD embedding
- Surface preparation tools
- Automatic meshing technology
- Physics modelling
- Turbulence modelling
- Post-processing

- CAE integration

For more information regarding these tools see STAR CCM+ user manual. This section is based on theory from CD-adapco online resources (CD-Adapco, 2014).

When solving equation 4-1 and 4-4 numerically using CFD, the following steps are performed. Note that some of the steps may be interchangeable:

- I. Mesh Generation
 1. Create/import the 3D model
 2. Choose a computational domain
 3. Create the volume mesh

- II. Physical and numerical setup
 1. Selecting physical models
 2. Defining initial conditions
 3. Setting boundary conditions
 4. Defining solvers and stopping criteria

- III. Visualization and Data analysis
 1. Set up desired visualisations and reports
 2. Running the simulation
 3. Post processing of results and visualizations
 4. Compare with experimental results, if applicable

4.7 3D modelling

When performing calculations using CFD software, the first step is to create a model. This can be both 2 and 3 dimensional depending on the case at hand. This model may be created in various CAD programs (Inventor, Catia etc.) and then implemented into the CFD software. Some CFD programs also support creation of simple models within the software, as possible in STAR CCM+. After importing the geometry, it is important to check the surface for errors. These errors occur from many different reasons, with typical reasons being; intersecting parts, internal geometry, surface mismatch, gaps between surfaces, and too complex geometry.

4.8 Computational domain

A computational domain is the region in 2D or 3D in which the equations of motion are solved in CFD, seen in Figure 4-5. The boundaries of a 2D domain are called edges, while those of a 3D domain are called faces. Size of the domain is one of the vital conditions' regarding validity of the results. Too small domain can lead to reflections from the walls and therefore pollute the results. On the other hand, too large domain is inefficient in terms of computational time. A key aspect to point out is if there is symmetry in geometry and forces, the model and domain might be cut in half at the symmetry line, and thus save significant amount of CPU resources.

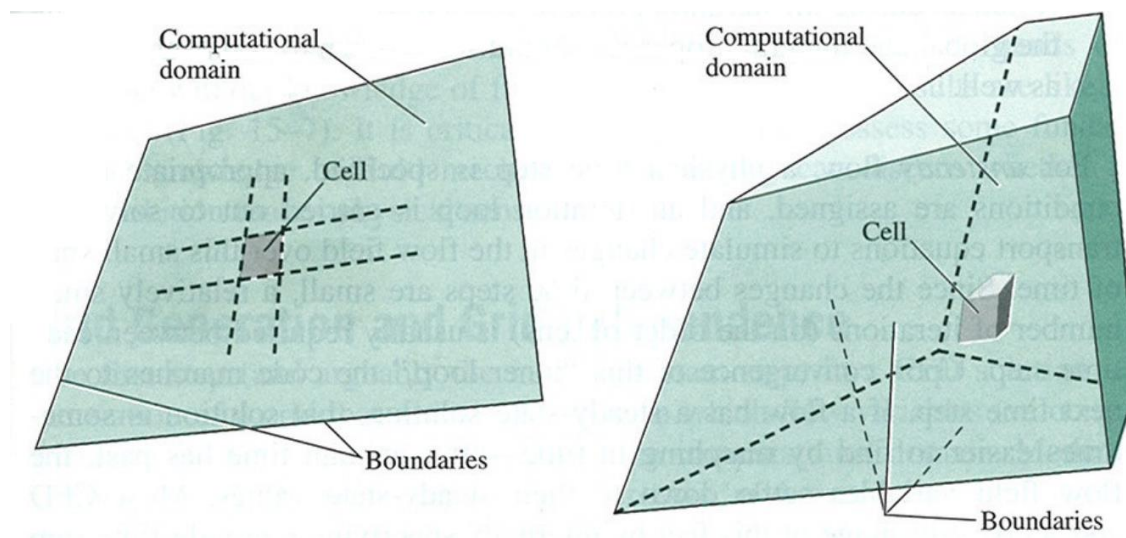


Figure 4-5 - Example of 2D and 3D domain (Cengel & Cimbala, 2010)

4.9 Meshing

A mesh is defined as the discretized representation of the computational domain, which the physics solvers use to provide a numerical solution. STAR-CCM+ provides meshers and tools that can be used to generate a quality mesh for various geometries and applications. This discretization divides the computational domain into many small elements called cells. For 2D domain, these cells are called areas, while for 3D domain they are called volumes. These cells are small control volumes in which discretized versions of Navier-Stokes equations are solved. STAR CCM+ is a cell centred finite volume CFD code, which computes conservation equations from the center of every cell. This may lead to errors called residuals. The quality of the CFD solution is highly dependent on the mesh quality. Therefore it is important to make sure the mesh is good before continuing to the next step. Two important mesh cycles needs to be done on the 3D model.

4.9.1 Surface remesher

In order to improve the overall quality of an imported or existing surface, and optimize it for the volume mesh models, the surface remesher can be used to re-triangulate the surface. Remeshing is mainly based on target edge length, but can also include refinement based on curvature and surface proximity. This mesher is typically used for remeshing surface-mesh, generated by the surface wrapper or imported geometry as for Roaldnes. Not only does this help for the volume mesher, it also aids the subsurface generator when prism layer thickness mesher is selected. Figure 4-6 shows an example of starting surface and remeshed surface.



Figure 4-6 - Example of before and after remeshing (CD-Adapco, 2014)

4.9.2 Volume mesher

There are several different volume meshers available in STAR CCM+; polyhedral mesher, trimmer, prism layer mesher, thin mesher, generalized cylinder, and extruder. This report will focus on the trimmer mesher for more information see STAR CCM+ user guide (CD-Adapco, 2014). The trimmer mesher provides a robust and efficient method for generating high-quality grids, capable of filling large volumes. It uses mainly hexahedral mesh with minimal skewness. This model also allows for local refinement control and uses less computer memory per cell than polyhedral mesh.

4.10 Physical models

Models in CFD are what tries to represent the physics in the numerics. CFD solutions are easy to obtain, and graphical outputs can look promising, but are not guaranteed to be physically meaningful. The validity depends on the correct input and knowledge about the flow field. In STAR CCM+ these model groups exist:

- Space, time and motion
- Materials
- Flow and energy
- Species
- Turbulence and transition
- Radiation
- Aeroacoustics
- Combustion
- Multiphase flow
- Solid stress
- Electromagnetism

(CD-Adapco, 2014)

Specific models used in this project will be covered in section 5.6. However, there are some models that specially apply to naval CFD worth a brief elaboration.

4.10.1 K-epsilon turbulence and realizable K-epsilon two-layer

The κ - ϵ model is a turbulence model used in RANS. It adds two more transport equations which must be solved simultaneously with the mass and momentum equations. This requires two more boundary conditions at inlet and outlet. For the κ - ϵ model, the turbulent kinetic energy κ , and the turbulent dispersion rate ϵ is specified. However in the realizable κ - ϵ model, a new transport equation for ϵ is added. In addition to this, a critical coefficient of the model C_μ is also added, which is expressed as a function of mean flow and turbulence properties, rather than assumed to be constant as in the standard model. The two-layer model is an alternative to a *low-Reynolds number* approach that allows the κ - ϵ model to be applied in viscous sub layers.

4.10.2 Eulerian multiphase

This model allows for several fluids of different viscosity and density to exist within the same boundary. It is necessary to use Eulerian multiphase when using VOF and segregated flow.

4.10.3 Volume of fluid (VOF)

VOF is one of the models that stand out in marine use of CFD. It is a simple multiphase model, suited for simulating flows of several immiscible fluids on numerical grids, capable of resolving the interface between the different phases of the mixture. This

model is suited for simulations of flow, where each phase makes up a large structure but with a small contact area between the phases. The 3D distribution of each phase at a given time is defined in terms of the volume fraction. The volume fraction is defined as the ratio between the volume occupied by the phase, over the total cell volume. This disturbance can be calculated by solving a transport equation for the phase volume fraction. This method uses the segregated flow model, which is also used in this project.

4.10.4 VOF Waves

The VOF wave model is used to simulate surface gravity waves on a light fluid to heavy fluid interface. This model is limited to 3D cases and is used along with the VOF model. The model is typically used for a 6-DOF marine model. This model also activates conditions in regions and boundaries to control damping of the waves near boundaries in order to reduce wave reflections.

4.10.5 Virtual Disk

The virtual disk model creates a momentum source, which intends to model spinning geometry such as propellers, rotors, fans, turbines, etc. as an actuator disk. This is a useful tool to obtain surrounding effects when propeller information is known. The actuator disk influences the flow field by entering the momentum equation (4-2) as a source term, which is distributed over the virtual disk. This disk is modeled as a propeller with an infinite amount of blades, which accelerates the propeller flow without inducing tangential velocities to the flow after the disk. This method also assumes and creates uniform inlet flow, and uniformly distributed added radial velocity behind the propeller (Steen, 2007).

Different models are available depending on the application. STAR CCM+ offers three different models: Body Force Propeller Method, 1D Momentum Method, and Blade Element Method. The blade element method is designed to analyze a complex flow field with asymmetrical loading, an example being helicopter rotors. The 1D momentum Method is based upon one-dimensional momentum theory with wake rotation, and is suitable for wind turbines. The last method, Body Force Method, is used to model the effect of a marine propeller. This method models the propeller – hull interaction. The disk induced flow depends on the flow around the hull. Correspondingly, the hull flow is influenced by the disk. It is used to model thrust and torque to create propulsion without actually resolving the propeller geometry. Use of this model, therefore requires less mesh refinement than the actual propeller geometry,

and will help reduce computational time. This method inflicts a rotationally averaged volume force f_b , distributed over the virtual disk. The radial distribution of the force component $f_{b\theta}$, follows the Goldstein optimum given by the following equations:

$$f_{bx} = A_x r \sqrt{1-r} \quad 4-11$$

$$f_{b\theta} = A_\theta \frac{r \sqrt{1-r}}{r(1-r'_h) + r'_h} \quad 4-12$$

$$r = \frac{r' - r'_h}{1 - r'_h} \quad 4-13$$

$$r'_h = \frac{R_H}{R_p} \text{ and } r' = \frac{r}{R_p} \quad 4-14$$

Here, f_{bx} is the body force in axial direction of the disk, and $f_{b\theta}$ is the body force in tangential direction. The radial coordinate is denoted by r , and R_H is the propeller hub radius, while R_p is the propeller radius. A_θ and A_x are two constants computed as:

$$A_x = \frac{105}{8} \frac{T}{\pi \Delta (3R_H + 4R_p)(R_p - R_H)} \quad 4-15$$

$$A_\theta = \frac{105}{8} \frac{Q}{\pi \Delta R_p (3R_H + 4R_p)(R_p - R_H)} \quad 4-16$$

Where Q is the torque, T is the thrust and Δ are the thickness of the actuator disk (CD-Adapco, 2014). This model uses the following inputs:

- Definition of position of disk and direction of thrust
- Specification of propeller performance curve:

$$K_T = \frac{T}{\rho n^2 D^4}, K_Q = \frac{Q}{\rho n^2 D^5}, J = \frac{V}{nD} \quad 4-17$$

- Specification of an operation point: rotation rate, thrust, or torque
- Specification of inflow velocity plane which defines average velocity and inflow density.

4.11 Initial conditions

Initial conditions in the simulation specify the initial data for the simulation. The converged solution should be independent of the initial conditions. However defining suitable initial conditions may affect the path to the converged solution and especially save computational time. Examples of initial conditions are:

- Pressure
- Velocity components
- Turbulence quantities
- Volume fraction

4.11.1 Segregated Flow

The flow equations are solved by the segregated flow model, one for each component of velocity, and one for pressure is solved in a segregated, or uncoupled manner. The linkage between the momentum and continuity equations is achieved with a predictor-corrector approach. More on this in STAR CCM+ user manual (CD-Adapco, 2014).

4.12 Boundary conditions

Boundaries are surfaces that surround and defines the domain. Every boundary has its own condition. The boundary conditions used in this project are: wall, symmetry plane, velocity inlet, and pressure outlet.

4.12.1 Wall

Wall is the simplest of boundary conditions. As fluids cannot pass through walls, the normal component of velocity is set equal to zero at all boundaries with this condition. Walls can be defined with or without slip.

4.12.2 Symmetry plane

A symmetry plane boundary represents an imaginary plane of symmetry in the simulation. The solution obtained with a symmetry plane boundary is identical to the solution that would be obtained by mirroring about the symmetry plane (half the resulting domain). The shear stress at a symmetry boundary is zero, and the face value of the velocity components and pressure is computed by extrapolating the parallel component of velocity and pressure in the neighbouring cell using *reconstruction gradients*, more on reconstruction gradients in STAR CCM+ user manual (CD-Adapco, 2014).

4.12.3 Velocity inlet

This condition represents the inlet of a duct with known velocity value. The pressure is not specified at velocity inlets, as this would lead to mathematically over-specification. The reason for this is pressure and velocity are coupled in the equation of motion.

4.12.4 Pressure outlet

At pressure outlet fluid flows out of the computational domain, with a specified outlet pressure. Outlet velocity is not specified at pressure outlets for the same reason as discussed in section 4.12.3. All boundaries can be defined with or without VOF Wave damping.

4.13 Rigid body motions

STAR CCM+ has several ways of simulating rigid body motions. For marine CFD simulations, use of Dynamic Fluid Body Interaction (DFBI) is used to simulate the motion of a rigid body in response to pressure and shear forces. STAR-CCM+ calculates the resultant force and moment acting on the body due to all influences and solves the governing equations of rigid body motion to find the new position of the rigid body. This module works in 6 DOF and lets the user decide which rotation and translation to lock or not. Angular velocity, centre of mass, moment of inertia, and velocities are also specified here.

4.14 Solvers and stopping criteria

Solvers control the solution, and are activated once per iteration, or per time step, depending on the type of solver. Physical models use and need solvers. Different models can use the same solvers, and sometimes several solvers. When setting up a simulation, required solvers are usually chosen automatically depending on the physical models selected.

Stopping criteria allow the user to specify for how long the solution runs for, and under what conditions it stops iterating. The main stopping criterions are maximum inner iterations, maximum physical time, maximum steps, and/or using a stop file.

4.15 Scaling of Resistance

Due to difference in Reynolds number on model scale and full scale, dynamic similarity is not satisfied completely. As a result of this, the friction force will be higher in model scale than what it would be in full scale. In brief; to resolve this problem and be able to estimate the full-scale ship resistance, the viscous forces are calculated both in model scale and full scale and the total force is scaled and calculated. This is done by 1: measuring resistance on model, 2: subtract the viscous force component, 3: assume that residual resistance are equal in model- and full-scale, 4: calculate full-scale viscous force coefficient and add to residual force coefficient, and 5: compute full scale resistance from total force coefficient. The theory surrounding scaling of forces will not be covered in this report, and can be viewed in detail in *Motstand og Propulsjon* (Steen, 2007).

In this report transverse stern and air resistance will not be included. Equations used to scale resistance are:

$$\text{Total resistance coefficient:} \quad C_{TM} = \frac{R_{TM}}{0.5 \rho_M V_M^2 S_M} \quad 4-18$$

$$\text{Residual resistance coefficient:} \quad C_{RM} = C_{TM} - (1 + k)C_{FM,ITTC} \quad 4-19$$

The form factor k , is calculated by comparing C_F from CFD calculations and C_F frictional resistance coefficient from ITTC 1957 Model-Ship correlation line:

$$\text{Form factor } k: \quad k = \frac{C_{FM,CFD}}{C_{FM,ITTC}} - 1 \quad 4-20$$

$$\text{ITTC friction resistance coefficient:} \quad C_{FM} = \frac{0.075}{(\log R_{nM} - 2)^2} \quad 4-21$$

$$\text{Residual resistance coefficient:} \quad C_{RM} = C_{RS} = C_R \quad 4-22$$

$$\text{Full scale resistance coefficient:} \quad C_{TS} = C_R + (1 + k)(C_{FS} - \Delta C_F) \quad 4-23$$

$$\text{Roughness Coefficient:} \quad \Delta C_F = [110(HV)^{0.21} - 403]C_F^2, H = 150 \quad 4-24$$

$$\text{Full scale resistance:} \quad R_{TS} = 0.5\rho_S V_S^2 S_S C_{TS} \quad 4-25$$

4.16 Thrust Reduction

Thrust-deduction factor is a term used to describe added resistance of having a propeller operating behind a ship. The propeller creates suction as it operates, and this suction results in higher velocities and, therefore, added friction acting on the hull. This friction adds to the shear forces and should be accounted for when deciding upon needed engine power.

The thrust deduction factor is usually computed from the model resistance, the propeller thrust and external tow force as in equation 4-26. In this master's thesis, a model test with and without propeller is performed. This makes it possible to calculate the thrust reduction directly from the total model forces, as described in equation 4-27. $R_{w prop}$ is resistance from simulation with propeller, and R_0 is resistance without propeller.

$$t = \frac{T_M - (R_{TM} - F_S)}{T_M} \quad 4-26$$

$$t = \frac{R_{w prop} - R_0}{R_{w prop}} \quad 4-27$$

4.17 Wake Field

The flow around the ship aft to where the propeller is located, changes due to friction shape of the hull and the propeller itself. This results in velocities in the propeller plane which is smaller than the ship velocity, which is called wake.

$$w = 1 - \frac{V_A}{V_S} \quad 4-28$$

Where V_S is the ship velocity, and V_A is the velocity "seen" by the propeller. Wake field without the presence of a propeller is called nominal wake, and will be covered in this thesis.

5 Method of analysis for Roaldnes

This chapter will cover the setting up of the simulations for the Roaldnes hull configurations. Method, solvers, models, and so forth are based on recommendations from CD-adapco, as well as special needs for this simulation. Note that all values related to base value are defined by a divisible of 2: 100, 50, 25, 12.5, 6.25 and so forth. If a mesh size between two refinements is larger than a multiple of two, STAR CCM+ will create an extra, and unnecessary layer of refinement. Figure 5-1 display an additional layer of refinement between two volumetric controls where the difference in the percentage of base is larger than twice the value. These simulations also have symmetry in geometry and forces, and only half the model and domain will be analyzed, see section 4.12.2. The final simulations will cover typical trawl speed of 4 knots and steaming speed of 10 knots full scale.

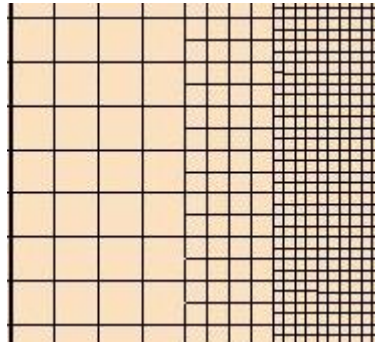


Figure 5-1 - Extra refinement layer between two volumetric controls.

5.1 3D modelling

The 3D model of this hull is received from Seacon as, as a CAD model created in Catia. It was sent to me as a surface mesh format; .igs. The model was then scaled by a factor of $\lambda = 10$. The reason for this was to simulate a model with the same length as the model for the towing test. The equal model length makes comparison easier, since scaling of forces is not needed. Presented below are table of dimensions for the model:

Table 1 - Table of dimensions Roaldnes

	Symbol	Unit	Model
Scale factor	λ	-	10
Length in waterline	L_{WL}	m	3.45
Beam	B	m	1.31
Mean draught	T	m	0.63
Volume displacement	∇	m^3	1219
Block coefficient	C_B	-	0.54
Longitudinal centre of gravity	LCG	m	[1.45 , 0 , 0]
Mass moment of inertia	I_Y	$Kg*m^2$	[-, 930 , -]

After importing the models into STAR CCM+, a surface validity check was performed. Even though the models appeared to look correct, a lot of work had to be done on them. Presented below are tables showing the errors in the original models, as discussed in section 4.7.

Table 2 - Errors in the 3D model, Hull 1

Error	Quantity
Pierced faces	101
Face quality	905
Face proximity	283
Free edges	30

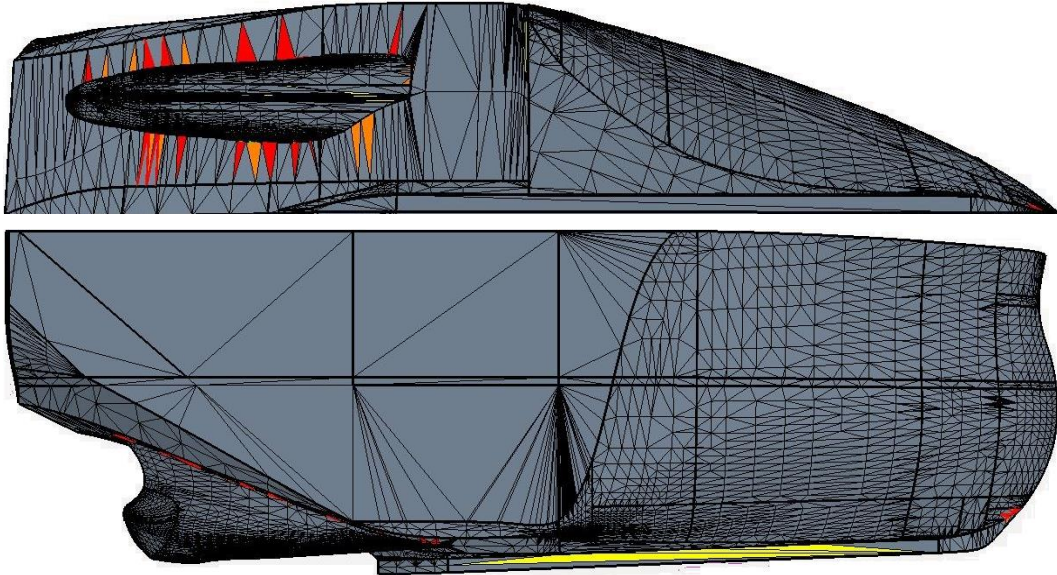


Figure 5-2 - Imported 3D model, Hull 1

Table 3 - Errors in the 3D model, Hull 2

Error	Quantity
Pierced faces	48
Face quality	2486
Face proximity	461
Free edges	0

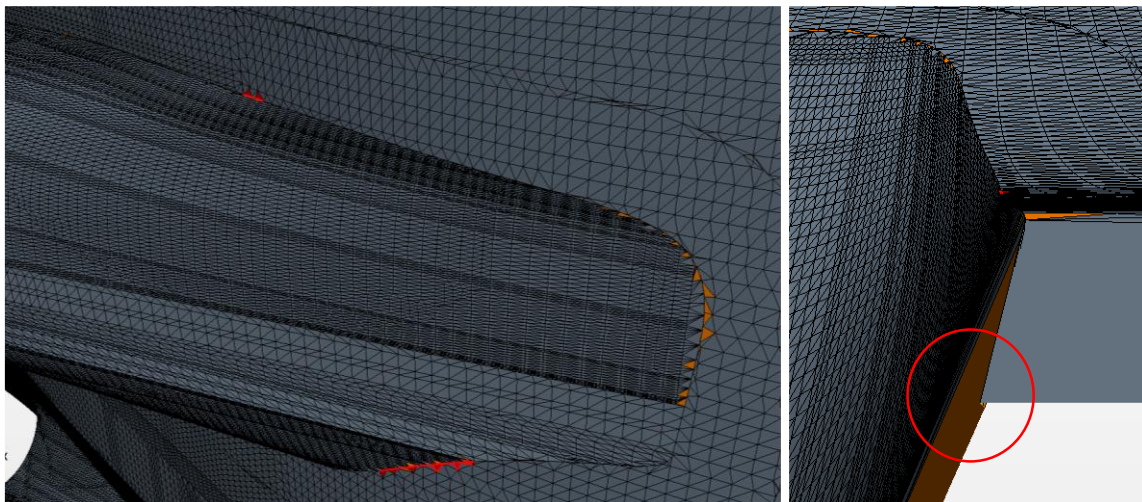


Figure 5-3 - Surface errors, Hull 2

As mentioned in section 4.9.1, STAR CCM+ contains a surface repair tool. The auto repair function is too rough for a complicated geometry like this. In order to ensure that the geometry kept its shape, all areas with surface errors had to be manually remeshed with polyhedral cells. As indicated by the red circle in Figure 5-3, sharp edges contained unneeded cells, which had to be deleted before a functional model was obtained, as seen in Figure 5-4. Note that this is the surface mesh that makes up the 3D model, not the mesh used when solving Navier-Stokes equations.

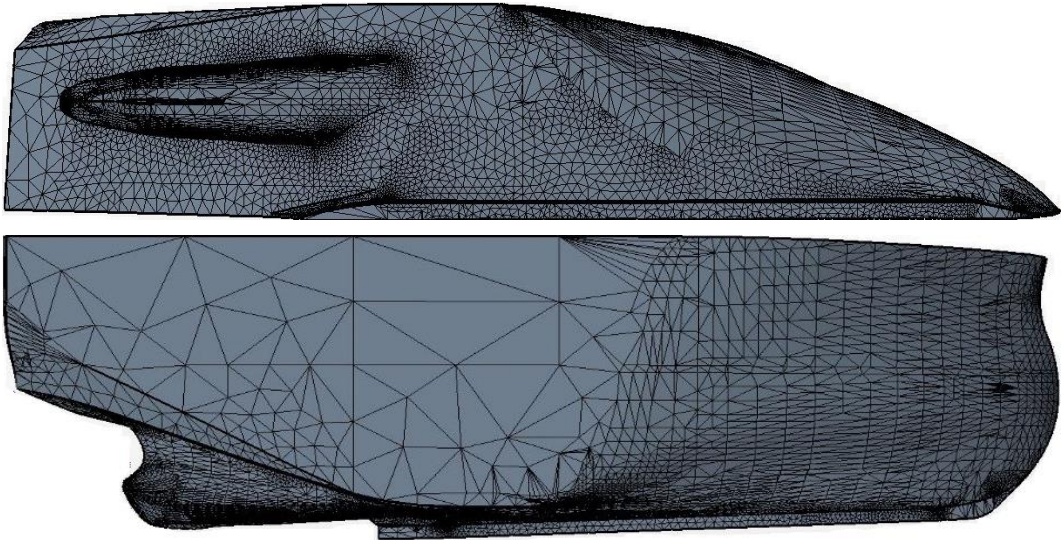


Figure 5-4 Remeshed 3D model, Hull 1

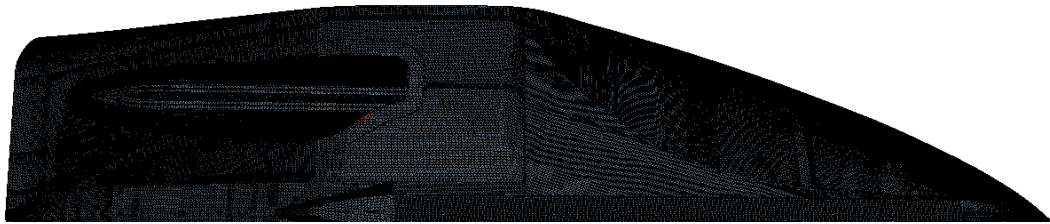


Figure 5-5 - Remeshed 3D model, Hull 2

When importing the model into STAR CCM+, some surfaces changed in shape. As seen in Figure 5-6 a large dent appeared at the port side skeg. Dents and rough surfaces would create drag and vortexes during simulation. These had to be taken care of manually within STAR CCM+.

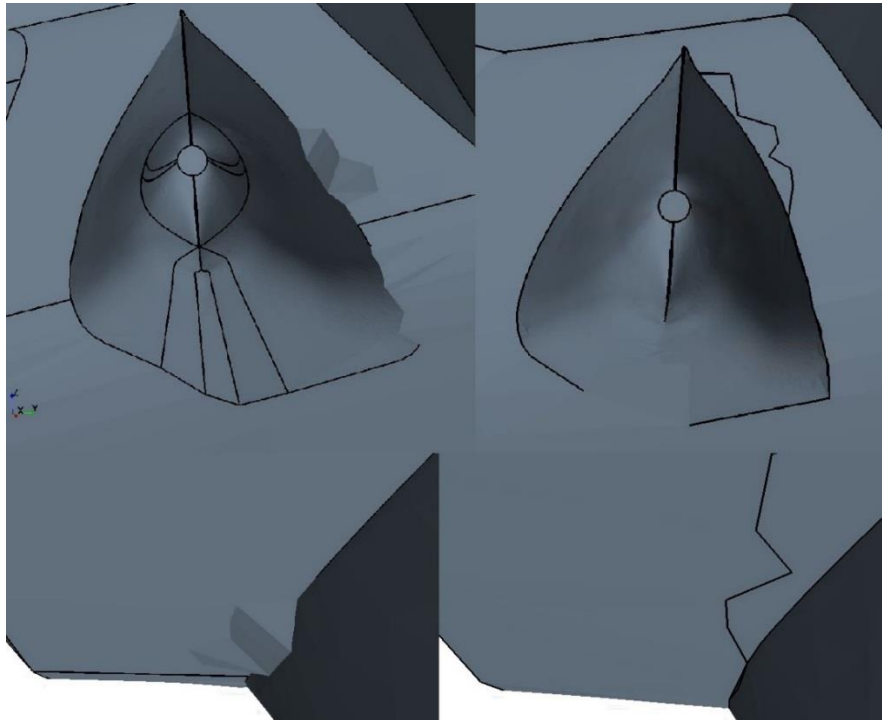


Figure 5-6 - Before and after repairing dent in skeg, Hull 1

From Figure 5-7 we observe that the keel was also seriously distorted. The reason for these surface changes, is the surface mesh that makes up the 3D model. For instance, when the mesh consists of too narrow and long cells, for instance, errors occur. Luckily these errors were noticed and fixed.

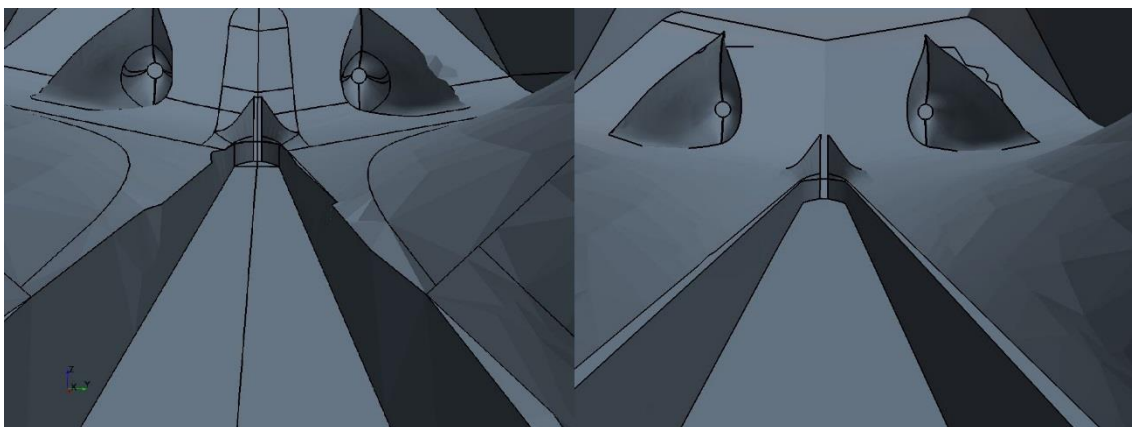


Figure 5-7 - Surface distortion in keel, Hull 1

5.2 Domain

The size of domain determines how much volume surrounding the object of interest shall be included in the computation. If we disregard computational time and computer power, increasing the domain will never result in a less accurate result, on the contrary. Decreasing it however, may cause fatal errors due to reflections, impact on the flow etc. For this setup, a domain large enough to avoid errors is needed before a convergence test may reveal the exact size needed. The preliminary domain size is based on findings from the project thesis associated with this master's thesis (Svoren, 2014), and can be seen in Figure 5-8.

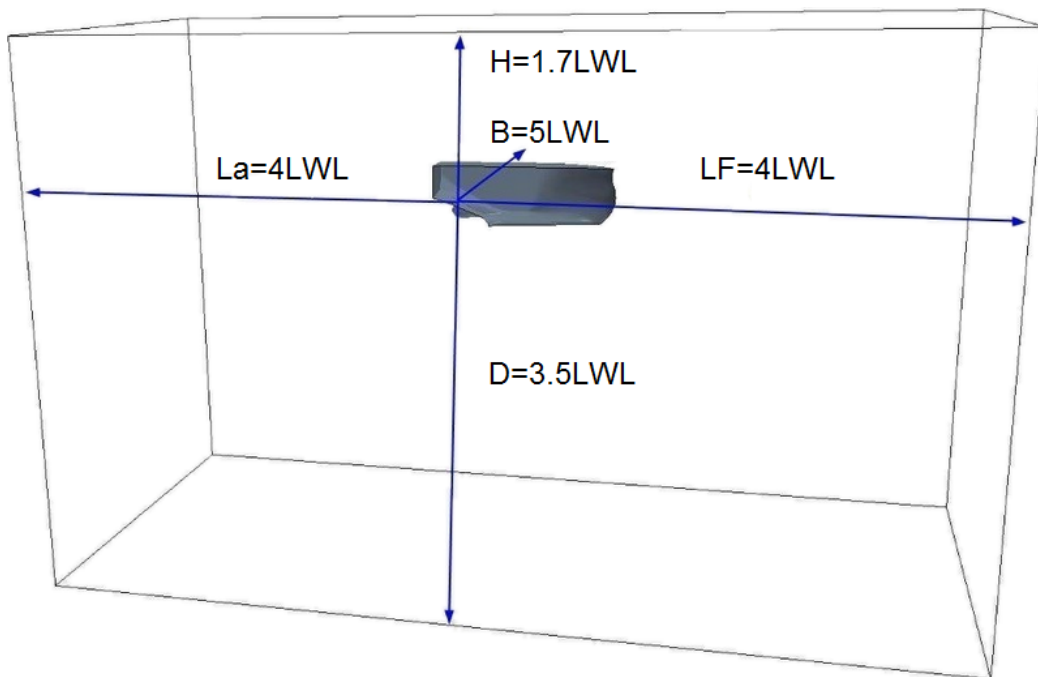


Figure 5-8 - Start domain for simulations

5.3 Meshing

Models used to mesh this hull based on needs for this particular simulation.

- Prism Layer Mesher
- Surface Remesher
- Trimmer

The prism layer mesher is needed to capture the correct velocity profile from the surface, as well as obtaining the desired y^+ value and wall shear stress, as mentioned in chapter 0. Surface remesher is used to remesh and improve the quality of the imported surface mesh. Finally, the trimmer is used to specify mesh properties on the specific volumetric controls, which makes up the final mesh.

5.3.1 Reference values

Reference values regarding meshing involve base size, prism layer control, surface growth rate, and allowed max and min cell size. These values are governing values for all regions, unless otherwise specified in regions.

- Base value: See convergence study, section 6.1.
- Maximum cell size: 400% of base
- Number of prism layers: 7
- Prism layer stretching: 1.5
- Prism layer thickness: 0.03m for the 10-knot simulation and .01 for the 4-knot simulation.
- Surface growth rate: 1.3
- Template growth rate: Default and boundary growth rate set to slow

Different prism layer thickness were used, due to large difference in velocity, and therefore velocity profile along the hull.

5.3.2 Volumetric control

The volumetric controls used are the same for both designs of the hull. They are set up to minimise unnecessary cells and get a more efficient simulation. They are also created in a way that helps capture the fine change in the free surface, to ensure that the waves develop in a proper way. As the stern area is most interesting, a finer grid resolution is created there.

- Free surface, thin

Anisotropic trimmer used with z equal to 10% of base and x, y equal to 800% of base.



- Free surface, medium

Anisotropic trimmer with z equal to 20% of base and x, y equal to 800% of base.



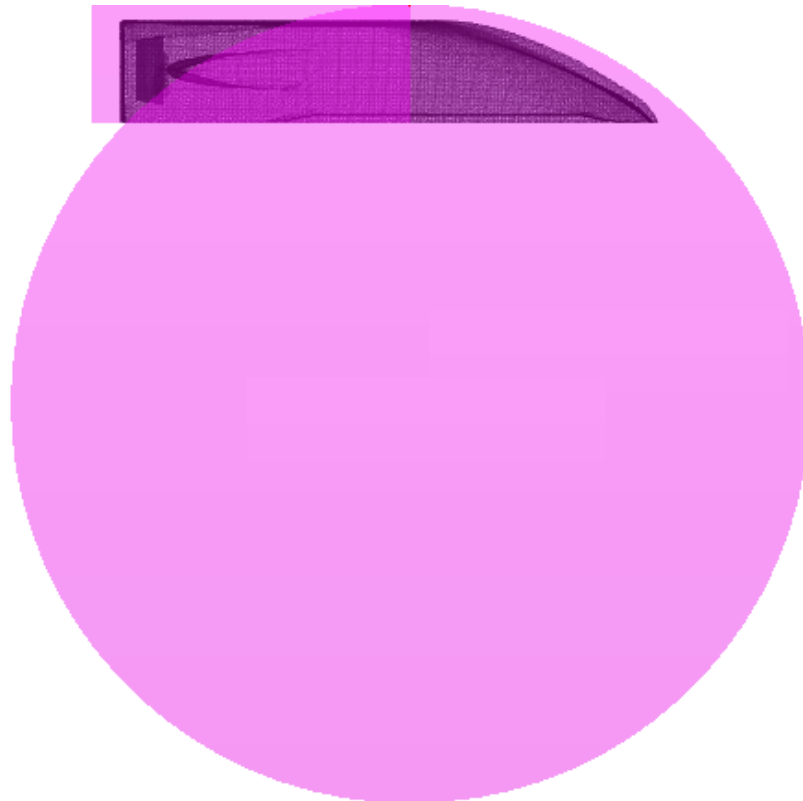
- Free surface, thick

Anisotropic trimmer with z equal to 40% of base and x, y equal to 800% of base.

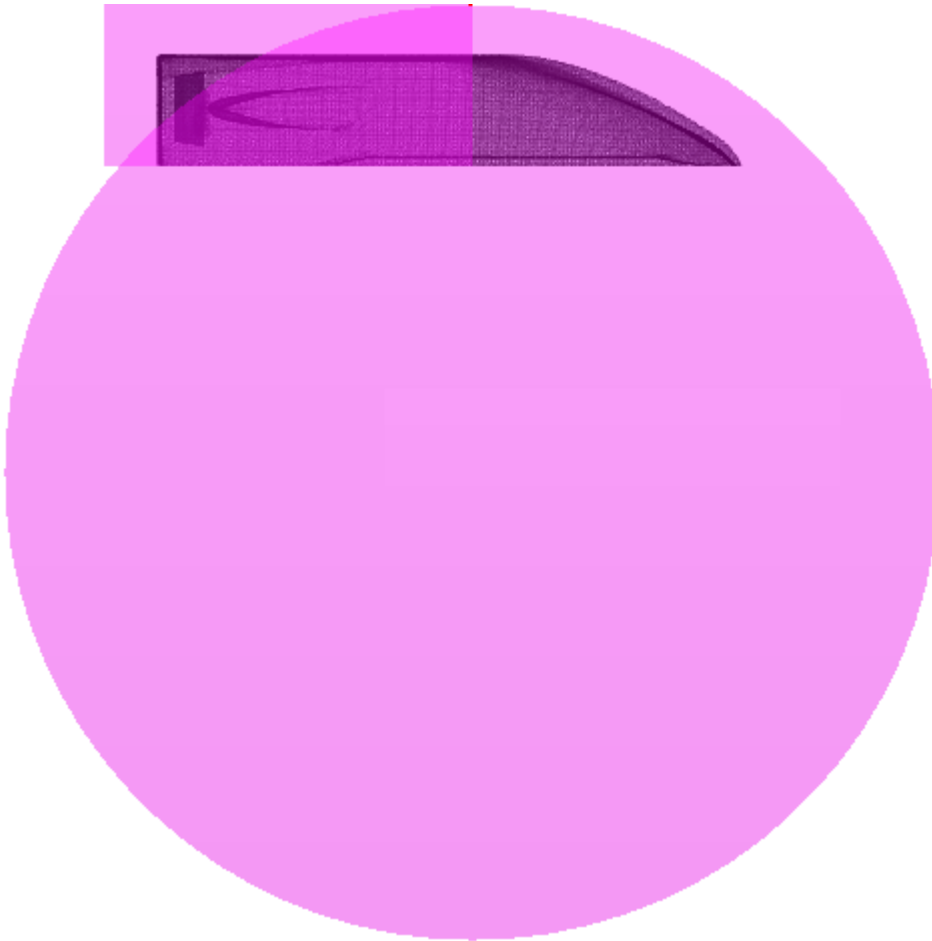


- Hull, very close

Anisotropic trimmer with x and y equal to 6.25% of base.



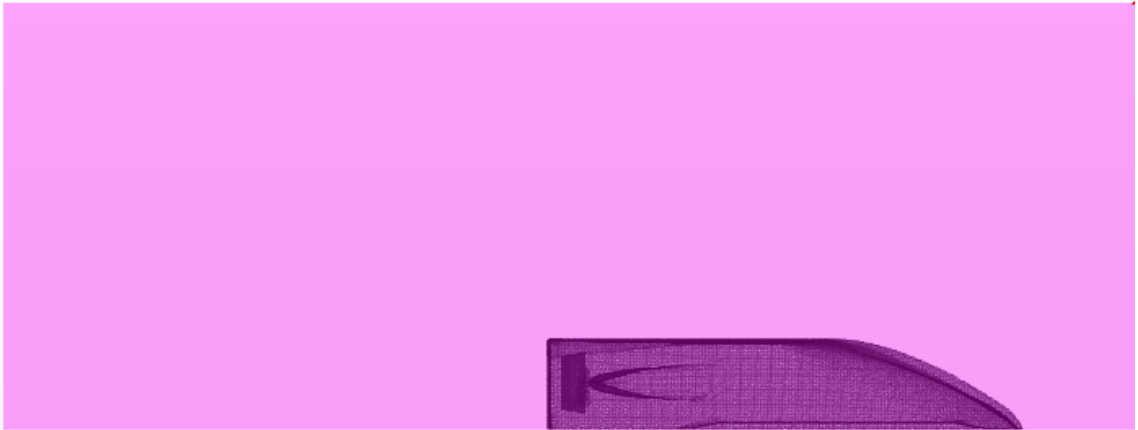
- Hull, close
Anisotropic trimmer with x and y equal to 12.5% of base.



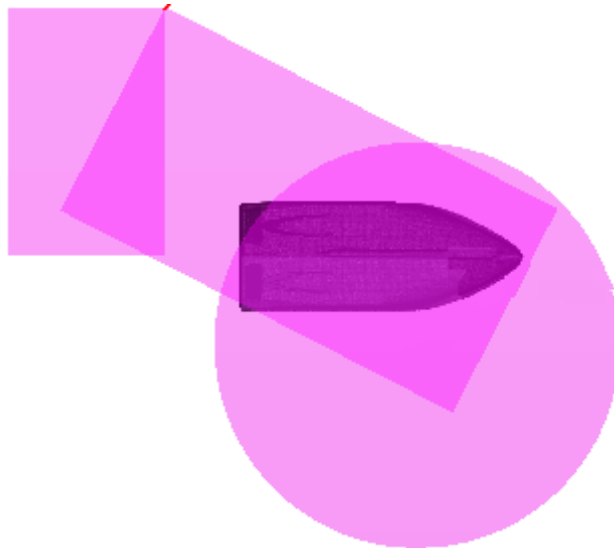
- Hull, medium
Anisotropic trimmer with z set to 50% of base, and x, y set to 100% of base.



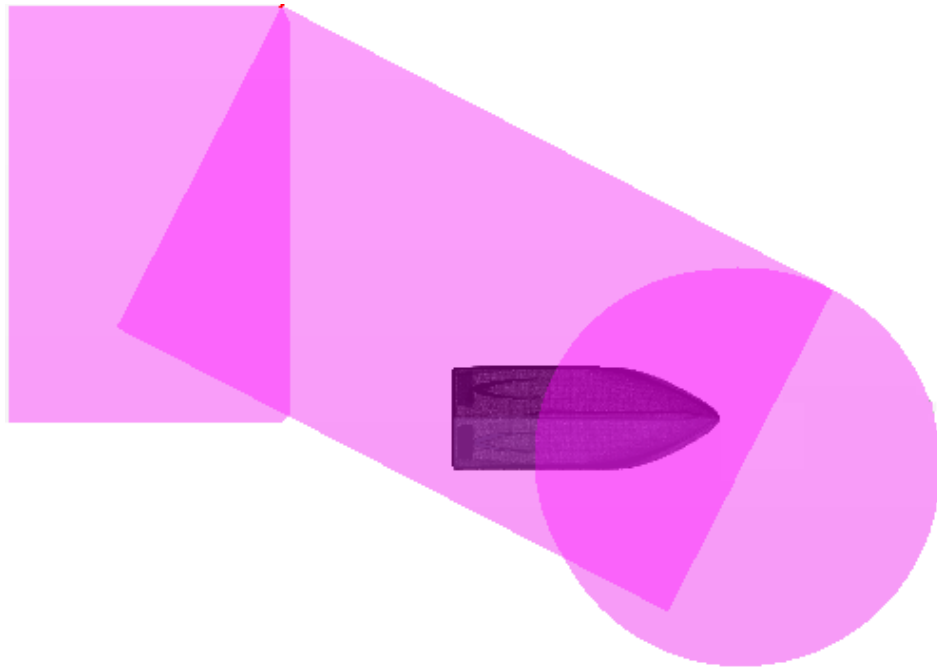
- Hull, far
Anisotropic trimmer with z set to 200% of base, and x, y set to 400% of base.



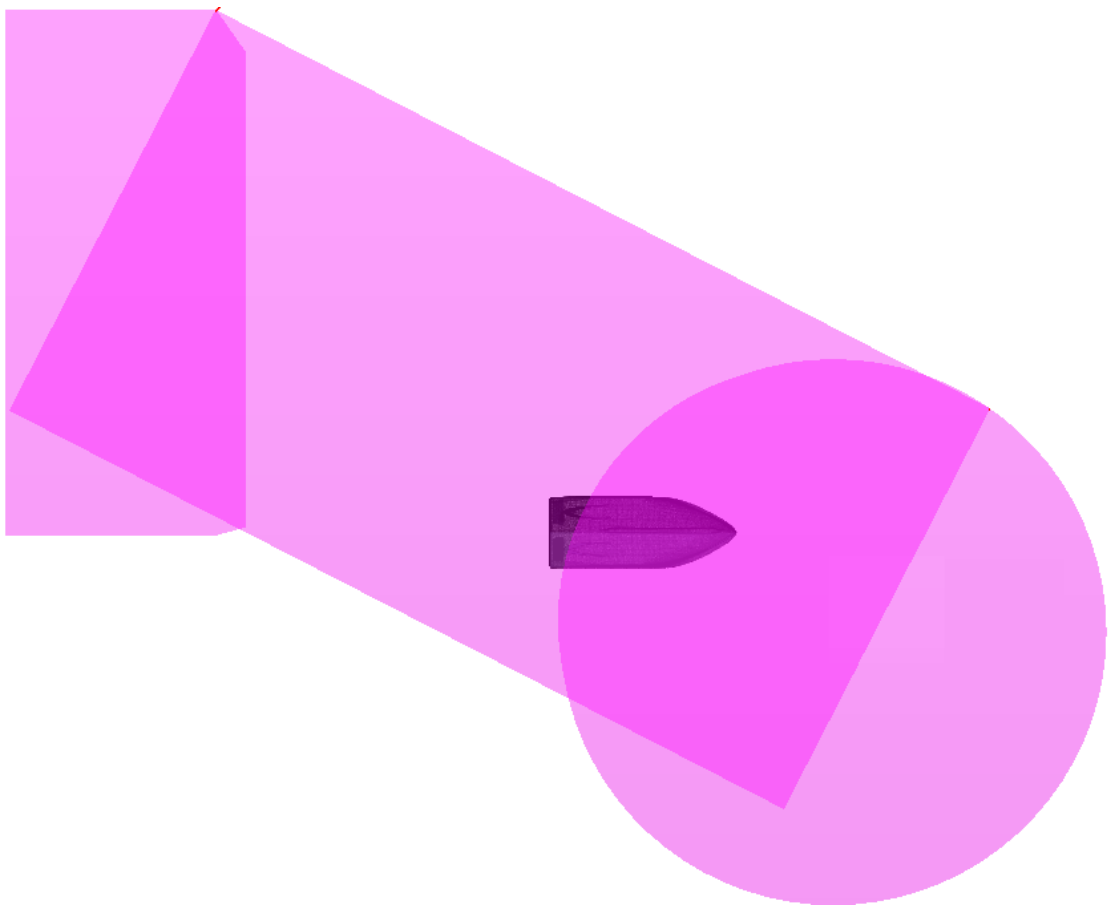
- Wake, close
Anisotropic trimmer with x and y set to 25% of base.



- Wake, medium
Anisotropic trimmer with x and y set to 50% of base.



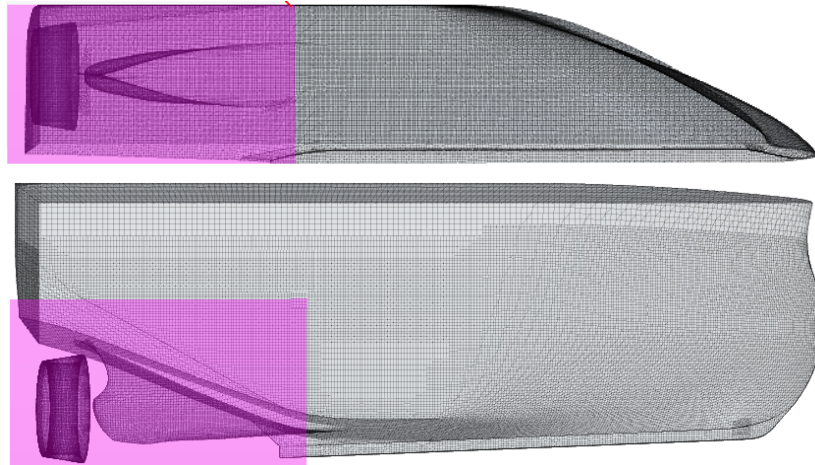
- Wake, far
Isotropic trimmer of 100% of base.



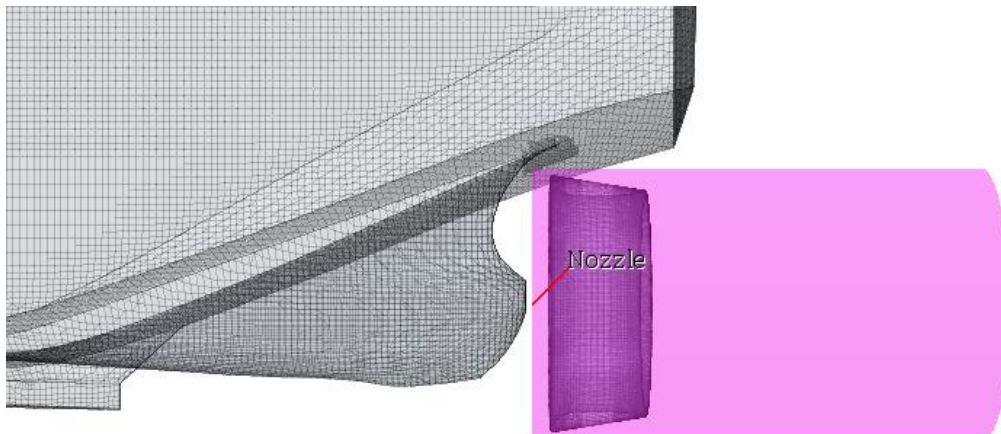
- Bulb
Isotropic trimmer set to 12.5% of base.



- Stern
Isotropic trimmer equal to 12.5% of base.



- Nozzle
Isotropic trimmer set to 12.5% of base.



5.4 Regions

Regions are what makes up the calculation domain in STAR CCM+. These simulations consist of 8 different regions. 6 for the virtual tank; top, bottom, side, symmetry plane, inlet, and outlet. The two last regions are for the ship hull and nozzle. The hull and nozzle require different prism layer values, and are therefore split up in two separate regions. VOF wave damping is also activated in the regions.

Top, bottom, side, symmetry, inlet and outlet have a custom surface size with a minimum size of 300% of base and a target size of 400% of base. The hull is also defined by a custom surface size with minimum size of 3.125% and target size of 12.5% of base. The hull's prism layer is defined by the reference values and the simulation speed. The 10-knot simulation was set up with 7 prism layers, stretching of 1.3 and a thickness of 0.03m. 7 prism layers and the low stretching, helps ensure y^+ value over 30. Values for the prism layer on the nozzle region is defined by 7 layers, a stretching of 1.5 and a thickness of 0.01m. Minimum cell size here is set to 0.78125 while target size set to 12.5. Small minimum size for the hull and nozzle were crucial in order to obtain a correct mesh.

5.5 Resulting mesh

With the setup described above (and base value from convergence study, 6.1) the resulting mesh are shown in Figure 5-9. Setting up a complete mesh for CFD calculations can be time consuming, and is very important for the validity of the solution. A vast amount of time has been used to set up the final mesh for this simulation. Several rounds of discussions with engineers from CD-adapco regarding refinement, models used, and free surface area have been conducted, to ensure a high-quality mesh.

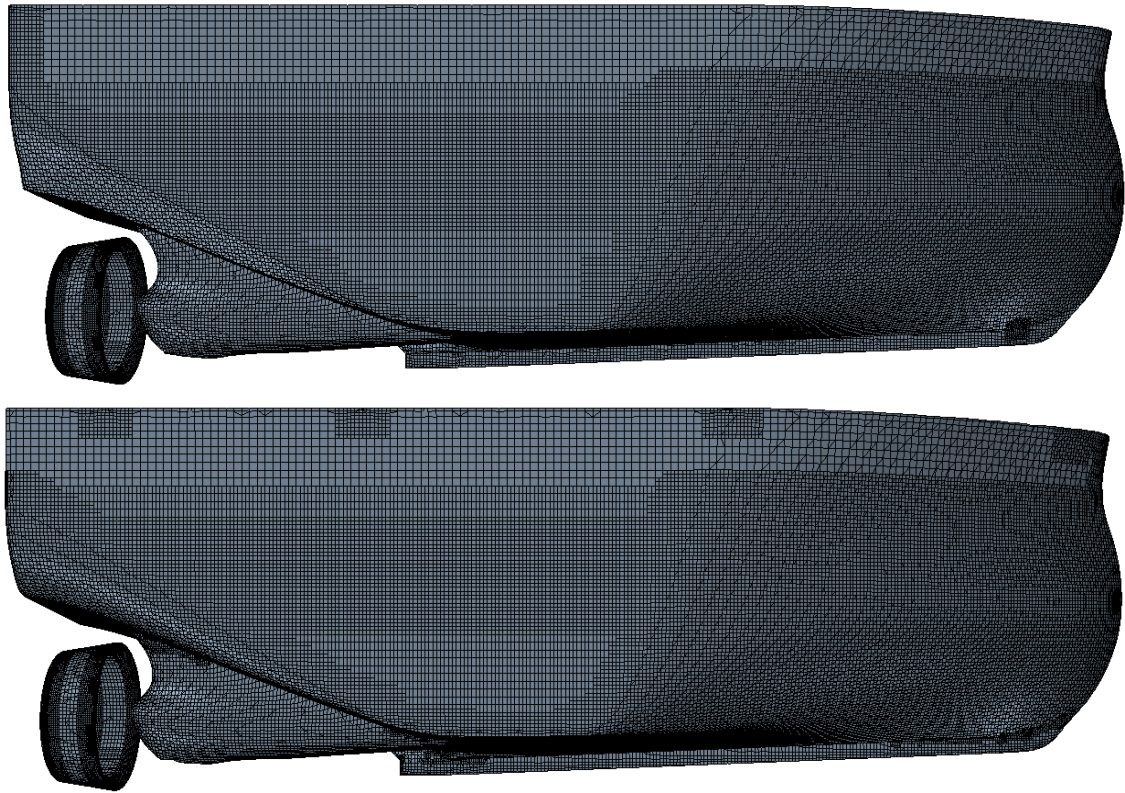


Figure 5-9 - Resulting mesh, Hull 1 and Hull 2

Figure 5-10 displays the gradual transition from prism layer mesh to the core mesh. Focus on this area has been to create a transition that doesn't have a large volume change.

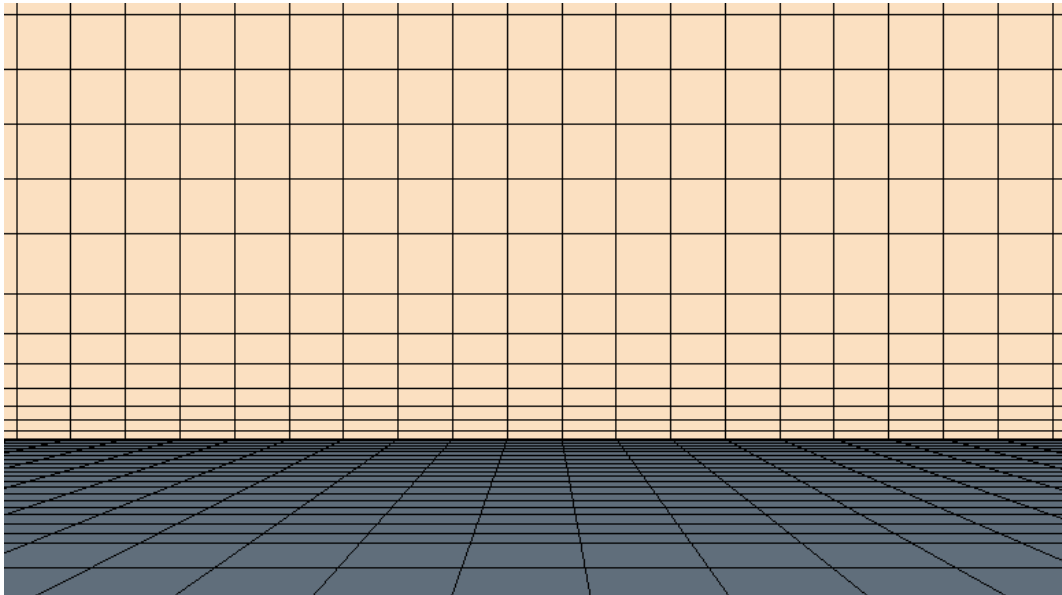


Figure 5-10 - Transition from prism layer to core mesh

In Figure 5-11 the different refinements can be observed. These are gradual with a target cell size of a multiple of two. This is done, as discussed in the introduction to this chapter, to optimize the resulting mesh. The gradual transition keeps numerical wave reflections/errors within mesh refinements from occurring.

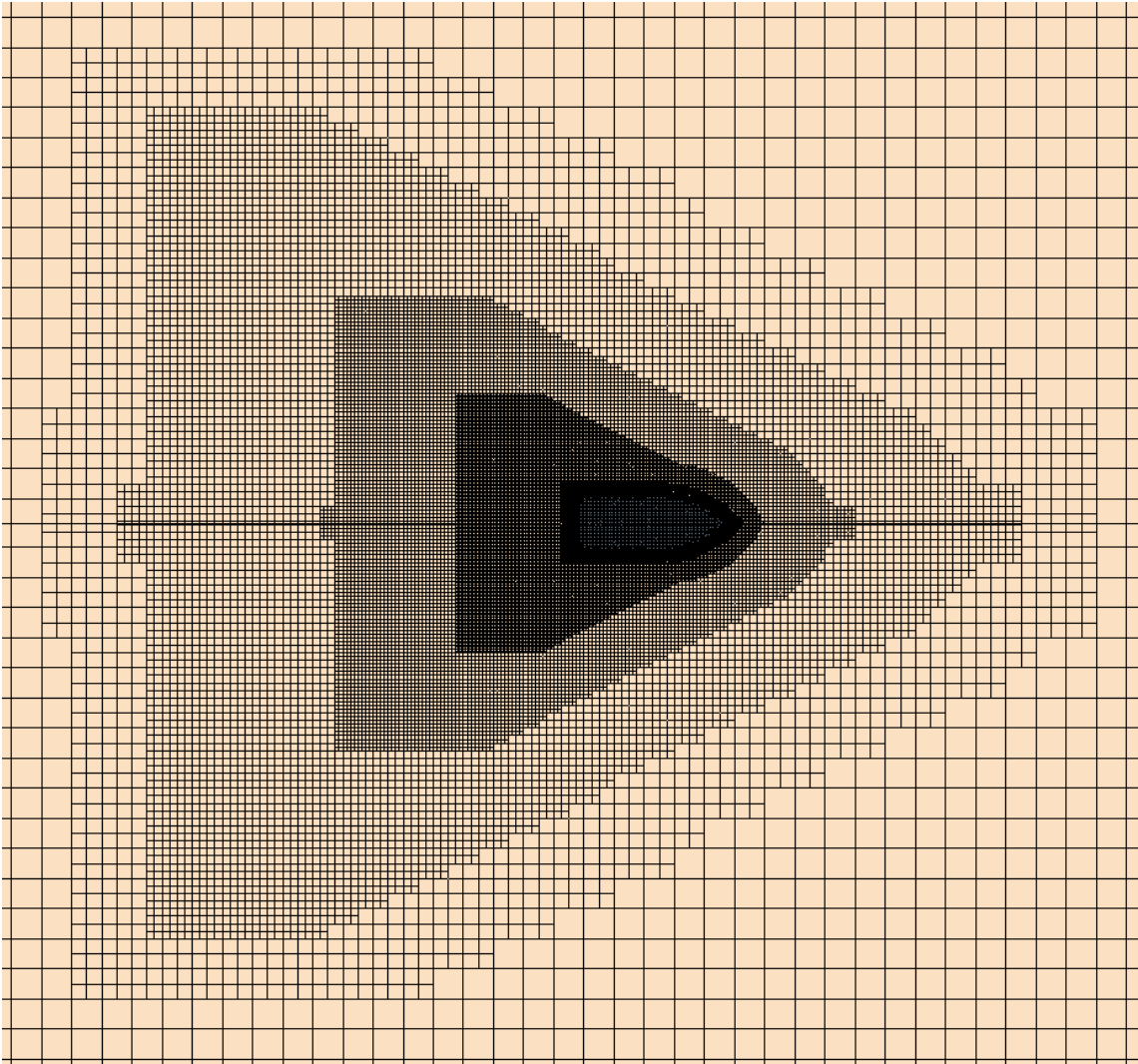


Figure 5-11 - Top view of mesh

In Figure 5-12 the surface refinement on the free surface can be viewed. These cells are nice and anisotropic, with large values in x and y-direction to optimize the mesh. It also has a small value in z-direction to capture the waves both through and crest.

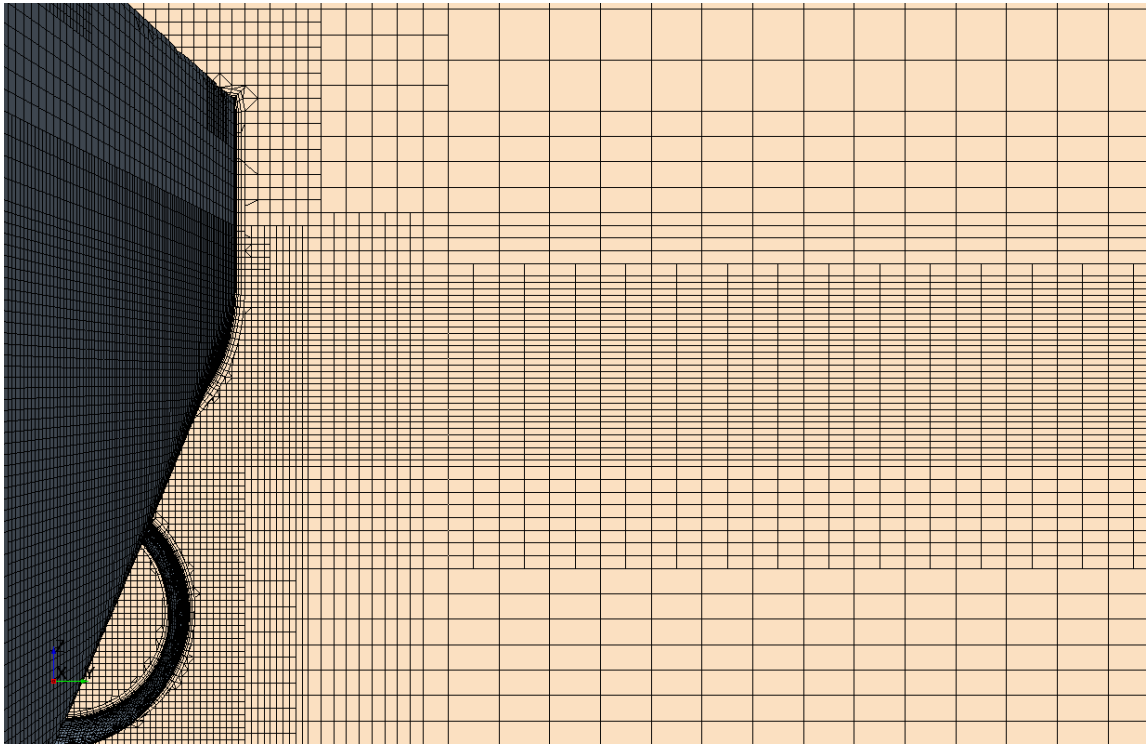


Figure 5-12 - Mesh refinement on free surface

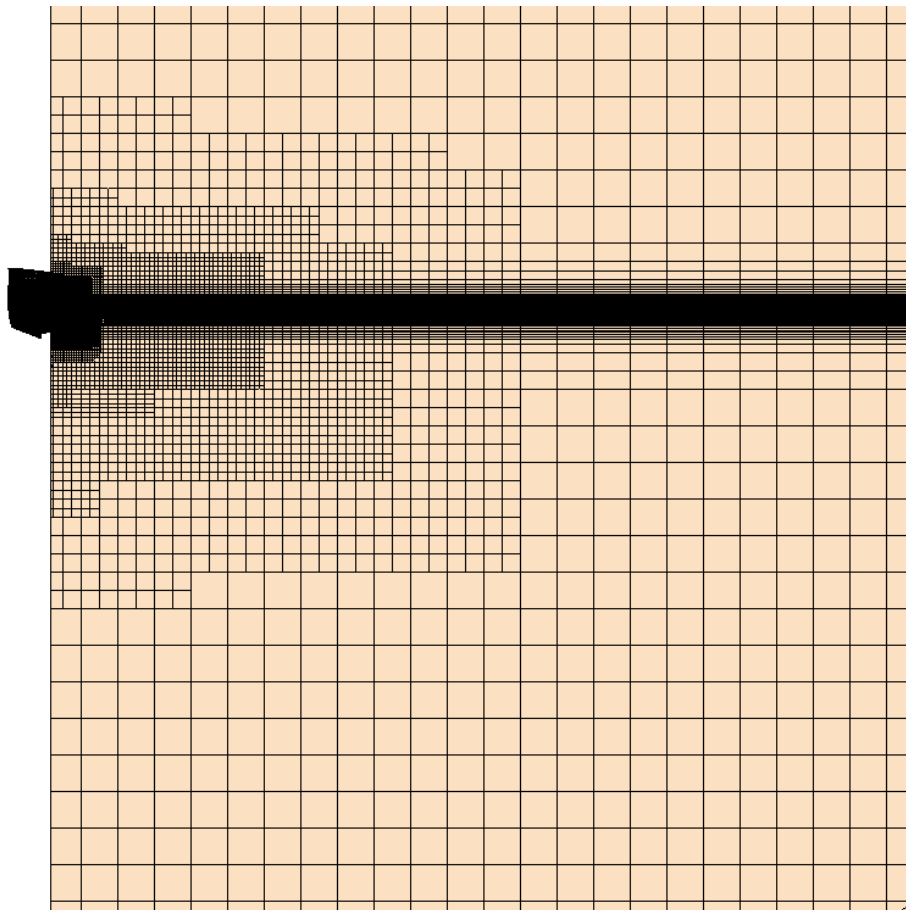


Figure 5-13 - Front view of mesh

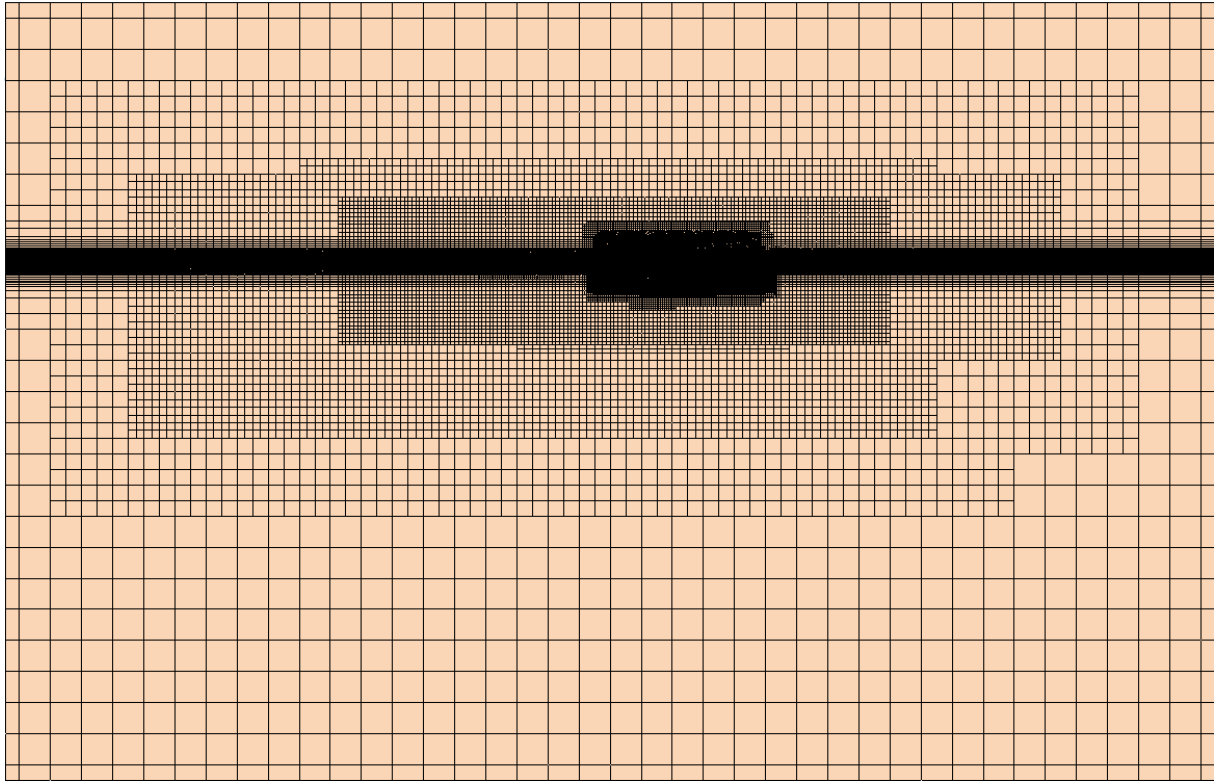


Figure 5-14 - Side view of mesh

From Figure 5-15 the mesh surrounding the nozzle can be seen. One can observe the refinement created by the surface remesher towards the trailing edge. This is a result of a minimum allowed cell size, small enough to capture the curvature.

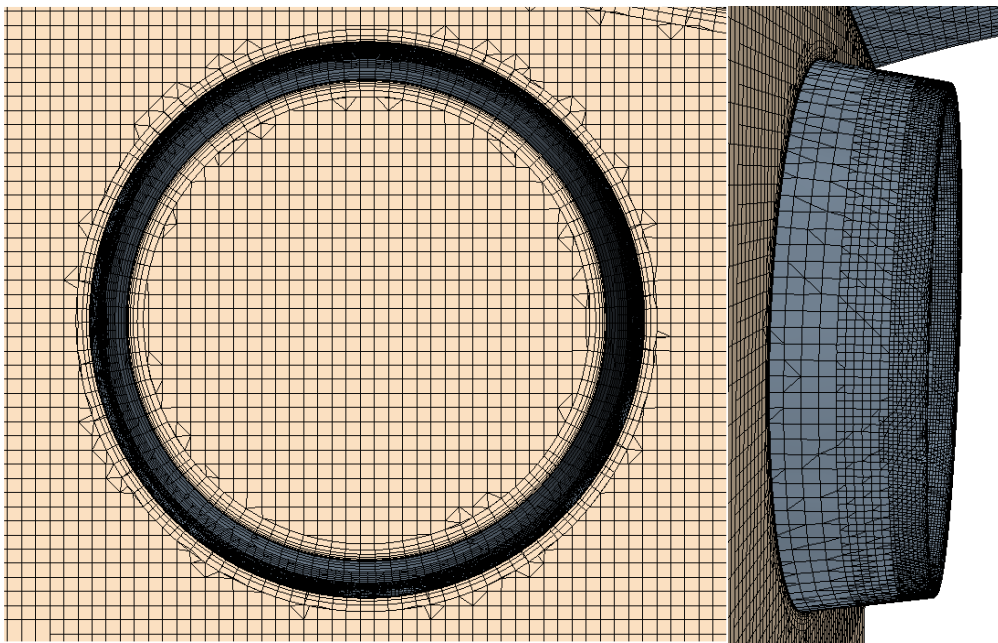


Figure 5-15 - Mesh of nozzle

5.6 Physical models

The specific models used in this project are:

- Eulerian multiphase
 - Water, $\rho = 997.2846 \text{ kg/ m}^3$
 - Air, $\rho = 1.18415 \text{ kg/ m}^3$
- Gradients
- Gravity
- Implicit unsteady
- κ - ϵ turbulence
- Multiphase equation of state
- Multiphase interaction
- Multiphase mixture
- Realizable κ - ϵ two-layer
- RANS
- Segregated flow
- Three dimensional
- Turbulent
- Two-layer all y +wall treatment
- Virtual disk
- VOF waves
 - Current speed = -0.651m/s , -1.627m/s (4 and 10 knots full scale)
- Volume of fluid (VOF)

A series of turbulence models are available in STAR CCM+, the κ - ϵ model is chosen for this project as it works well with the software (CD-Adapco, 2014). Selection of physical models for this simulation is based on results from project thesis (Svoren, 2014), and specific needs for these simulations.

5.6.1 Virtual disk

In order to simulate effective wake, an actuator disc in the form of a Body Force Method is used, as described in section 4.10.5. The body force propeller method is used to simulate the effect of the actual propeller. For this simulation, the operation point input was set to the rotation rate, which allows the user to input open water diagram values only for the specific simulation speed. Open water result for this propeller was obtained from Finnøy Gear AS. This dataset can be seen in Appendix A and Appendix B. Propeller data was a table input to STAR CCM+ as a .csv file as seen in the table below.

Table 4 - Open water data for propeller (Appendix A-B)

1	J	Kt	Kq	η
4 knot	0.5	0.30061	0.05491	0.6177
10 knot	0.902	0.23041	0.04364	0.7316

When creating the geometry for the actuator disk, the real propellers data was used, along with recommendations from STAR tutorial.

- Inner radius: 0.0425m
- Outer radius: 0.19m
- Thickness: 0.019m, 5% of diameter (A. Östman, personal communication, April 20, 2015)
- Velocity plane radius: 0.209m, 110% of diameter
- Velocity plane offset: 0.019m, 5% of diameter
- Propeller rotation rate: Left-handed
- Operation point input: Rotation rate

The propeller rotation direction was selected based on results from project thesis (Svoren, 2014), see Appendix C. In this way, the propeller operates against parts of the rotational hull induced velocities in the propeller plane with highest velocity, and may gain some “free” thrust.

5.7 Initial conditions

The applicable conditions are regarding pressure and velocity of the fluids. These are set as field functions with water speed (speed of current) adjusted to the selected run and the reference pressure to 101325Pa.

5.8 Boundary conditions

Boundary conditions in this simulation are straight forward, and does not vary a lot from the benchmark. The length of the VOF damping is increased due to the width of the model. This choice is based upon guidance from support engineers at *Steve portal* (CD-Adapco, 2014).

Table 5 - VOF damping boundaries, Roaldnes

	Roaldnes	VOF damping
VOF damping	14m	
Bottom	Velocity inlet	No
Inlet	Velocity inlet	Yes
Outlet	Pressure outlet	Yes
Side	Velocity inlet	Yes
Symmetry	Symmetry plane	No
Top	Velocity inlet	No
Hull	Wall	No
Nozzle	Wall	No

5.9 Rigid body motions

As mentioned in section 4.13 STAR CCM+ allows for 6-DOF, all six ship motions; surge, sway, heave, roll, pitch, and yaw. In a calm water resistance prediction, simulation like this only two degrees of freedom are needed; heave and pitch. This is to account for sinkage and trim during simulation. From Figure 5-16 one can observe that the sinkage, indicated in red, quickly stabilizes, while the trim increased continuously. Problem with the trim was most likely related to centre of mass. Communication with several experienced CFD users led nowhere, and the problem was not resolved. After discussions with P.h.D candidate Jarle Kramer, supervisor professor Sverre Steen, and Professor Bjørnar Pettersen, simulations in this thesis were set up with no motions allowed. This was based upon three arguments; It speeds up the simulations considerably, avoids problems with oscillating forces that occurred due to sensitive input regarding centre of mass, and it is presumed that pitch will have little effect for this case. As a countermeasure, a simulation on 10 knots with heave and pitch allowed was performed to obtain the correct sinkage. The calculated sinkage was then implemented to all simulations of 10 knots.

A MatLab script was used to find the mean sinkage of the last 35% percentile of the simulation. Mean sinkage was calculated to be equal to -0.0141772m for 10 knots simulations, see Figure 5-17. For the 4-knot simulation, zero sinkage was assumed.

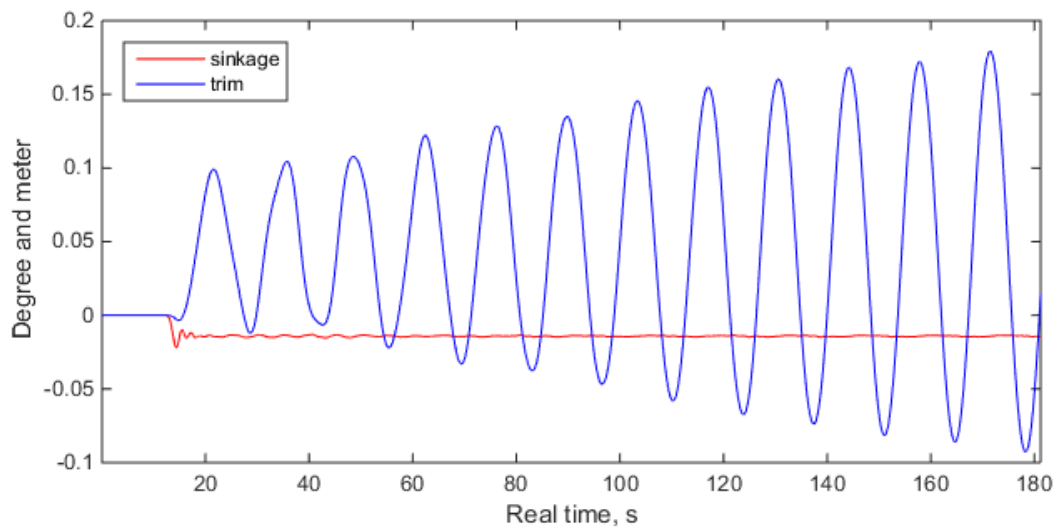


Figure 5-16 - Sinkage and trim from 10-knot simulation with heave and pitch allowed

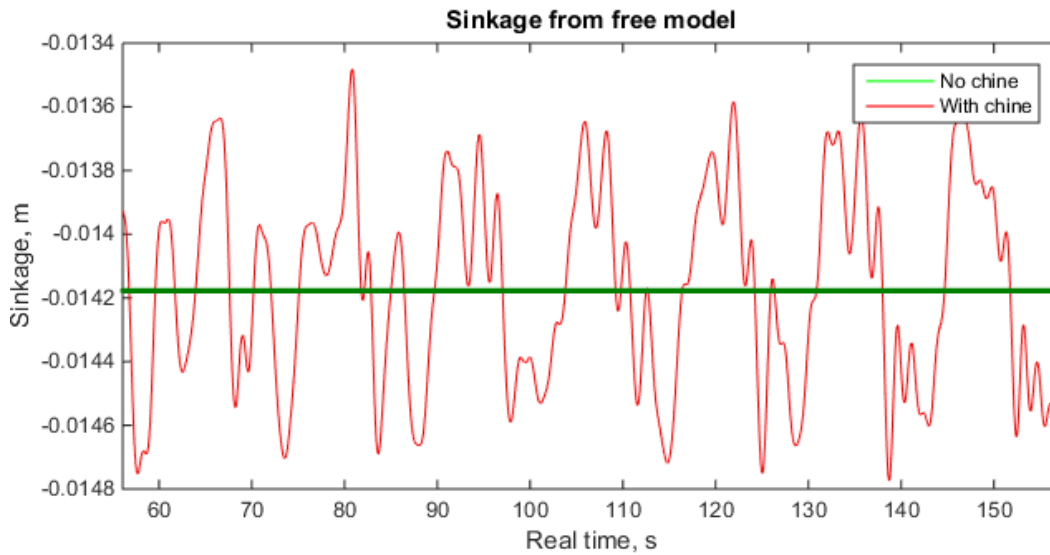


Figure 5-17 - Last 35% percentile of simulation with heave

The mass used in these simulations are obtained from Seacon as, and set to 625Kg. This value correspond to half of the ship weight displacement, note that this is due to symmetry in the simulation. Moment of inertia in pitch was calculated using equation 5-1. Moment of inertia in roll and yaw are not needed in these simulations, and set to the value of 1 (CD-Adapco, 2014).

$$I_5 = Mr_5^2 = mass(0.25 * lwl)^2 = 625kg(0.25 * 3.45m)^2 = 465Kgm^2 \quad 5-1$$

5.10 Solvers and stopping criteria

The solvers used for all simulations are the same. The most interesting solver to mention is the implicit unsteady. The VOF wave model is unable to solve pressure and velocity components in a coupled manner. Therefore, the implicit model is chosen because it is more stable than what explicit unsteady is. It is to be mentioned that explicit unsteady is capable of obtaining a more accurate result, but also needs more knowledge to use (CD-Adapco, 2014).

- Implicit unsteady
 - 1st order
- 6-DOF solver
- 6-DOF Motion
- Partitioning
- Wall distance
- Damping boundary distance
- Segregated flow
- Segregated VOF
- K-Epsilon turbulence
- K-Epsilon turbulent viscosity

Stopping criteria used in all simulations are maximum inner iteration, set equal to 5 iterations.

5.11 Setup of 4 knot simulations

Requirements for a low velocity simulation vary for the once with high velocity, where the big difference lies with the free surface. The hull will not induce any waves of significance at 4 knots, but by running the simulation at low speed, waves will still exist in the numerics. These waves are tiny, and an even finer mesh refinement at the free surface is needed to capture these in a good way. To avoid errors and reduce computational time, the effect of waves are neglected by setting up a simulation without free surface. Physical models used for this setup are:

- Cell Quality Remediation
- Constant Density
- Gradients
- Implicit unsteady
- κ - ϵ turbulence
- Liquid
- Realizable κ - ϵ two-layer
- RANS
- Segregated flow
- Three dimensional
- Turbulent
- Two-layer all y^+ wall treatment
- Virtual disk

And the only difference regarding mesh setup is that the domain is now cut at the free surface. This boundary is defined as a slip wall which means no shear stress along this boundary.

6 Results and discussion

After setting up a mesh capable to capture the free surface in a proper manner, prevent energy reflection between mesh refinements (ref 5.5), and define the curvature of the geometry in an adequately way, the next step is to run the simulations. In order to know what mesh cell size, domain size, and time step to use, a convergence test has to be performed.

6.1 Convergences study

A convergence test is a mathematic method of testing the convergence of an infinite series. In CFD it would be practically impossible to test all configurations. Instead, some chosen configurations are selected based upon lessons learned from project thesis (Svoren, 2014). These will be presented in this chapter. There are several ways of which a convergence study can be performed in CFD. One way of doing it, is by changing the mesh size and time step simultaneously, another by changing one operator at a time. The method for the convergence study in this thesis is based upon lessons learned in the course TMR15 Numerical Methods at NTNU. Convergence was tested on Mesh, time step, and domain individually. For this study Hull 1, without the nozzle. The simulation speed was set to 12 knots full scale, 1.952m/s model scale. Higher velocity demands finer grid and time step, which means that if convergence is found here, it will also be valid for 10 and 4 knots full scale.

6.1.1 Mesh

When setting up the simulation for convergence test on mesh size, base size was chosen based upon the project thesis, and set equal to 0.2m. This start mesh produced a setup consistent of 1.5mil cells. A time step of 0.02s was selected for the mesh study. This would ensure CFL numbers within reasonable values, and make for quicker simulations. In the table below the chosen base values and resulting number of cells can be viewed.

Table 6 - Base value and number of cells

Base value	Number of cells
0.14	3 920 580,00
0.16	2 739 163,00
0.18	2 050 627,00
0.20	1 538 683,00
0.22	1 225 485,00
0.24	1 021 128,00

After running the simulation with a base value of 0.2m, simulations with higher and lower base value was also simulated. This was done to check at which point a finer mesh resolution would not produce any better results. Figure 6-1 display the total force acting on the hull, while Figure 6-2 display pressure and shear forces separately. All six simulation converged within the time frame, and from Figure 6-2 it can be seen that the shear force converged quickly with very low oscillations while the pressure forces continued to oscillate for a while. This has to do with large pressure forces induced in the virtual towing tank. This is where the VOF wave damping comes to play (ref. 4.10.4). At the beginning of a simulation, high peak values occur before the water i.e. the numerics, settles down. For this reason, a simulation time of 200 seconds have been chosen, so that the solution may converge.

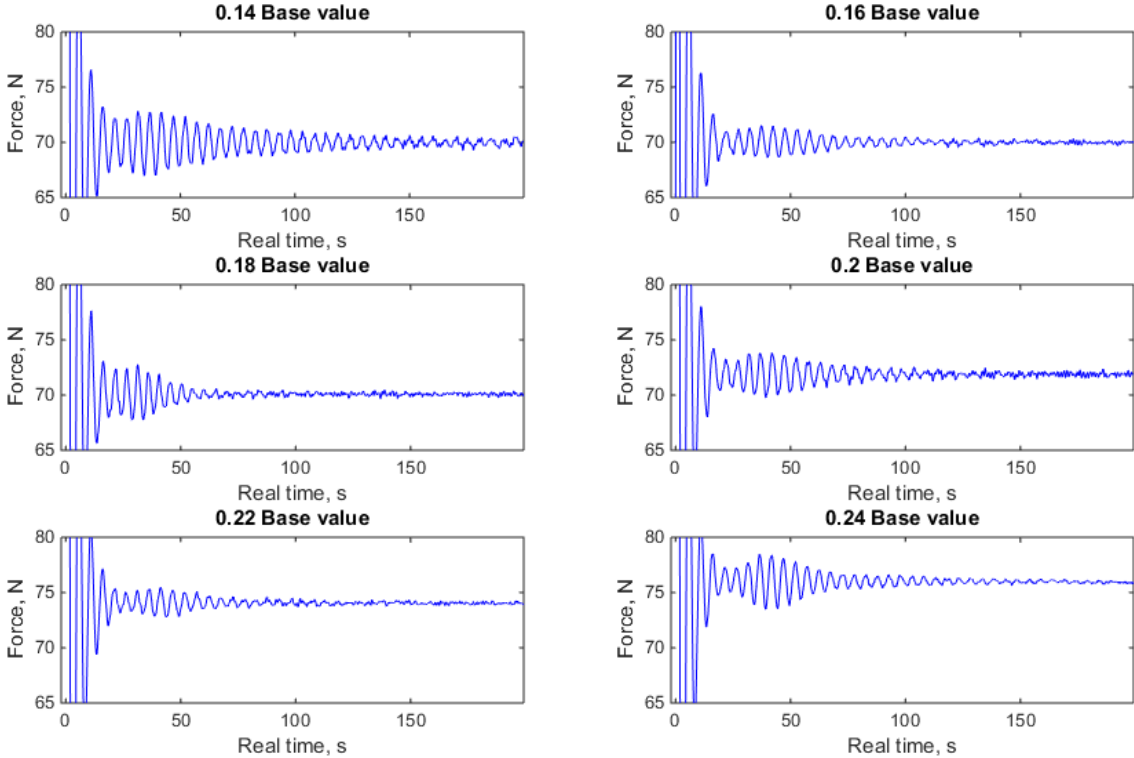


Figure 6-1 - Total force, full runtime – Mesh

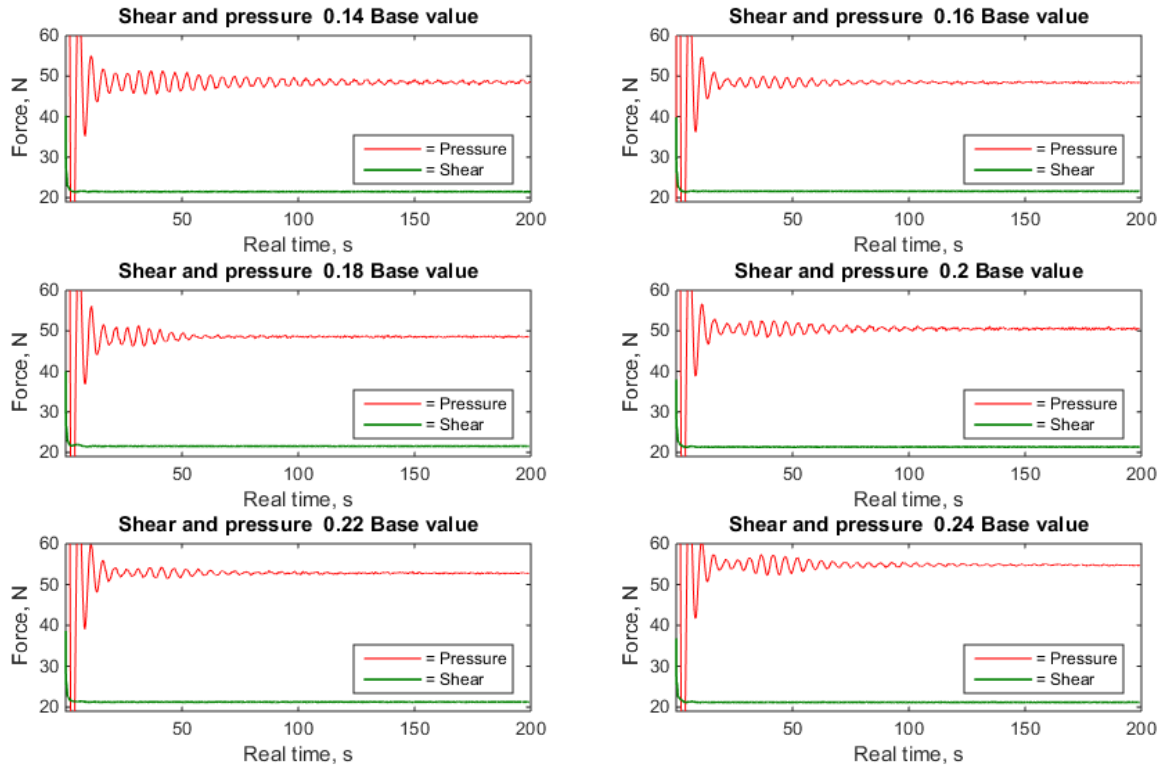


Figure 6-2 - Pressure and shear force, full runtime - Mesh

Figure 6-3 display the converged solutions on the mesh analysis, along with the mean total force on the hull. One may see that the simulation with a base of 0.14m oscillates the most with an average amplitude of 0.38N which is about 0.54%. In Figure 6-4, the pressure and shear forces are split up, and the resulting forces displayed on top of each plot. From this figure, we see that there are little oscillations left, and the forces have converged towards a final value.

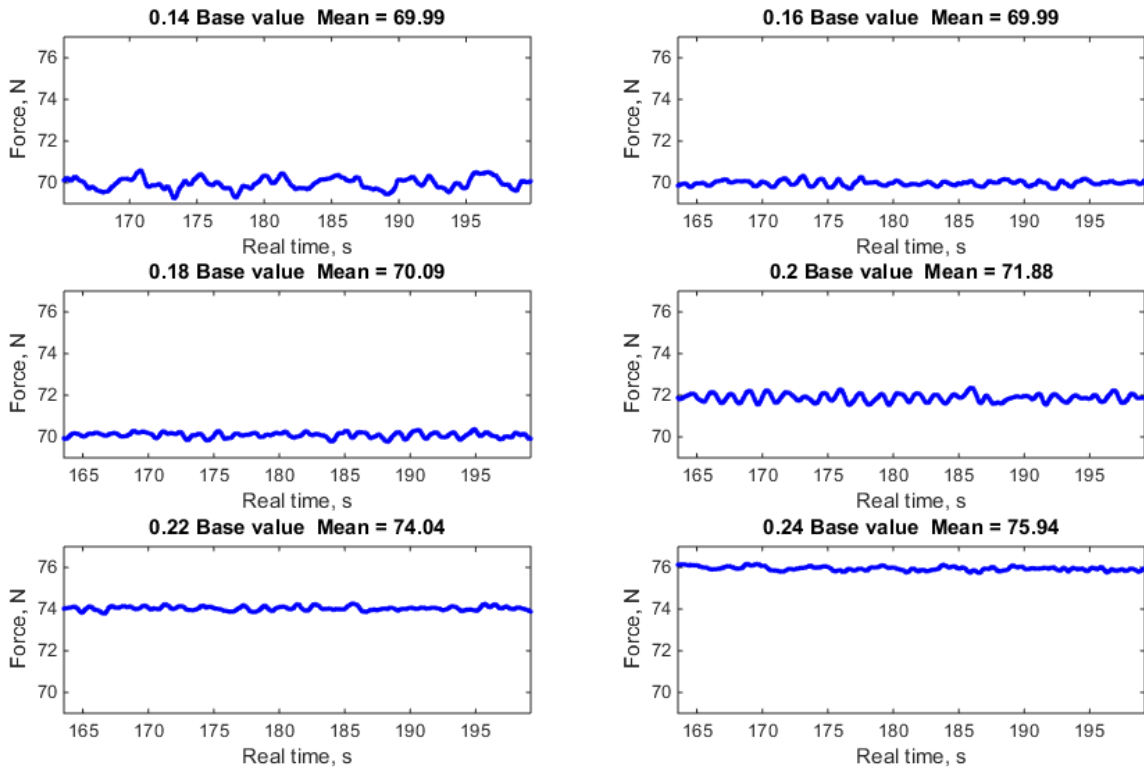


Figure 6-3 - Last 20% percentile of runtime - Mesh

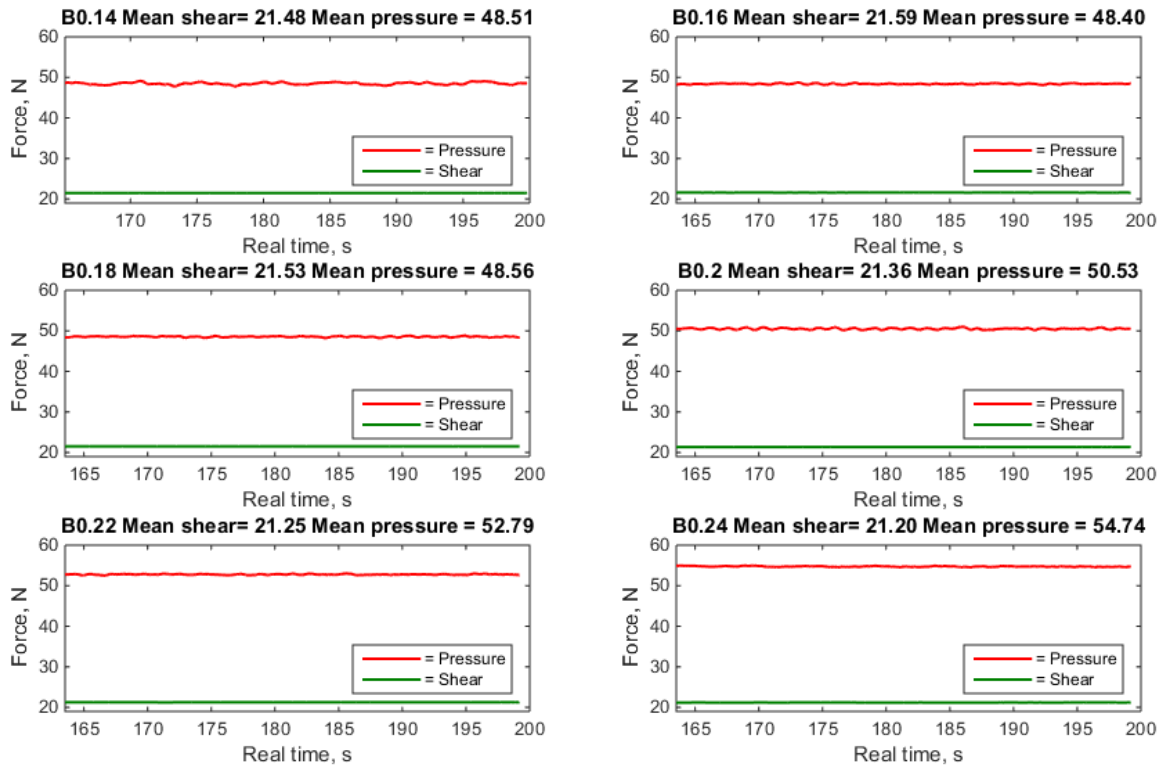


Figure 6-4 - last 20% of runtime shear and pressure - Mesh

After running these simulations, Matlab was used to plot the mean force to the number of cells. This can be viewed in Figure 6-5. A clear convergence can be found after 2 million cells. From Table 7 a difference of under 1% between the last three solutions can be seen, hence there is no need to check for finer cell sizes.

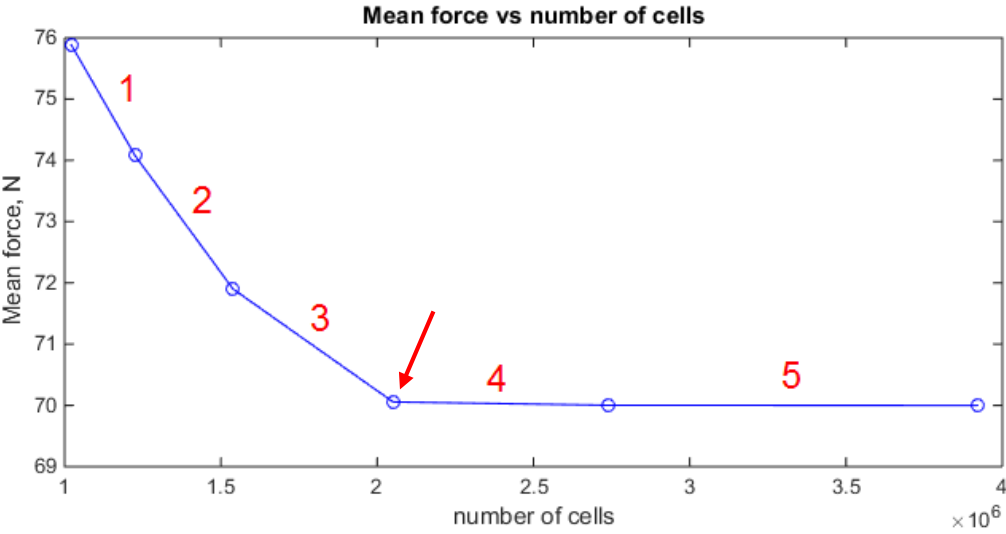


Figure 6-5 - Mean force vs number of cells – Mesh

Table 7 - Difference between mesh simulations

Base value	Interval	Difference [%]
0.24 – 0.22	1	2.386
0.22 – 0.20	2	2.937
0.20 – 0.18	3	2.563
0.18 – 0.16	4	0.077
0.16 – 0.14	5	0.004

From these results a base value of 0.18m with 2 050 627 cells was chosen for further analysis, indicated by red arrow in Figure 6-5. Since number of cells directly influence the amount of times the governing equations are solved (see Section 4.2), it is desirable to use the least amount of cells which still produce an accurate result.

6.1.2 Time step

After deciding upon which mesh size to use, finding the right time step was next. The time step in STAR CCM+ is the time between each set of iterations i.e. the physical time between each time the governing equations are solved. Similar to the base size, time step have an influence on CFL number, wall y^+ number, and convergence of the solution (and more). Finding the right time step is, therefore, crucial. For the mesh test, a time step of 0.02s was used. In this section a total of 8 different time steps were tested; 0.001, 0.002, 0.004, 0.006, 0.01, 0.02, 0.03 and 0.04s. In Figure 6-6 the total runtime are presented. As can be seen, the 0.004s and 0.006s simulations took a while before the amplitude subsided. Reasons for this were investigated and numerical interference might be the cause, but not concluded upon. The rest converged nicely.

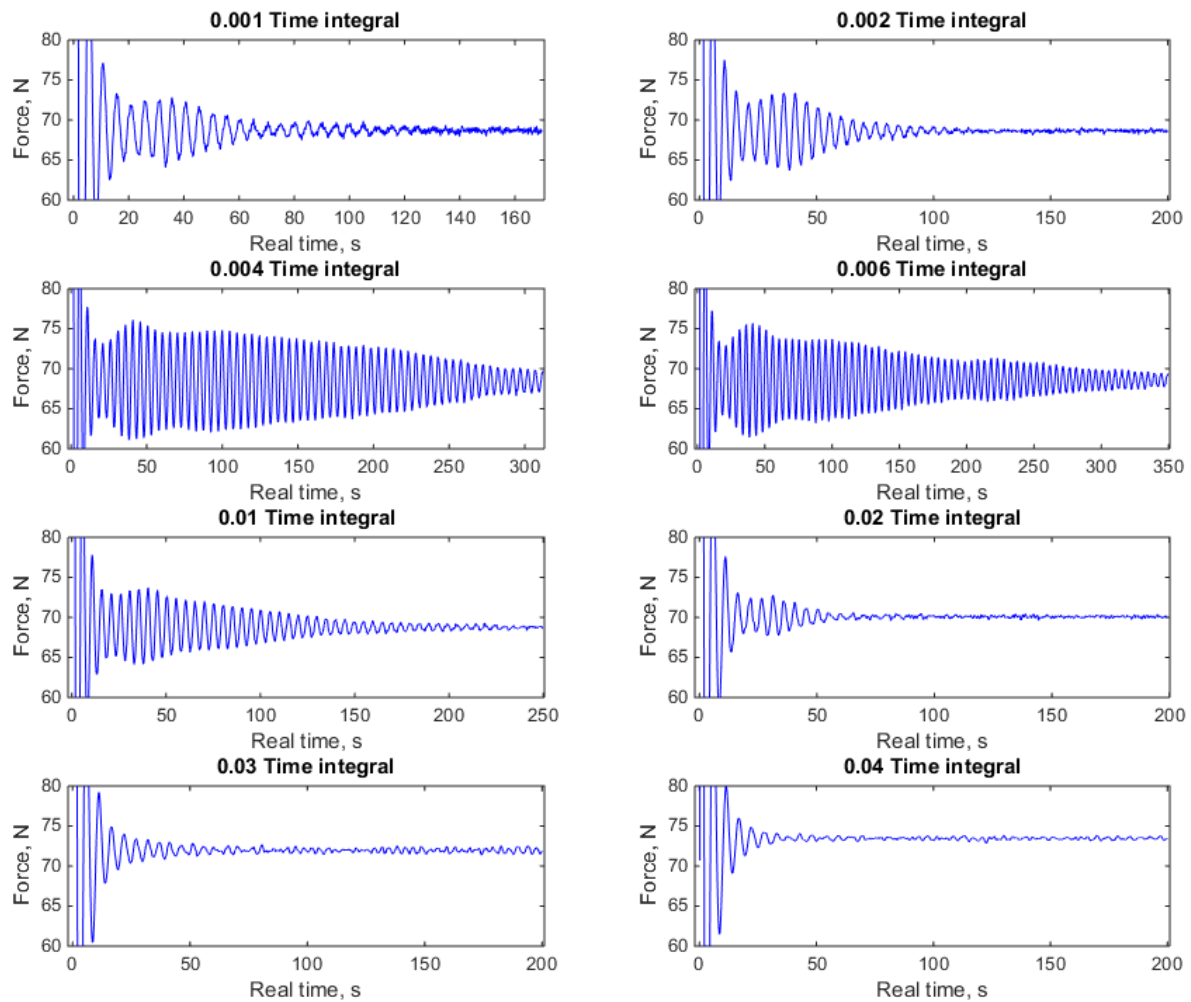


Figure 6-6 - Total force, full runtime - Time step

In Figure 6-7 forces are decomposed and shown with pressure forces indicated in red and shear forces indicated in green. Just like for the mesh test the shear force converge right away while the pressure force oscillates back and forth for a while.

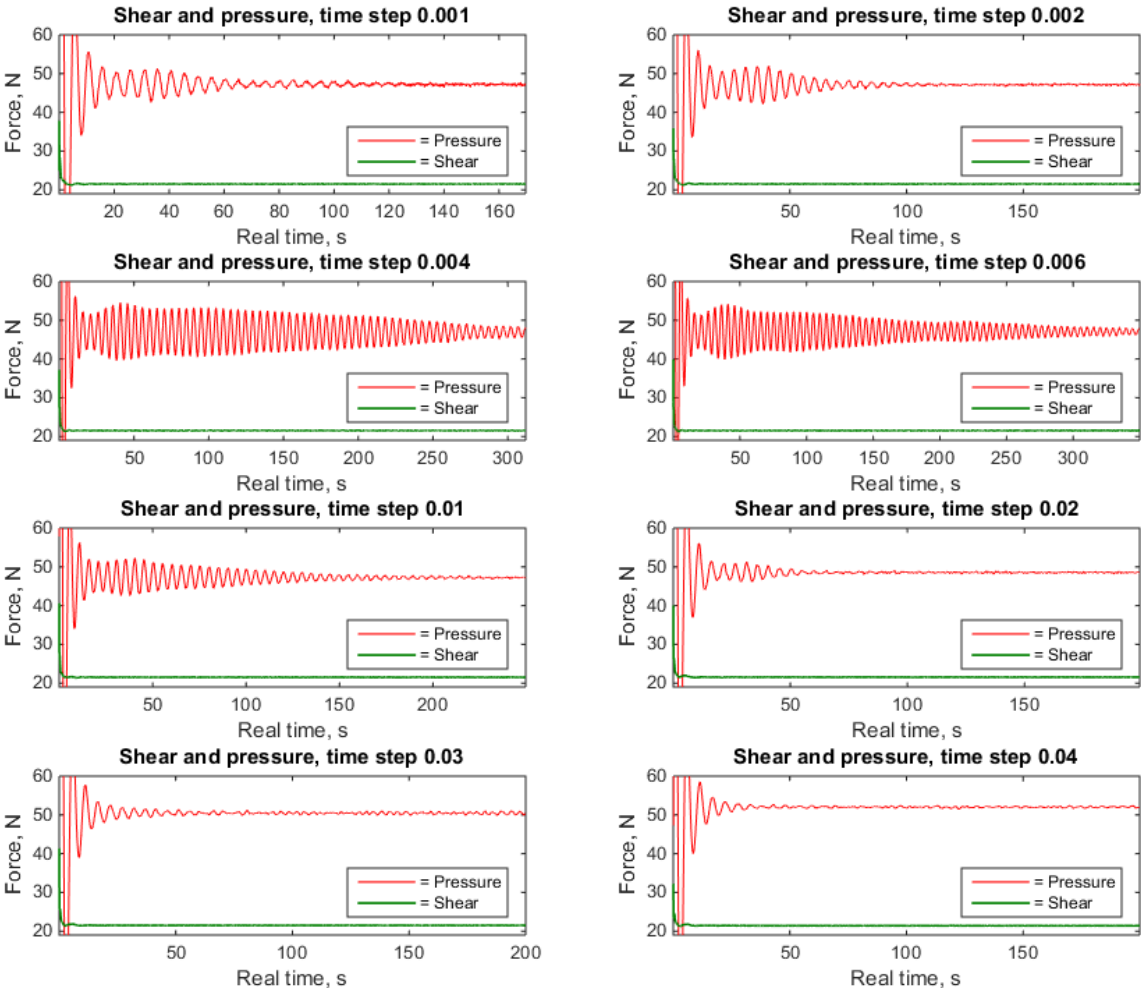


Figure 6-7 - Pressure and shear force, full runtime - Time step

From the figures above one can see a clear convergence in the forces at the end of each simulation. The last 20% percentile is then cut out and used to calculate the mean forces, displayed in Figure 6-8 and Figure 6-9. The simulation with a time step of 0.001s might have been simulated longer, but due to limited computer resources, this had to suffice. As mentioned the 0.004s and 0.006s simulations still oscillates with a mean amplitude of 1.37N and 1.08N respectively, which is below 2% of the mean force.

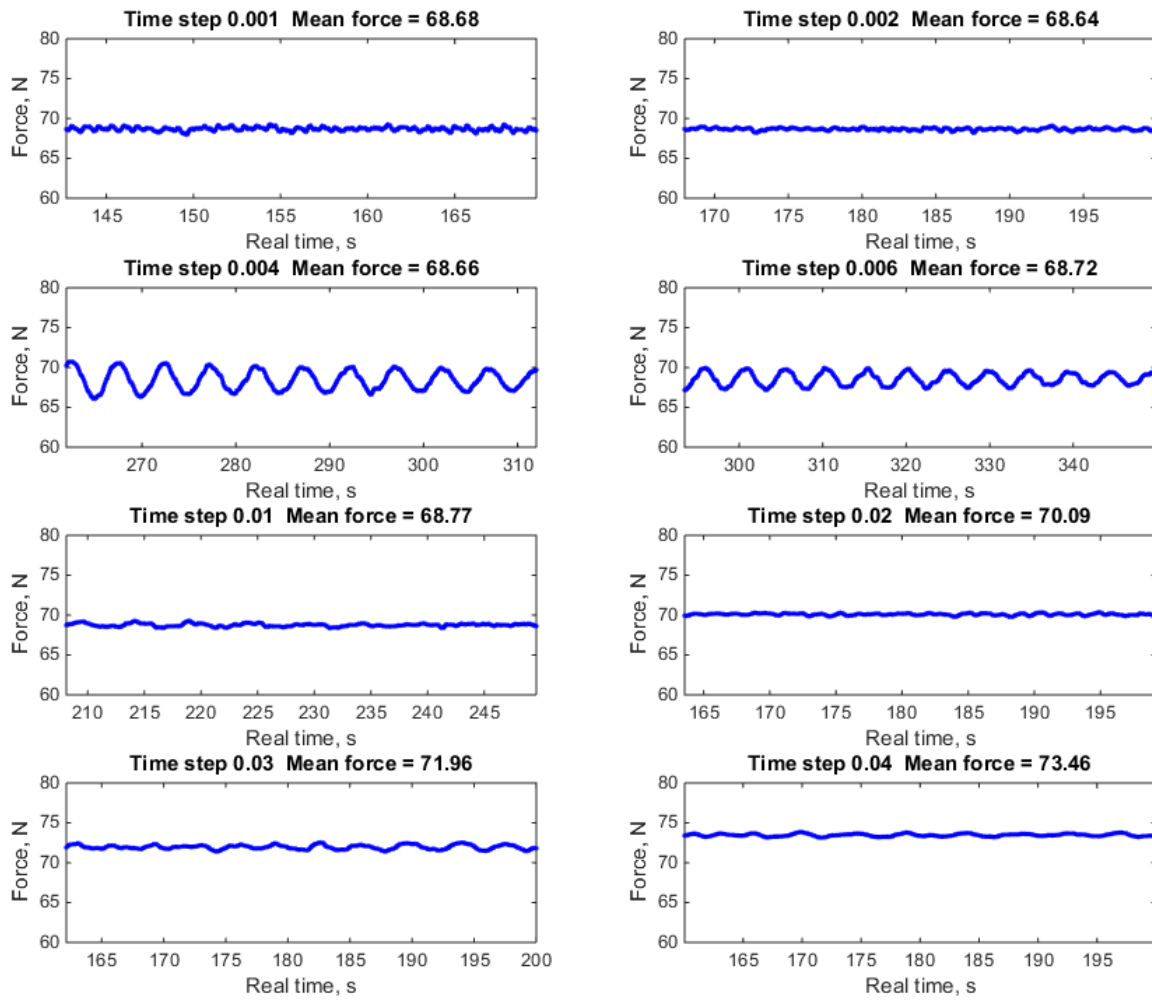


Figure 6-8 - Last 20% percentile of runtime – Time step

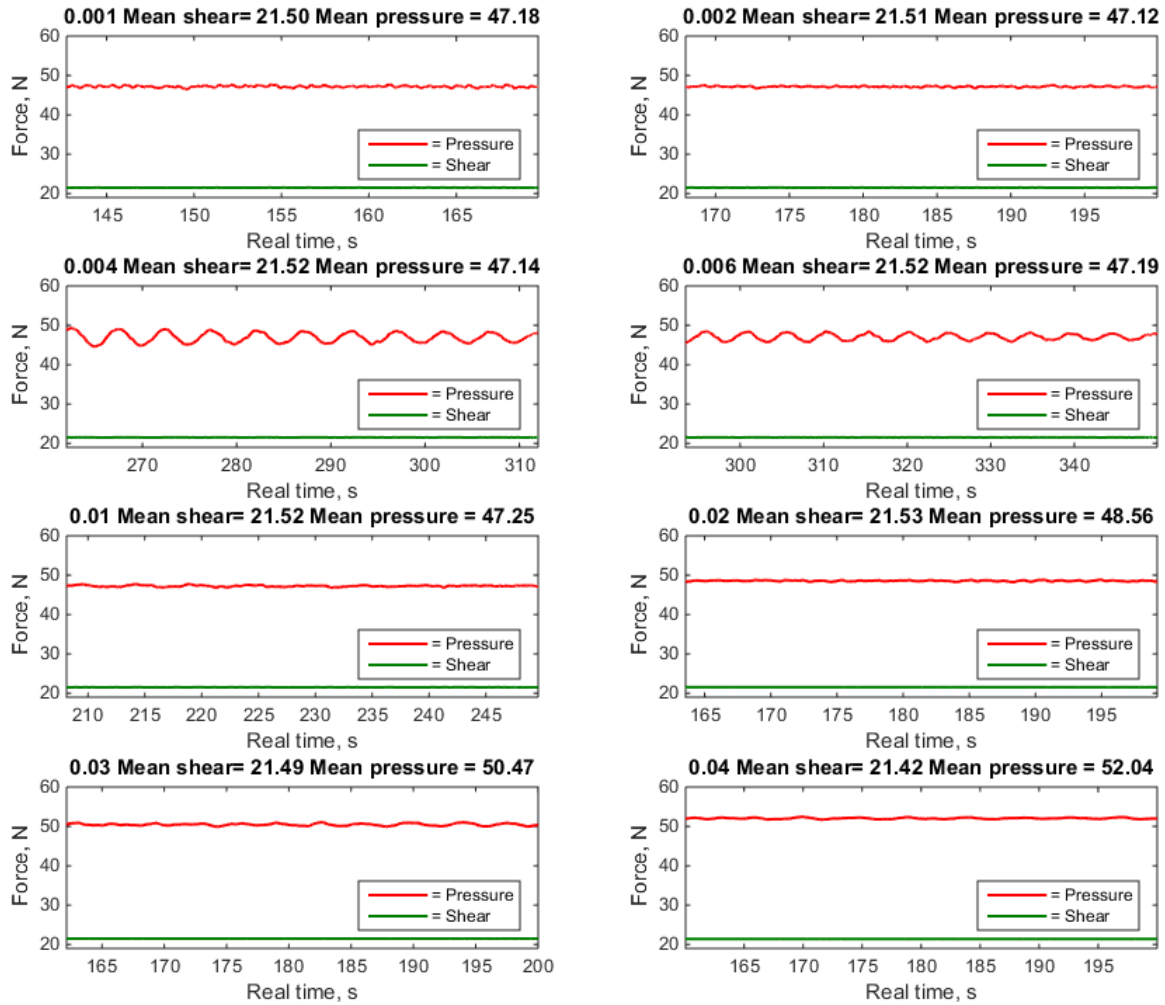


Figure 6-9 - last 20% of runtime shear and pressure – Time step

In Figure 6-10 mean forces are plotted to time step. Note that the x-axis are plotted logarithmic. This is done to better show the leaps between each time step. Several simulations are tested after the graph seems to converge. This was done to check whether the graph was continually descending or oscillating with low frequency. After the increase in mean force at the 0.001s simulation, it was assumed that the solution had converged.

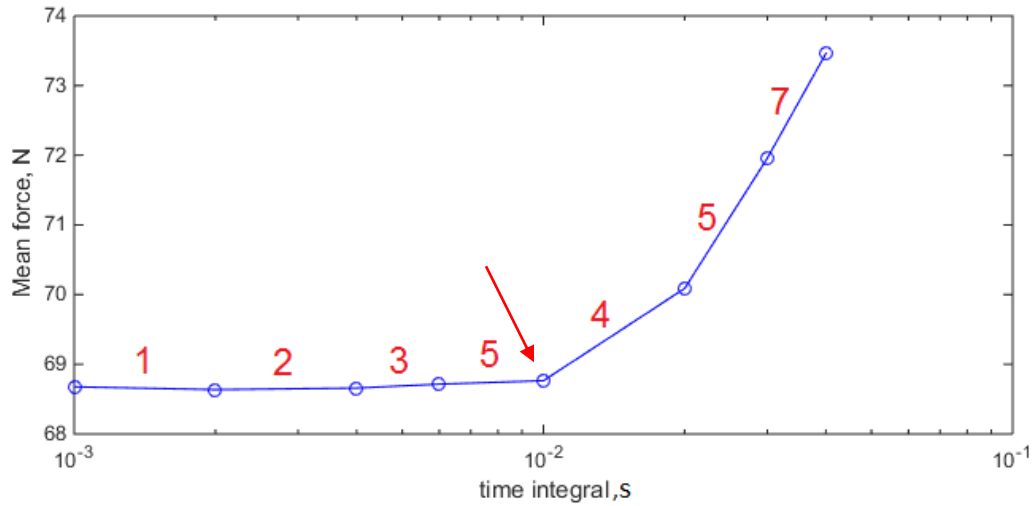


Figure 6-10 - Mean force vs logarithmic time step

Table 8 - Difference between time steps

Time step [s]	Interval	Difference [%]
0.001-0.002	1	0.156
0.002-0.004	2	0.033
0.004-0.006	3	0.081
0.006-0.01	4	0.072
0.01-0.02	5	1.889
0.02-0.03	6	2.597
0.03-0.04	7	2.047

Table 8 display the difference in mean forces between the simulations. From this result, a time step of 0.01s was chosen for further analysis. This corresponds to expectations when comparing this setup and the setup from a similar Master's Thesis performed by Jarle Kramer (Kramer, 2014), which also landed upon 0.01s as an appropriate time step.

The importance of time step can easily be seen in the wave pattern from each simulation. Figure 6-11 displays the developed wave pattern from the simulation with 0.01s time step. In this figure, one can see the Kelvin wake pattern which can be expected on a ship in motion. The snapshot in Figure 6-12 is taken from a simulation with a time step = 0.1s. This figure clearly shows a different pattern, the waves here are unnatural for a ship with Froude number of 0.33. This is a result of a coarse time step, which prevents fine wave elevations from being captured.

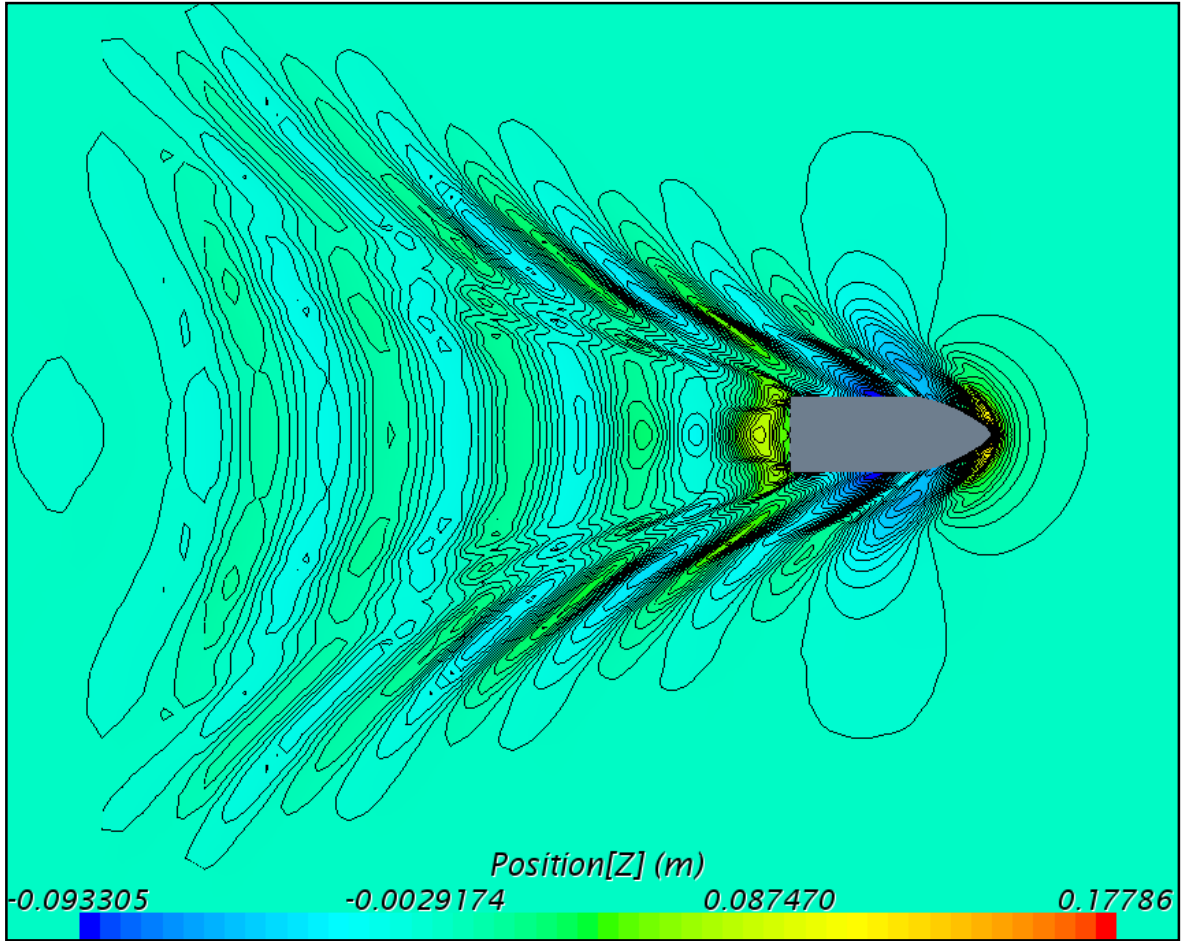


Figure 6-11 - Wave pattern with time step of 0.01s

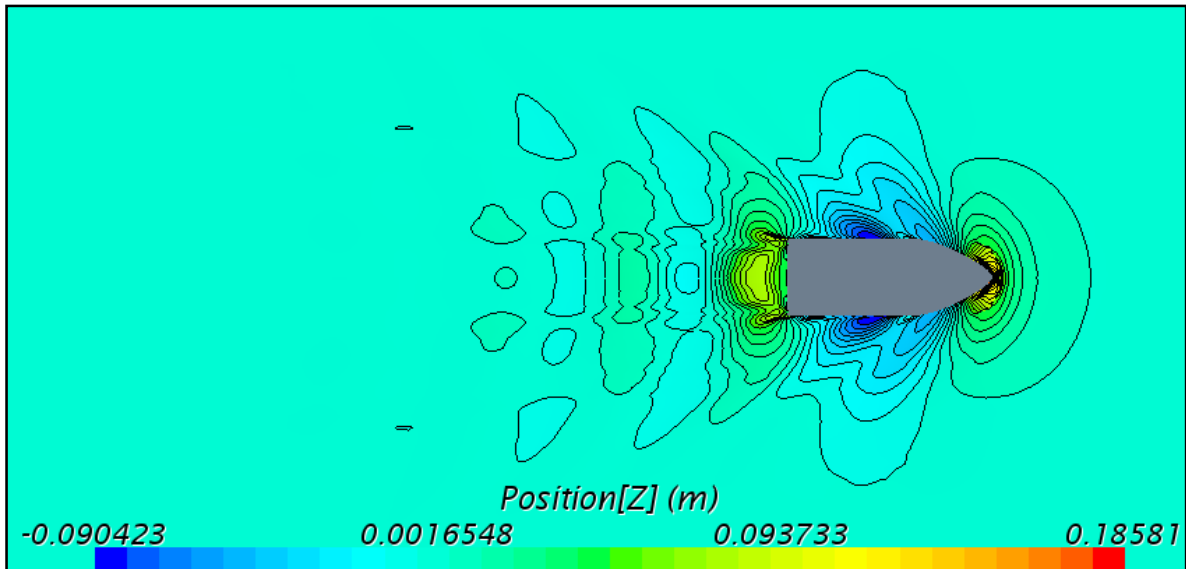


Figure 6-12 - Wave pattern with time step of 0.8s

6.1.3 Domain

As described in section 5.2 a start domain was set for this case. In order to check whether this domain was suitable or not, a convergence test had to be performed. Three additional domains was tested; 50%, 80% and 150% of the start mesh. These can be viewed in Figure 6-13. VOF damping length was set to a length where it reached the first mesh refinement from the walls. The pink area displays the hull geometry included in the calculations, and gives a sense of the relative size of the domains.

Table 9 - Number of cells in each domain size

Domain size	50%	80%	100%	150%
No. Cells	1 848 676	1 974 892	2 050 627	2 164 623

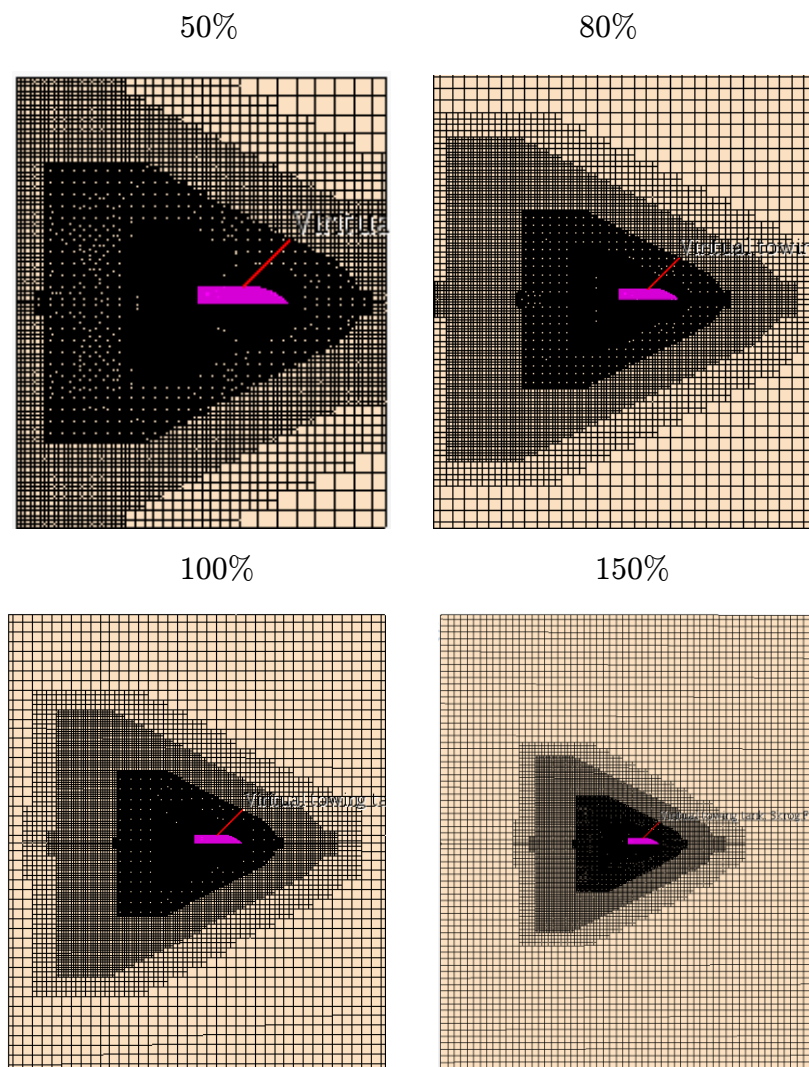


Figure 6-13 – Different domain size.

Plots of the complete runs both for total force and decomposed force shown in the figures below. As for the previous runs in time and mesh trials, the simulations converges but at a different time. As seen from the previous simulations, the shear force stabilizes right away while the pressure force keeps oscillating for some time, due to low frequent waves induced at the start of the simulation.

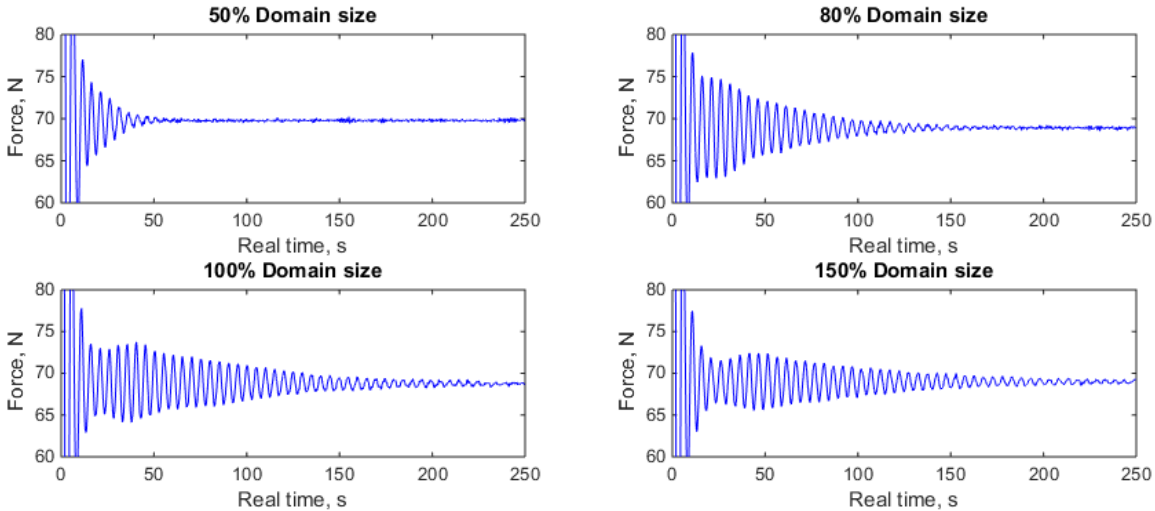


Figure 6-14 - Total force, full runtime – Domain

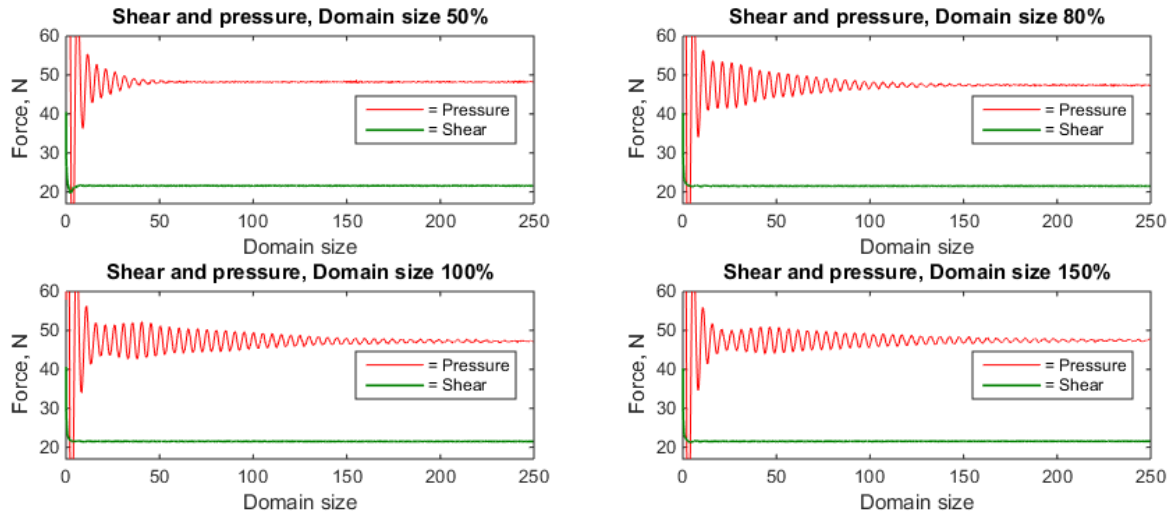


Figure 6-15 - Pressure and shear force, full runtime – Domain

Figure 6-16 display the last 20% of the total run. Here we see that almost all oscillations are gone. The 150% simulation still oscillates with a mean amplitude of 0.32N, which is the same as 0.46% of the mean. These are all recognized as converged. Figure 6-17 display the tail decomposed as shear and pressure force.

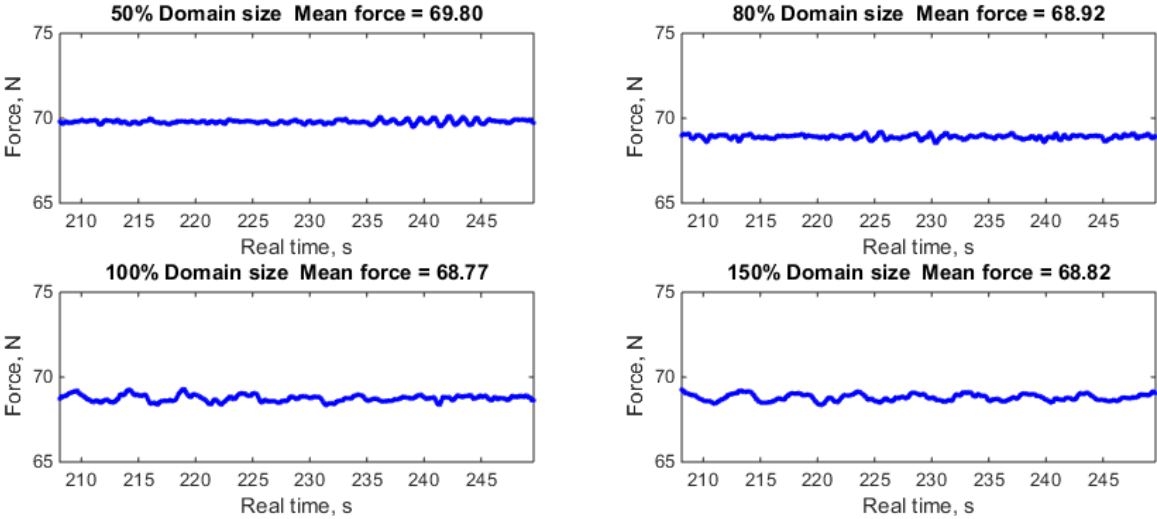


Figure 6-16 - Last 20% percentile of runtime - Domain

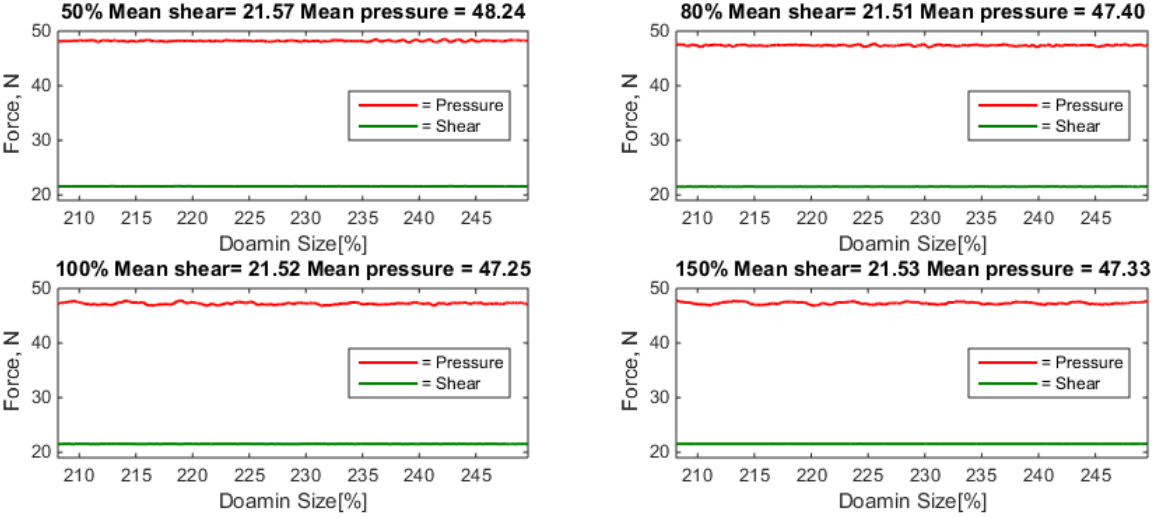


Figure 6-17 - last 20% of runtime shear and pressure - Domain

In Figure 6-18 mean force is plotted to the size of domain. One thing to notice is the small difference in mean force for all the simulations. It varies from 69.80N to 68.77N which is only a difference of 1.5%. This indicates that using the wrong domain may not ruin the simulation regarding forces on the hull, although there may be other negative effects on streamlines, waves, and flow field.

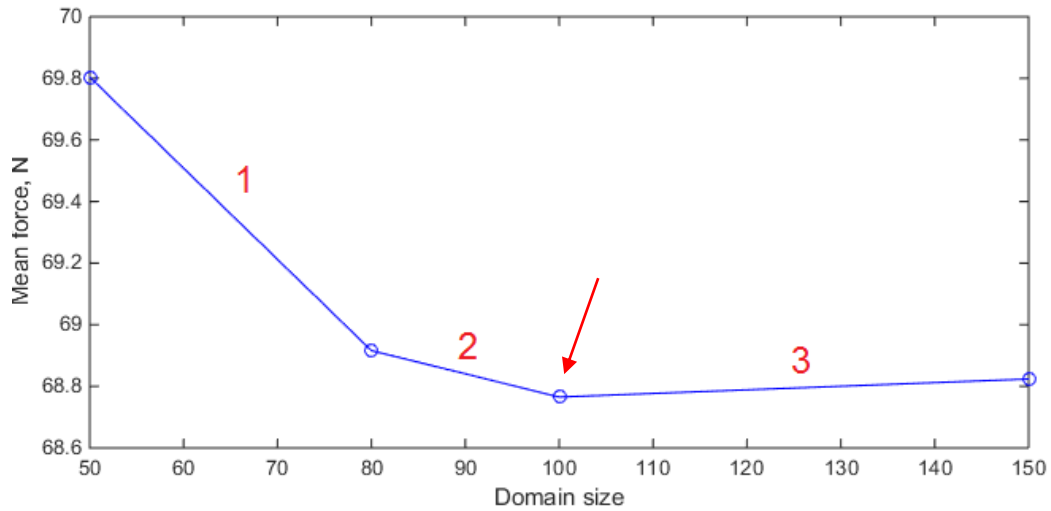


Figure 6-18 - Mean force vs domain size

Table 10 - Difference between domain sizes

Domain size	Interval	Difference [%]
50% - 80%	1	1.288
80% - 100%	2	0.219
100% - 150%	3	0.085

By looking at the mean force; 80, 100, and 150% domain is acceptable. But by observing the wake fields it is shown that the 80% domain might be too short in the aft of the ship to capture the wake. For this reason, it was decided upon sticking with the preliminary domain, 100%.

6.1.4 Summary of Convergence Study

From the convergence tests described in this chapter, an optimal simulations setup was found. All simulations showed good tendency to converge, and the thorough work done, strengthens confidence in the chosen setup. The resulting setup consists of base size of 0.18m with approximately 2 million cells, time step of 0.01s and the domain from Figure 6-19. This will be used for further analysis in this thesis.

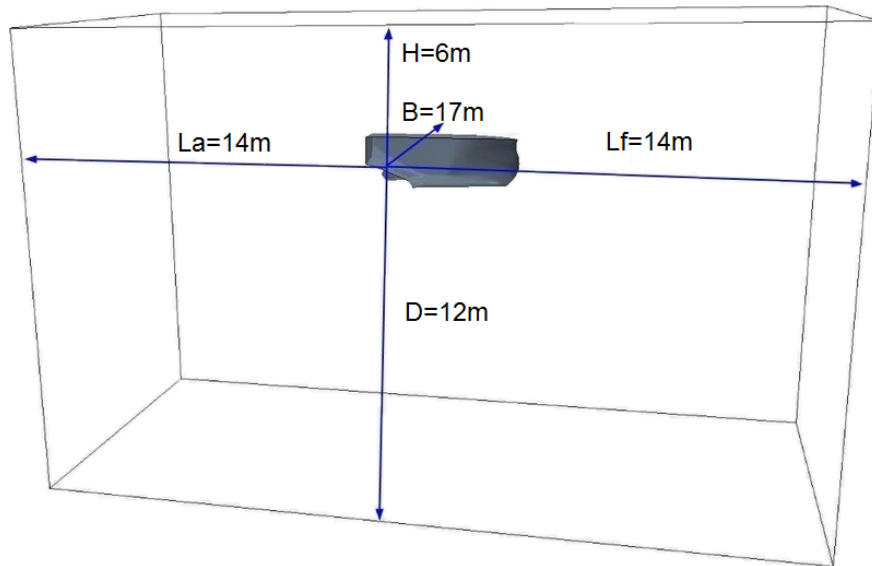


Figure 6-19 - Chosen domain

As mentioned in Chapter 5, the following analysis will cover trawl speed of 4 knots, and steaming speed of 10 knots. A total of eight simulations will be analyzed further. These involve the two hull designs, with different speeds, and with and without propeller-nozzle, as described in Figure 6-20.

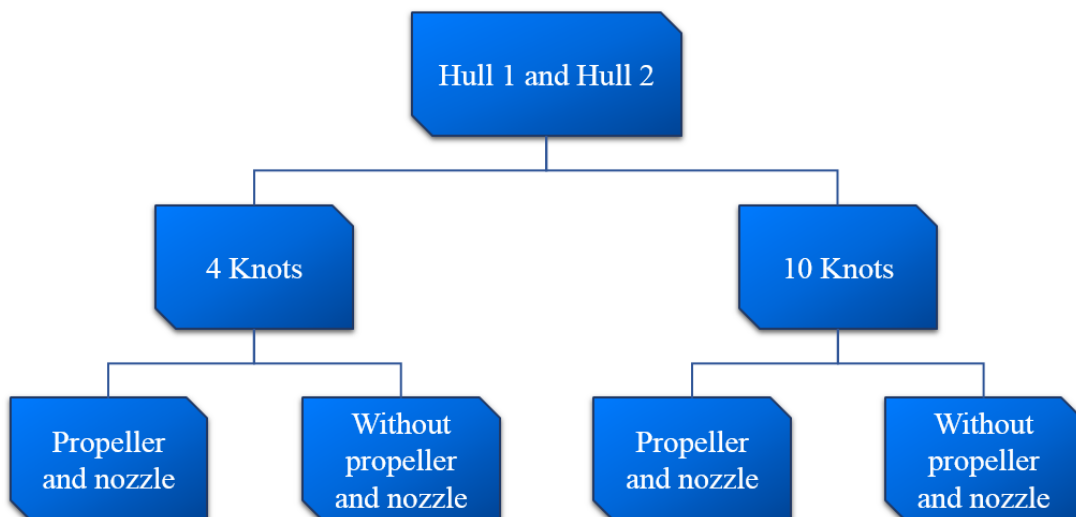


Figure 6-20 - Simulation hierarchy

Since the convergence study was performed with 12-knot full-scale speed, differences in CFL number and y^+ values is to be expected. CFL numbers are hard to keep below 1 at free surface setups. By using a tool called High-Resolution Interface Capturing (HRIC) courant numbers up to 25, is allowed (J. Scott, personal communication, May 14, 2015). CFL-low in HRIC was set to 50 and CFL-high set to 100. The preliminary obtained courant number is therefore sufficiently accurate. When setting up the final simulations change in the wall y^+ value must be accounted for. Wall y^+ value for the 10-knot simulation with mesh setup from the convergence study is shown in Figure 6-21. Large parts of the hull fall above y^+ value of 30, which is good, however maybe too much of the aft does not. In order to fix this, the stretching factor was reduced from 1.5 to 1.3 by trial and error. This resulted in a better coverage of y^+ values above 30 on the hull. Some sharp corners and surfaces still fall below a y^+ value of 30, but this is to be expected, see Section 0. The new wall y^+ value can be seen in Figure 6-22.

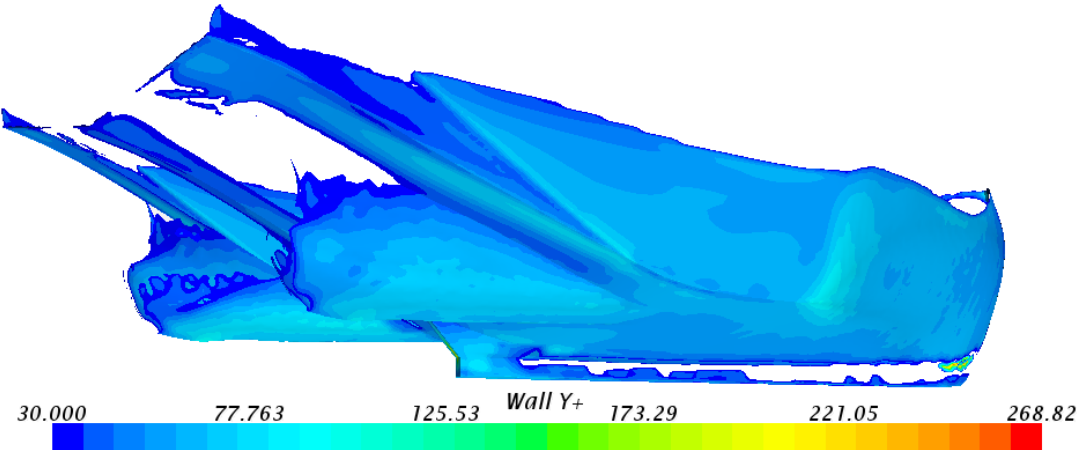


Figure 6-21 - wall y^+ value 10-knot mesh setup from convergence study

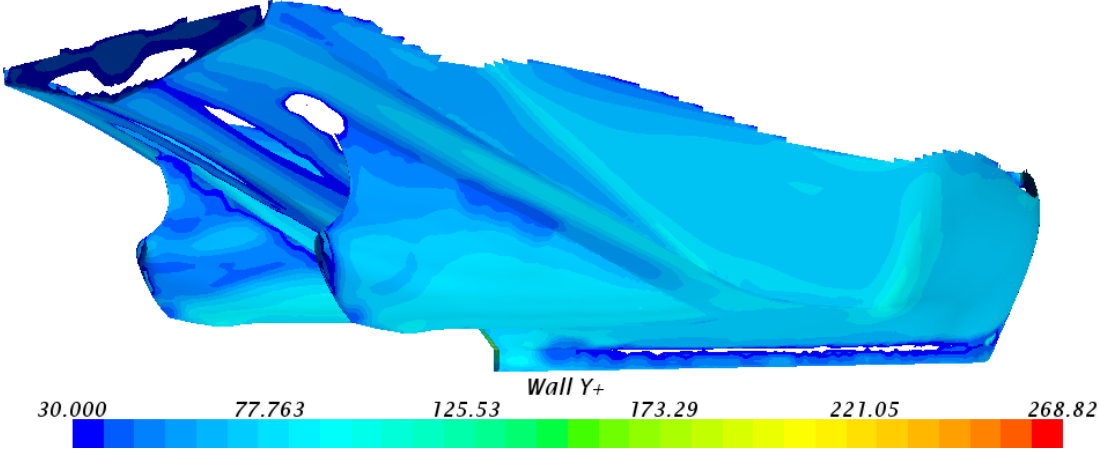


Figure 6-22 - wall y^+ value 10-knot new mesh setup

Figure 6-23 display the wall y^+ value at 4 knots with the same mesh setup as used above. Almost the whole hull have y^+ values which fall within the logarithmic blended region referring to Figure 4-4. To account for this the prism layer thickness was adjusted down from 0.03m to 0.01m, and the stretching from 1.5 to 1.7m. This was a result of meshing iterations performed. Figure 6-24 display the new y^+ value from this setup, where nearly all y^+ values fall below 5 where the viscous sub-layer is resolved.

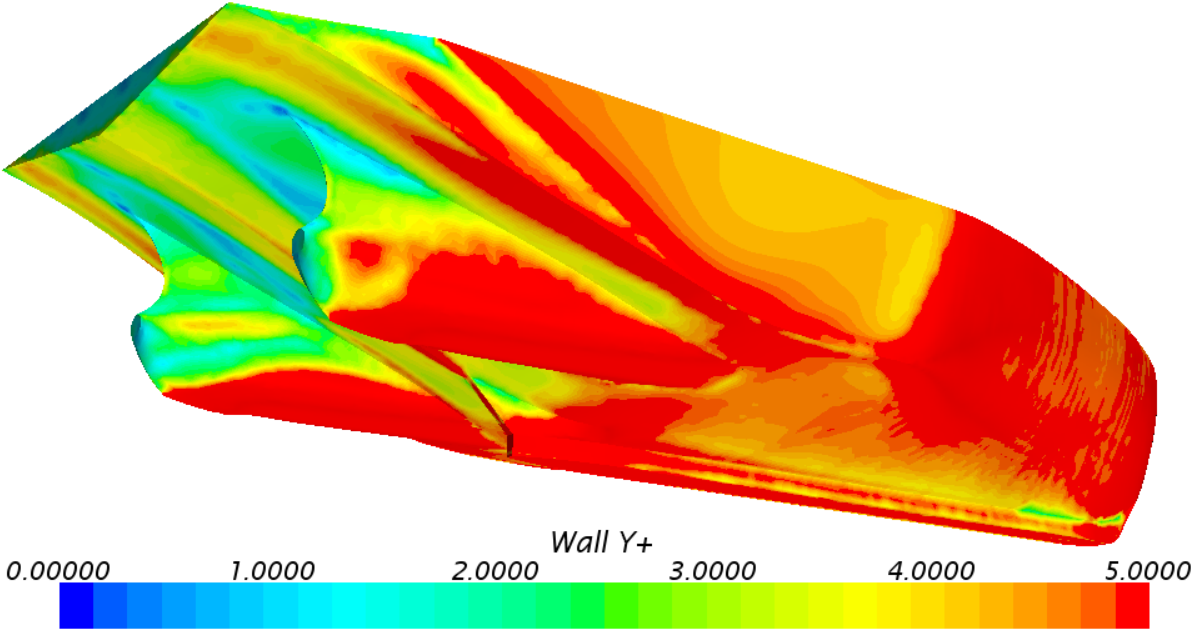


Figure 6-23 - Wall y^+ value 4 knots with mesh setup from convergence study

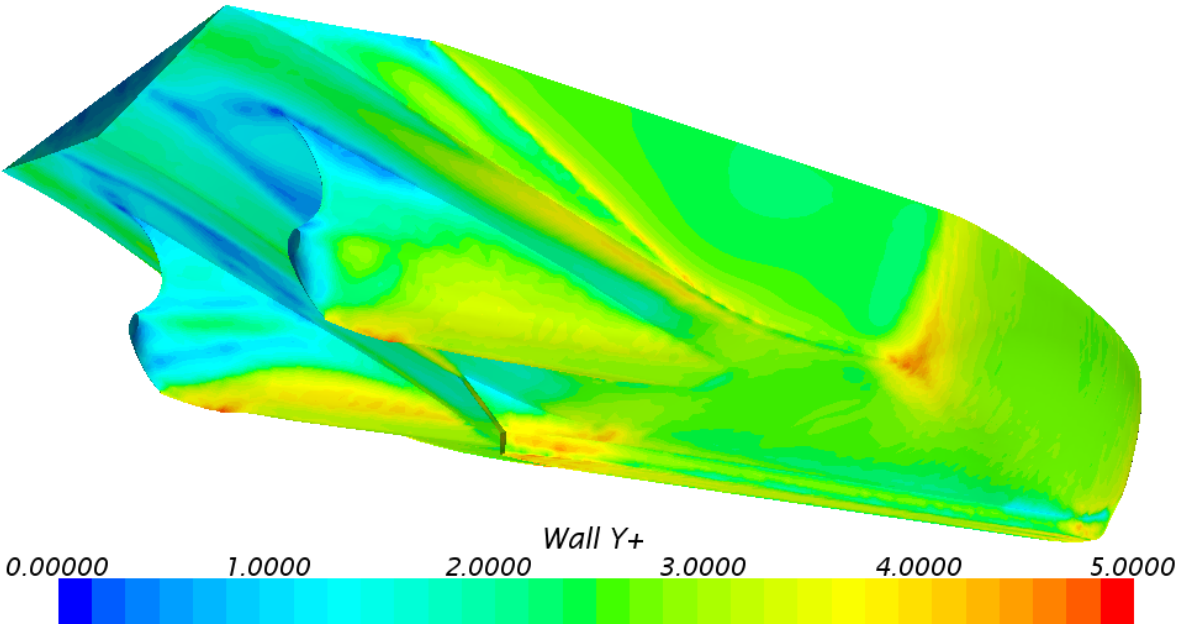


Figure 6-24 - Wall y^+ value 4 knots with final mesh setup

6.2 Results with Optimal Simulations Setup

In this section, results from the optimal simulation setup will be presented. This setup was found and described in the previous section. Some results are exported as .csv files from STAR CCM+ post processed in MatLab, other results are plotted directly in STAR with built in post processing tool and field functions.

6.2.1 Comparison of Dynamic Pressure

In the two figures below the dynamic pressure is observed, and compared between the two hulls at 10 knots. As anticipated the dynamic pressure is negative along the ship side, where the velocities are high, and higher where the velocities are low. A comparison between these hulls shows a difference in the aft shoulder. This is also where the difference in geometry can be found. Hull 1 show low pressure over the first sharp edge created by the chines, indicated by red circle. This coincides with suspicions discussed in Section 3.1.2. Hull 2, on the other hand, show a more uniform pressure over the aft shoulder. Same tendency can be seen in the simulation with nozzle and actuator disk, these can be found in Appendix F. The effect on the flow from this sharp edge where the pressure drops will be investigated in the next section.

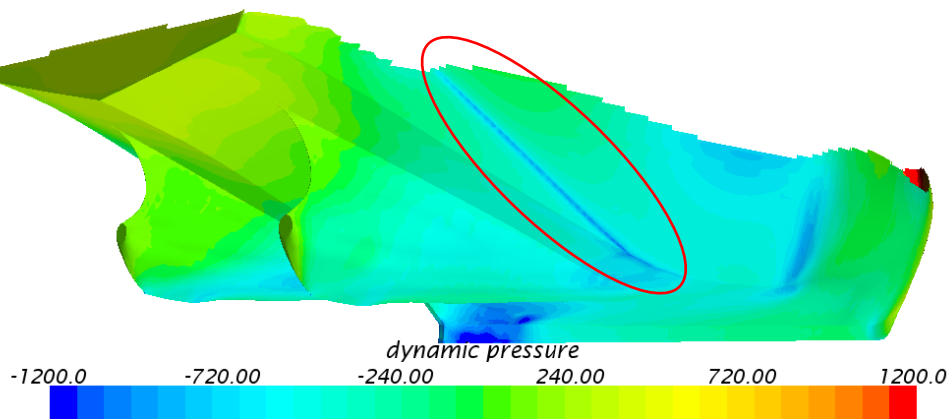


Figure 6-25 – Pressure [Pa], Hull 1 at 10 knots without nozzle and disk

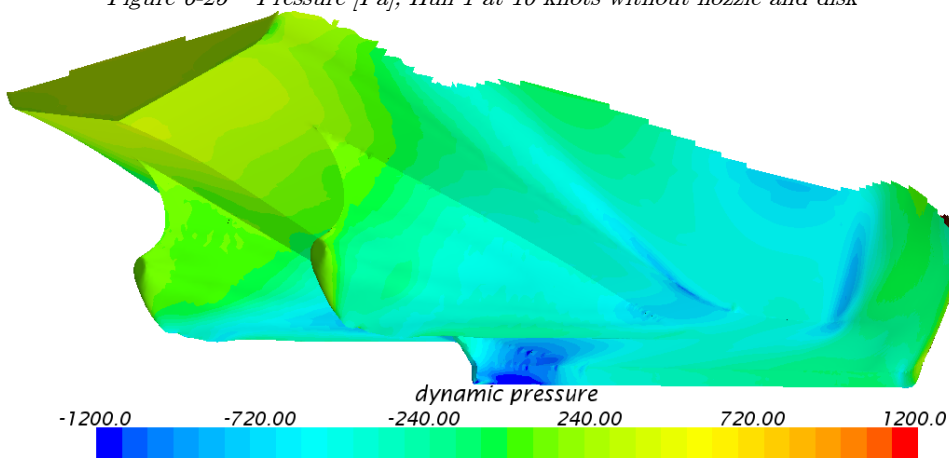


Figure 6-26 – Pressure [Pa], Hull 2 at 10 knots without nozzle and disk

6.2.2 Comparison of Vorticity

Effects on sharp edges can be seen in the flow pattern as vorticities. This is the case for the stern shape on Hull 1. Figure 6-27 and Figure 6-28 are showing vorticity on two waterlines, respectively -0.2m and -0.3m model scale, while Figure 6-29 and Figure 6-30 are showing the same, including nozzle and actuator disk. There are two interesting things to point out here. The first being that the vorticity increases with the depth of the measurement. This can be seen by comparing the two first figures. The second and most interesting phenomenon is the difference between the two hull designs. Each of the following figures displays the two hulls at the same water level, and Hull 1 consistently produce more vorticity than what Hull 2 does. This corresponds well to results from the previous section. A consequence of this can be increased resistance, due to the creation of these vorticities. However, what might be more crucial to this ship, is the disturbance in the inflow of the propeller wake field. This ship has large propellers working on high load which increases the risk of drag. For this reason, it is desirable to design a hull which produce the best possible wake field. These figures show that Hull 1 produce more vorticities at the aft shoulder than what Hull 2 does.

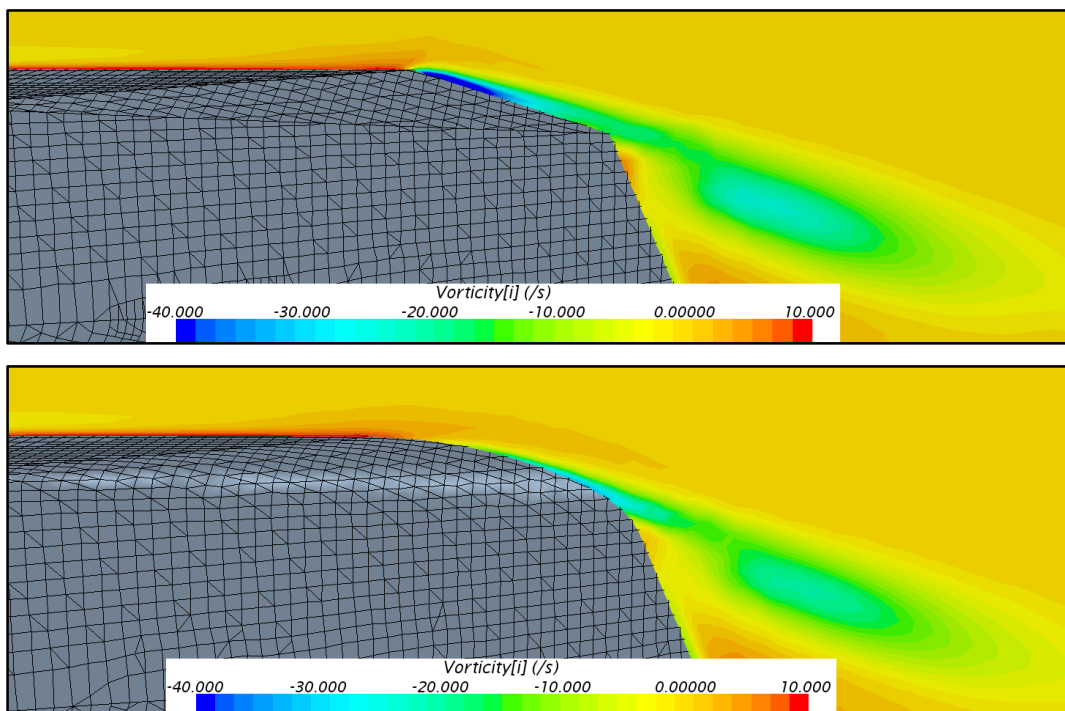


Figure 6-27 - Vorticity Hull 1 and 2 at 10 knots with nozzle and disk, -0.2m

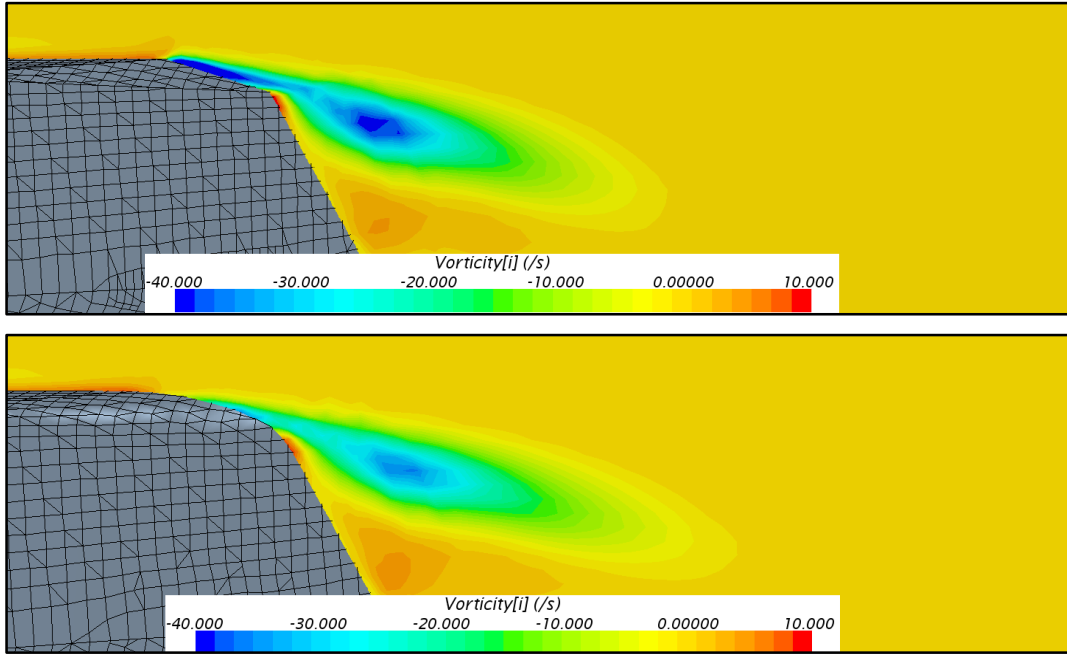


Figure 6-28 - Vorticity Hull 1 and 2 at 10 knots with nozzle and disk, -0.3m

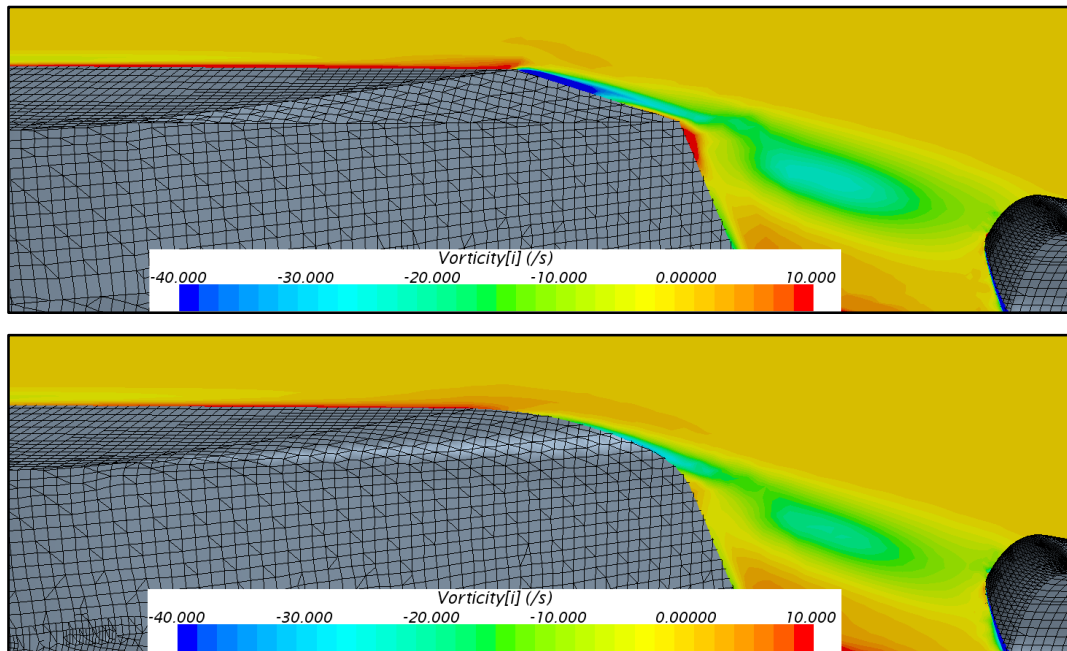


Figure 6-29 - Vorticity Hull 1 and 2 at 10 knots with nozzle and disk, -0.2m

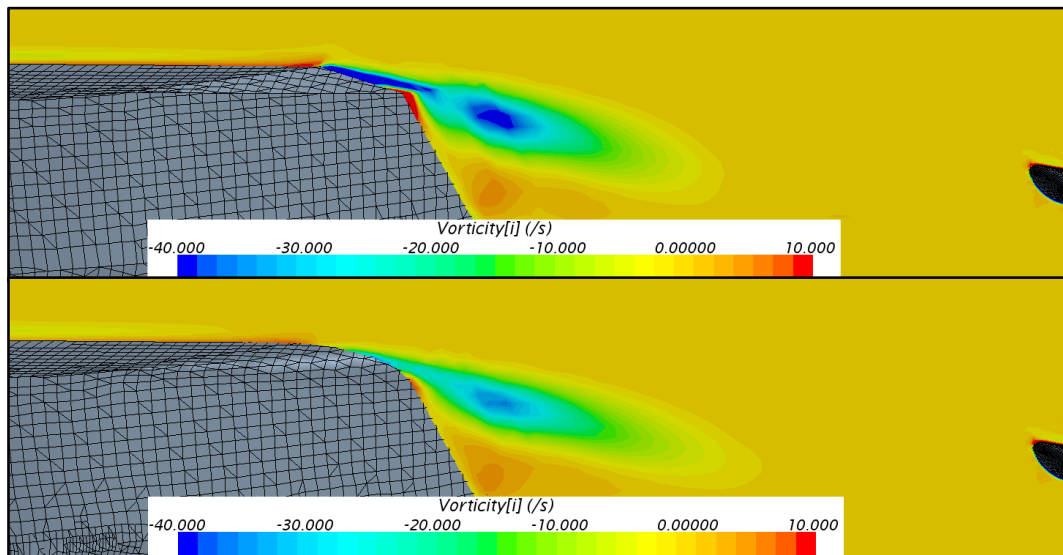


Figure 6-30 - Vorticity Hull 1 and 2 at 10 knots with nozzle and disk, -0.3m

Figure 6-29 indicates that the vorticities may influence the propeller wake field. In order to investigate whether this is the case, the vorticity is plotted onto a plane 0.02m in front of the propeller. It is plotted in front of the propeller plane to avoid influences from the actuator disk. The two following figures are taken from the simulations with nozzle and actuator disk of Hull 1 and Hull 2. Here, one clearly sees that the vorticity from the shoulder still has an effect on the propeller inflow. When comparing them, it can also be seen that the vorticity at Hull 1 has greater red zones both at the outer parts and at the hub. The blue zone with negative vorticity is also more prominent on the propeller plane on Hull 1 than what can be seen on Hull 2. This corresponds well with what is discussed above. Vorticity can also be seen in the simulations without nozzle and propeller, see Appendix G for plots. However, they are smaller and almost identical. Why they appear better on the simulations with nozzle and disk may be explained by the suction created by the actuator disk, although this is not investigated further.

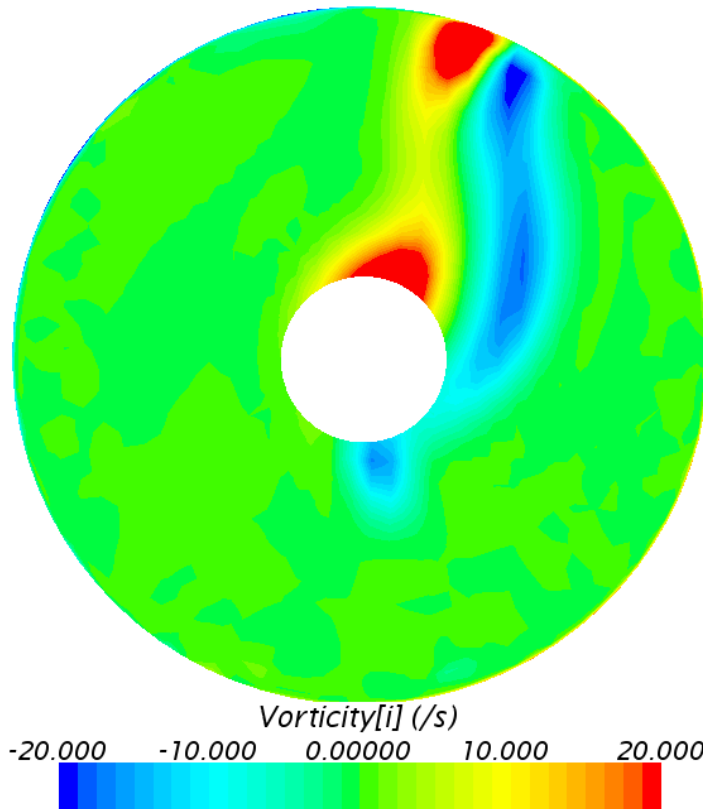


Figure 6-31 - Vorticity propeller plane Hull 1 at 10 knots with nozzle and disk

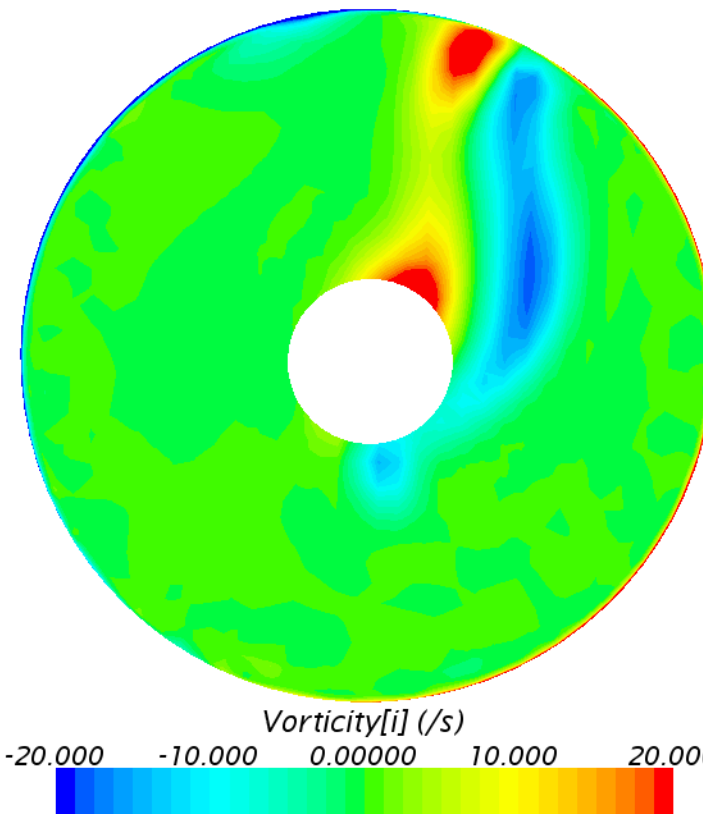


Figure 6-32 - Vorticity propeller plane Hull 2 at 10 knots with nozzle and disk

6.2.1 Axial Velocity

The axial velocity is plotted onto the same plane as used in section above. In Figure 6-33 and Figure 6-34 the nominal axial velocity can be seen. These are obtained from the simulations without nozzle and actuator disk. By observing the blue area, which correspond to low axial velocity, one may see that velocities are lower in the propeller plane for Hull 1 than what they are for Hull 2. This may lead to an increased wake fraction, as shall be discussed in the next section. The same result can also be seen in Figure 6-35 and Figure 6-36 to some extent. Note that velocity plots with virtual disk includes propeller induced velocities, which has not been covered in this thesis due to the complexity of calculation and restricted time-frame. For this reason, effective wake will not be covered in this thesis.

From the simulations at 10 knots, smaller differences can be seen between the two hull designs. For this reason it is expected that the difference in nominal wake field will be larger for the 4 knots simulations, than for the 10 knots simulation.

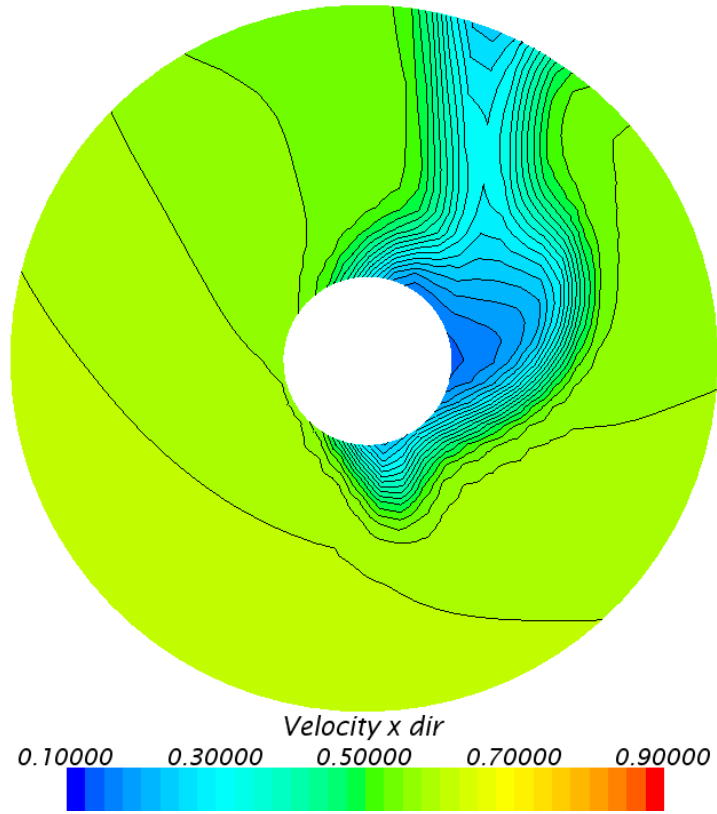


Figure 6-33 - Axial velocity Hull 1 at 4 knots without nozzle and disk

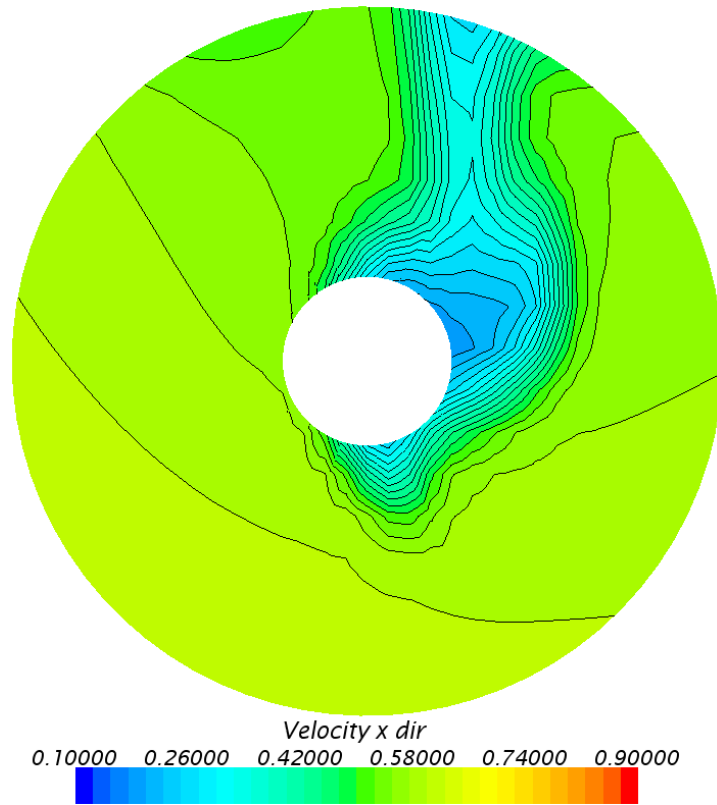


Figure 6-34 - Axial velocity Hull 2 at 4 knots without nozzle and disk

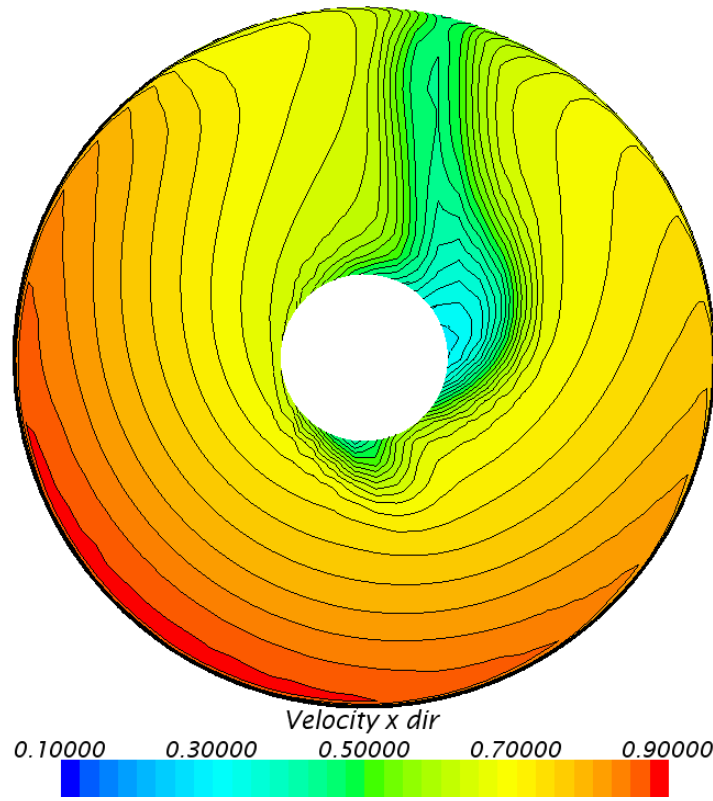


Figure 6-35 - Axial velocity Hull 1 at 4 knots with nozzle and disk

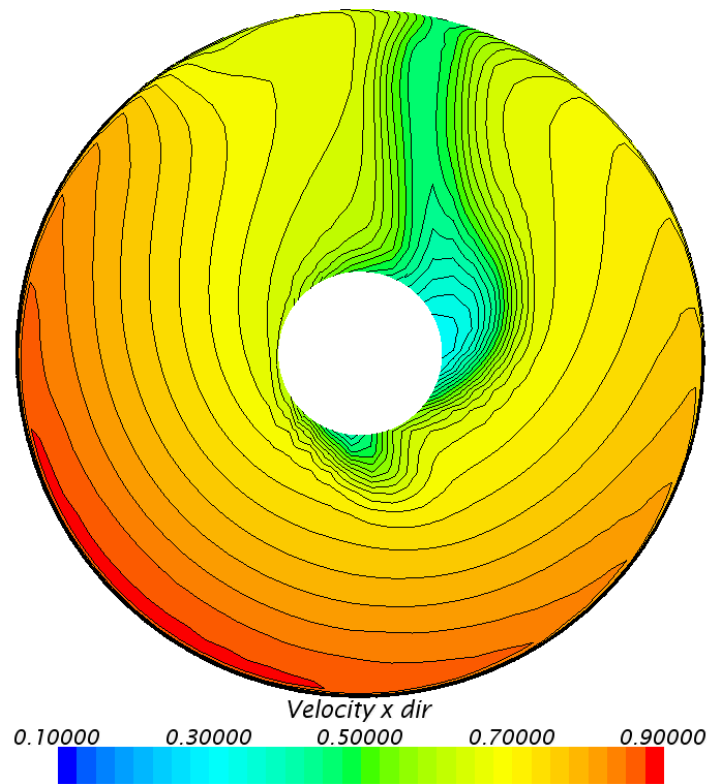


Figure 6-36 - Axial velocity Hull 2 at 4 knots with nozzle and disk

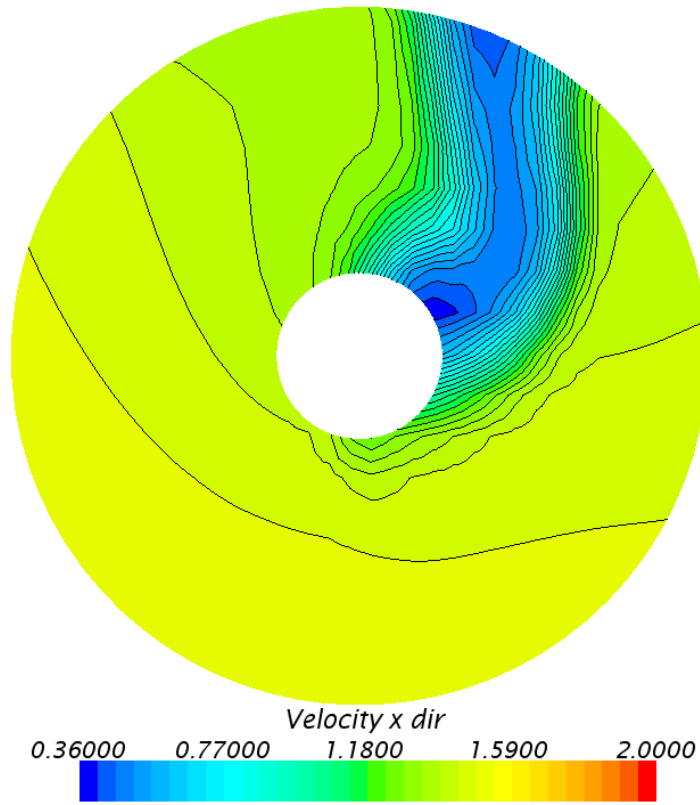


Figure 6-37 - Axial velocity Hull 1 at 10 knots without nozzle and disk

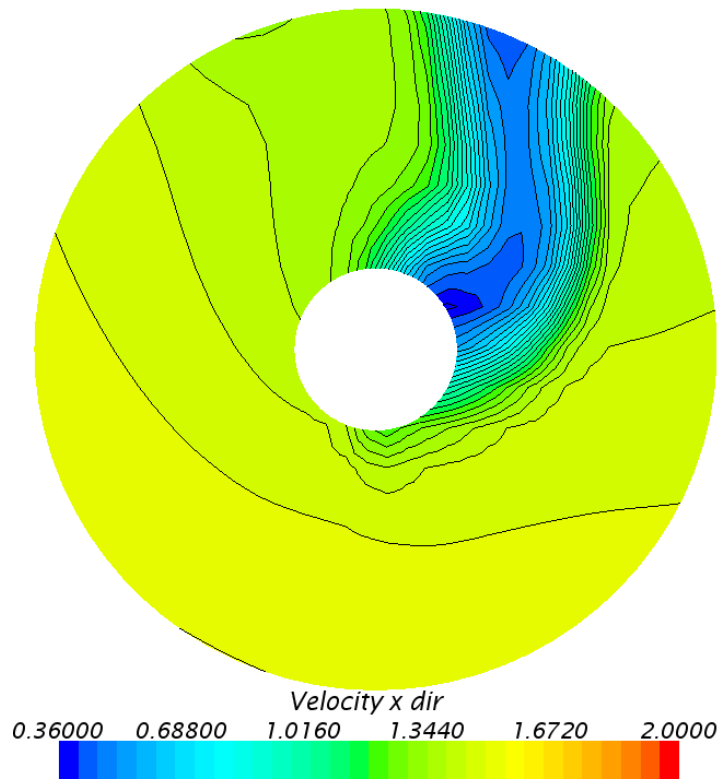


Figure 6-38 - Axial velocity Hull 2 at 10 knots without nozzle and disk

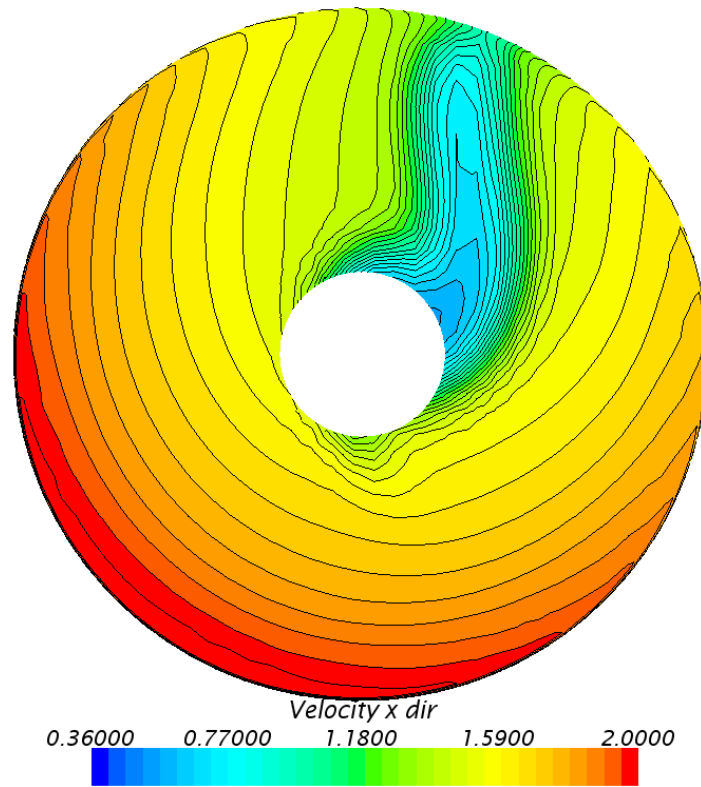


Figure 6-39 - Axial velocity Hull 1 at 10 knots with nozzle and disk

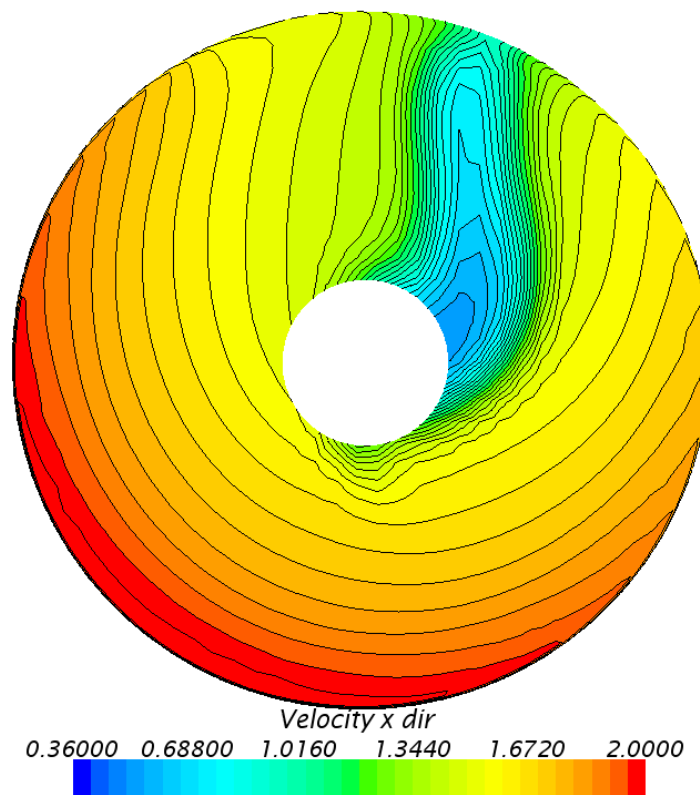


Figure 6-40 - Axial velocity Hull 2 at 10 knots with nozzle and disk

6.2.2 Wake field

As described in Section 4.17, the wake field is also an important factor when observing the inflow on the propeller plane. From the following four figures, the nominal wake is plotted on a plane 0.02m in front of the actuator disk. Figure 6-41 display the propeller wake field on Hull 1 while Figure 6-42 on Hull 2, both at 4 knots full-scale speed. When comparing them, they show a difference in the upper right section of the propeller plane. The wake field from Hull 1 show a larger area, with darker colors than what is visible from Hull 2. Turning to the results from the 10 knots simulations, the same trend can be seen. Hull 1 show a somewhat broader band of higher wake values than what is seen from Hull 2, although the difference at 10 knots is less compared to the 4 knots simulations. This corresponds well with what was shown in the previous section. This suggests that at Hull 2 may have a better propeller wake field with higher axial velocities than what Hull 1 does.

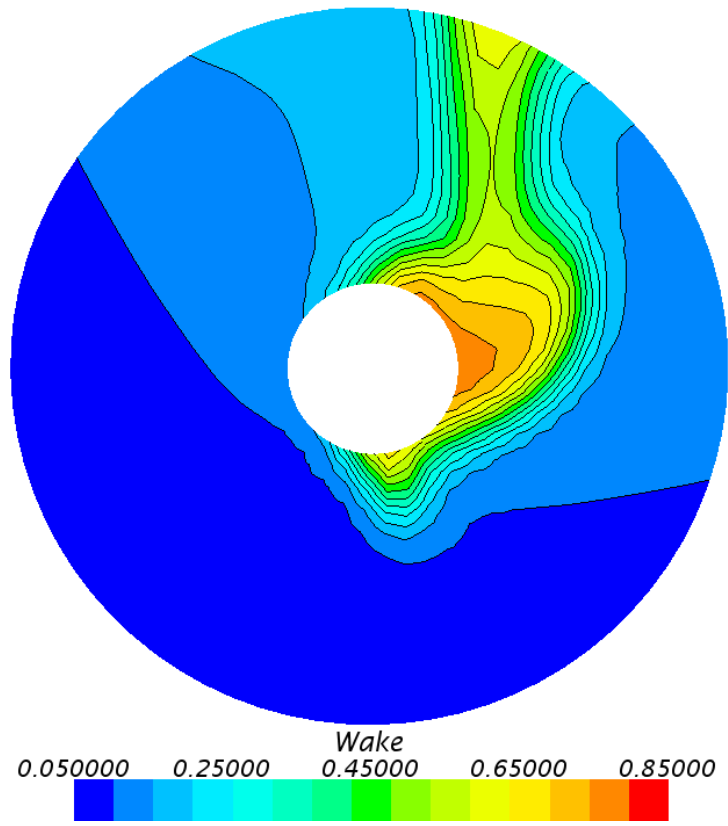


Figure 6-41 - Nominal wake field Hull 1 at 4 knots

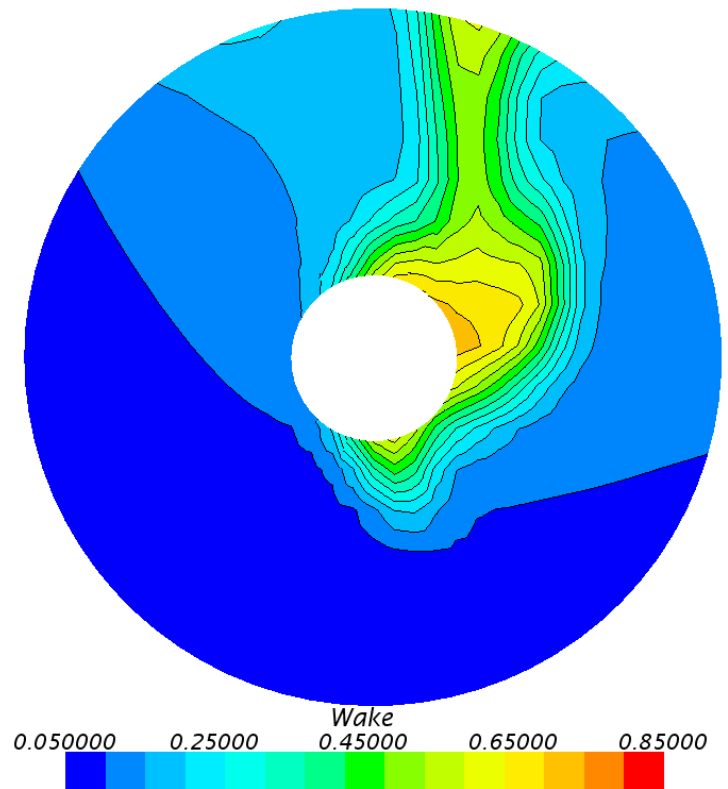


Figure 6-42 - Nominal wake field Hull 2 at 4 knots

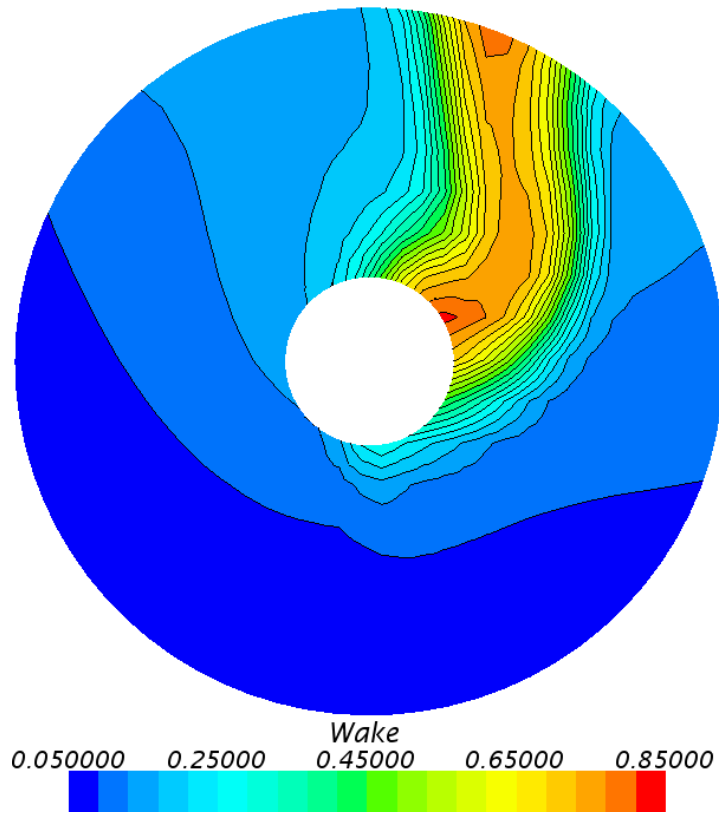


Figure 6-43 - Nominal wake field Hull 1 at 10-knots

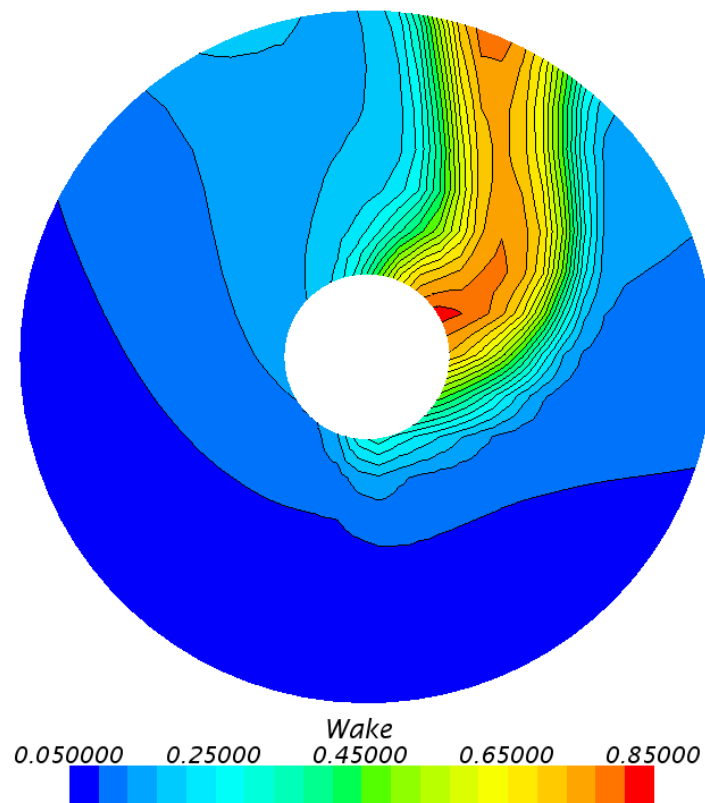


Figure 6-44 - Nominal wake field Hull 2 at 10-knots

6.2.3 Tangential Velocity

In Figure 6-45 the tangential velocities from Hull 2 without nozzle and disk can be viewed. In Section 6.2.3 the propeller rotation direction was chosen based on results from the project thesis (Svoren, 2014). Results from simulations in this master's thesis show tangential velocities as viewed in the figure below. The view of this plot is seen from the back and forth. The parts with highest tangential velocities have a rotation clockwise and covers about half of the propeller area. This backs up the counter-clockwise rotational direction chosen in section 6.2.3. Tangential velocities from the remaining simulations can be found in Appendix I.

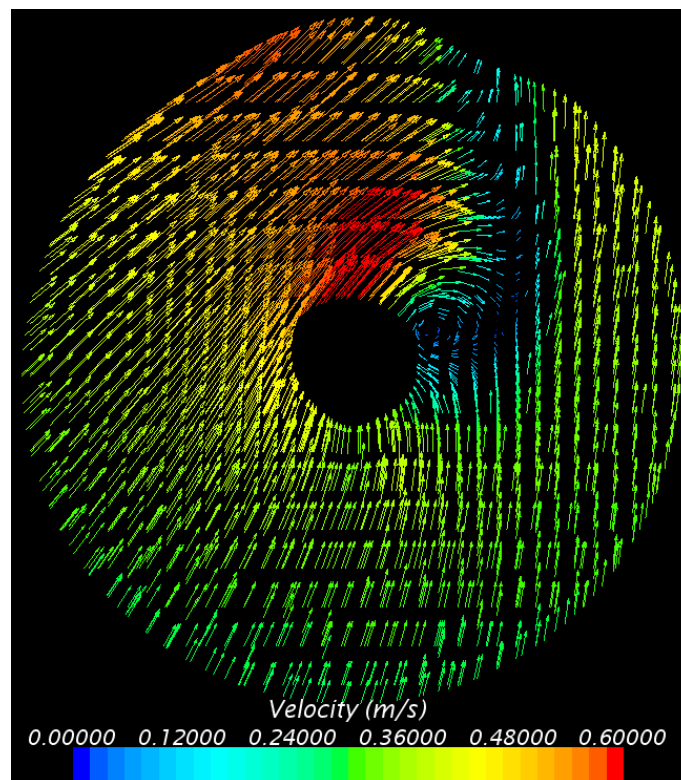


Figure 6-45 - Tangential velocity Hull 2 at 10 knots

6.2.4 Dynamic Pressure

As cavitation is of concern for this ship and ships in general (Section 3.1.3), the pressure field on the propeller plane should be looked at. In the following figures, the dynamic pressure is plotted on the same plane as the wake field for Hull 2. As anticipated, the pressure increases towards the inside if the skeg while it decreases towards static pressure on the outside of the propeller. No significant differences can be seen on the pressure field between the two hull designs, see Appendix J for dynamic pressure from Hull 1.

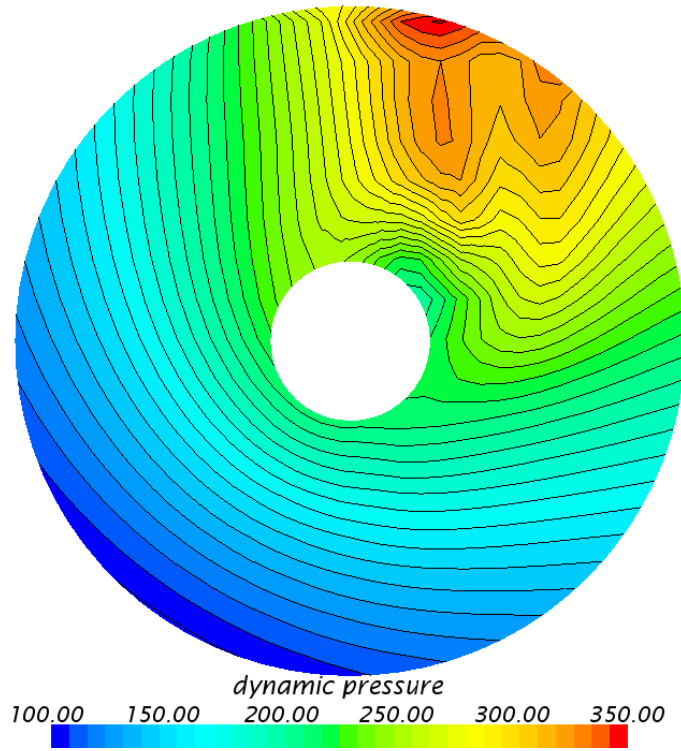


Figure 6-46 - Dynamic pressure [Pa] Hull 2 without nozzle and disk at 10 knots

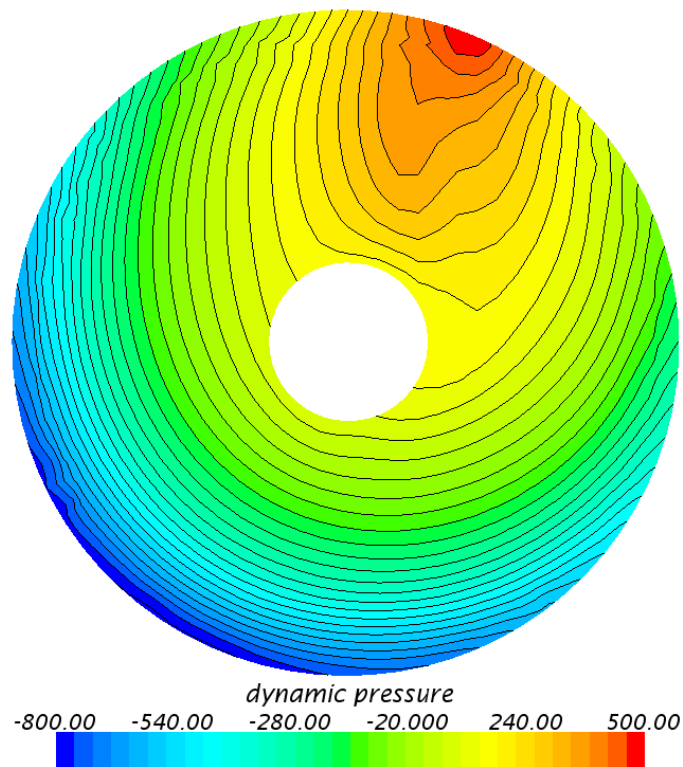


Figure 6-47 - Dynamic pressure [Pa] Hull 2 with nozzle and disk at 10 knots

6.2.5 Streamlines

In this section, the streamlines are going to be investigated. The path of a water particle is plotted as a line corresponding to the path it has taken, and a color corresponding to the velocity it had. Figure 6-48 show streamlines on Hull 1 at 4 knots. In the first picture, one may see a swirl of low-velocity particles on the inside of the skeg. This is not favorable, as it might disturb the wake field for the propeller. On the second picture, we can see that the suction from the virtual disk helps “clean” this area and create a better inflow plane. There are still some low-velocity areas left, but considerable better than shown in the simulation without the virtual disk. This trend was seen visible equal on both Hulls. Streamlines from Hull 2 can be found in Appendix H.

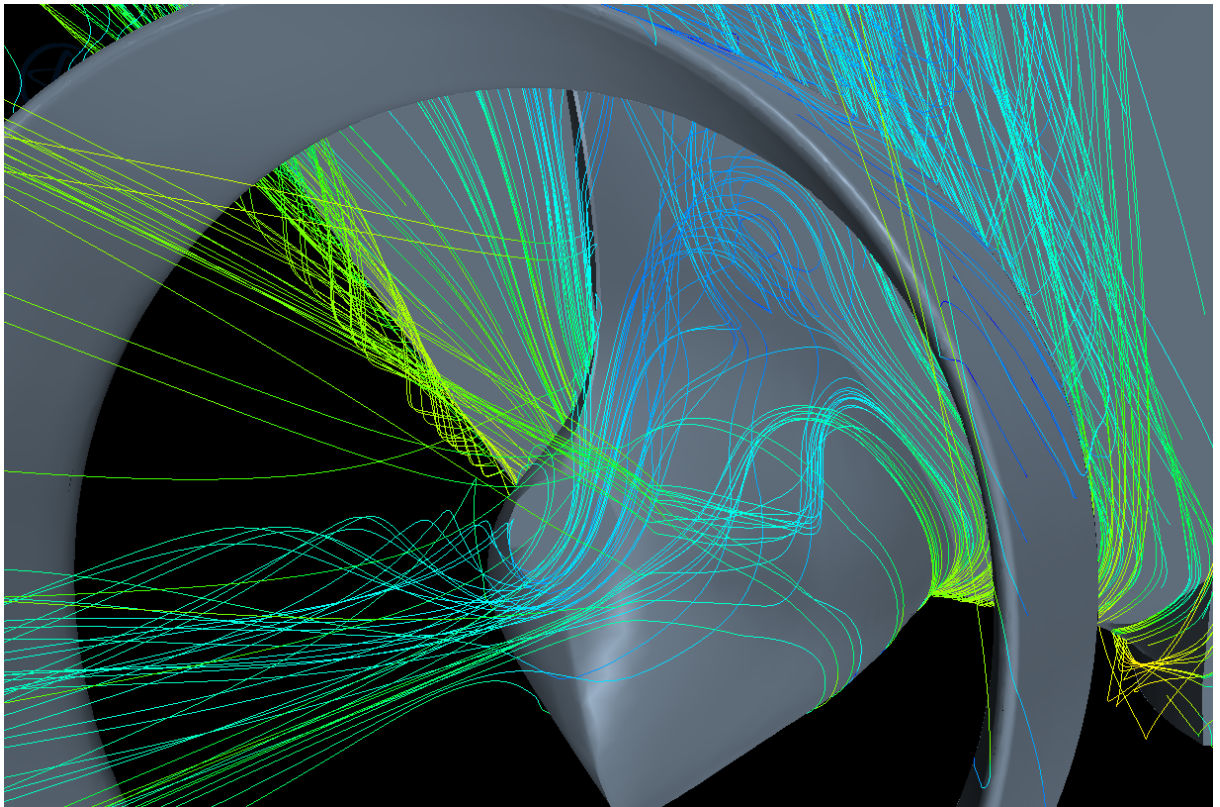
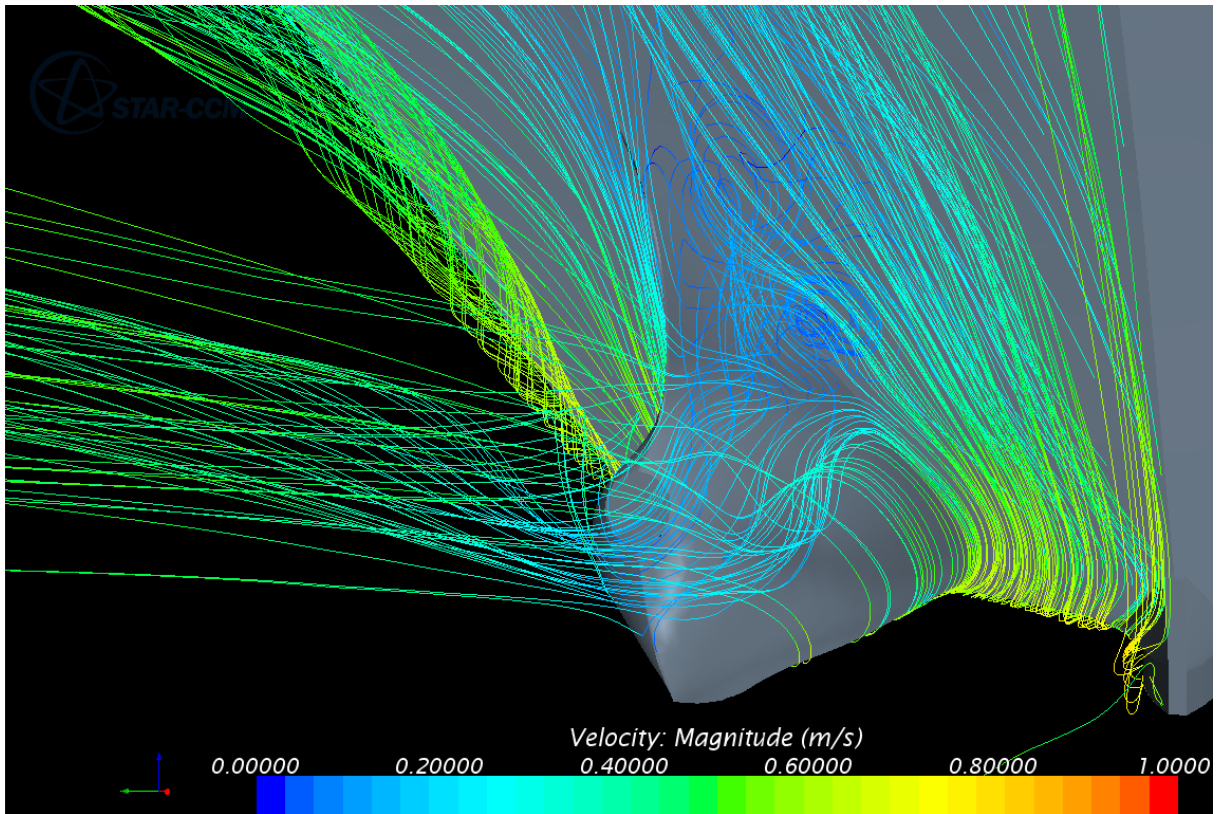


Figure 6-48 - Streamlines Hull 1, at 4 knots without and with propeller and nozzle

In the two plots below one may see the difference in flow over the nozzle between the two hulls. A swirl of water gathers on top of the nozzle on Hull 1.

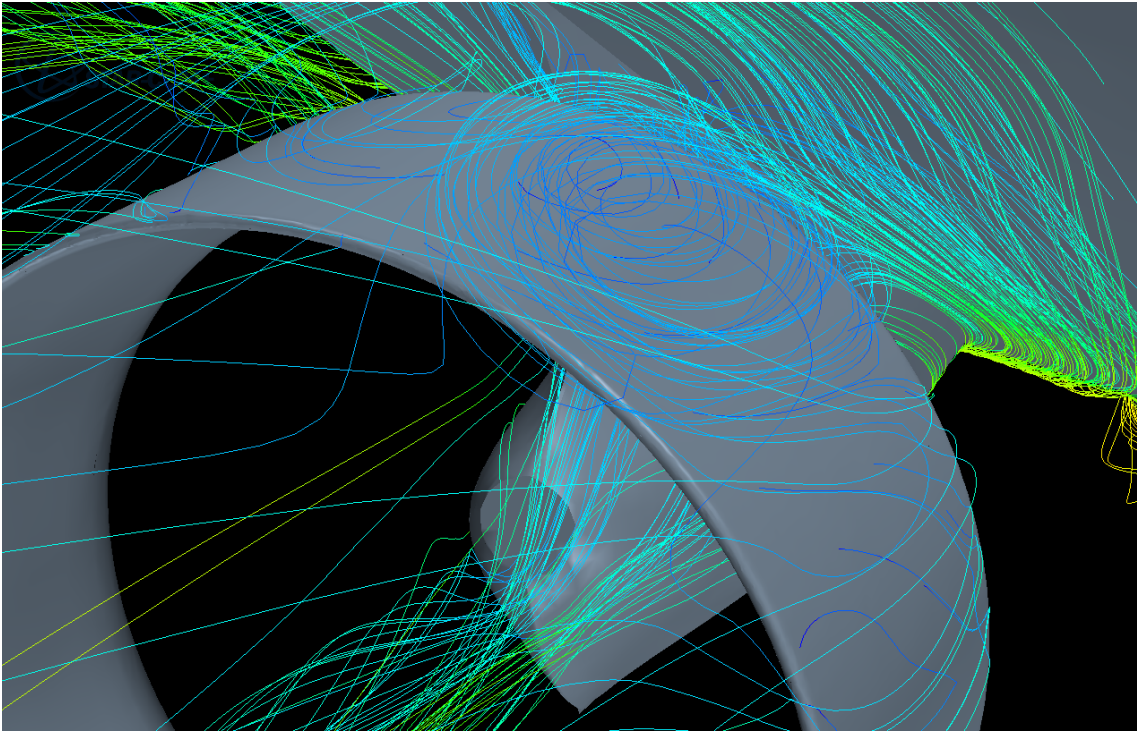


Figure 6-49 - Streamlines Hull 1, at 4 knots with propeller and nozzle, top of nozzle

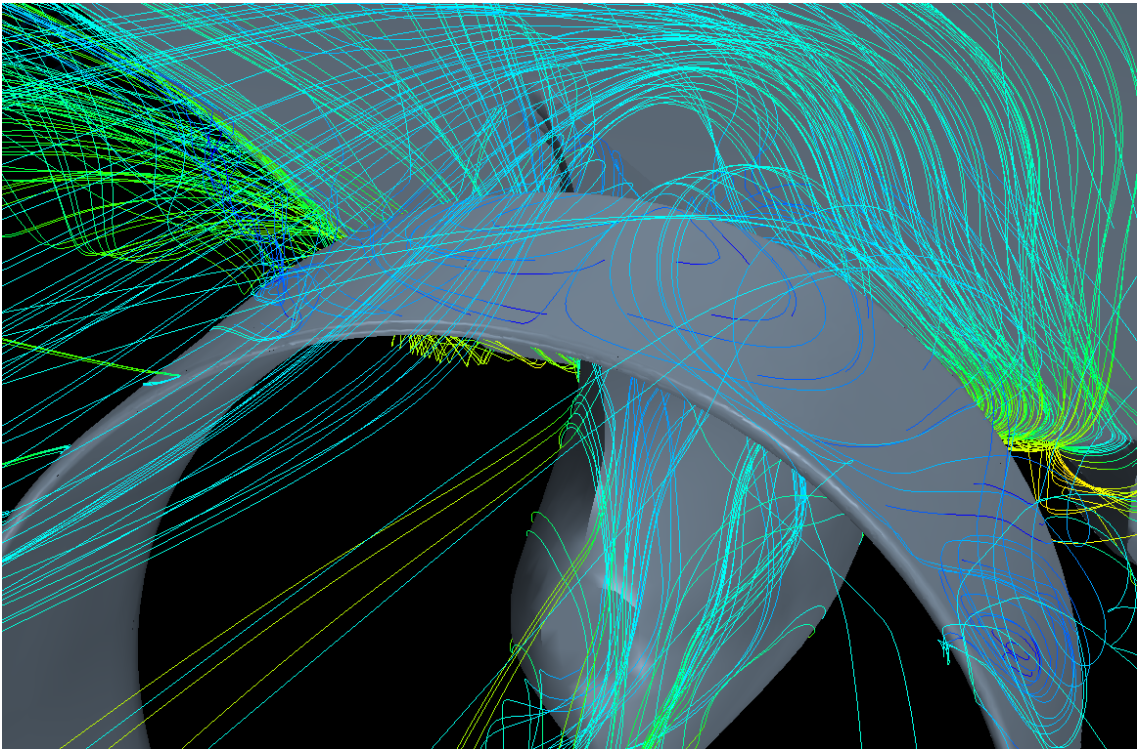


Figure 6-50 - Streamlines Hull 2, at 4 knots with propeller and nozzle, top of nozzle

This effect can also be seen on Hull 2, but rotating around a different axis. Stagnation points on top of the nozzles can be seen in Figure 6-51 and Figure 6-52. Exactly what causes these differences between the two designs are yet to be determined.

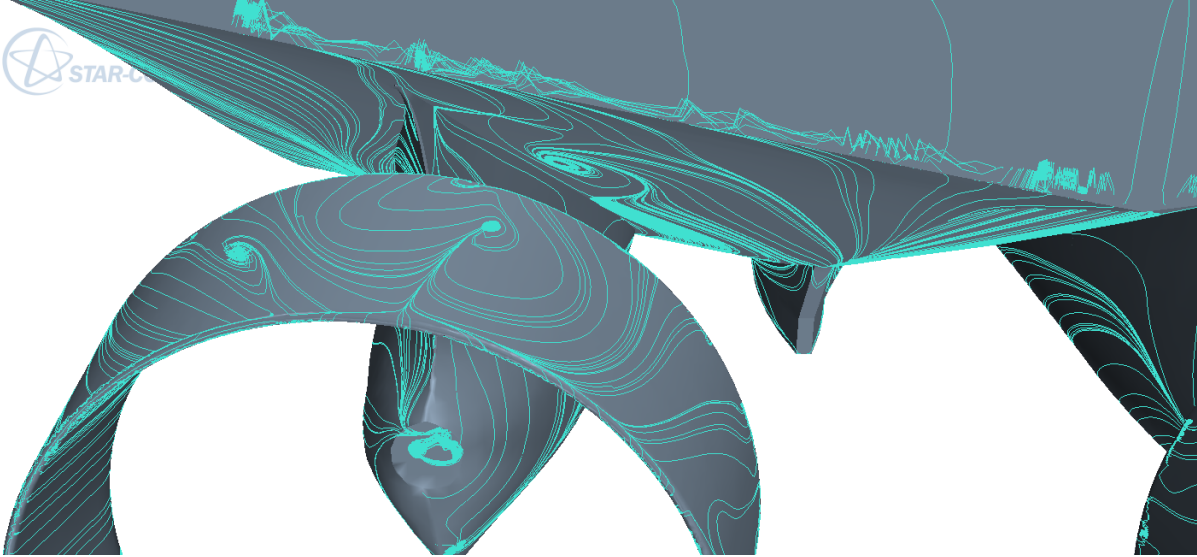


Figure 6-51 - Streamlines showing particle path on top of nozzle, Hull 1 at 4 knots

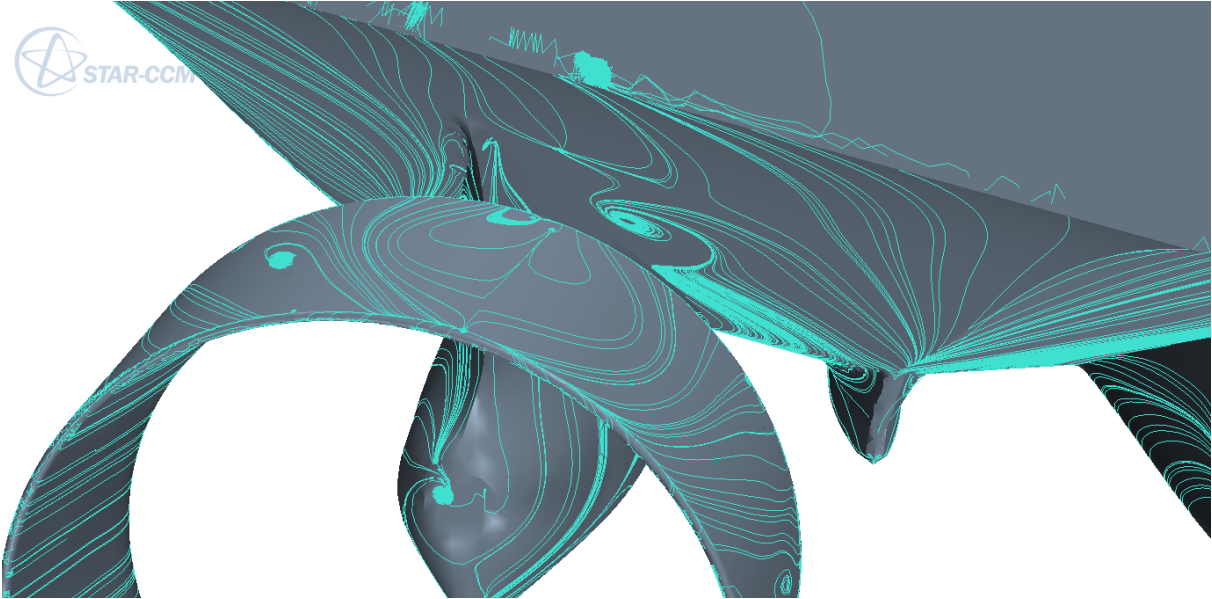


Figure 6-52 - Streamlines showing particle path on top of nozzle, Hull 2 at 4 knots

Figure 6-53 display streamlines at Hull 1 from the 10 knots simulations. Similar to the 4 knots simulation, a swirl on the inside of the skeg was found here, only bigger. This swirl also settled to some extent, yet low velocities can be still found. Figures from the remaining simulations can be seen in Appendix H.

An identical effect was also visible in the simulations from the project thesis leading up to this master's thesis. In a meeting with all involved parties of this research project, these problems were brought up, and discussed. Possible solutions to this problem would be to adjust the skeg angle, shape, and/or width, as mentioned in Section 3.1.3. This was nevertheless not prioritized in this master's thesis.

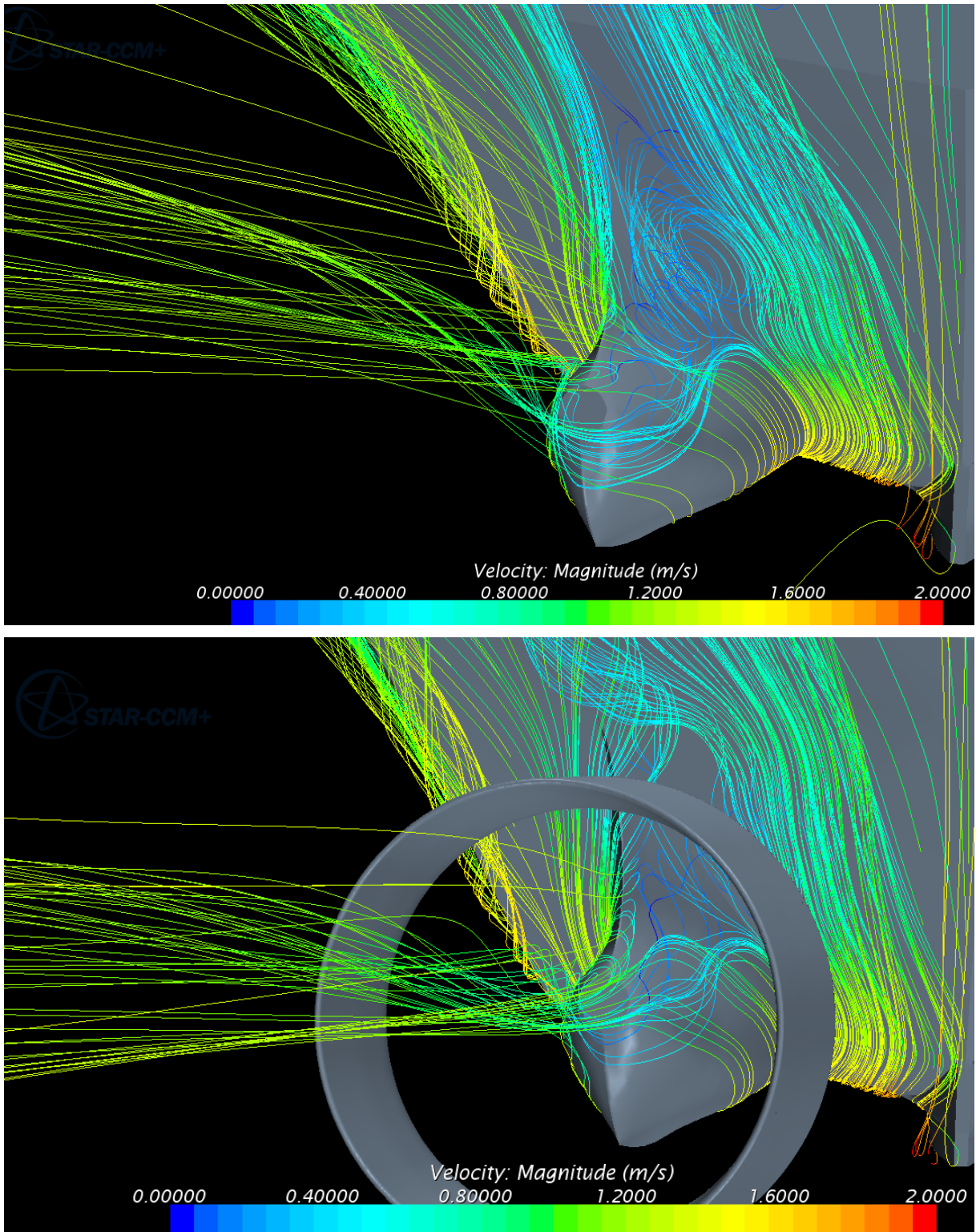


Figure 6-53 - Streamlines Hull 1, at 10 knots without and with propeller and nozzle

The two figures below display the streamlines along the surface of the hull. One may see that the swirl on the inside of the skegs is smaller in the second figure with nozzle and disk. This agrees well with the figure above. Equal figures for Hull 2 can be found in Appendix H.

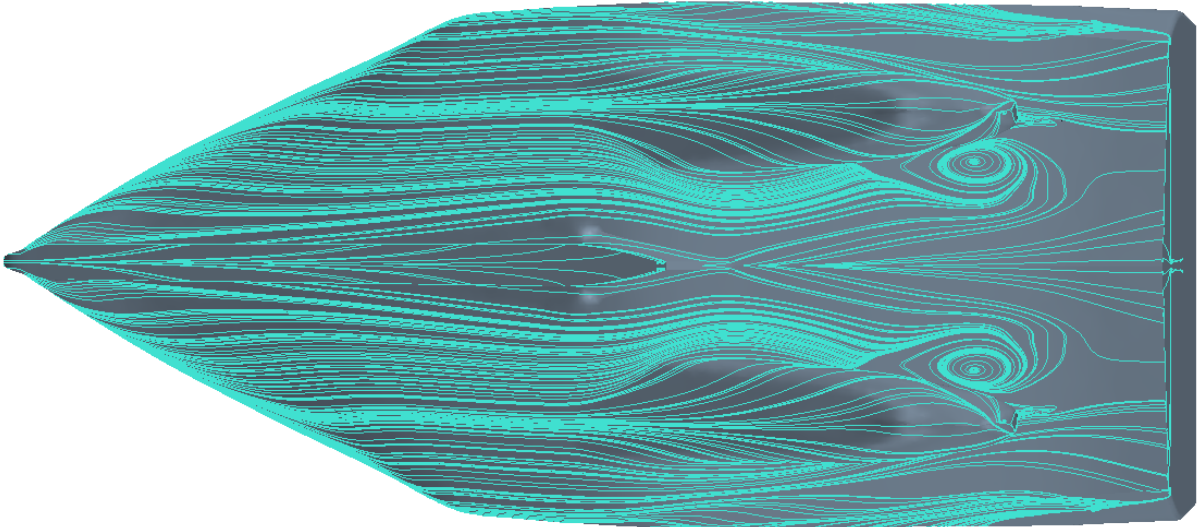


Figure 6-54 - Streamlines Hull 1 at hull surface without propeller and nozzle, 10 knots

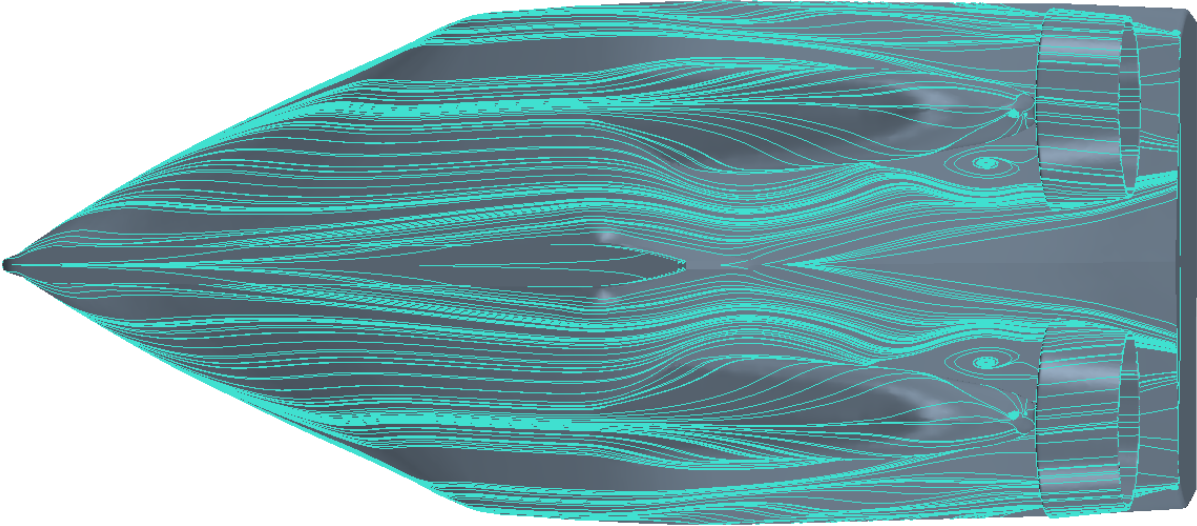


Figure 6-55 - Streamlines Hull 1 at hull surface with propeller and nozzle, 10 knots

6.2.1 Wave pattern Hull 1

Below the wave pattern and wave elevation is plotted for Hull 1 at 10 knots full scale. A nice wake pattern can be seen with a maximum elevation at the bow of 0.125 meters, and minimum trough of -0.085 meters. This is equivalent to 1.25m and 0.85m full scale.

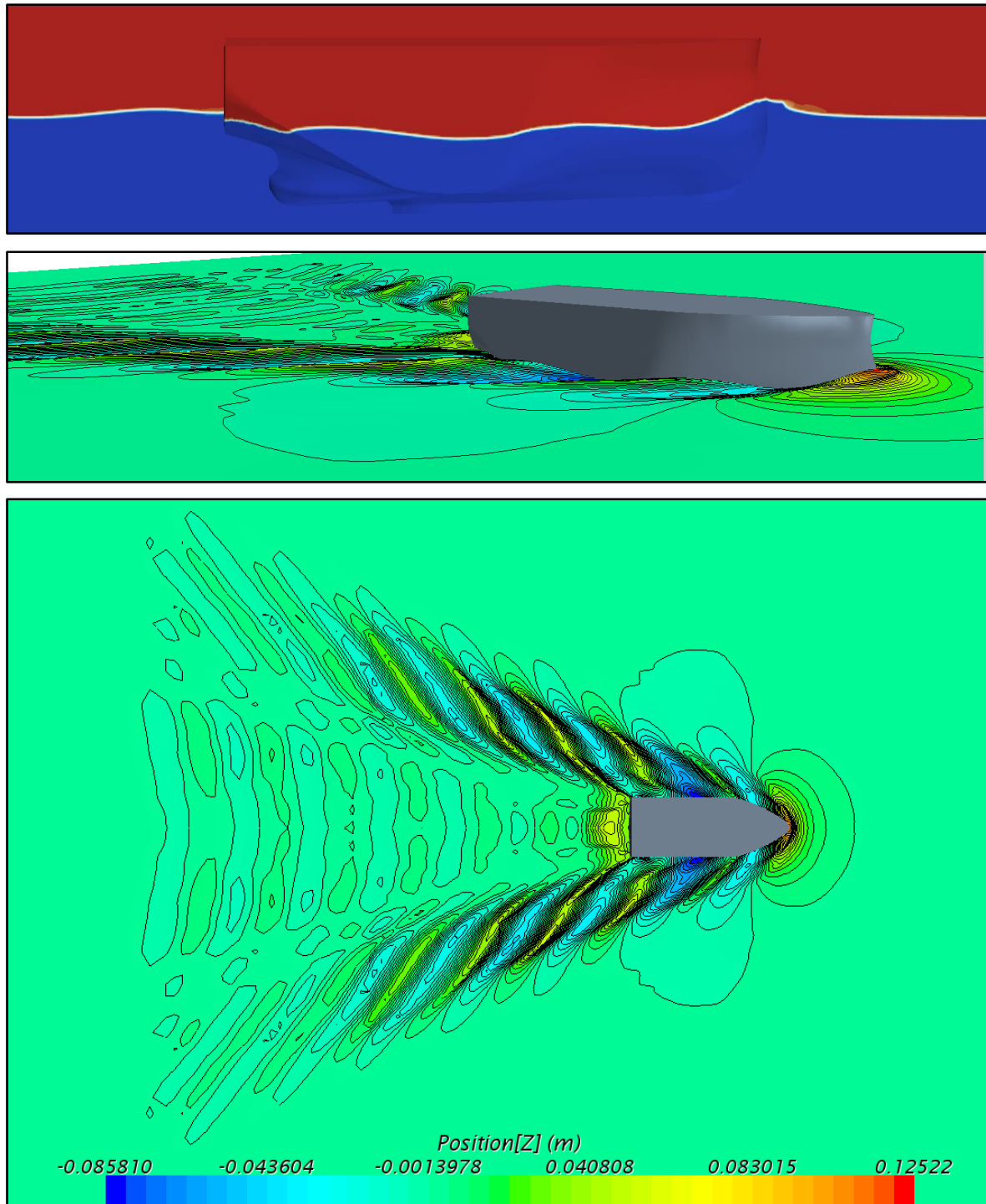


Figure 6-56 - Wave elevation and pattern, Hull 1 at 10 knots

6.2.1 Wave Pattern Hull 2

The wave pattern of Hull 2 are similar to the one of Hull 1, except for the max value which is slightly higher. There is no reason to believe this is a result of changes made to the stern, rather than a result of time at which the plot was taken.

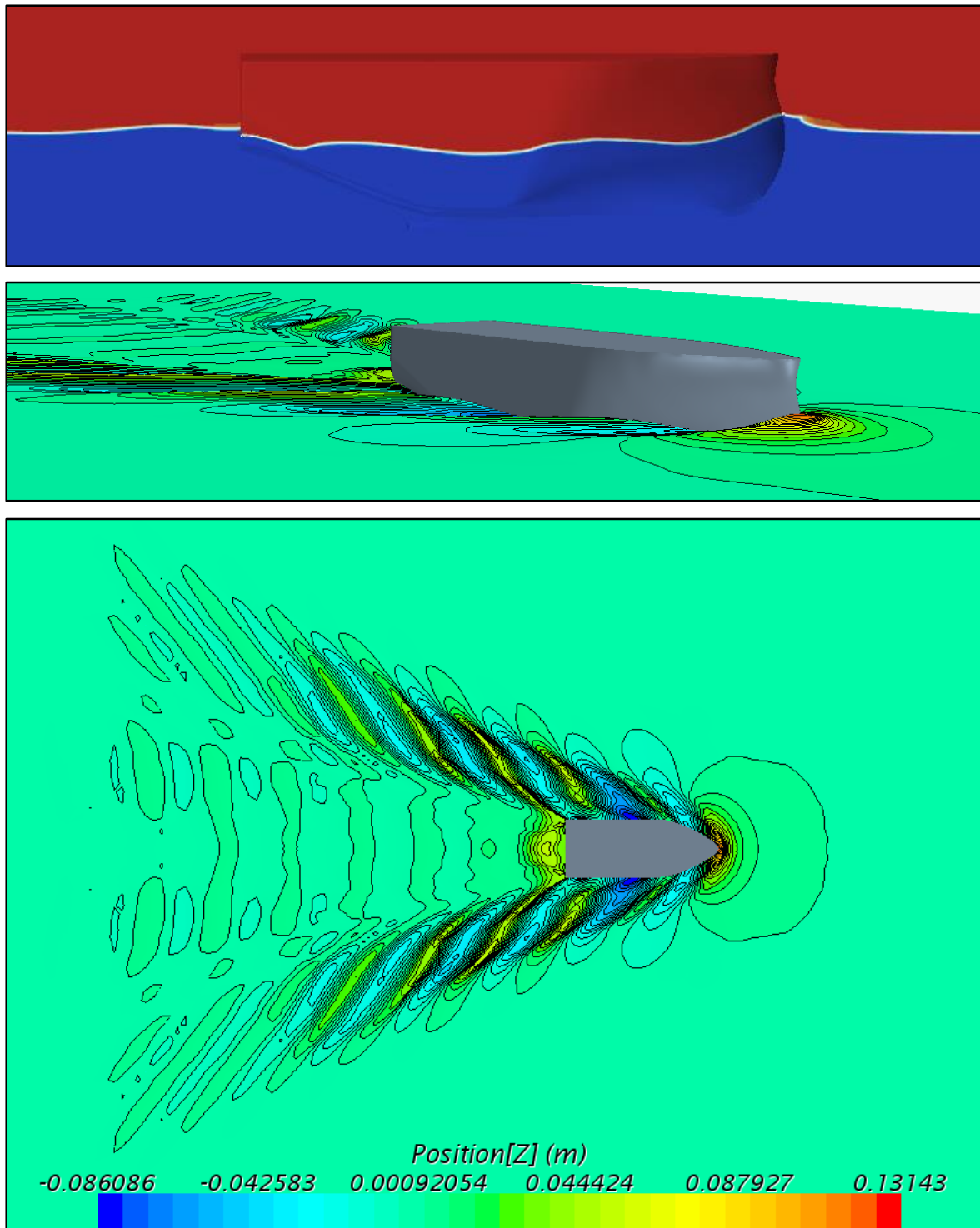


Figure 6-57 - Wave elevation and pattern, Hull 2 at 10 knots

6.2.2 Hull Forces at 4 Knots

As expected the simulations without free surface converged quickly, as seen in the figures below. Convergence in forces were found after 10 seconds but left running for 80 seconds to confirm the result. Figure 6-59 show that the shear and pressure forces both settles almost right away compared to what the simulations with free surface does.

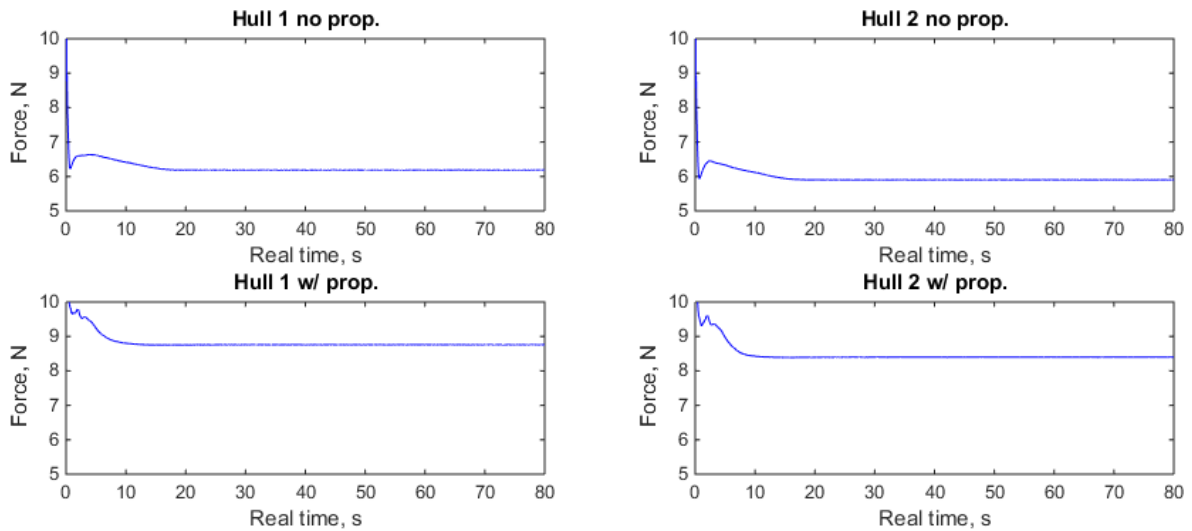


Figure 6-58 - Total runtime at 4 Knots

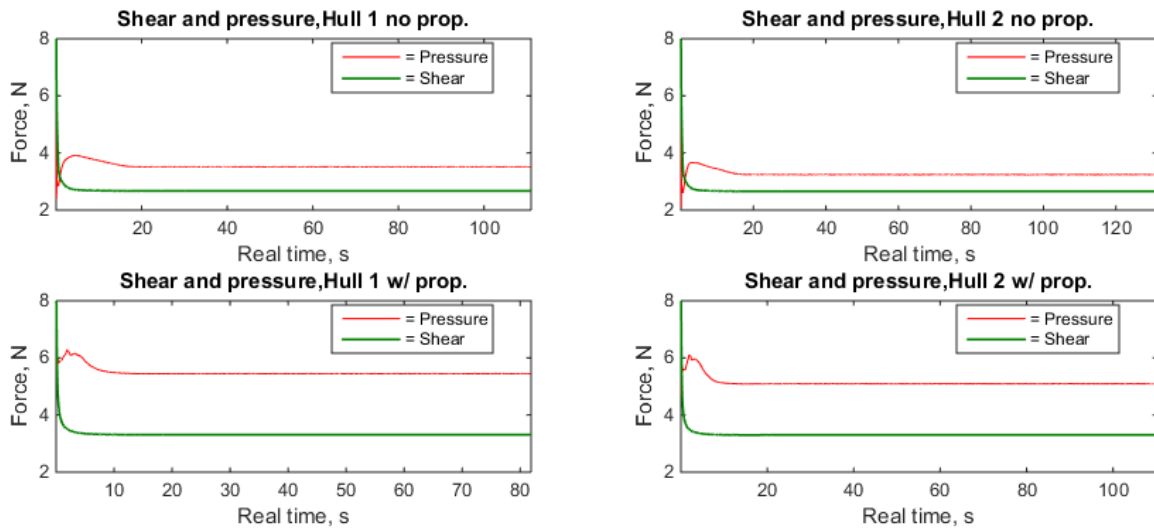


Figure 6-59 - Total runtime at 4 Knots, decomposed to shear and pressure forces

The two following figures both show the last 20 seconds of the simulations. The total force and the belonging simulation-case is displayed above every graph in Figure 6-60 and decomposed components are displayed in Figure 6-61.

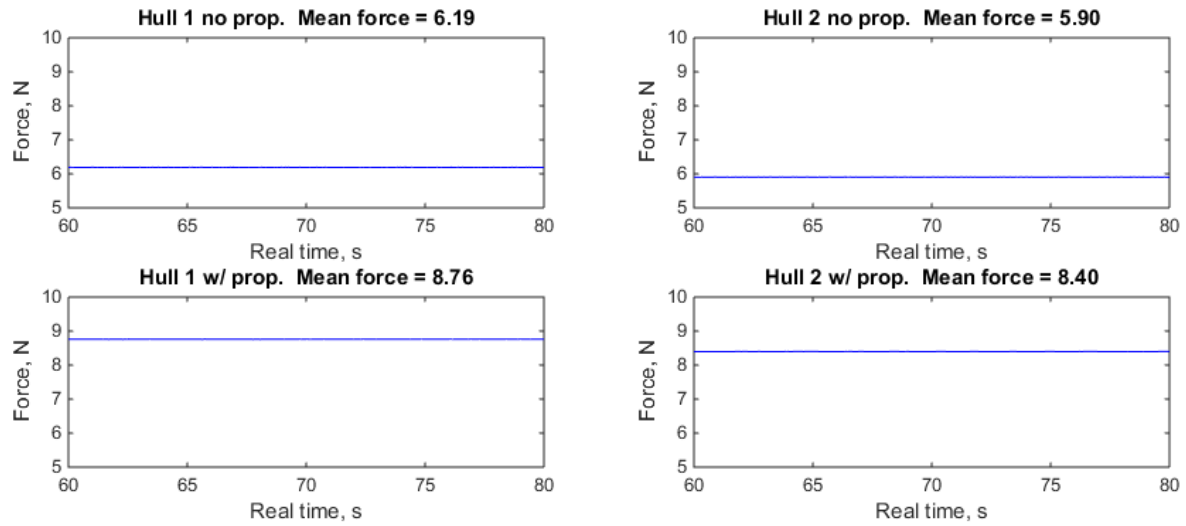


Figure 6-60 - Converged forces at 4 Knots

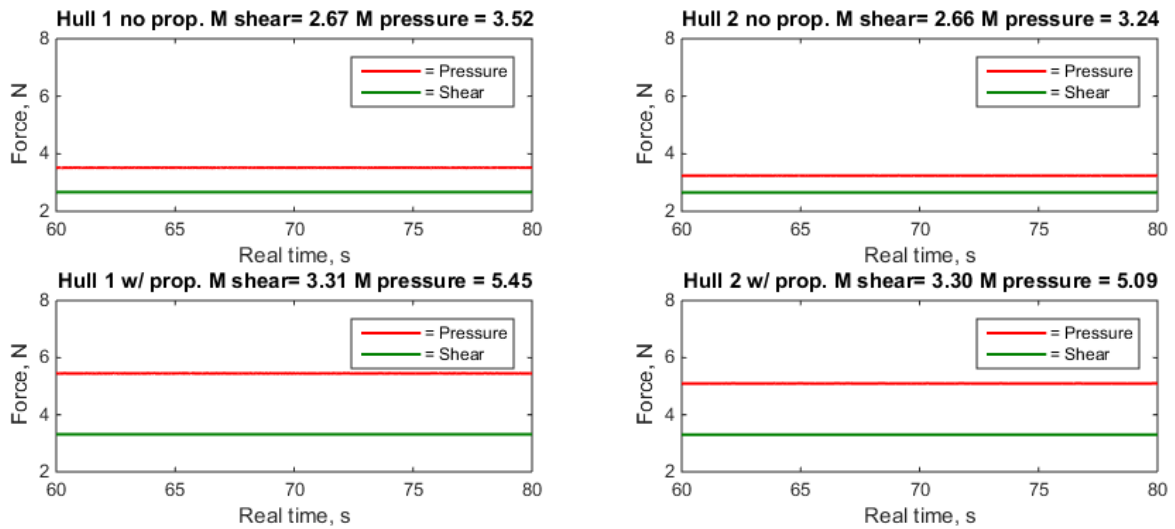


Figure 6-61 - Converged shear and pressure forces at 4 Knots

6.2.3 Hull Forces at 10 Knots

In this section results from the 10-knot simulation is presented. In the first figure, one can see that the simulation had to run all the way up to 350 seconds for the oscillations to decrease. This trend can also be seen at the chosen time step from the convergence study.

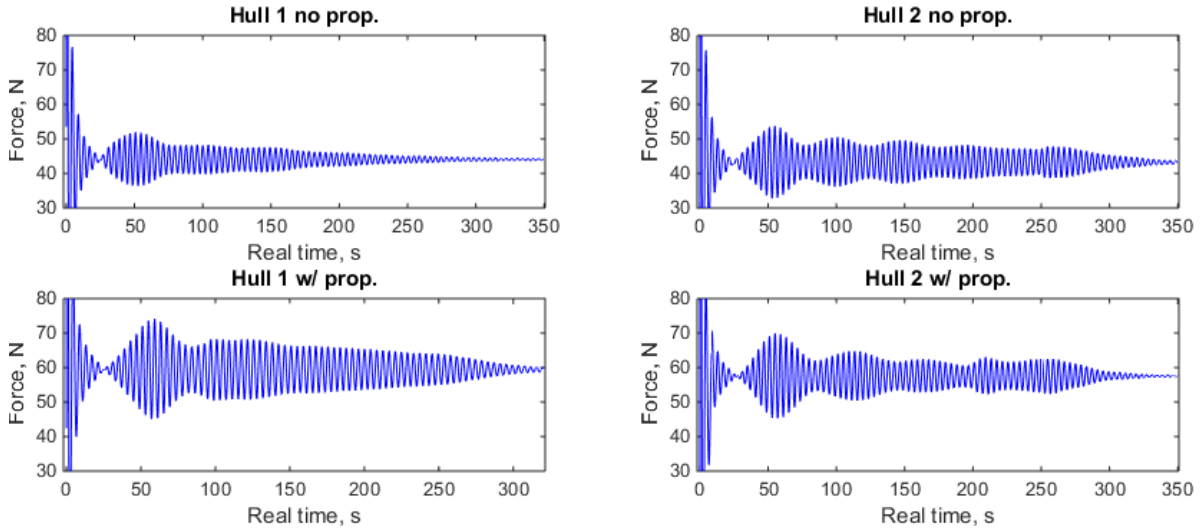


Figure 6-62 - Total runtime at 10 Knots

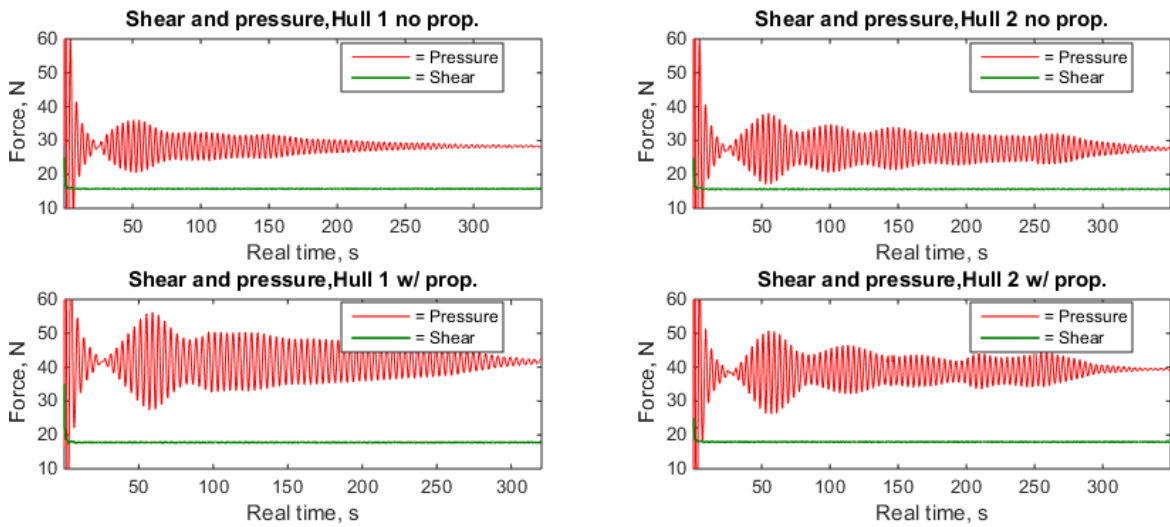


Figure 6-63 - Total runtime at 10 Knots, decomposed to shear and pressure forces

In the two following figures, the last 15% percentile of the simulations are presented. As in the previous section, the forces are presented above each graph. It can be seen that the resistance of the hull with nozzle and disk is higher than without. One component of this increased resistance is drag on the nozzle, while another component is thrust reduction from added resistance due to the presence and effects of the propeller.

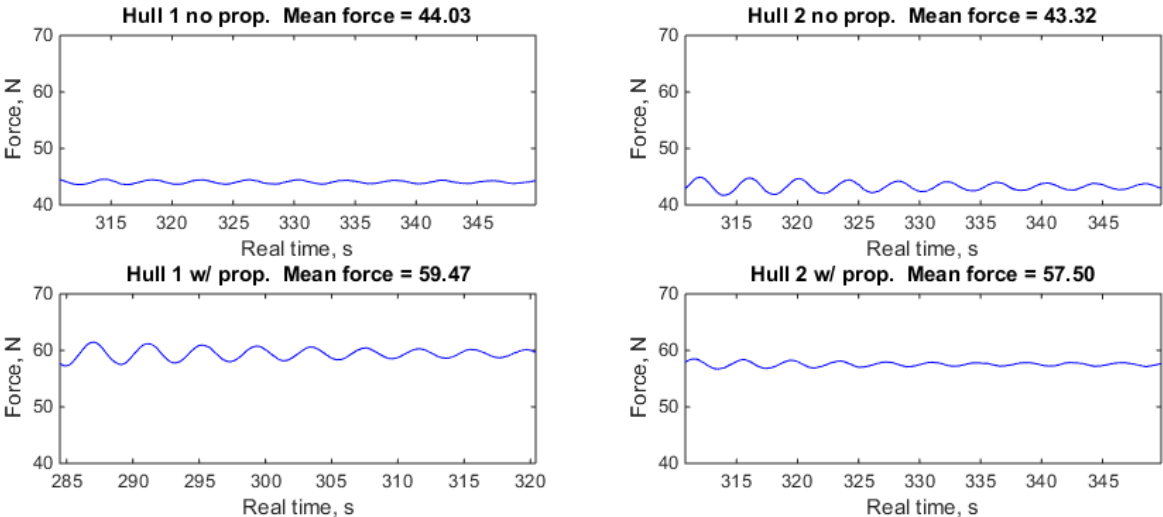


Figure 6-64 - Converged forces at 10 Knots

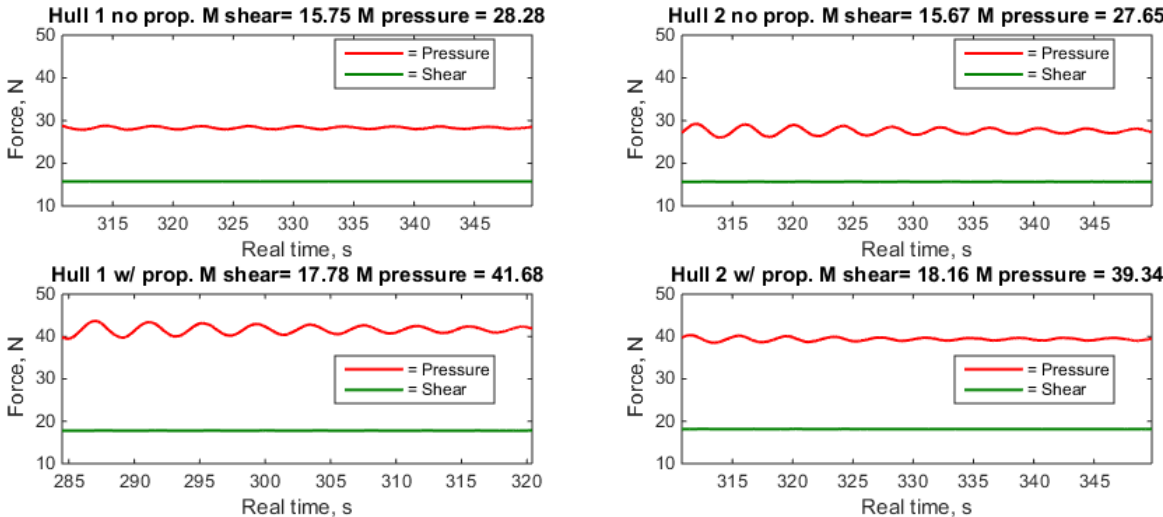


Figure 6-65 - Converged shear and pressure forces at 4 Knots

6.2.1 Thrust Reduction

As described in Section 4.16 the thrust reduction can be calculated. From Figure 6-64 the hull resistance with and without propeller at 10 knots is calculated, but values from the simulations with propeller also includes the nozzle resistance, which is not included in the simulations without propeller effects. For this reason, the simulations with disk are run for another 25 seconds without the nozzle. Results from this can be viewed in Figure 6-66. The thrust deduction factor t , is then calculated by using equation 4-27. Hull 1 yields a thrust deduction factor of 0.160 while Hull 2 yields a factor of 0.154. This is an improvement of 3.75% on the suggested hull design.

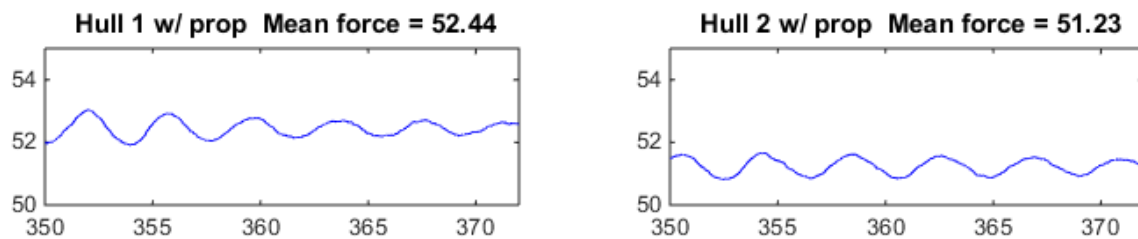


Figure 6-66 - Hull resistance with virtual disk and without nozzle

Table 11 – Thrust deduction factor

	Hull 1	Hull 2
t	0.160	0.154

6.2.2 Form Factor

The form factor is calculated as was described in Section 4.15 from the 10 knots simulations without nozzle and disk. A form factor of 0.290 was found for Hull 1 and form factor of 0.317 for Hull 2.

Table 12 - Form factors

	Hull 1	Hull 2
k	0.290	0.317

6.2.3 Full-Scale Hull Resistance

In this section, the scaled hull resistance will be presented. By using equations from Section 4.15 and values from the previous sections the full-scale hull resistance was calculated, and can be viewed in the table below.

Table 13 - Scaled results

	4 knots		10 knots	
	Hull 1	Hull 2	Hull 1	Hull 2
$R_{TM}[N]$	12.377	11.806	88.059	86.646
C_{TM}	0.00937	0.00894	0.01067	0.01050
C_{FM} CFD	0.00404	0.00402	0.00382	0.00380
C_{FM} ITTC	0.00398		0.00334	
C_R	0.00423	0.00370	0.00636	0.00610
ΔC_F	-0.0019, set = 0		0.00017	
C_{TS}	0.00720	0.00671	0.00916	0.00895
$R_{TM} [N]$	9 739	9 092	77 612	75 891
$P_E[kW]$	20.0	18.7	399.3	390.4

To validate these values, one may compare the coefficients to the actual recorder forces. From the table above the residual coefficient from the 4 knots simulations is 45% of the total force coefficient, which agrees well to what can be seen in Figure 6-60 and Figure 6-61. Same goes for the 10-knot simulation where the residual force coefficient corresponds to little over 64% of the total force coefficient, which also corresponds well with Figure 6-64 and Figure 6-65. It is also worth noticing that the friction coefficient has been reduced by about 15% when scaling the shear force from model to full scale. This correspond to what was discussed briefly in Section 4.15.

By looking at the second last row in Table 13, the full scale total hull resistance can be seen. This show a 6.7% decrease in total hull resistance from Hull 1 to Hull 2 at 4 knots, and 2.2% decrease in hull resistance at 10 knots. This corresponds well to findings discussed in Section 3.1.2. The next section will cover comparison of these results with values from a similar ship, R/V Gunnerus, in order to check the validity of the results.

6.3 Comparison with R/V Gunnerus

When performing numerical calculations, it is always useful to have experimental data to compare with, to check whether the numerical results are in the same order of magnitude. One ship that may be comparable with Roaldnes is NTNU's research vessel R/V Gunnerus. An experimental model test on R/V Gunnerus was performed by Marintek in 2005, see Appendix K for excerpts of the report. Length in waterline of this vessel is 30.005m compared to Roaldnes' 35m. The breadth of Gunnerus is somewhat smaller than Roaldnes' with 9.6m to 13m. Unfortunately, the volume displacements tested is quite different with Gunnerus' 400 m³ from experiment to Roaldnes' 1250 m³ in CFD (full-scale displacement). Nevertheless, these results can be used to check that the CFD results from Roaldnes is within a reasonable size. Gunnerus was scaled by $\lambda = 10.345$ while Roaldnes by $\lambda = 10$.

Figure 6-67, Figure 6-69, Figure 6-70, and Figure 6-70 presents model test results for Gunnerus and CFD results on the two hull designs for Roaldnes. The red dot indicates value from experimental tests on Gunnerus, the blue dot from CFD on Hull 1 while the magenta colored dot on Hull 2.

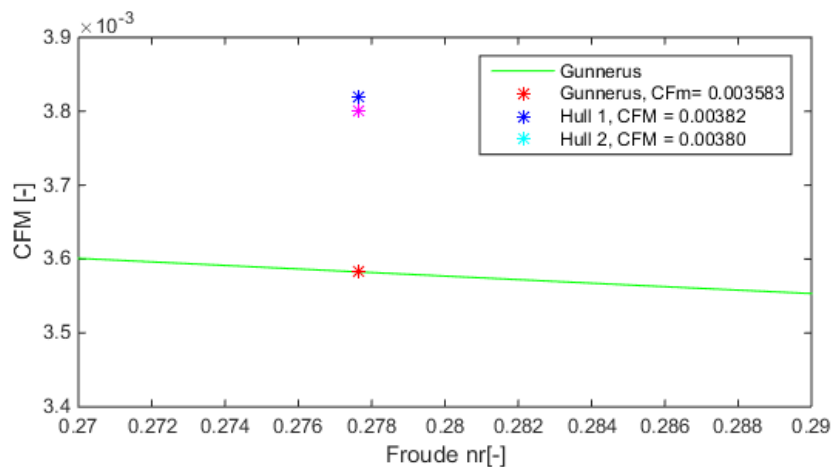


Figure 6-67 - Comparison CFM at $F_n = .02776$

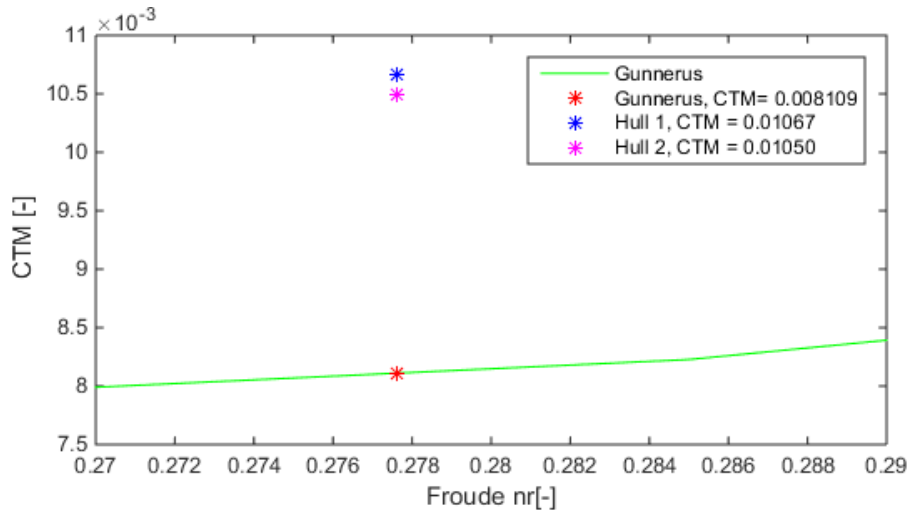


Figure 6-68 - Comparison CTM at $F_n = .02776$

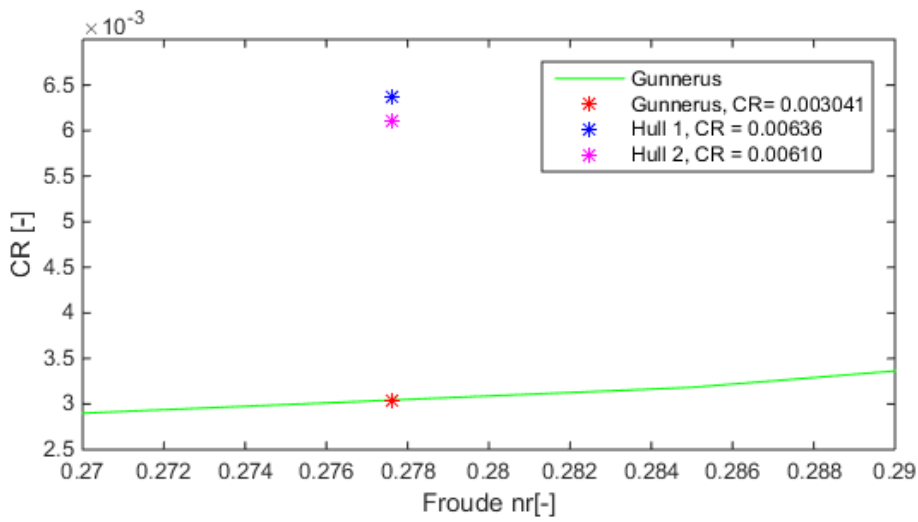


Figure 6-69 - Comparison of CR at $F_n = .02776$

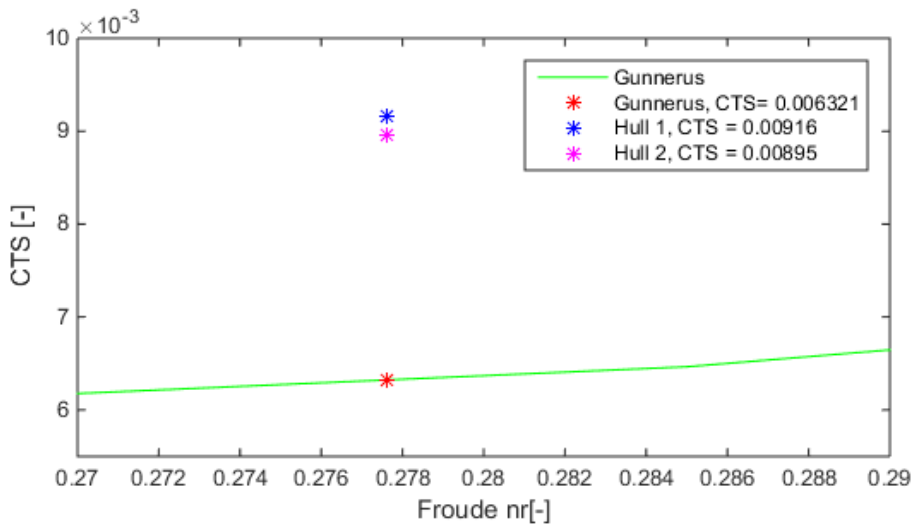


Figure 6-70 - Comparison of CTS at $F_n = .02776$

When comparing these hulls at $Fn = 0.2776$, the results show that C_{TS} on Hull 1 is 44.9% larger than C_{TS} on Gunnerus while C_{TS} on Hull 2 is 41.6% lower than Gunnerus'. Based on these results the numerical calculations performed on the two hulls seem to be within an acceptable range compared to the reference vessel.

6.4 Uncertainties of results

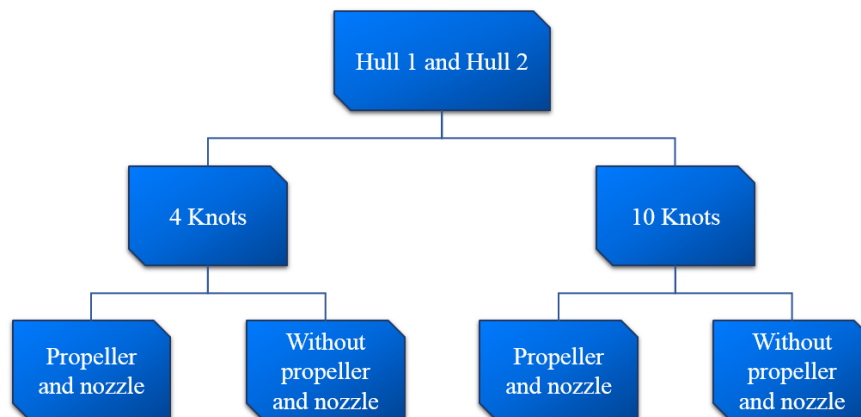
As numerical simulations is a way of reproducing the real world by use of numbers, there will always exist uncertainties. Evaluation of the uncertainty of a CFD simulation is complex, due to the many factors involving and the complexity of the software. For this reason, it is important to have a critical view of the results. The turbulence models used in this thesis is RANS with k-epsilon turbulence model. As discussed in Section 4.3 the RANS model does not even try to capture even the largest eddies, but models them numerically. This creates a source of error on its own. The K-epsilon model also involves inputs which also may lead to deviation from the real world. As mentioned in Chapter 1, CFD may produce results with varying degree of accuracy, but can at least be used to spot trends. In this thesis results with several decimals have been used. This does not necessary correlate to the level of accuracy between these numerical results and future model test and sea trial. They are merely used to compare different numerical values to one another.

7 Conclusion

This combined project and master's thesis has covered verification and optimization of the hull shape of a trawler for the ship owner Roaldnes. A resistance prediction and flow calculation on the Seacon design was performed in the project thesis (Svoren, 2014). Results from this report formed the basis for a new hull design, referred to as Hull 2, with rounded aft part compared to the previous design with chines, Hull 1.

A convergence study was completed on mesh size, time step, and domain size in order to achieve the best possible simulation setup for this case. The convergence study was performed with a velocity of 1.952m/s or 12 knots full scale. The domain was chosen based on findings from project thesis. A total of six simulations with different mesh size, eight simulations with different time step, and four different domain sized was tested. All simulations converged well on its own, and the result from this study formed an optimal simulation setup. This setup consisted of a base size of 0.18m with approx. 2mill cells, a time step of 0.02s, and a domain which stretched 4 lwl aft and forth, 5 lwl to the side, 1.7 lwl up and 3.5 lwl down. The difference in results from the chosen values to the next, towards the asymptotic value, was 0.077% on mesh, 0.072% on time step, and 0.085% on domain size. This proves that the convergence study was successful.

The final simulations covered in total eight simulations, one set for each hull, as viewed in the hierarchy below.



From these simulations, Hull 1 revealed a low pressure over the sharp edge created by the chines, which is consistent with the hypothesis from the project thesis. Hull 2 displayed a more gradual pressure transition over the aft shoulder. Due to the finding of this low-pressure edge, vorticities in this area was investigated. This study showed more vorticities and stronger vorticities on Hull 1, than what was found on Hull 2 at

this area. These vorticities propagated in the inflow of the propeller, where slightly higher values were recorded in the propeller plane for Hull 1 compared to Hull 2.

A plot of nominal axial velocities in the propeller plane show lower velocities in the upper left sector where vorticities are strong. The nominal wake is also plotted and compared. Some differences can be seen between the two designs. At 4 knots, Hull 1 exhibits somewhat higher values in a broader area than what can be seen on Hull 2, while at 10-knots the difference is almost insignificant. A plot of nominal tangential velocity backs up the choice of rotational direction as was set outwards. The dynamic pressure on the propeller plane is plotted and found very similar.

Streamlines are also observed for all simulations. These show the same tendency as found in the project thesis, with a low-velocity swirl of water rotating inside the skeg tunnel. However, the inflow display remarkably better streamlines after adding suction from the virtual disk. Wave pattern at 10 knots full scale is plotted, and display a realistic Kelvin wake with max elevation at the bow of 1.3m, wave crests of 0.6m, and deepest trough of 0.8m full scale.

Results from the logged forces on these simulations show that the 4 knots simulations converged right away, and the residual force covered 3/5 of the total force. The 10 knots simulations took much longer to converge, and here the residual force covered 2/3 of the total logged force. Thrust deduction factor was calculated for the 10 knots simulations, and found to be equal to 0.160 for Hull 1 and 0.154 for Hull 2, which is an improvement of 3.75%. Results from scaling can be viewed in the table below.

	4 knots		10 knots	
	Hull 1	Hull 2	Hull 1	Hull 2
$R_{TM}[N]$	12.377	11.806	88.059	86.646
C_{TM}	0.00937	0.00894	0.01067	0.01050
$C_{FM} \text{ CFD}$	0.00404	0.00402	0.00382	0.00380
$C_{FM} \text{ ITTC}$		0.00398		0.00334
C_R	0.00423	0.00370	0.00636	0.00610
ΔC_F		-0.0019, set = 0		0.00017
C_{TS}	0.00720	0.00671	0.00916	0.00895
$R_{TM} [N]$	9 739	9 092	77 612	75 891
$P_E[kW]$	20.0	18.7	399.3	390.4

From this an improvement in full scale hull resistance is found to be 6.7% at 4 knots and 2.2% at 10 knots. This agrees well with results discussed above.

A validation of the result is performed with a similar reference ship, R/V Gunnerus. Note that the volume displacement for these two ships are 400 m³ on Gunnerus, and 1250 m³ on Roaldnes. The scaled total force coefficient for Gunnerus equals 0.00632 while this report shows C_{TS} for Hull 1 equal 0.00916, C_{TS} of 0.00895 for Hull 2.

As CDF is a numerical tool to replicate reality, error sources and uncertainty will always be of presence. Nevertheless, it can be used to show trends. Results obtained in this report suggests that Hull 2 might produce a more uniform inflow, and a better wake field for the propellers than what can be seen from Hull 1. It also indicates that Hull 2 might produce lower thrust reduction as well as an overall lower hull resistance at both trawling and transit. For reasons described, Hull 2 seems to be an improvement compared to the current design, and is recommended for further study and model test.

8 Further Work

Upon finishing this thesis, several interesting research possibilities have been discovered. The first one being an improvement of the simulations performed in this work. Simulations in this thesis were performed with constant sinkage and no trim. It would be interesting to perform calculations with heave and pitch allowed, and compare results with this thesis.

It would also be interesting to carry out the same simulations, but with different input method for the virtual disk, and see if this makes any difference. In this thesis, a rotation rate is specified along with K_Q , K_T , and η for that specific velocity. Another method is to input the whole propeller curve and specify thrust and torque.

Other changes to the virtual disk would also be of interest. This thesis covers simulations with the disk revolving outwards. By performing calculations with the opposite rotation direction, one could compare and find out whether the choice of rotation direction was the right one, or if it had little effect on thrust.

This thesis covered nominal wake calculations. A method of calculating propeller induced velocities was found, but considered too time-consuming to be included in this master's thesis. By either calculating these velocities or performing a simulation with the virtual disk in open water alone, the effective wake could also be considered.

Changes to the simulation setup, in order to simulate this ship in turn could also be made. This would make it possible to observe the inflow for the propeller, and compare it to straight ahead cruising. In sharp turn, the flow around the skegs might create low velocities and a high wake field for the inflow to the relatively large ducted propellers. This research question is highly relevant, as this ship will operate with large rudder angles.

The hull from Seacon was designed with chines in an attempt to reduce roll motion. As this thesis covers results in straight ahead cruising of this design, it would be of interest to perform calculations in roll, and observe whether this design had any effect as intended.

9 Reference

CD-Adapco. (2014). STAR CCM+ User Guide version 9.06.

Retrieved from <https://steve.cd-adapco.com/>

Cengel, Y., & Cimbala, J. (2010). Fluid Mechanics Fluid Mechanics, 2, 853-920.

Mc Graw Hill Professional.

CFD-online. (2015). CFD online. Retrieved from:

<http://www.cfd-online.com/Wiki/Lawofthewall>

Dejhalla, R., & Prpi, J. (2006). *A Review of the State-of-the-Art in Marine*

Hydrodynamics. Retrieved from Faculty of Engineering University of Rijeka

Department of Naval Architecture and Ocean Engineering

DNVGL. (2014). Class Rules Ships / High Speed, Light Craft and Naval Surface

Craft, 6. Retrieved from <https://exchange.dnv.com/servicedocuments/dnv>

Dokkum, K. V. (2007). Ship knowledge: ship design, construction and operation.

Enkhuizen: DOKMAR.

Ellingsen, H., & Endal, A. (2007). Fishing Vessels and Workboats. Trondheim:

NTNU.

Ferziger, J. H., & Peric, M. (2002). Computational Methods for Fluid Dynamics, 3.

Berlin: Springer.

Fitzpatrick, R. (2014). *Fluid Mechanics*. Retrieved from

<http://farside.ph.utexas.edu/>

Havfisk. (2014). Gadus Neptun. Retrieved from:

<http://www.havfisk.no/no/flaten/oversikt-over-flaten/gadus-neptun>

Havforskningsinstituttet, (2011). Retrieved from

www.imr.no/nyhetsarkiv/2011/august/lukeritraldorengirbedrekontroll/nb-no

- Kramer, J. (2014). *Hydrodynamic performance of sail-assisted merchant vessels*.
(Master's's thesis), Retrieved from
<https://daim.idi.ntnu.no/masteroppgaver/011/11603/masteroppgave.pdf>
- Marintek. (1988). Fremdriftsforsøk, 27meter fiskefartøy. Retrieved from Marintek,
Sintef.
- Maritime, S. (2008). Steerable nozzle. Retrieved from
<http://www.splashmaritime.com.au/Marops/data/Stories/Pkort.htm>
- NHO. (2008). NOx-fondet. Retrieved from
<https://www.nho.no/Prosjekter-og-programmer/NOx-fondet/>
- Park, D.-W., & Chun, H.-H. (2009). Design practice for the stern hull form of a
twin-skeg ship. *Journal of Marine Science and Technology*, *14*(3), 310-321.
doi: 10.1007/s00773-009-0046-5
- Seacon. (2014). Torbas. Retrieved from
<http://seacon.no/fartoyserier/sc-70/ms-torbas>
- SSB. (2015). Norskregistrerte skip ikke inkludert i handelsflåten. Retrieved from
<http://www.ssb.no/160261/norskregistrerte-skip-ikke-inkludert-i-handelsfl%C3%A5ten.antall-skip-og-bruttotonnasje-etter-skipstype>
- Steen, S. (2007). *Motstand og propulsjon propell og foil teori, 2*. Trondheim: Institutt
for Marin Teknikk.
- Svoren, N. Ø. (2014). *Use of CFD to estimate hull performance*. Unpublished Project
Thesis, MTS, NTNU, Trondheim, Norway
- Traung, J.-O. (1960). *Fishing boats of the world 2*. Farnham: Fishing News Books.

10 Appendix

Appendix A. Open water data, 4 knots

=====
"AKPA-CP-DT/SPA". STEADY PROPULSOR ANALYSIS.

version 6.0
=====

SUMMARY OF THE DATA ON PROPULSOR ARRANGEMENT AND INTEGRAL PERFORMANCE

Project name: P85-380-ROA 4 knop

POD (HUB, GONDOLA):

Pod length Lpod = 1.3200 m
Maximum pod diameter DPm = 0.8500 m
Shaft immersion ho = 3.5000 m

Axial force..... Fxo = 0.17900E+03 [N] KFxo=
0.00073 (based on n and D of FRW stage)
Vertical force..... Fyo = -0.43640E-10 [N] KFyo=
0.00000 (based on n and D of FRW stage)
Side force..... Fzo = 0.77846E-11 [N] KFzo=
0.00000 (based on n and D of FRW stage)
Axial moment..... Myax= 0.16718E-11 [N*m] KMyax=
0.00000 (based on n and D of FRW stage)

RUDDER(/STRUT): NO

DUCT: DUCT (NOZZLE PROPELLER)

Duct diameter..... DD = 4.0000 m
Duct length..... LD = 1.7100 m
Distance between duct L.E. and propeller plane..... XLEDT = 0.6750 m
X-coordinate of the duct L.E. XPDTLE = 0.6750 m

Duct thrust..... Td = 0.26356E+05 [N] Ktd=
0.10789 (based on n and D of FRW stage)
Axial force..... Fxo = 0.26356E+05 [N] KFxo=
0.10789 (based on n and D of FRW stage)
Vertical force..... Fyo = 0.89942E+01 [N] KFyo=
0.00004 (based on n and D of FRW stage)
Side force..... Fzo = 0.12917E+02 [N] KFzo=
0.00005 (based on n and D of FRW stage)

NUMBER OF PROPELLERS: 1

FORWARD PROPELLER:

Cavitation analysis: non-cavitating flow

Direction of rotation..... Right
x-coordinate of the disk..... XP = 0.000 [m]

```

Diameter..... D = 3.800 [m]
Rotational speed..... n = 1.083 [Hz]
Number of the blades..... Z = 4
Hub ratio..... rh/R = 0.224
Expanded area ratio..... Ae/Ao = 0.400
Advance coefficient..... Jv = 0.500
Axial wake fraction..... WT = 0.2654
Inductive axial inflow coefficient..... WTI = -0.4167
Thrust..... T = 0.73432E+05 [N]      KT=
0.30061 (based on n and D of FRW stage)
Effective thrust..... Te = 0.66089E+05 [N]      KTe=
0.27055 (based on n and D of FRW stage)
Torque..... Q = 0.50967E+05 [N*m]      KQ=
0.05491 (based on n and D of FRW stage)
Shaft delivered power..... PD = 0.34692E+06 [W]      KPD=
0.34499 (based on n and D of FRW stage)
Spindle moment of one blade..... Mys = 0.31882E+04 [N*m]      KMys=
0.00343 (based on n and D of FRW stage)
Propeller efficiency in wake..... ETAB = 0.4360 ( ETAB=T*V/PD )
"Open-water" propeller efficiency..... ETAO = 0.6177 ( ETAO=(1-
WTI)*ETAB )
Conditional propulsive efficiency..... ETAD = 0.3924 (
ETAD=Te*V/PD=(1-t)*ETAB )

```

Appendix B. Open water data, 10 knots

```

=====
"AKPA-CP-DT/SPA". STEADY PROPULSOR ANALYSIS.          version 6.0
=====

```

SUMMARY OF THE DATA ON PROPULSOR ARRANGEMENT AND INTEGRAL PERFORMANCE

Project name: P85-380-ROA 10 knop

POD (HUB, GONDOLA):

```

Pod length ..... Lpod = 1.3200 m
Maximum pod diameter ..... DPm = 0.8500 m
Shaft immersion ..... ho = 3.5000 m

Axial force..... Fxo = -0.18703E+04 [N]      KFxo=-
0.00399 (based on n and D of FRW stage)
Vertical force..... Fyo = -0.15435E-09 [N]      KFyo=
0.00000 (based on n and D of FRW stage)
Side force..... Fzo = 0.26587E-10 [N]      KFzo=
0.00000 (based on n and D of FRW stage)
Axial moment..... Myax = 0.63768E-11 [N*m]      KMyax=
0.00000 (based on n and D of FRW stage)

```

RUDDER(/STRUT): NO

DUCT: DUCT (NOZZLE PROPELLER)

```

Duct diameter..... DD = 4.0000 m
Duct length..... LD = 1.7100 m
Distance between duct L.E. and propeller plane..... XLEDT = 0.6750 m
X-coordinate of the duct L.E. .... XPDTLE = 0.6750 m

```

Duct thrust..... Td = 0.96470E+04 [N] Ktd=
 0.02060 (based on n and D of FRW stage)
 Axial force..... Fxo = 0.96470E+04 [N] KFxo=
 0.02060 (based on n and D of FRW stage)
 Vertical force..... Fyo = -0.17087E+01 [N] KFyo=
 0.00000 (based on n and D of FRW stage)
 Side force..... Fzo = -0.19211E+01 [N] KFzo=
 0.00000 (based on n and D of FRW stage)

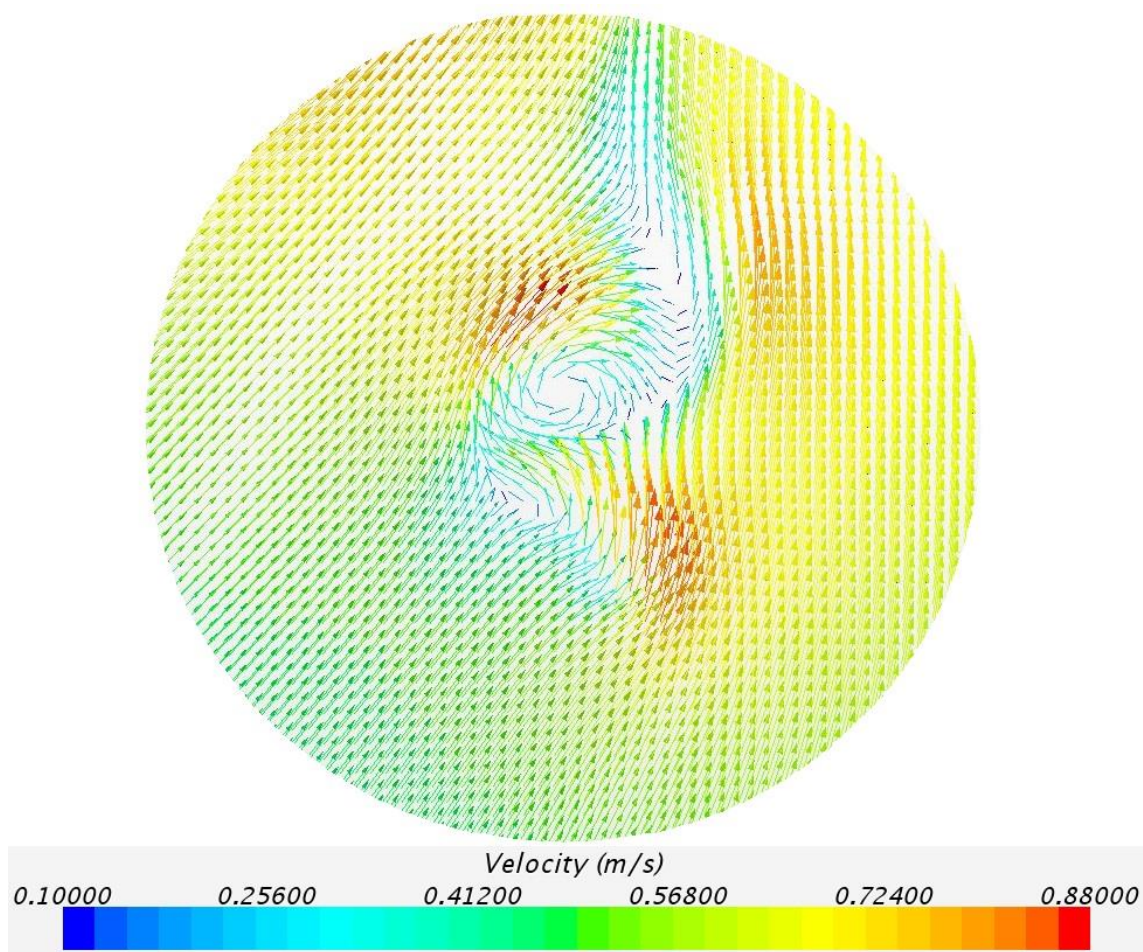
NUMBER OF PROPELLERS: 1

FORWARD PROPELLER:

Cavitation analysis: non-cavitating flow

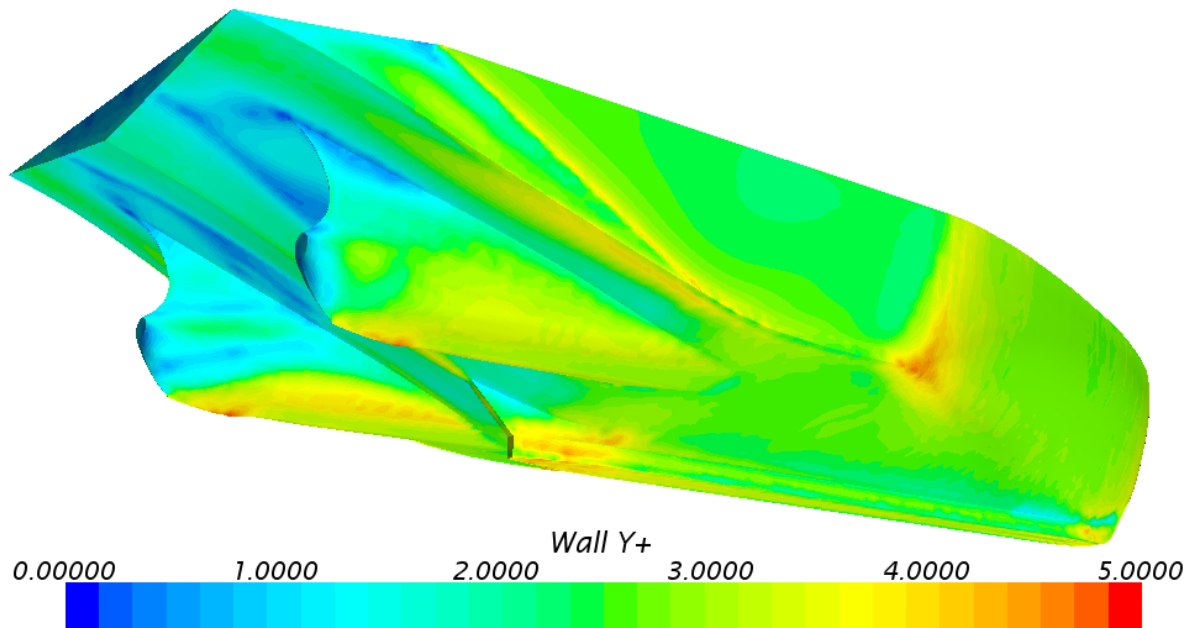
Direction of rotation..... Right
 x-coordinate of the disk..... XP = 0.000 [m]
 Diameter..... D = 3.800 [m]
 Rotational speed..... n = 1.500 [Hz]
 Number of the blades..... Z = 4
 Hub ratio..... rh/R = 0.224
 Expanded area ratio..... Ae/Ao = 0.400
 Advance coefficient..... Jv = 0.902
 Axial wake fraction..... WT = 0.2654
 Inductive axial inflow coefficient..... WTI = 0.0352
 Thrust..... T = 0.10790E+06 [N] KT=
 0.23041 (based on n and D of FRW stage)
 Effective thrust..... Te = 0.97112E+05 [N] KTe=
 0.20737 (based on n and D of FRW stage)
 Torque..... Q = 0.77660E+05 [N*m] KQ=
 0.04364 (based on n and D of FRW stage)
 Shaft delivered power..... PD = 0.73193E+06 [W] KPD=
 0.27420 (based on n and D of FRW stage)
 Spindle moment of one blade..... Mys = 0.44336E+04 [N*m] KMys=
 0.00249 (based on n and D of FRW stage)
 Propeller efficiency in wake..... ETAB = 0.7583 (ETAB=T*V/PD)
 "Open-water" propeller efficiency..... ETAO = 0.7316 (ETAO=(1-
 WTI)*ETAB)
 Conditional propulsive efficiency..... ETAD = 0.6825 (
 ETAD=Te*V/PD=(1-t)*ETAB)

Appendix C. Tangential velocity from project thesis

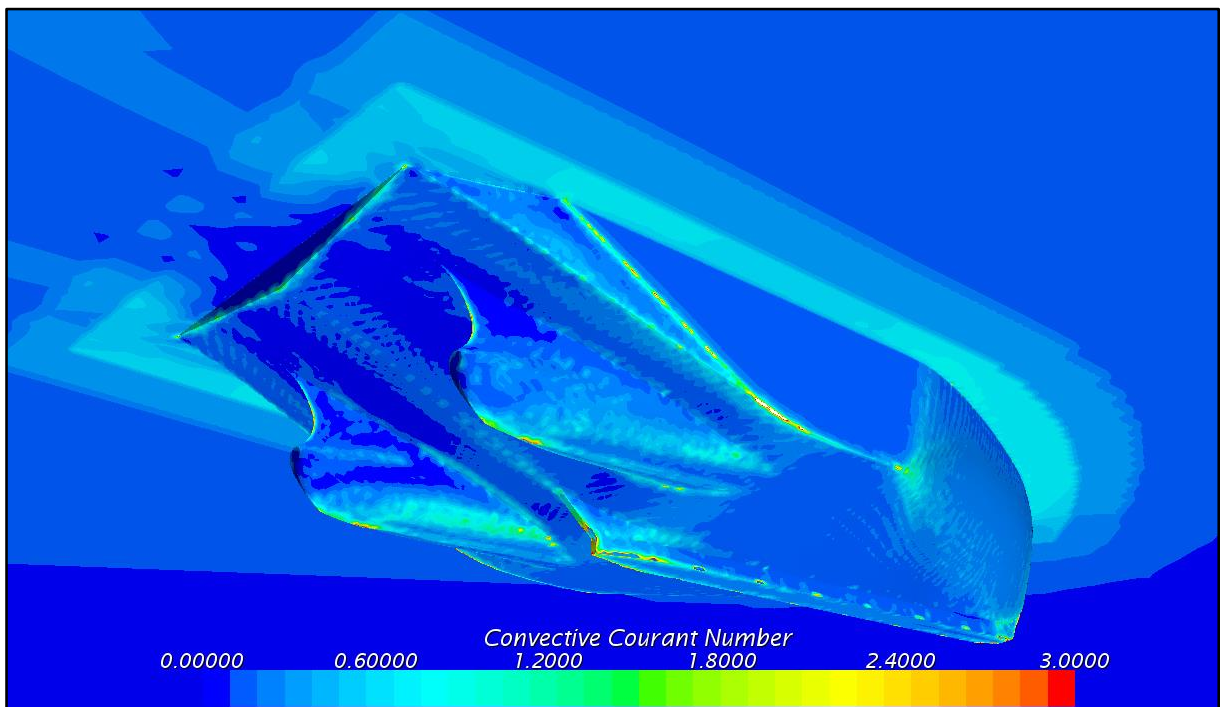


1 - Velocity field Roaldnes hull with chines, 10 knot seen from back to forth(Svoren, 2014)

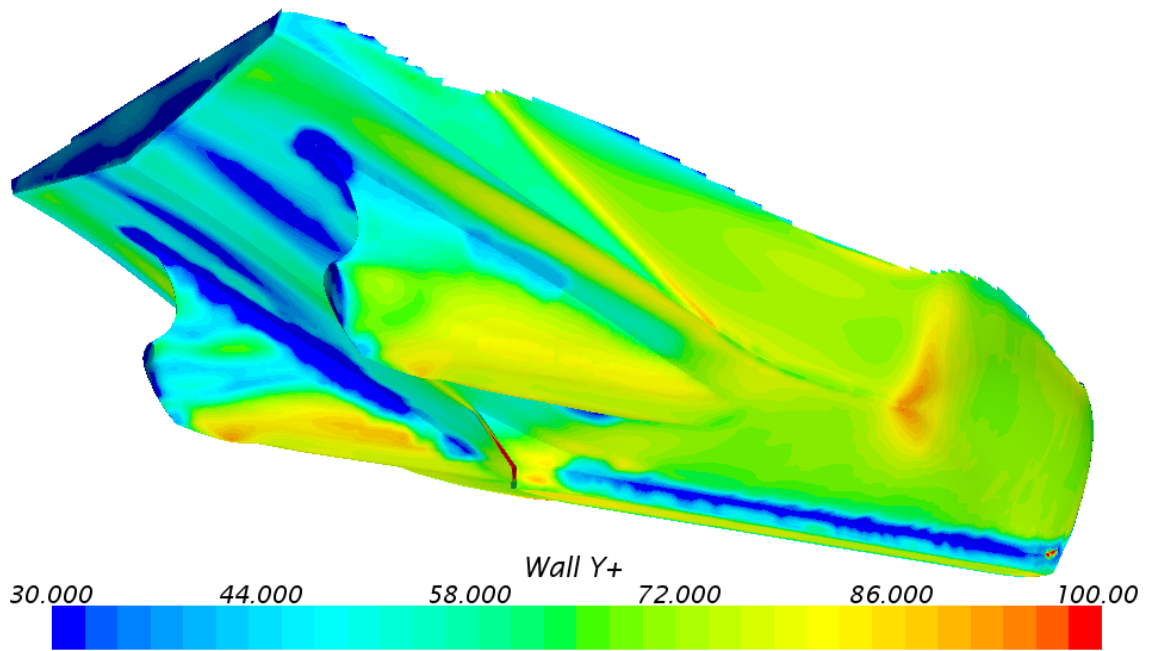
Appendix D. CFL Number and Wall y^+ Value Hull 1



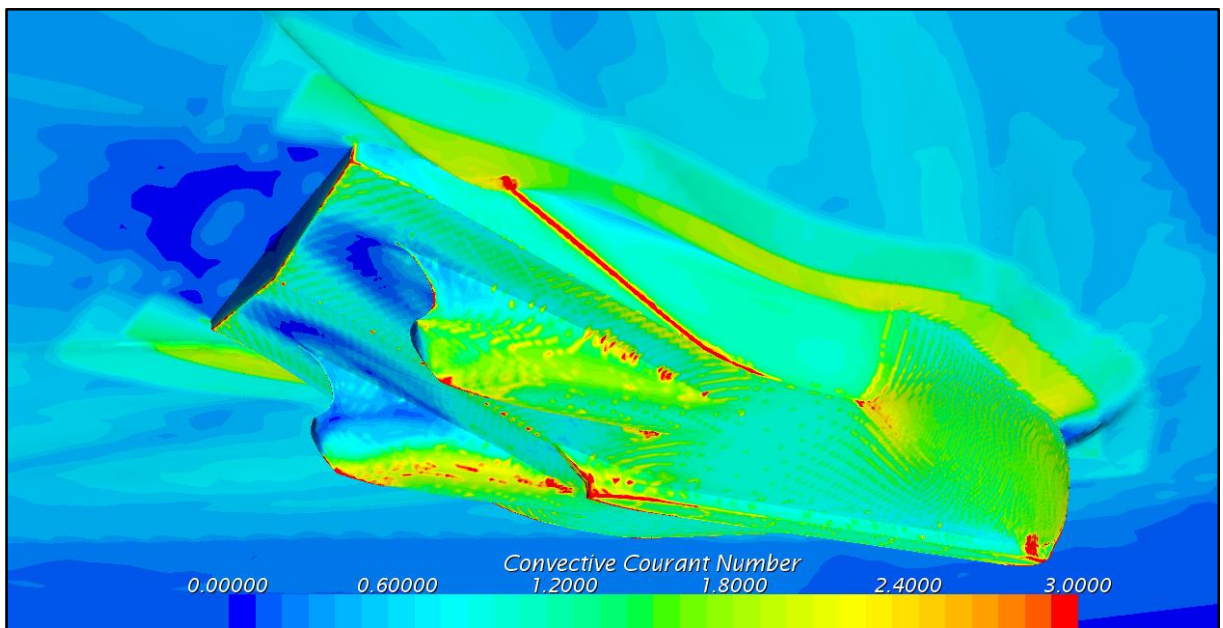
2 - Wall y^+ values, Hull 1 at 4 knots without nozzle and disk



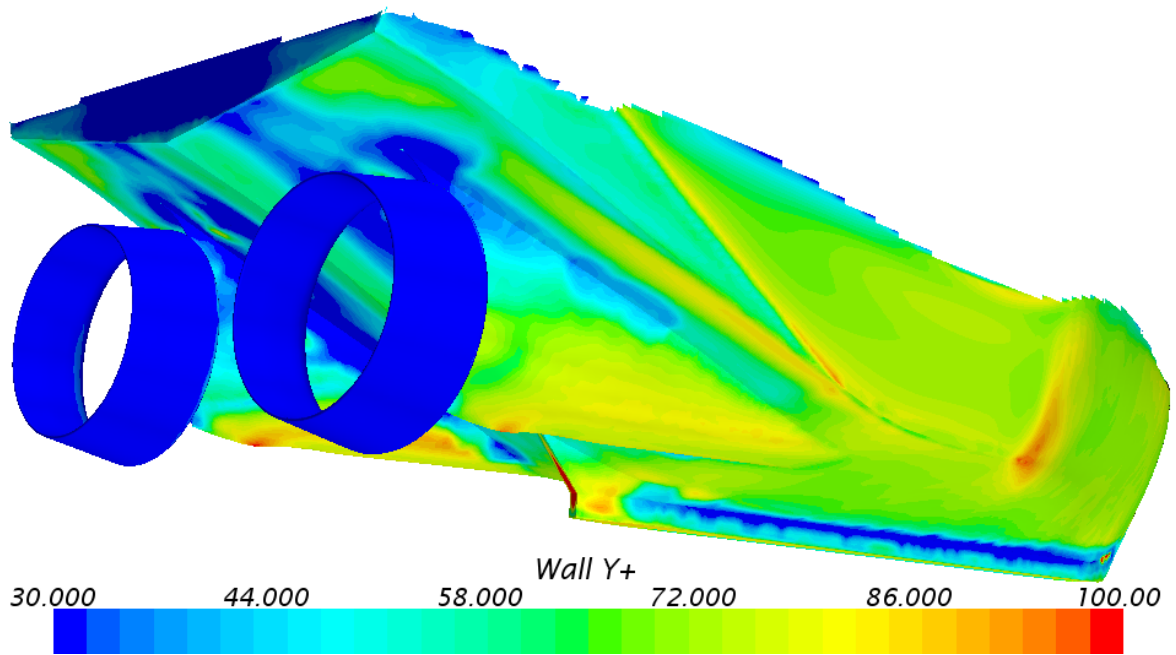
3 - Courant number, Hull 1 at 4 knots without nozzle and disk



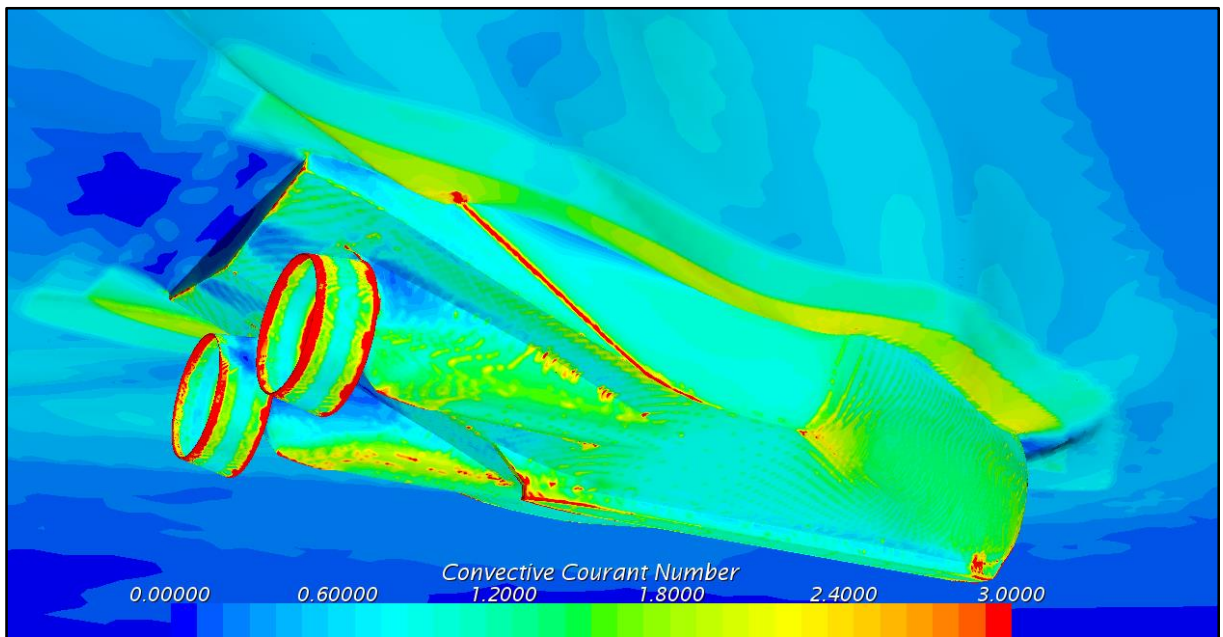
4- Wall y^+ values, Hull 1 at 10 knots without nozzle and disk



5- Courant number, Hull 1 at 10 knots without nozzle and disk

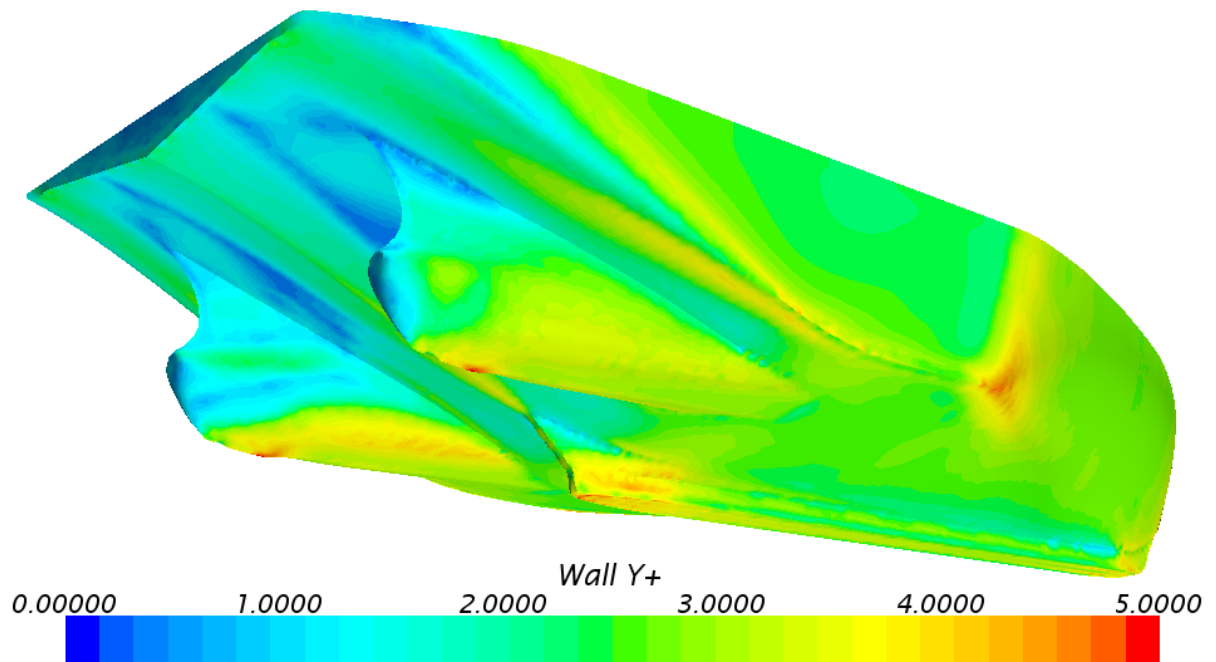


6- Wall y^+ values, Hull 1 at 10 knots with nozzle and disk

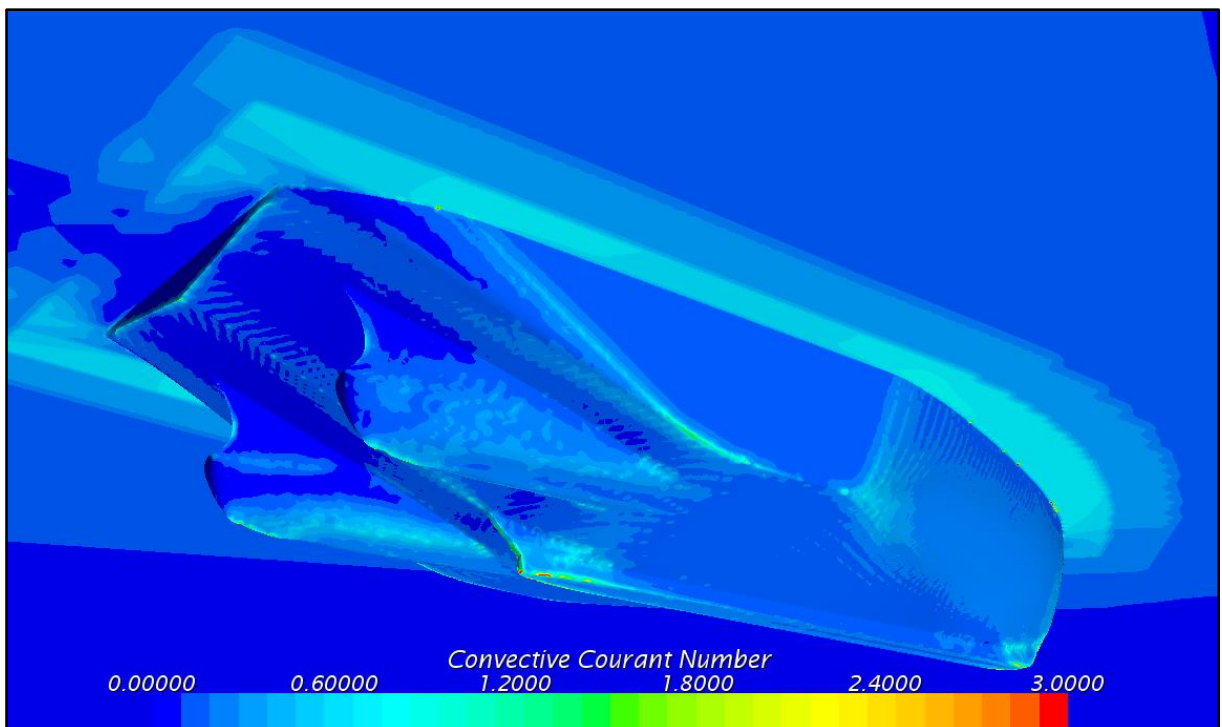


7- Courant number, Hull 1 at 10 knots with nozzle and disk

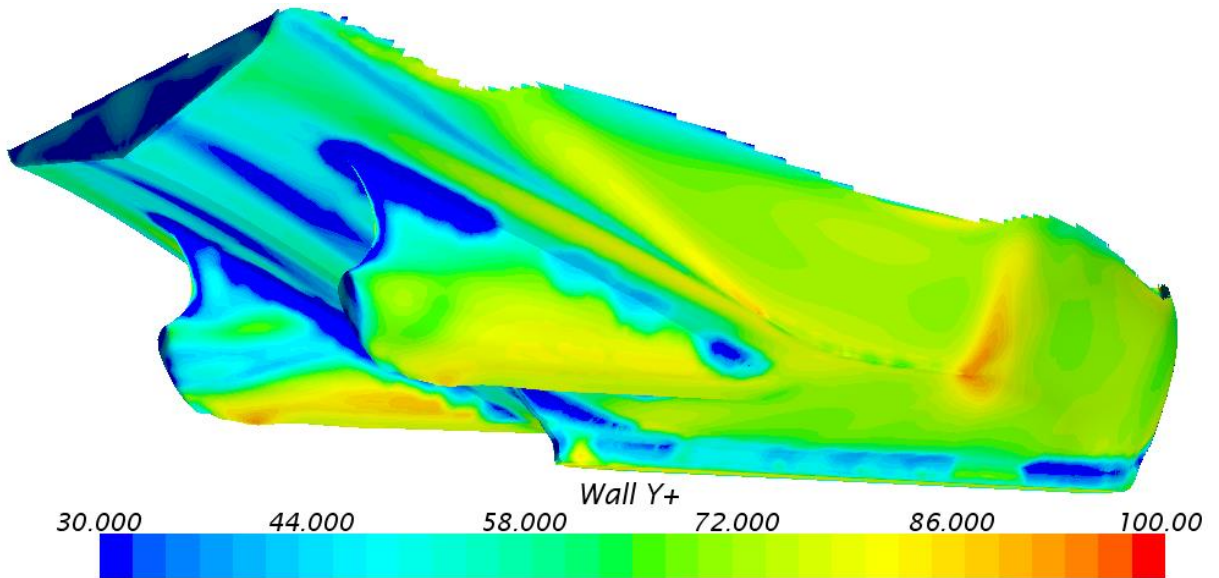
Appendix E. CFL Number and Wall y^+ Value Hull 2



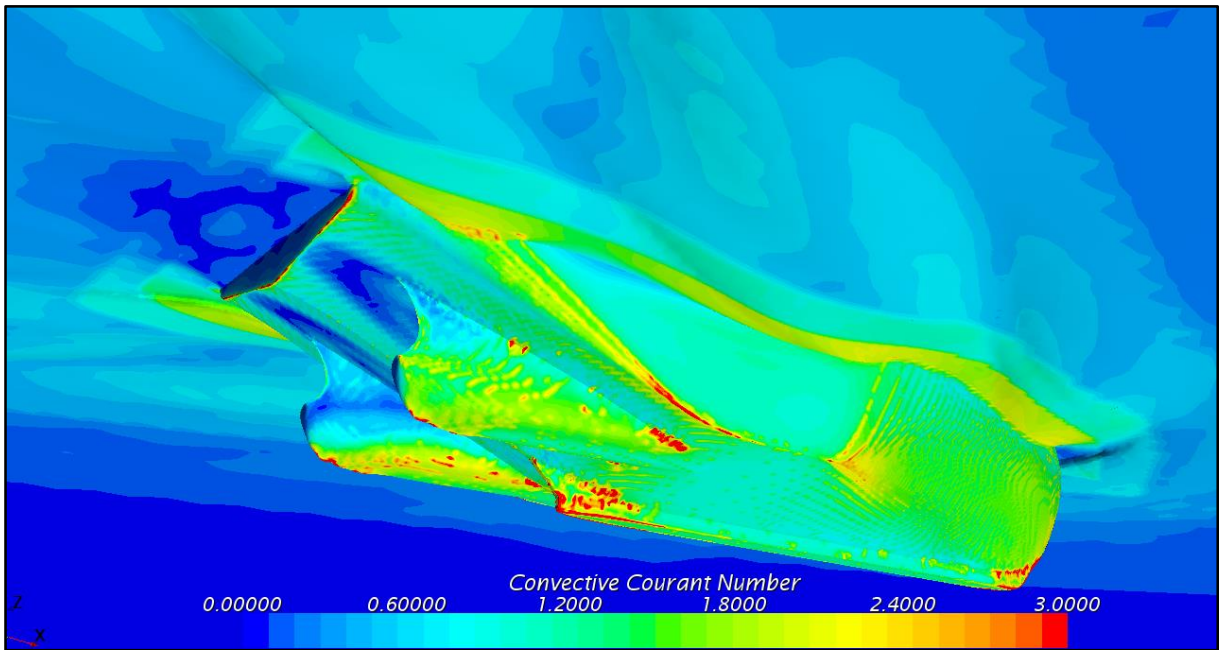
8 - Wall y^+ values, Hull 2 at 4 knots without nozzle and disk



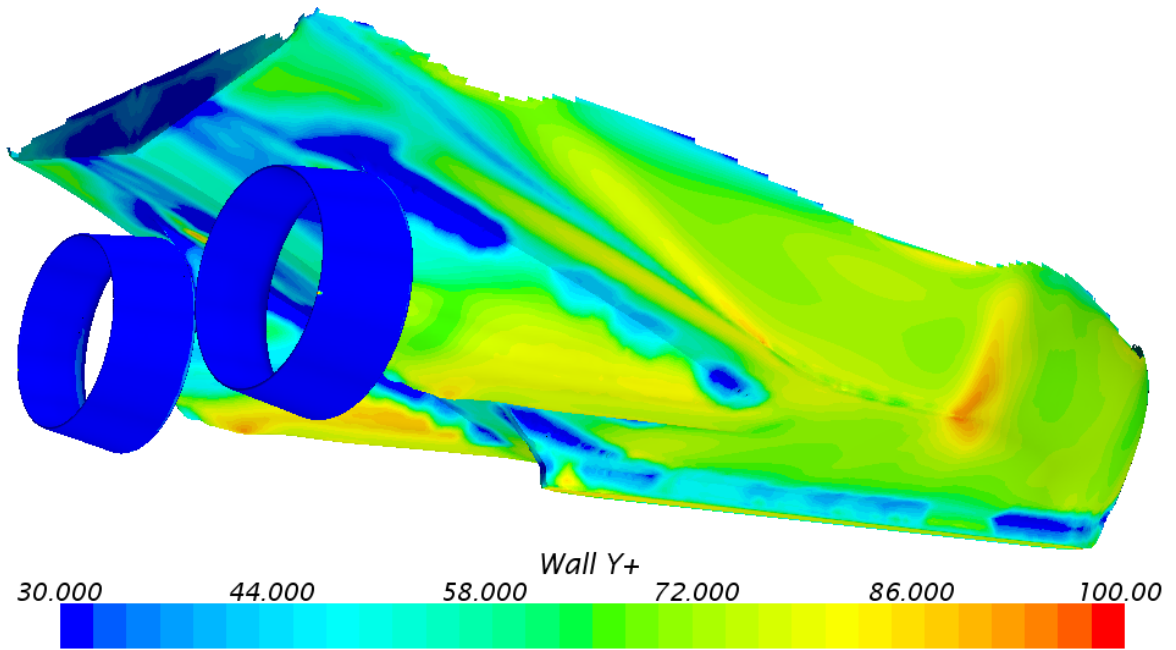
9 - Courant number, Hull 2 at 4 knots without nozzle and disk



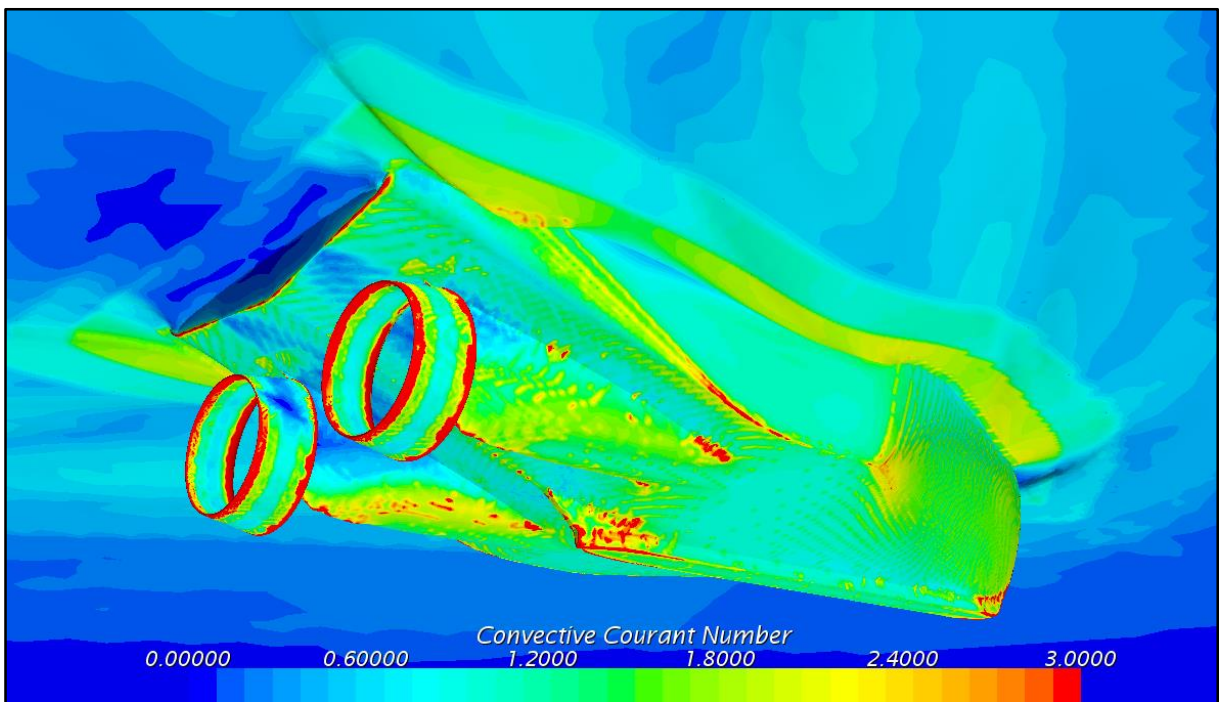
10 - Wall y^+ values Hull 2 at 10 knots without nozzle and disk



11 - Courant number, Hull 2 at 10 knots without nozzle and disk

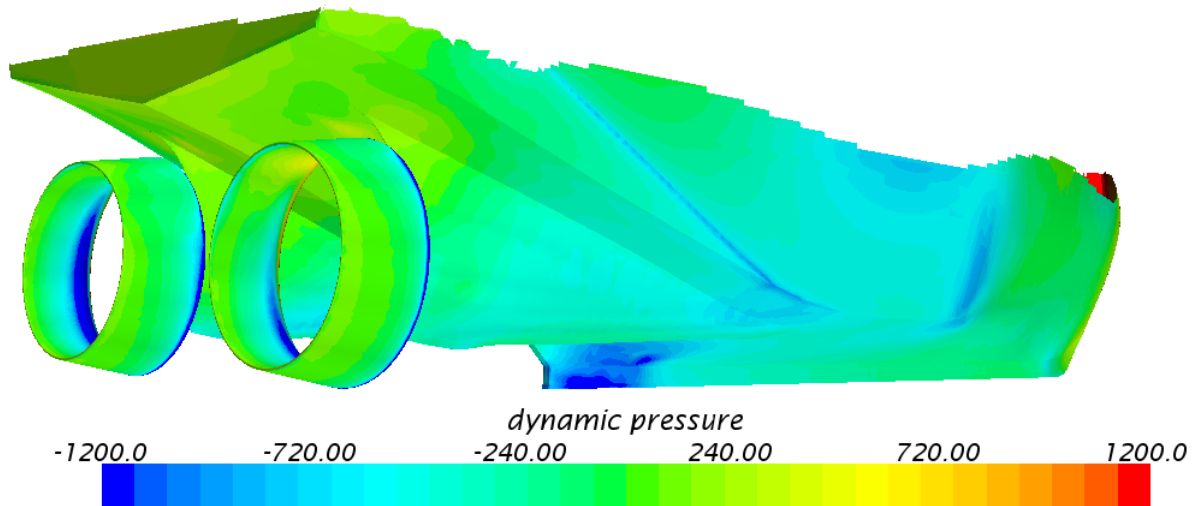


12 - Wall y+ values Hull 2 at 10 knots with nozzle and disk

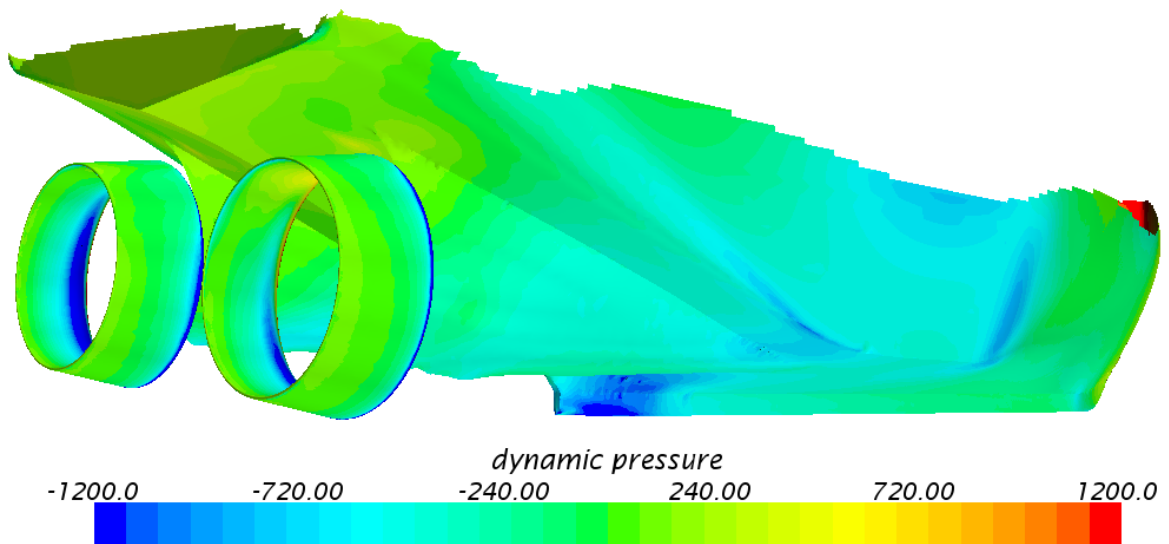


13 - Courant number, Hull 2 at 10 knots with nozzle and disk

Appendix F. Dynamic Pressure

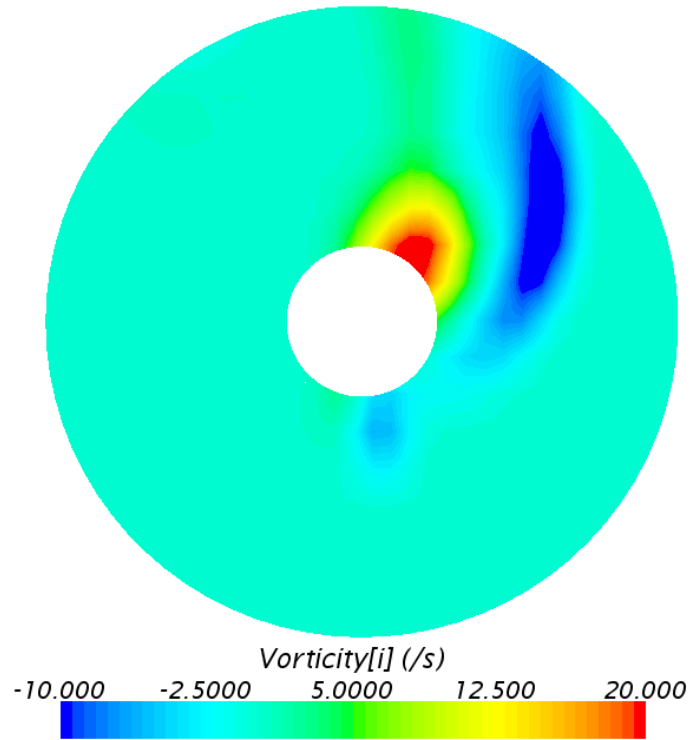


14 – Pressure [Pa], Hull 2 at 10 knots with nozzle and disk

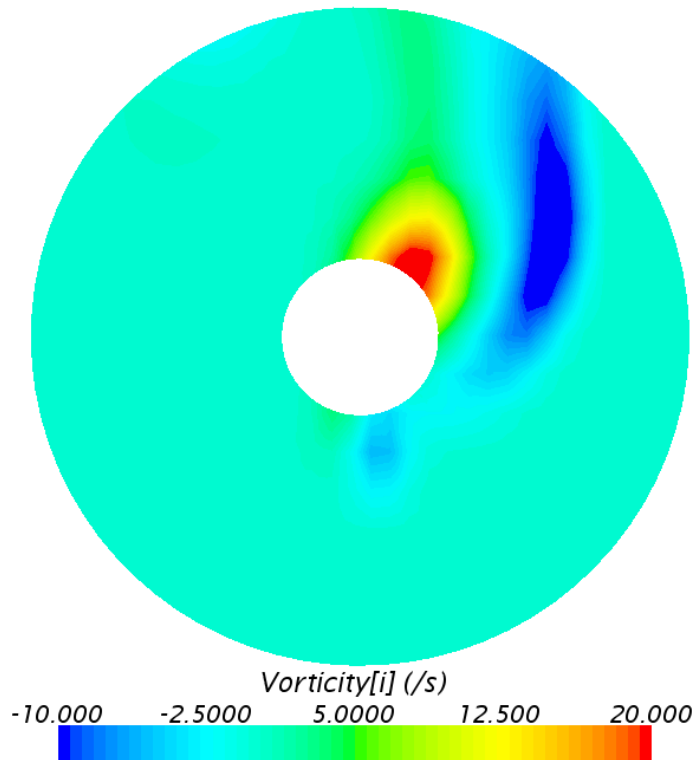


15 – Pressure [Pa], Hull 2 at 10 knots with nozzle and disk

Appendix G. Vorticity in Propeller Plane

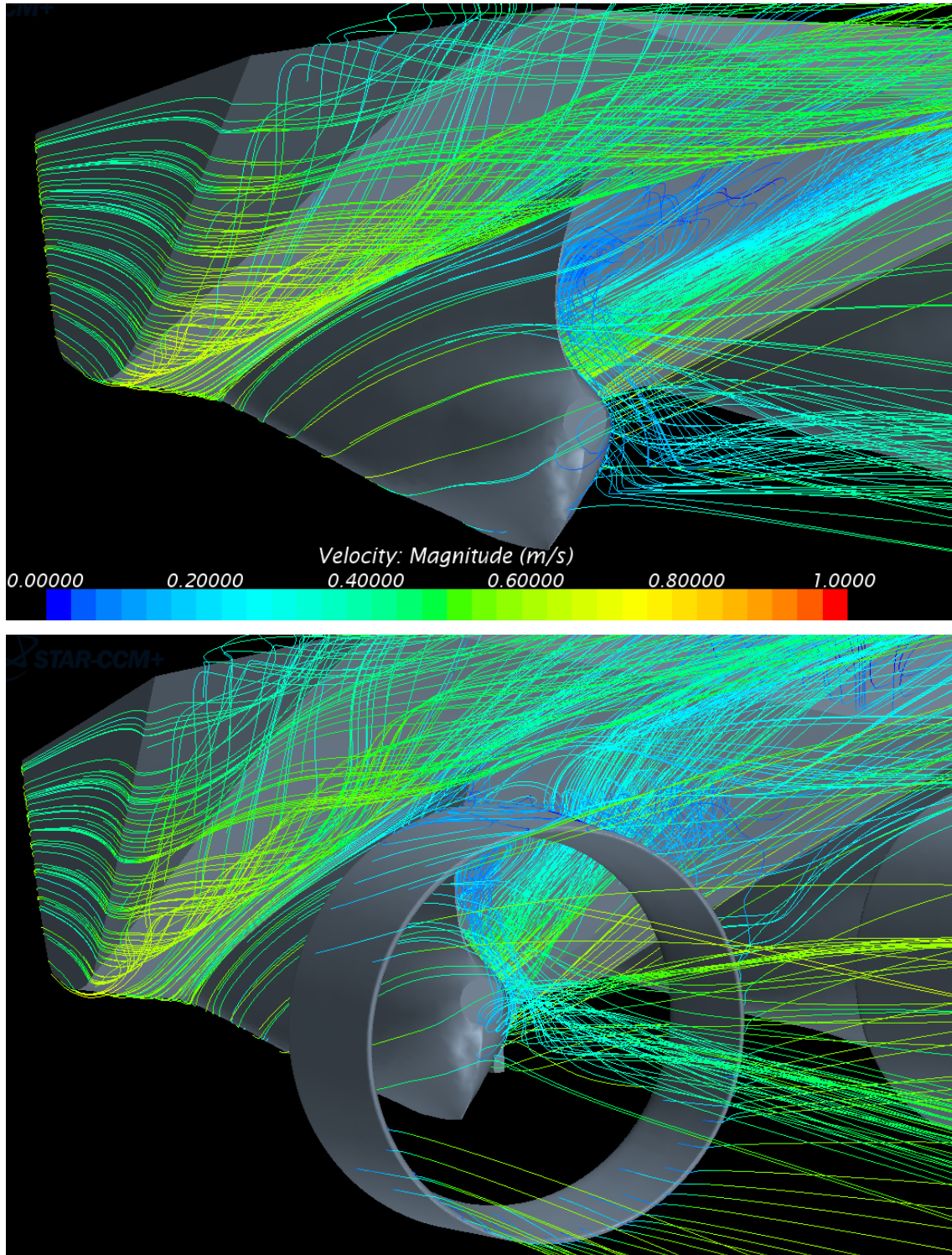


16 - Vorticity propeller plane Hull 1 at 10 knots without nozzle and disk

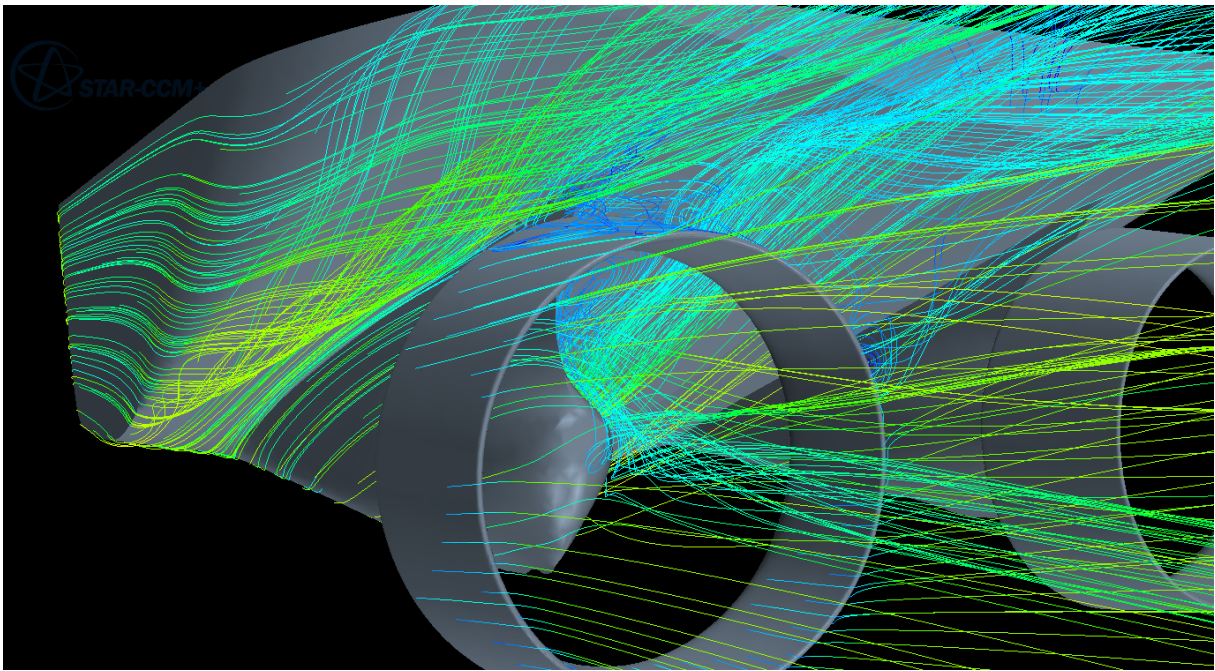
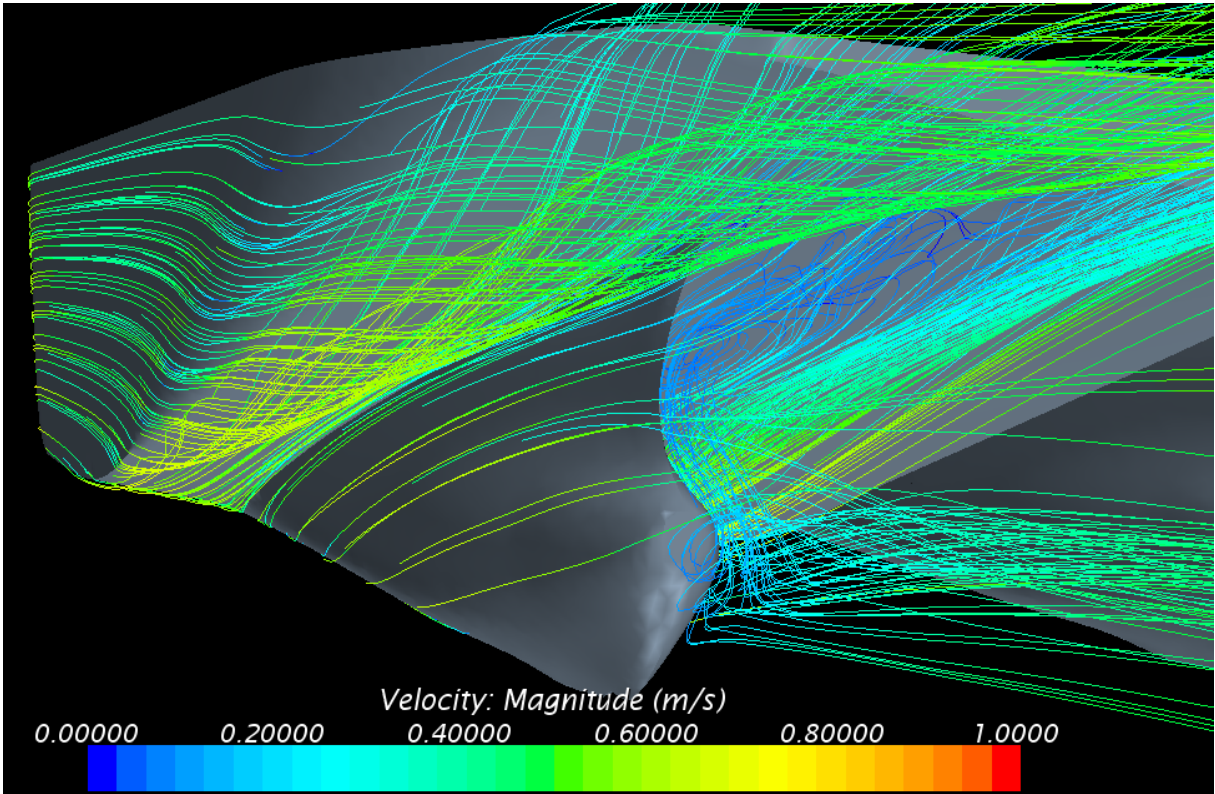


17 - Vorticity propeller plane Hull 2 at 10 knots without nozzle and disk

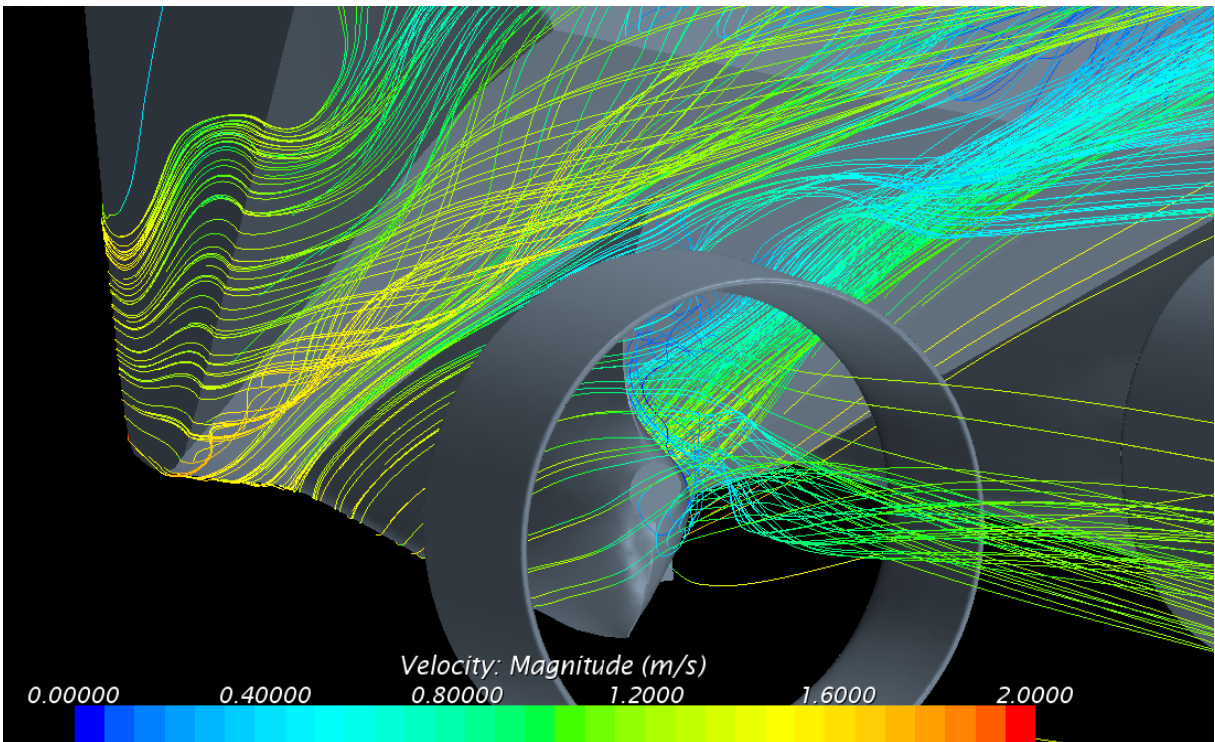
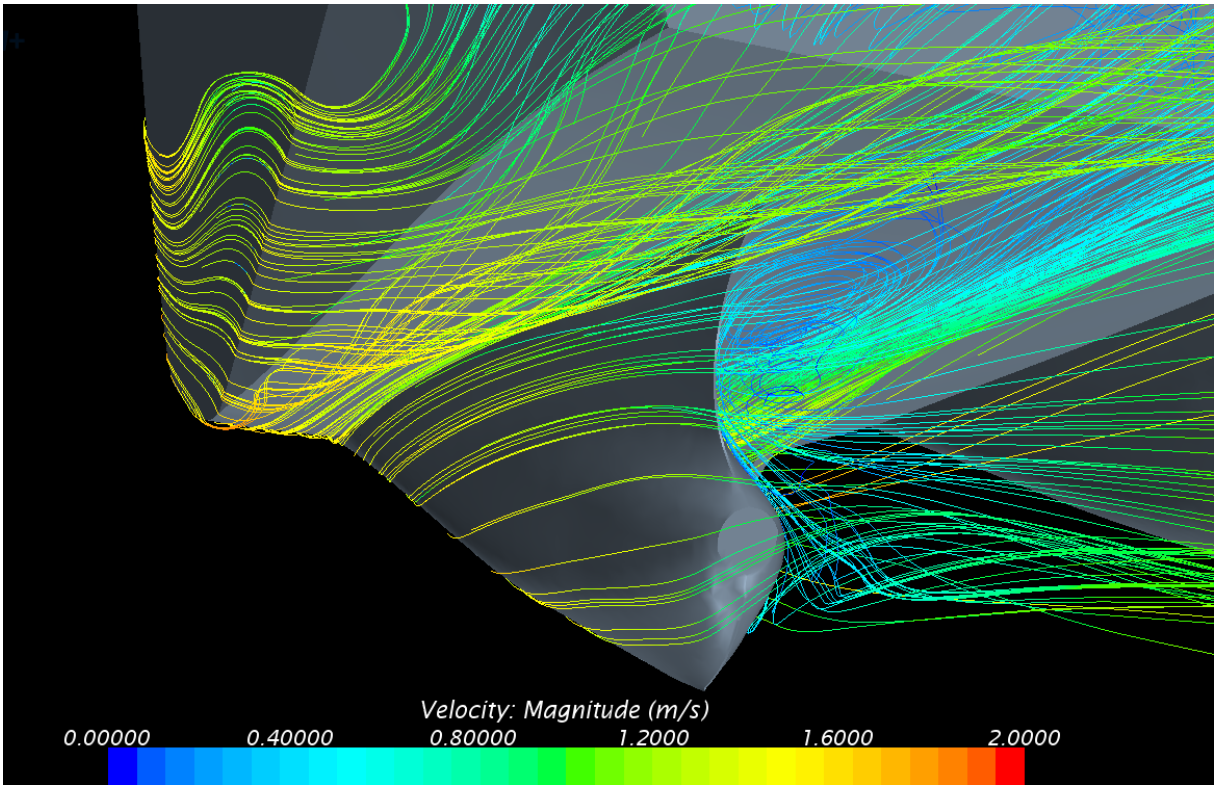
Appendix H. Streamlines



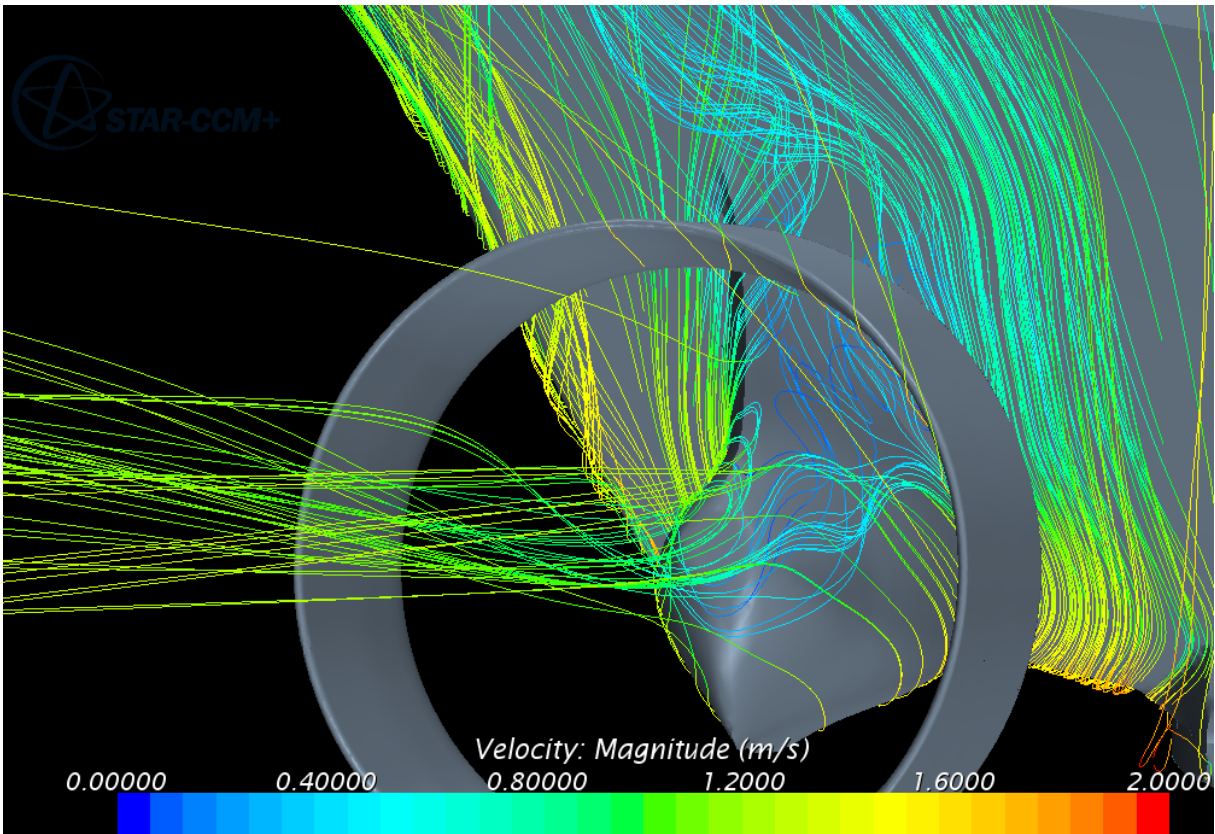
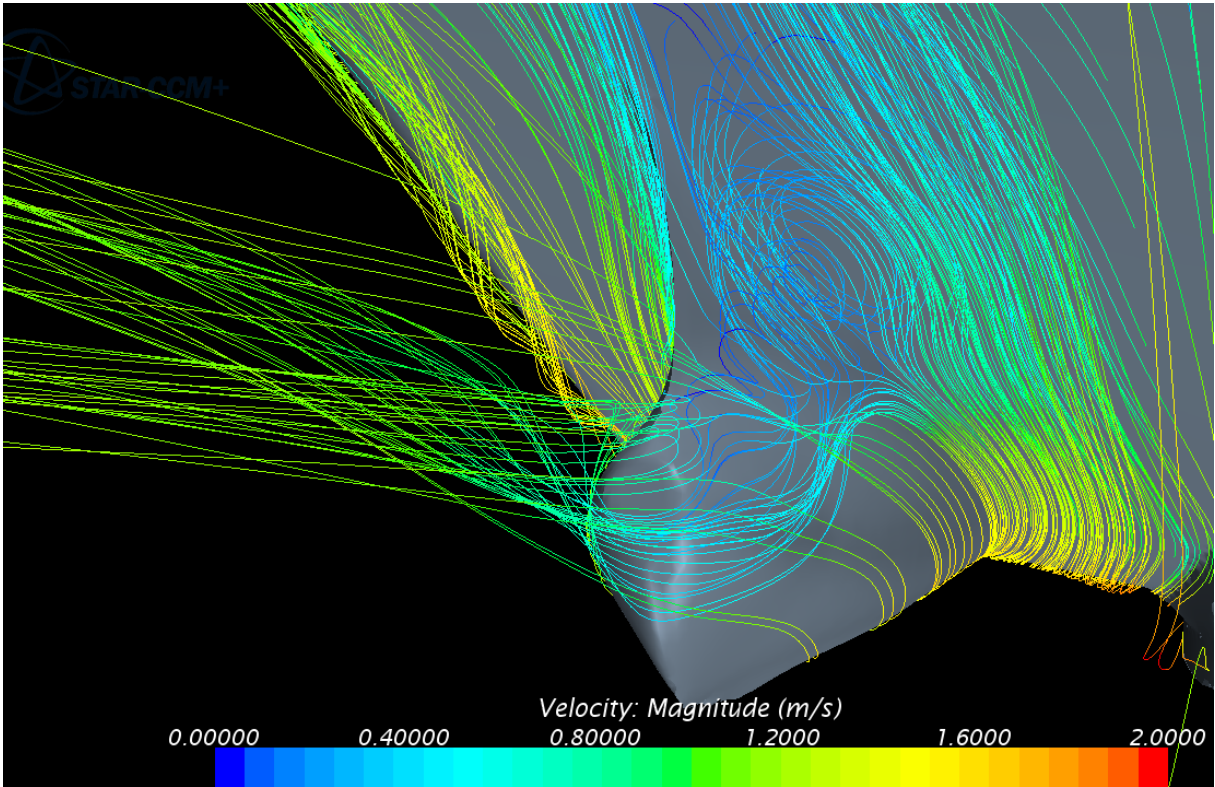
1 - Streamlines Hull 1, at 4 knots with and without nozzle and disk



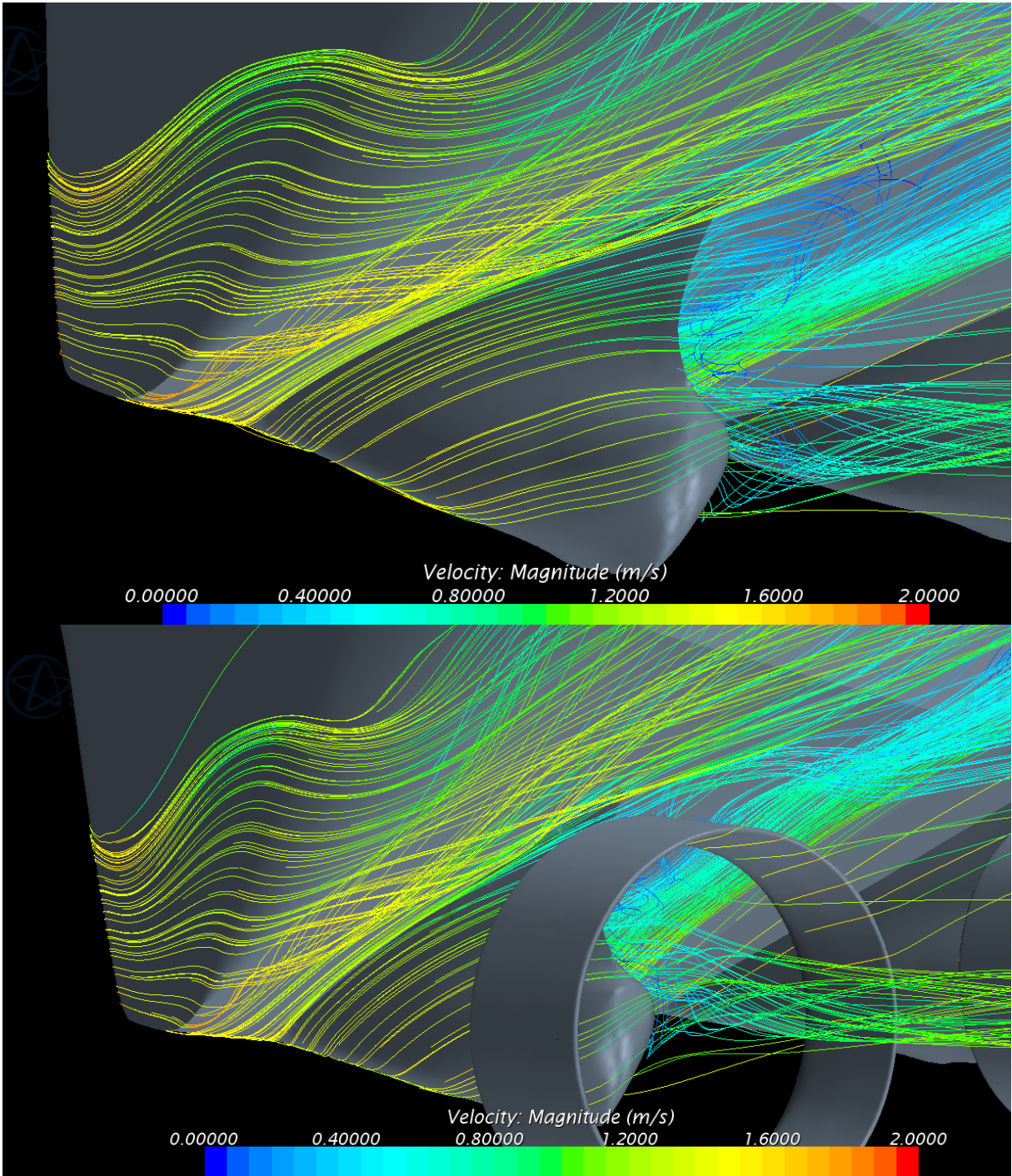
2 - Streamlines Hull 2, at 4 knots with and without nozzle and disk



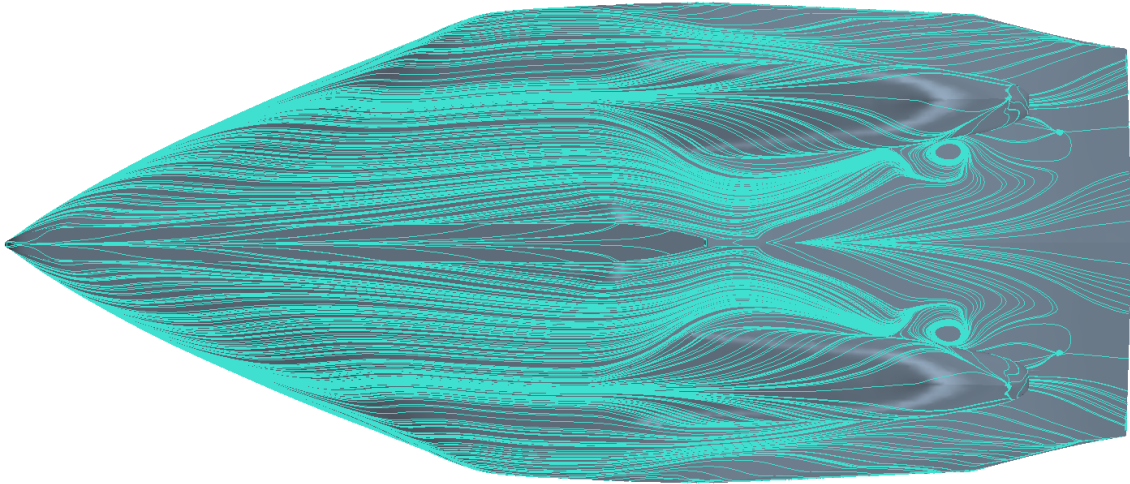
18 - Streamlines Hull 1, at 10 knots with and without nozzle and disk



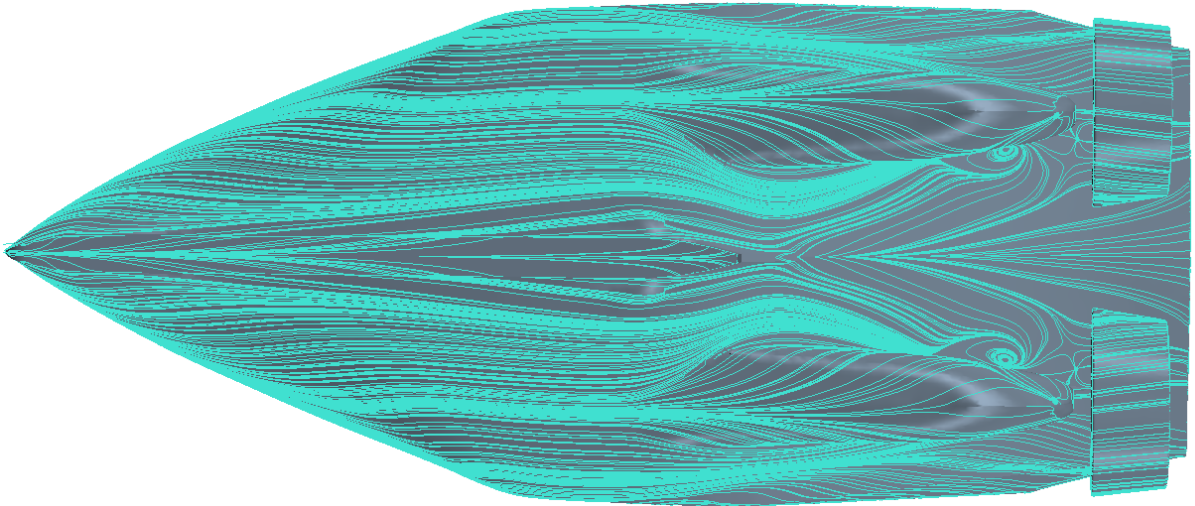
19 - Streamlines Hull 2, at 10 knots with and without propeller and nozzle



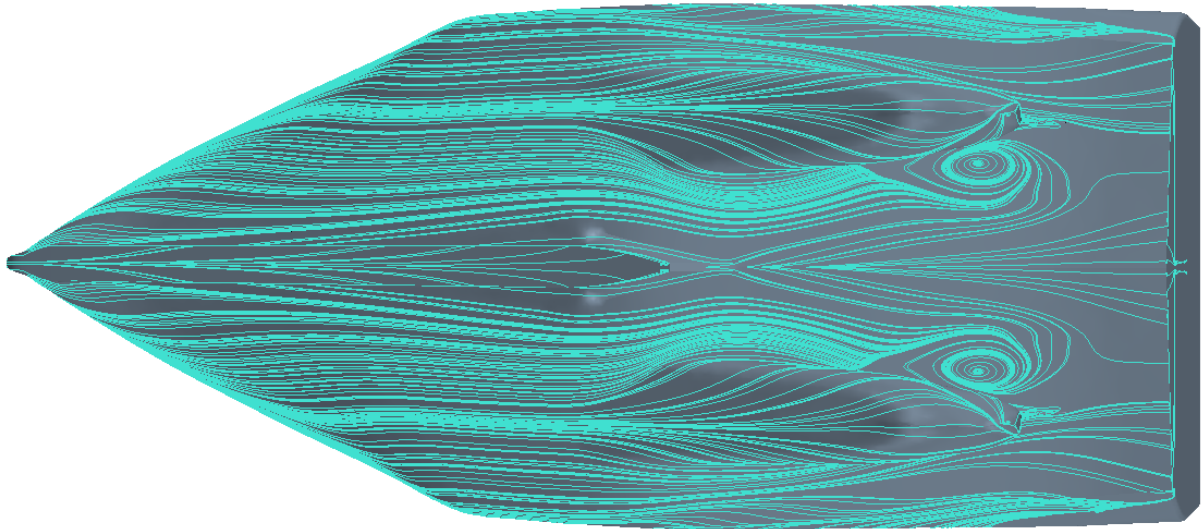
20 - Streamlines Hull 2, at 10 knots with and without propeller and nozzle



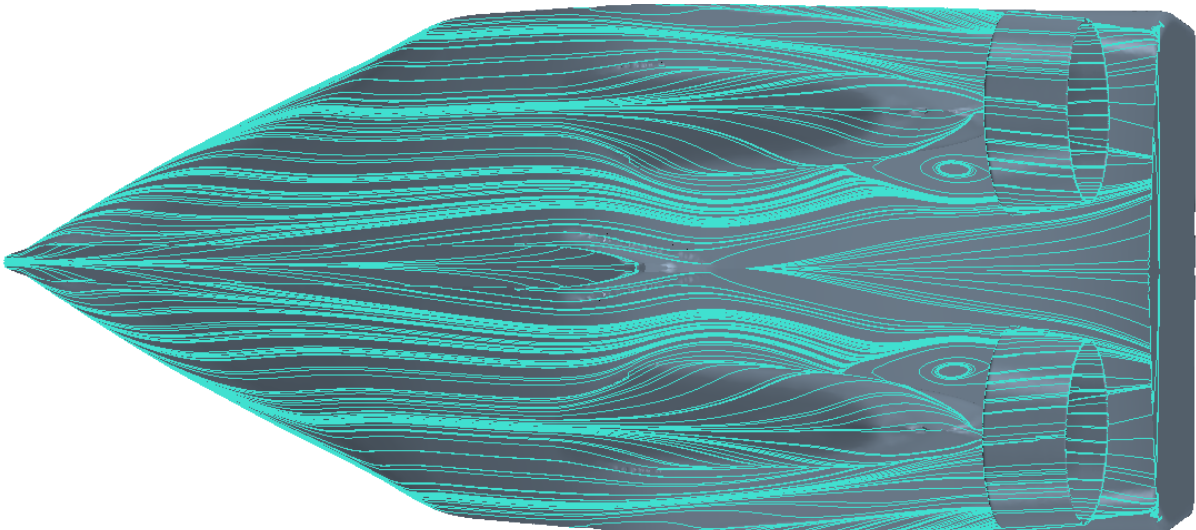
21 - Streamlines Hull 1 at hull surface without propeller and nozzle, 4 knots



22 - Streamlines Hull 1 at hull surface with propeller and nozzle, 4 knots

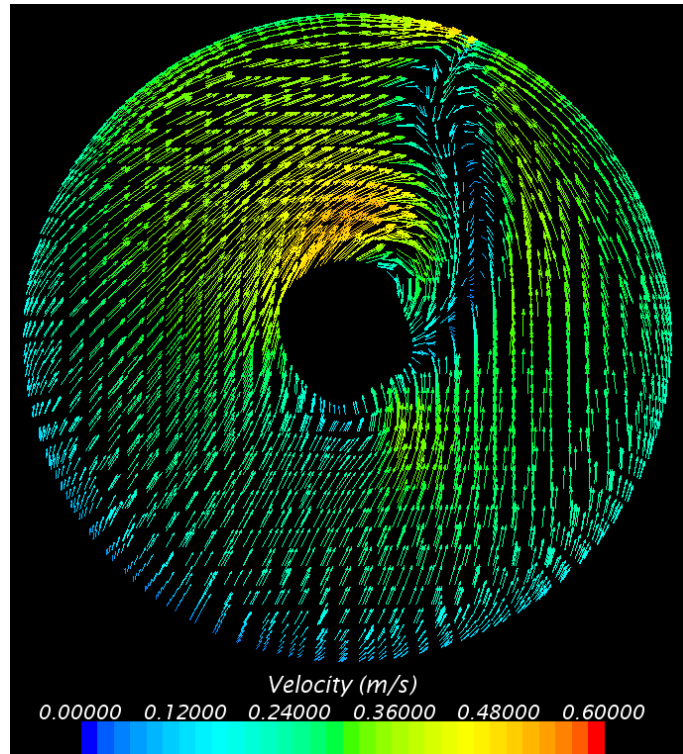


23 - Streamlines Hull 1 at hull surface without propeller and nozzle, 10 knots

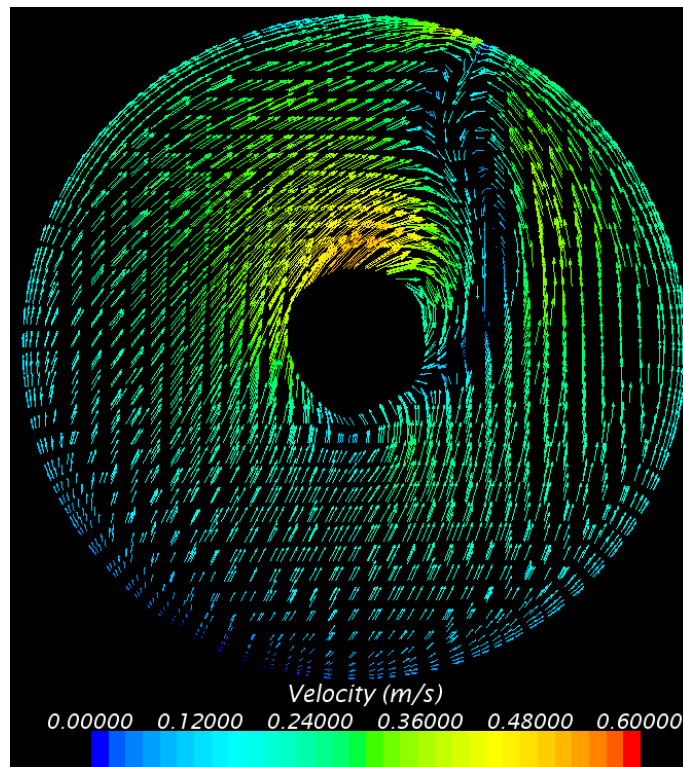


24 - Streamlines Hull 1 at hull surface with propeller and nozzle, 10 knots

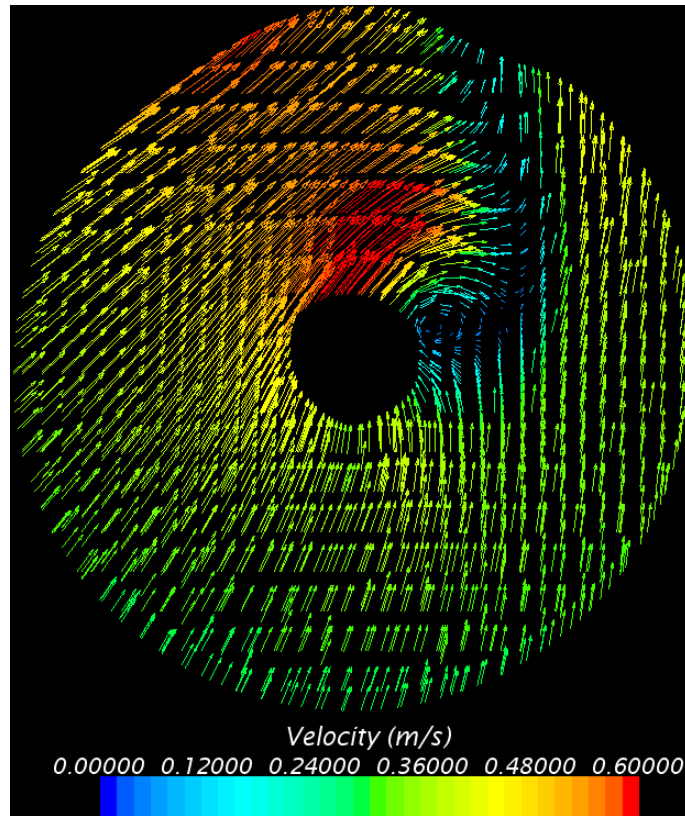
Appendix I. Tangential Velocity



25 – Tangential velocity Hull 1 at 10 knots with nozzle and disk

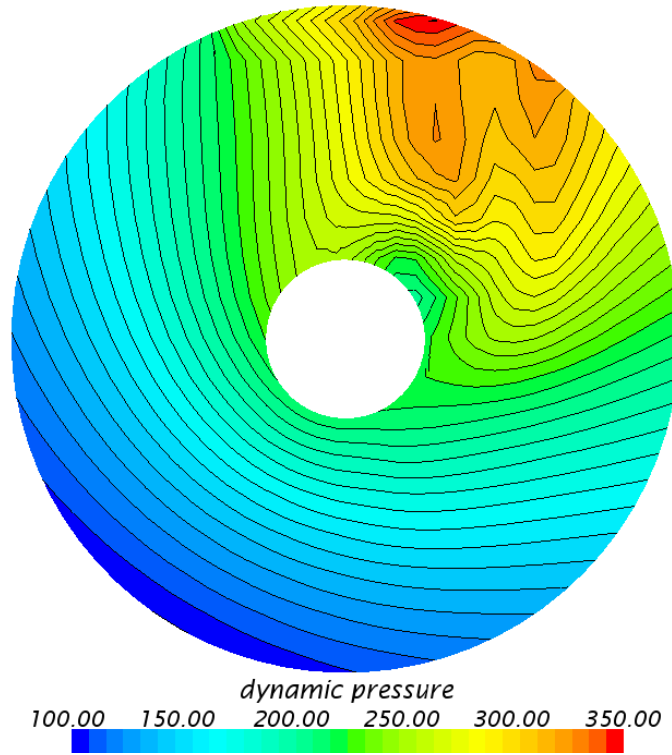


26 – Tangential velocity Hull 2 at 10 knots with nozzle and disk

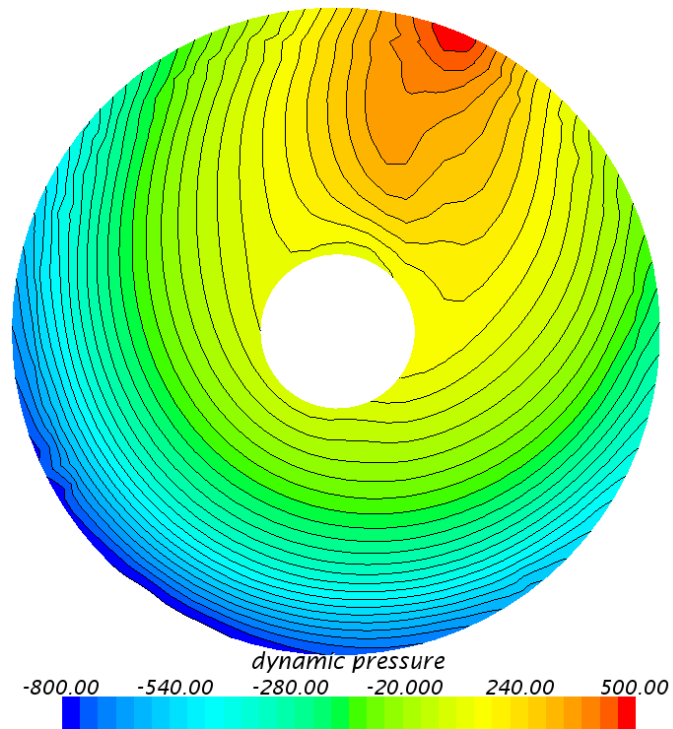


27 – Tangential velocity Hull 1 at 10 knots without nozzle and disk

Appendix J. Dynamic Pressure




28 - Dynamic pressure [Pa] Hull 1 without nozzle and disk at 10 knots



29 - Dynamic pressure [Pa] Hull 1 with nozzle and disk at 10 knots

Appendix K. R/V Gunnerus

	RESISTANCE TEST	ENCL. 18
		REPORT 530112.00.01
		DATE 2005-04-05
		REF M2705A

HULL MODEL No.: M2705A Model Scale: 10.345
Loading condition: WL1 - Normal Operative
Draught AP/FP: 2.600 / 2.600 [m]


	Symbol	Unit	SHIP	MODEL
Length betw. perp.	L_{FP}	[m]	28.900	2.794
Length on waterline	L_{WL}	[m]	30.005	2.900
Breadth waterline	B_{WL}	[m]	9.600	0.928
Draught at $L_{FP}/2$	T	[m]	2.600	0.251
Wetted surface	S	[m ²]	381.51	3.565
Wetted surf. of transom stern	A_T	[m ²]	2.96	0.028
Transv. proj. area above WL	A_V	[m ²]	74.00	0.426
Volume displacement	V	[m ³]	404.64	0.365
Block coefficient	C_{BLW}	[-]	0.540	0.540

1+k	=	1.2295	Tankwater temp. [°C]	=	14.9
$C_{NM} \cdot 10^3$	=	0.1237			

V_B [knots]	V_M [m/s]	F_N [-]	R_{RM} $\cdot 10^{-6}$	R_M [N]	C_M $\cdot 10^3$	C_M $\cdot 10^3$	C_{APP} $\cdot 10^3$	C_{RM} $\cdot 10^3$	C_R $\cdot 10^3$
8.00	1.280	0.240	3.253	22.758	7.806	3.684	0.215	0.327	2.611
8.50	1.360	0.255	3.456	25.761	7.827	3.641	0.212	0.328	2.686
9.00	1.440	0.270	3.660	29.484	7.990	3.601	0.209	0.330	2.900
9.50	1.519	0.285	3.863	33.824	8.227	3.565	0.206	0.332	3.183
10.00	1.599	0.300	4.066	39.735	8.723	3.530	0.203	0.334	3.722
10.50	1.679	0.315	4.269	47.327	9.423	3.498	0.200	0.335	4.463
11.00	1.759	0.330	4.473	55.419	10.054	3.468	0.198	0.337	5.132
11.50	1.839	0.345	4.676	63.808	10.591	3.439	0.196	0.338	5.705
12.00	1.919	0.360	4.879	72.709	11.084	3.412	0.194	0.339	6.232
12.50	1.999	0.375	5.083	85.883	12.066	3.386	0.192	0.341	7.246
13.00	2.079	0.390	5.286	104.312	13.549	3.362	0.190	0.342	8.760
13.50	2.159	0.405	5.489	128.636	15.494	3.339	0.188	0.343	10.734
14.00	2.239	0.420	5.693	158.951	17.802	3.317	0.187	0.344	13.070

Setup: Towing test:
 m2705a1s1 m2705a1_slep_1 (Cw)

ShipX (RepGen version 2.0.15) 11-Mar-2005 14:42:15
 ShipX (RepGen version 2.0.11) 11-May-2004 14:12:35

	SHIP RESISTANCE COEFFICIENS	ENCL. 19
		REPORT 530112.00.01
		DATE 2005-04-05
		REF M2705A

HULL MODEL No.: M2705A Model Scale: 10.345
 Loading condition: WL1 - Normal Operative
 Draught AP/FP: 2.600 / 2.600 [m]

	Symbol	Unit	SHIP	MODEL
Length betw. perp.	L_{PP}	[m]	28.900	2.794
Length on waterline	L_{WL}	[m]	30.005	2.900
Breadth waterline	B_{WL}	[m]	9.600	0.928
Draught at $L_{PP}/2$	T	[m]	2.600	0.251
Wetted surface	S	[m ²]	381.51	3.565
Wetted surf. of transom stern	A_T	[m ²]	2.96	0.028
Transv. proj. area above WL	A_V	[m ²]	74.00	0.426
Volume displacement	∇	[m ³]	404.64	0.365
Block coefficient	C_{BLW}	[-]	0.540	0.540

$1+k$ = 1.2295 Correlation coef $\cdot 10^3$ = -0.1300
 $C_{MAS} \cdot 10^3$ = 0.1222 Seawater temp. [°C] = 15.0

V_B [knots]	V_M [m/s]	F_R [-]	R_{NS} $\cdot 10^{-9}$	C_R $\cdot 10^3$	C_{TS} $\cdot 10^3$	C_{VS} $\cdot 10^3$	C_{IBS} $\cdot 10^3$	C_{APPS} $\cdot 10^3$	C_{TS} $\cdot 10^3$
8.00	1.280	0.240	0.104	2.611	2.071	2.663	0.435	0.174	5.875
8.50	1.360	0.255	0.111	2.686	2.053	2.667	0.437	0.175	5.957
9.00	1.440	0.270	0.117	2.900	2.037	2.670	0.439	0.175	6.177
9.50	1.519	0.285	0.124	3.183	2.021	2.673	0.441	0.176	6.465
10.00	1.599	0.300	0.130	3.722	2.006	2.676	0.442	0.177	7.009
10.50	1.679	0.315	0.137	4.463	1.993	2.679	0.444	0.177	7.755
11.00	1.759	0.330	0.143	5.132	1.979	2.681	0.445	0.177	8.428
11.50	1.839	0.345	0.150	5.705	1.967	2.683	0.447	0.178	9.005
12.00	1.919	0.360	0.156	6.232	1.955	2.685	0.448	0.178	9.535
12.50	1.999	0.375	0.163	7.246	1.944	2.686	0.449	0.179	10.553
13.00	2.079	0.390	0.169	8.760	1.934	2.688	0.451	0.179	12.070
13.50	2.159	0.405	0.176	10.734	1.923	2.689	0.452	0.179	14.046
14.00	2.239	0.420	0.182	13.070	1.914	2.690	0.453	0.179	16.385

Setup: Towing test:
 m2705ais1 m2705a1_slep_1 (Cw)

ShipX (RepGen version 2.0.15) 11-Mar-2005 14:42:15

	SHIP RESISTANCE	ENCL.	20
		REPORT	530112.00.01
		DATE	2005-04-05
		REF	M2705A

HULL MODEL No.: M2705A Model Scale: 10.345
Loading condition: WL1 - Normal Operative
Draught AP/FP: 2.600 / 2.600 [m]

	Symbol	Unit	SHIP	MODEL
Length betw. perp.	L_{FP}	[m]	28.900	2.794
Length on waterline	L_{WL}	[m]	30.005	2.900
Breadth waterline	B_{WL}	[m]	9.600	0.928
Draught at $L_{FP}/2$	T	[m]	2.600	0.251
Wetted surface	S	[m ²]	381.51	3.565
Wetted surf. of transom stern	A_T	[m ²]	2.96	0.028
Transv. proj. area above WL	A_V	[m ²]	74.00	0.426
Volume displacement	∇	[m ³]	404.64	0.365
Block coefficient	C_{BLW}	[-]	0.540	0.540

1+k	=	1.2295	Correlation coef $\cdot 10^3$	=	-0.1300
$C_{MAS} \cdot 10^3$	=	0.1222	Seawater temp. [°C]	=	15.0

V_B [knots]	V_H [m/s]	F_N [-]	R_{TS} [kN]	P_E [kW]	C_{ADK} [-]	Trim [deg]	Sinkage [m] AP	FP
8.00	1.280	0.240	19.47	80.1	47.58	-0.421	-0.026	-0.239
8.50	1.360	0.255	22.29	97.5	46.93	-0.524	-0.022	-0.287
9.00	1.440	0.270	25.91	120.0	45.26	-0.618	-0.023	-0.335
9.50	1.519	0.285	30.22	147.7	43.24	-0.707	-0.027	-0.384
10.00	1.599	0.300	36.30	186.7	39.89	-0.796	-0.032	-0.434
10.50	1.679	0.315	44.28	239.2	36.05	-0.888	-0.038	-0.486
11.00	1.759	0.330	52.82	298.9	33.17	-0.992	-0.043	-0.544
11.50	1.839	0.345	61.68	364.9	31.05	-1.163	-0.033	-0.620
12.00	1.919	0.360	71.11	439.0	29.32	-1.347	-0.019	-0.699
12.50	1.999	0.375	85.39	549.1	26.49	-1.474	-0.021	-0.764
13.00	2.079	0.390	105.64	706.5	23.16	-1.552	-0.037	-0.820
13.50	2.159	0.405	132.58	920.8	19.90	-1.548	-0.078	-0.859
14.00	2.239	0.420	166.32	1197.9	17.06	-1.467	-0.143	-0.883

Setup: Towing test:
 m2705a1s1 m2705a1_slep_1 (Cw)

ShipX (RepGen version 2.0.15) 11-Mar-2005 14:42:15